PART A: STUDIES DIRECTED TOWARD THE TOTAL SYNTHESIS OF CHEBULAGIC ACID

PART B: DNA RECOGNITION BY METALLOINTERCALATOR-PEPTIDE CONJUGATES

Thesis by

Curtis Asa Hastings

In Partial Fulfillment of the Requirements

for the Degree of

Doctor of Philosophy

California Institute of Technology

Pasadena, California

1998

(Submitted March 16, 1998)

Acknowledgement

At the outset, I would like to thank Prof. Jackie Barton for giving me the opportunity to work in her laboratory. I am deeply grateful to her for her support and advice, and for encouraging me to pursue my ideas. I thank Prof. Erick Carreira, in whose group I did the work described in Part A of this thesis. His enthusiasm for science is infectious, and I can only hope that some of it rubbed off on me. I am grateful to him for supporting me in pursuing my scientific interests. I thank the rest of my thesis committee, Profs. Dennis Dougherty and Bill Goddard, for their advice and support during my time at Caltech.

I owe a debt of gratitude to the many people who helped me to reach this stage. Prof. Mike McBride first afforded me an opportunity to do chemistry research. His enthusiasm and patience were instrumental in my decision to pursue a graduate education. During my time in his laboratory, Dr. Lev Ryzhkov, Randy Carter, and John Toscano taught me much about research. At Caltech, I have had the opportunity to learn from many fine colleagues. In particular, I wish to acknowledge Justin du Bois in Erick Carreira's group. Also, I wish to acknowledge the many members of Jackie Barton's group who helped me learn how to work with and think about DNA.

A number of the projects in Part B of this thesis are collaborative. Many people have made valuable contributions to the metallointercalator-peptide projects in Jackie's lab, and we have all benefited from each other's work. During my time in Jackie's group, I have had the pleasure of working with Marilena Fitzsimons, Bob Houser, Sonya Franklin, and Kim Copeland. I am grateful to Brian Jackson, Brian Hudson, and Tim Johann for their insights into the development of a protocol for dissociation constant determination of the metallointercalator-peptide conjugates. On a more personal level, I have had many

enjoyable and fruitful scientific discussions with my "neighbors" in 139 Noyes, Erik Holmlin and Dr. Pete Dandliker.

I acknowledge the assistance of John Racs and Suzanna Horvath of the Biopolymer Synthesis and Analysis Resource Center at Caltech for the synthesis of resin-bound peptides. I thank Gary Hathaway for performing mass spectrometric analysis of the metallointercalator-peptide conjugates.

On a personal level, I am deeply grateful to Donna Campisi for her patience and love during the past four years. I am also deeply indebted to my parents, who have been a constant, positive influence on me. Without their support, none of this would have been possible.

Abstract

Part A. The development of asymmetric allene/enone and allene/enoate intramolecular [2+2]-photocycloadditions is described. Irradiation of optically active allenes (89-92% ee) appended to enones and enoates afforded alkylidenecyclobutane photoadducts with high levels of asymmetric induction (83-100%) derived exclusively from the allene fragment. Substrates examined include allenyl alcohols appended to 1,3-cyclopentanedione, 1,3-cyclohexanedione, and 4-hydroxycoumarin. The absolute sense of induction in these reactions was determined by photocycloaddition of an allene containing an internal stereochemical label. The *exo*-methylenecyclobutanes obtained upon irradiation of allene-coumarins were isolated as single olefin diastereomers. A model for the high levels of enantioinduction observed in these transformations is presented.

The asymmetric intramolecular allene/enoate [2+2]-photocycloaddition was applied to the synthesis of the topoisomerase I inhibitor chebulagic acid. The synthetic utility of this reaction was demonstrated by the preparation of an advanced intermediate containing all of the stereochemical information present in the chebulic acid fragment of chebulagic acid. In the course of these synthetic studies an unusual δ-alkynyl lactone photoproduct was obtained upon photocyloaddition of a substrate that was expected to afford a [7.6.6.4]-tetracyclic system. A 1,5-hydrogen shift in a biradical intermediate was implicated in the formation of this product by isotopic labeling studies; the mechanistic implications of these results for enantioselectivity in photochemical reactions of optically active allenes tethered to enones and enoates are discussed.

Part B. The DNA recognition properties of peptide conjugates of phenenthrenequinone diimine complexes of rhodium(III) have been studied. The structural and thermodynamic basis for the 5'-CCA-3'-selectivity of the metallointercalator-peptide conjugate $[Rh(phi)_2(phen')]^{3+}$-AANVAIAAWERAA-$CONH_2$ was investigated. A protocol for measuring dissociation constants of DNA cleaving ligands by cleavage titration is described. Using this protocol, the energetic contribution of the peptide to sequence-selective binding was assessed, and evidence for the origin of the enhanced sequence-selectivity observed at elevated temperature was obtained. Micromolar quantities of $[\Delta$-$Rh(phi)_2(phen')]^{3+}$-AANVAIAAWERAA-$CONH_2$ were synthesized to examine the structure of the metallointercalator-peptide conjugate and the metallointercalator-peptide conjugate•DNA complex by NMR. NMR results for the metallointercalator-peptide conjugate in the absence of DNA are reported.

A family of peptide conjugates of $[Rh(phi)_2(phen')]^{3+}$ (phi = 9,10-phenanthrenequinone diimine, phen' = 5-(amidoglutaryl)-1,10-phenanthroline) was also synthesized. The peptide sequences were obtained by single amino acid modification of the 5'-CCA-3'-selective metallointercalator-peptide conjugate $[Rh(phi)_2(phen')]^{3+}$-AANVAIAAWERAA-$CONH_2$ to explore the correlation between the amino acid sequence of the peptide and the nucleotide sequence of the DNA target. Changing the position of the glutamate at position 10 in the sequence of the appended peptide resulted in the identification of a 5'-ACA-3'-selective metallointercalator-peptide conjugate, $[Rh(phi)_2(phen')]^{3+}$-AANVAEAAWARAA-$CONH_2$. Locating the glutamate on one face of a putative α-helix was found to be essential for sequence specificity; peptide conjugates with the glutamate at positions 7, 8, 12, and 13 did not afford sequence-selective DNA recognition. Further amino acid substitutions were made at positions 6 and 10. Mutating the glutamate at position 6 to arginine caused complex changes in the recognition characteristics of the resulting conjugate. To probe the interactions that give rise to

sequence specificity, we have measured thermodynamic dissociation constants for these sequence-selective metallointercalator-peptide conjugates and $[Rh(phi)_2(phen')]^{3+}$.

The observed sequence preferences are consistent with the model of Sardesai *et al.* for the sequence selectivity of $Rh(phi)_2(phen')]^{3+}$-AANVAIAAWERAA-$CONH_2$. This model states that sequence-specific DNA recognition requires the peptide to adopt an α-helical conformation, and that Glu^{10} makes a critical base-specific contact with the 5'-terminal cytosine of the recognition sequence. Using the additional sequence-selectivity data, this model is refined. This refined model suggests that recognition of the central C•G base pair of the 5'-CCA-3' recognition sequence of [Rh]-E10 is accomplished by Ile^6 through shape-selection, and that recognition of the 5'-terminal A•T base pair of the 5'-ACA-3' recognition sequence of [Rh]-E6 is accomplished by van der Waals contacts between alanine and thymine methyl groups. The implications of these results for the *de novo* design of sequence-selective DNA binding peptides are discussed.

Table of Contents

Acknowledgement iii

Abstract v

Table of Contents viii

List of Figures xvi

List of Schemes xxi

List of Tables xxiii

Chapter 1: Introduction

1.1. Part A: Studies directed toward the total synthesis of chebulagic acid

1.1.1. Biological activity of chebulagic acid 1

1.1.2. Structure of and synthetic approach to chebulagic acid 2

1.2. Part B: DNA recognition by metallointercalator-peptide conjugates

1.2.1. DNA recognition by proteins 3

1.2.2. Engineering proteins with altered sequence selectivity 8

1.2.3. DNA recognition by peptides 9

1.3. References and Notes 11

Chapter 2: Studies Directed Towards the Total Synthesis of Chebulagic Acid I: The Asymmetric Intramolecular [2+2]-Photocycloaddition of Allenes with Enones and Enoates

2.1. Introduction

2.1.1. Introduction 17

2.1.2. Mechanistic aspects of photocycloadditions 18

2.1.3. Previous investigations of asymmetric photocyclizations 19

2.2. Experimental 20

2.3. Results

2.3.1. Synthesis of photosubstrates 45

2.3.2. Photocyclizations of 1,3-cyclopentanedione and 1,3-cyclohexanedione derived substrates 47

2.3.3. Photocyclization of 4-hydroxycoumarin-derived substrate 51

2.3.4. Determination of sense of stereochemical induction in photocyclizations 52

2.4. Discussion 55

2.5. Conclusions 58

2.6. References and Notes 58

Chapter 3: Studies Directed Toward the Total Synthesis of Chebulagic Acid II: Synthesis of an Advanced Intermediate Containing All Stereocenters of Chebulic Acid

3.1. Introduction

3.1.1. Introduction 63

3.1.2. Structure of chebulic and chebulagic acids 63

3.1.3. Retrosynthetic analysis of chebulic acid 64

3.2. Experimental 65

3.3. Results

3.3.1. Synthesis of the chebulic acid core: synthesis of the allene component of the chebulic acid precursor photosubstrate in enantioenriched form 104

3.3.2. Synthesis of the chebulic acid core: synthesis of the allene component of the chebulic acid precursor photosubstrate in racemic form 105

3.3.3. Synthesis of the chebulic acid core: synthesis of the chebulic acid precursor photosubstrate 106

3.3.4. Synthesis of the chebulic acid core: formation of an unexpected photoproduct 107

3.3.5. Mechanistic study of stereospecific 1,7-hydrogen atom transfer in the formation of an unusual allene/enoate photoproduct 109

3.3.6. Synthesis and photocycloaddition of allene containing a pendant olefin 111

3.3.7. Removal of photocycloaddition stereocontrolling group by ring-closing metathesis 115

3.3.8. Attempted elaboration of metathesis product to chebulic acid 115

3.4. Discussion

3.4.1. Preparation of an advanced intermediate for the synthesis of chebulic acid 117

3.4.2. Formation of an unexpected photoproduct arising from 1,5-hydrogen atom transfer 119

3.5. Conclusions 122

3.6. References and Notes 123

Chapter 4: Chapter 4: Probing the Origins of the DNA 5'-CCA-3' Sequence Selectivity of the Metallointercalator-Peptide Conjugate $[Rh(phi)_2(phen')]^{3+}$-AANVAIAAWERAA-$CONH_2$: Implications for Design

4.1. Introduction

4.1.1. Introduction 128

4.1.2. DNA binding and cleavage by phenanthrenequinone diimine complexes of rhodium(III) 128

4.1.3. Recognition of DNA by metallointercalator-peptide conjugates 129

4.2. Experimental

4.2.1. Materials and Methods 132

4.2.2. Instrumentation 133

4.2.3. Synthesis of oligonucleotides 134

4.2.4. Synthesis of peptides 135

4.2.5. Synthesis of $[Rh(phi)_2(phen')]^{3+}$ 135

4.2.6. Enantiomer separation of $[Rh(phi)_2(phen')]^{3+}$ 135

4.2.7. Synthesis of [Rh]-E10 136

4.2.8. Synthesis of [Δ-Rh]-E10 137

4.2.9. Model of dissociation constant determination by photocleavage titration 137

4.2.10. Dissociation constant determination of sequence-selective metallointercalator-peptide conjugates by photocleavage titration 139

4.2.11. Bulk dissociation constant determination of non-sequence-selective metallointercalators by photocleavage titration 140

4.3. Results

4.3.1. Synthesis of [Rh]-E10 and [D-Rh]-E10 140

4.3.2. NMR study of a metallointercalator-peptide conjugate 141

4.3.3. Modeling of dissociation constant determination experiments 146

4.3.4. Determination of the dissociation constant of [Rh]-E10 for a 5'-CCA-3' sequence under conditions affording optimum selectivity 148

4.3.5. Effect of temperature on metallointercalator-peptide conjugate selectivity and affinity 150

4.3.6. Circular dichroism study of a metallointercalator-peptide conjugate bound sequence-selectively to DNA 152

4.4. Discussion

4.4.1. Energetics of DNA binding by [Rh]-E10 155

4.4.2. Conformational effects of DNA binding by [Rh]-E10 158

4.5. Conclusions 159

4.6. References and Notes 160

Chapter 5: Perturbing the DNA Sequence Selectivity of Metallointercalator-Peptide Conjugates by Single Amino Acid Modification

5.1. Introduction

5.1.1. Correlations between the amino acid sequences of DNA binding proteins and the nucleotide sequences of their targets 167

5.1.2. Model for DNA recognition by metallointercalator-peptide conjugates derived from the P_{22} repressor 168

5.2. Experimental

5.2.1. General procedures 170

5.2.2. Instrumentation 170

5.2.3. Synthesis of $[Rh(phi)_2(ethynylphen')]^{3+}$ 170

	5.2.4.	Synthesis of metallointercalator-peptide conjugates	174
	5.2.5.	Characterization of metallointercalator-peptide conjugates	175
	5.2.6.	Photocleavage of DNA restriction fragments	175
	5.2.7.	Photocleavage of oligonucleotides	176
5.3.	Results		
	5.3.1.	Synthesis and characterization of metallointercalators	177
	5.3.2.	Synthesis and characterization of metallointercalator-peptide conjugates	179
	5.3.3.	Site-selectivity of DNA photocleavage on restriction fragments by metallointercalator-peptide conjugates derived from [Rh]-E10 by varying the position of the critical glutamate	183
	5.3.4.	Photocleavage of oligonucleotides by metallointercalator-peptide conjugates derived from [Rh]-E10 by varying the position of the critical glutamate	185
	5.3.5.	DNA photocleavage by metallointercalator-peptide conjugates containing further amino acid sequence changes at positions 6 and 10	189
	5.3.6.	Photocleavage of oligonucleotides by [Rh]-E6E10	192

	5.3.7.	Photocleavage efficiency of metallointercalator-peptide conjugates	197
	5.3.8.	Circular dichroism of metallointercalator-peptide conjugates	198
5.4.	Discussion		
	5.4.1.	DNA recognition by metallointercalator-peptide conjugates derived from [Rh]-E10 by varying the position of the critical glutamate	199
	5.4.2.	Model for DNA recognition by [Rh]-E6 and [Rh]-E10	201
	5.4.3.	Implications of the model	202
	5.4.4.	Effect of the E6R mutation on the DNA sequence selectivity of [Rh]-E6	206
5.5.	Conclusions		207
5.6.	References and Notes		208
Chapter 6:	Conclusions and Perspectives		
6.1.	Conclusions		213
6.2.	Perspectives		214
6.3.	References and Notes		216
Appendix I:	X-ray Crystallographic Data for (±)-15 (Chapter 2)		217
Appendix II:	COSY and TOCSY Spectra and COSY, TOCSY, and NOESY Cross Peak Assignments for [Δ-Rh]-E10 (Chapter 5)		220

List of Figures

Chapter 1:

1.1. Ellagitannin synthesis targets: chebulagic acid amd chebulic acid. 1

1.2. Synthetic plan for the establishment of the correct relative stereochemistry at C4 and C5 of chebulic acid using [2+2]-photocycloadditions. 2

1.3. Shape complementarity in the *434* repressor dimer–operator complex. 6

Chapter 2:

2.1. Model substrates for enantioselective photocyclizations. 46

2.2. Enantiomeric excess determination of photoproducts derived from 1,3-cyclopentanedione and 1,3-cyclohexanedione. 48

2.3. Selected ^{1}HNMR NOE difference data for photoproducts derived from 1,3-cyclopentanedione and 1,3-cyclohexanedione. 49

2.4. Confirmation of asymmetric induction in photocyclization of 1,3-cyclopentanedione and 1,3-cyclohexanedione derived substrates by conversion to a cycloalkanol and (*S*)-MTPA ester derivatization. 50

2.5. Enantiomeric excess determination of photoproduct derived from 4-hydroxycoumarin. 51

2.6. Determination of relative stereochemistry of photoproduct derived from 4-hydroxycoumarin. 52

2.7. Determination of relative stereochemistry of photoproduct containing an internal stereochemical label. 55

2.8. Proposed transition state geometry leading to diastereoselective product formation in photocyclizations of 4-hydroxycoumarin derived substrates. 56

Chapter 3:

3.1. Ellagitannin synthesis targets: chebulagic acid; chebulic acid; carpinusnin; corilagin. 64

3.2. Enantiomeric excess determination of alkyne photoproduct. 108

3.3. Comparison of diastereoselection in deuterium incorporation at C^2 upon enolate tautomerization and upon photocycloaddition. 110

3.4. Determination of stereoselectivity of 1,5-hydrogen atom transfer in the formation of alkyne photoproduct. 111

3.5. Determination of relative stereochemistry of photoproduct derived from dimethylpentenyl allene. 114

3.6. Determination of enantiomeric excess of photoproduct derived from dimethylpentenylallene. 116

3.7. Confirmation of correct relative stereochemistry of advanced intermediate containing all stereocenters of chebulic acid. 117

3.8. Conformational basis for stereoselectivity in installation of the C^3 stereocenter of chebulic acid. 119

3.9. Conformational basis for stereoselectivity in 1,5-hydrogen atom transfer. 121

Chapter 4:

4.1.	Solution structure of a rhodium(III) phi complex bound to DNA by intercalation from the major groove.	130
4.2.	Helix-turn-helix DNA binding proteins used as sources of DNA recognition α-helices.	130
4.3.	^{1}H NMR spectrum of [Δ-Rh]-E10.	143
4.4.	NOESY spectrum of [Δ-Rh]-E10	144
4.5.	Sequential assignment process for [Δ-Rh]-E10 showing H_N-H_α region and summary of interresidue NOEs.	145
4.6.	Modeled dissociation constant determination experiment.	146
4.7.	Effect of 10 low-affinity binding sites on observed fraction of site of interest cleaved as a function of DNA concentration and ligand–DNA ratio.	147
4.8.	Autoradiogram of dissociation constant determination of [Rh]-E10 for 5'-CCA-3' by photocleavage titration.	149
4.9.	Photocleavage isotherms for [Rh]-E10 and $[Rh(phi)_2(phen')]^{3+}$.	150
4.10.	Temperature dependence of the dissociation constant of [Rh]-E10 for 5'-CCA-3'.	151
4.11.	Comparison of CD spectra of [Rh]-E10 in the absence and presence of its DNA target sequence.	153
4.12.	Effect of intercalative binding by $[Rh(phi)_2(phen')]^{3+}$ on CD spectrum of K_2-29.	154

Chapter 5:

5.1. Absorbance spectrum of $[Rh(phi)_2(ethynylphen')]^{3+}$ as a function of pH. 178

5.2. UV-visible spectrum of a representative peptide conjugate of $[Rh(phi)_2(phen')]^{3+}$. 181

5.3. MALDI-TOF mass spectrum of a representative metallointercalator-peptide conjugate. 182

5.4. UV-visible spectrum of a representative peptide conjugate of $[Rh(phi)_2(ethynylphen')]^{3+}$. 183

5.5. Photocleavage of pUC18 3'-endlabeled *Eco*RI/*Pvu*II 180-mer by first-generation metallointercalator-peptide conjugates at 55 °C in the presence of 5 mM $MnCl_2$. 184

5.6. Photocleavage of a 31-mer oligonucleotide containing all four 5'-NCA-3' sites by [Rh]-E6 as a function of concentration. 186

5.7. Dissociation constant determination for [Rh]-E6. 188

5.8. Photocleavage isotherm for [Rh]-E6. 189

5.9. Photocleavage of pUC18 5'-endlabeled *Eco*RI/*Pvu*II 180-mer by second-generation metallointercalator-peptide conjugates at 55 °C in the presence of 5 mM $MnCl_2$. 191

5.10. Cleavage of a 31-mer oligonucleotide containing all 4 5'-NCA-3' sequences by [Rh]-E6 and [Rh]-E10 in the absence of Mn^{2+}. 194

5.11. Photocleavage isotherm for [Rh]-E6E10. 195

5.12. CD spectrum of [Rh]-E6 (50 μM) in 5 mM $MnCl_2$, 10 mM Tris•HCl, pH 7.0. 198

5.13. $C_\alpha \rightarrow C_\beta$ vectors for arginine residues from the *E. Coli* CAP protein, the glucocorticoid receptor, and Zif268 that target guanine, after superimposition of the contacted residues. 201

5.14. Model for DNA recognition by [Rh]-E10. 203

5.15. Recognition of C•G by shape-selectivity. 204

5.16. Structure of the P_{22} α_3 helix and structure the E10 peptide drawn using canonical α-helix torsion angles. 205

Appendix II:

II.1. COSY spectrum of [Δ-Rh]-E10 (500 MHz, D_2O). 220

II.2. TOCSY spectrum of [Δ-Rh]-E10 (600 MHz, 90:10 H_2O–D_2O). 221

List of Schemes

Chapter 2:

2.1. Synthetic equivalence of asymmetric [2+2]-photocycloaddition–exocyclic olefin oxidative cleavage and asymmetric ketene-enone cycloaddition. 17

2.2. Mechanism of enone-olefin photocycloadditions. 18

2.3. Synthesis of photocyclization model substrates. 46

2.4. Synthesis of photocyclization substrate containing an internal stereochemical label. 53

2.5. Determination of relative stereochemistry of allene containing an internal stereochemical label. 54

2.6. Model for diastereofacial selectivity in allene-enone and allene-enoate enantioselective photocyclizations. 56

Chapter 3:

3.1. Retrosynthetic design for chebulic acid employing [2+2]-intramolecular photocycloaddition. 65

3.2. Preparation of allene component for chebulic acid synthesis in enantioenriched form. 104

3.3. Preparation of allene component for chebulic acid synthesis in racemic form. 105

3.4. Preparation of the photosubstrate for chebulic acid synthesis. 106

3.5. Derivitization of alkyne photoproduct for enantiomeric excess determination. 108

3.6. Synthesis of deuterium-labeled photosubstrate. 109

3.7. Olefin metathesis strategy for stereocontrolling auxiliary removal. 112

3.8. Synthesis and photochemistry of dimethylpentenyl-substituted allene in enantiomerically enriched form. 113

3.9. Installation of the C^3 stereocenter of chebulic acid. 116

3.10. Mechanistic possibilities for the formation of alkyne photoproduct. 120

3.11. Origin of enantioselectivity in the formation of alkyne [2+2]-photocycloaddition products. 122

Chapter 4:

4.1. Synthesis of [Rh]-E10 and [Δ-Rh]-E10. 141

Chapter 5:

5.1. Synthesis of alkynylphenanthroline-based metallointercalator. 177

5.2. Synthesis of peptide conjugates of $[Rh(phi)_2(phen')]^{3+}$. 179

5.3. Synthesis of peptide conjugates of $[Rh(phi)_2(ethynylphen')]^{3+}$. 181

List of Tables

Chapter 1:

1.1. Base-specific contacts by amino acids in crystal structures of selected transcription factor-DNA complexes. 7

Chapter 4:

4.1. DNA recognition by P_{22}-repressor derived peptide conjugates of $[Rh(phi)_2(phen')]^{3+}$. 131

4.2. ^1H NMR (600 MHz, 90:10 H_2O–D_2O) chemical shifts for Δ-[Rh]-E10. 142

4.3. Summary of measured dissociation constants. 152

Chapter 5:

5.1. Base-specific contacts by amino acids in crystal structures of selected transcription factor-DNA complexes. 168

5.2. Peptide conjugates of $[Rh(phi)_2(phen')]^{3+}$ synthesized. 180

5.3. Peptide conjugates of $[Rh(phi)_2(ethynylphen')]^{3+}$ synthesized. 180

5.4. Nucleotide sequences from the *EcoRI/PvuII* 180-mer restriction fragment of pUC18 that show enhanced photocleavage by [Rh]-R6A10. 193

5.5. Summary of DNA recognition by peptide conjugates of $[Rh(phi)_2(phen')]^{3+}$ and $[Rh(phi)_2(ethynylphen')]^{3+}$. 196

5.6. Helical content of peptide conjugates of $[Rh(phi)_2(phen')]^{3+}$. 199

Appendix I:

I.1. Crystallographic data for (±)-15. 217

I.2. Positional parameters for (±)-15. 217

I.3. General displacement parameters - U for (±)-15. 218

Appendix II:

II.1. Observed COSY (500 MHz, D_2O) cross peaks for [Δ-Rh]-E10. 222

II.2. Observed TOCSY (600 MHz, 90:10 H_2O–D_2O) cross peaks for Δ-[Rh]-E10. 223

II.3. Observed NOESY (600 MHz, 90:10 H_2O–D_2O) cross peaks for Δ-[Rh]-E10. 226

Chapter 1: Introduction

1.1. Part A: Studies directed toward the total synthesis of chebulagic acid

1.1.1. Biological activity of chebulagic acid. DNA topoisomerases alter the linking number of supercoiled DNA, a reaction that is crucial to a number of cellular processes including replication, transcription, and recombination.[1,2] Type I topoisomerases transiently break and religate a single strand of DNA, while type II topoisomerases transiently break and religate both strands of DNA. Inhibitors of DNA topoisomerases are potential tools for studying the mechanism by which these enzymes catalyze strand passage.[3] Several topoisomerase inhibitors have antitumor activity,[4] including the chemotherapeutic agent camptothecin.[5]

In 1992 Berry *et al.* reported that bioassay-guided fractionation of methanol extracts of *Erodium stephanium* had identified the known ellagitannin natural product chebulagic acid (**1**, Figure 1.1) as the most potent known inhibitor of topoisomerase I mediated DNA relaxation.[6] The topoisomerase-catalyzed relaxation of supercoiled DNA proceeds through the open circular form to the relaxed form. Camptothecin inhibits conversion of open circular DNA to relaxed DNA by both topoisomerase I and topoisomerase II.[5] In contrast, chebulagic acid inhibits both the conversion of supercoiled DNA to open circular DNA and

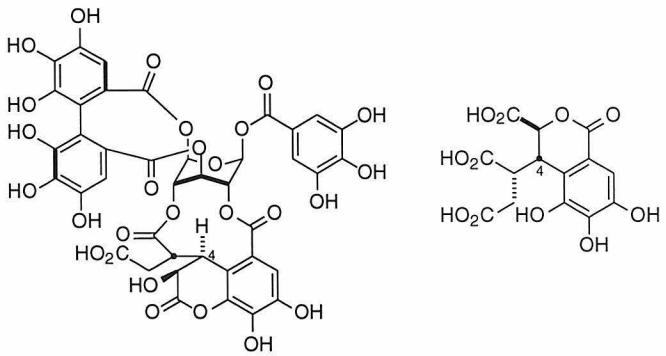

Figure 1.1. Ellagitannin synthesis targets: chebulagic acid (**1**); chebulic acid (**2**).

the conversion of open circular DNA to relaxed DNA by topoisomerase I. Unlike camptothecin, chebulagic acid has no effect on the gel mobility of the DNA. Chebulagic acid is a significantly more potent inhibitor of type I topoisomerases than type II topoisomerases. These results suggest that, unlike camptothecin, chebulagic acid acts by binding to topoisomerase I rather than by stabilizing a covalent enzyme•DNA complex.

1.1.2. Structure of and synthetic approach to chebulagic acid.

Chebulagic acid, first isolated from the dried fruits of *Terminalia chebula*,[7] is a member of the ellagitannin class of natural products. Chebulagic acid contains a highly acylated glucose core locked in a $^1C_4$ conformation by dicarboxylate substituents at C2-C4 and C3-C5. The C2-C4 component is found in two tautomeric forms; the tautomer chebulic acid (**2**, Figure 1.1) is also found in *Terminalia chebula* extracts. The chebulic acid component of these natural products is highly oxygenated and contains a synthetically challenging array of three contiguous stereocenters. Because of the potent biological activity of ellagitannin natural products, the synthetic challenges posed by the chebulic acid subunit, and the unusual molecular architecture of chebulagic acid, it is an attractive target for total synthesis.

We have chosen to establish the contiguous stereocenters of chebulic acid using olefin-enone and olefin-enoate photocycloaddition chemistry. These reactions provide access to complex carbocyclic structures with the desired *anti* stereochemistry at C4 and C5

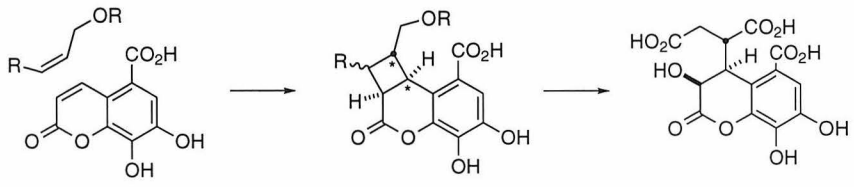

Figure 1.2. Synthetic plan for the establishment of the correct relative stereochemistry at C4 and C5 of chebulic acid using [2+2]-photocycloadditions.

(Figure 1.2). Elaboration of the cyclobutane product of the photocycloaddition reaction *via* ring expansion was expected to lead to **2**.[8] However, prior to this study there was no reliable method for controlling or predicting the absolute sense of stereochemical induction in such cyclizations. Therefore, in order to prepare chebulic acid in enantiomerically pure form, the development of an asymmetric variant of this reaction was necessitated.

Part A of this thesis describes studies directed toward the total synthesis of chebulagic acid. 1,3-Disubstituted allenes were investigated as sources of asymmetry in intramolecular [2+2]-photocycloadditions. The development of an asymmetric variant of the [2+2]-photocycloaddition reaction of olefins with enones and enoates that addresses the complex stereochemical challenge posed by the chebulic acid subunit of chebulagic acid is described in Chapter 2.[9,10] This chemistry was applied to the synthesis of the chebulic acid subunit of chebulagic acid. The preparation of an advanced intermediate containing the three stereocenters of the target in the correct relative and absolute configuration, demonstrating the synthetic utility of the asymmetric [2+2]-photocycloaddition reaction of olefins with enones and enoates, is described in Chapter 3.[11]

1.2. Part B: DNA recognition by metallointercalator-peptide conjugates

1.2.1. DNA recognition by proteins. A myriad of biological processes are mediated by noncovalent interactions such as hydrogen bonding, electrostatic and van der Waals contacts, and stacking interactions.[12] Although the individual energies of these weak interactions are comparable to thermal energies, the additive free energy of multiple weak interactions can lead to a stabilization of >5 kcal•mol^{-1} for the formation of preferred complexes.[12b] Consequently, specificities of greater than 4 orders of magnitude can be achieved.[13] Among other functions, these interactions determine the stability of the folded states of proteins and nucleic acids, and mediate important events of molecular recognition such as protein–nucleic acid recognition, enzyme–substrate recognition and receptor–ligand

binding. Part B of this thesis focuses on interactions that determine specificity in protein-DNA recognition.

Nucleic acid binding proteins play important roles in the fundamental cellular processes of transcription, translation, and repair. Transcription factors comprise one of the most diverse classes of DNA-binding proteins. Understanding the DNA-binding properties of these proteins is important for understanding how genetic information is processed and utilized. The first reported three-dimensional structures of transcription factors were the λ Cro protein, the *E. Coli* CAP protein, and the DNA binding domain of the λ repressor.[14] Since that time a wealth of high-resolution structural data has appeared. Nature has devised many solutions to the problem of sequence-selective DNA binding. However, despite the structural variety of these proteins a number of common folds have been identified; examples include the helix-turn-helix,[15] helix-loop-helix,[16] homeodomain,[17] basic region-leucine zipper,[18] zinc finger,[19] and β-ribbon motifs.[20] A common feature of all of these protein classes is the presence of a "recognition element" that makes base-specific contacts with the DNA target while the remainder of the protein provides nonspecific DNA affinity and orients the recognition element relative to the DNA. Although the α-helix is the most common recognition element, antiparallel β-sheet DNA binding proteins are known. With one exception,[21] all of the transcription factors characterized to date bind to DNA as dimers or linked multimers, and control over the aggregation state of the protein is an important regulatory pathway.[22]

Analysis of three-dimensional structures of protein-DNA complexes has identified a wealth of interactions that contribute to overall affinity and sequence specificity. Sequence specificity is attained through shape complementarity (indirect readout) as well as through the formation of base-specific hydrogen bonds and van der Waals contacts (direct readout). In general base-specific contacts are made by amino acid side chains in the major groove, perhaps because the major groove is wide enough to accommodate the protein secondary

structural elements used for recognition and because the major groove edge of the base pairs presents a more diverse array of functionality. However, DNA binding proteins that make base-specific contacts in the minor groove are known.[23]

The importance of shape complementarity may be realized by considering the thermodynamics of complex formation. The free energy change (ΔG) of complex formation is a combination of enthalpic (ΔH) and entropic ($T\Delta S$) contributions. Enthalpic stabilization is achieved through short-range noncovalent interactions. There is an entropic penalty for complex formation associated with the reduction in dynamic fluctuations at the interface. However, release of ordered water molecules on the interacting surfaces of the protein and the nucleic acid target can provide compensation. A recent elegant example of this effect was reported for glucocorticoid receptor binding to two idealized response elements that differed by one base pair.[24] Binding to the response element containing C•G at the variable site was enthalpically favored but entropically disfavored over binding to the response element containing A•T at the variable site. The authors postulated that the entropic penalty for removal of the thymine methyl group was due to a cavity at the interface that is filled by an immobilized water molecule.

Both the enthalpic and entropic driving forces for complex formation are maximized when the three-dimensional surface of the protein is highly complementary to the DNA target. Not surprisingly, essentially all of the protein-DNA complexes that have been crystallographically characterized to date have a remarkably high level of shape complementarity (Figure 1.3). Some proteins bend their DNA targets and in doing so create a larger contact interface; consequently, the inherently greater flexibility of some DNA sequences provides an additional means of discriminating among otherwise related binding sites.

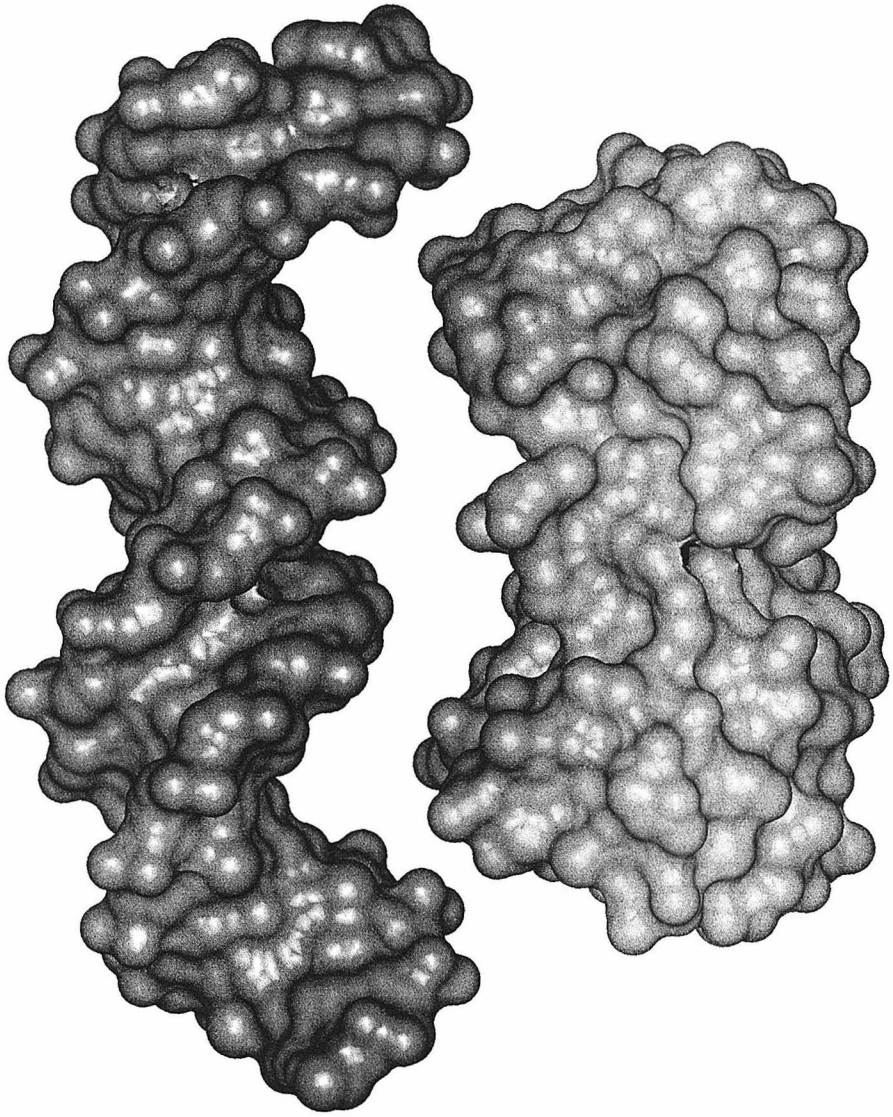

Figure 1.3. Shape complementarity in the *434* repressor dimer–operator complex.[25] The protein has been separated from the DNA slightly to illustrate the complementary nature of the binding surfaces.

Table 1.1. Base-specific contacts by amino acids in crystal structures of selected transcription factor-DNA complexes.[a,26]

	A	T	C	G
Arg		CAP		GR; Trp; Zif; CAP; Arc; Gli
Asn	en; GATA	Arc	Arc	λ
Asp			Gli	
Gln	λ; 434; Arc	434		434
Glu			CAP	
Gly		λ; Gr		
His				Zif
Ile		en		
Lys				GR; λ; MetJ; Gli
Ser	Gli			λ; Gli
Thr	MetJ			

[a]CAP, *E. Coli* CAP protein; en, *Drosophila* engrailed homeodomain; λ, λ-repressor; 434, *434* repressor; GR, glucocorticoid repressor; MetJ, *E. Coli* MetJ repressor; Trp, *E. Coli* Trp repressor; Zif, Zif268 zinc fingers; Arc, P_{22} Arc repressor; Gli, human *GLI* oncogene zinc fingers; GATA-1, erythroid-specific transcription factor GATA-1.

Paradoxically, increases in our knowledge of the structural details of protein-DNA interaction have raised additional questions about how the amino acid sequence of the protein determines the nucleotide sequence of the target. There is no universal code that correlates the amino acid sequence of a DNA recognition domain with the nucleotide sequences that are recognized. Multiple amino acid residues are capable of recognizing a given base and multiple bases may be recognized by a given amino acid (Table 1.1). However, there are some common themes. Arginine and glutamine possess long side chains and are capable of making bidentate hydrogen bonds to individual bases. Van der Waals contacts between the thymine methyl group and the hydrophobic amino acid side

chains of Ala, Val, Leu, Ile, Ser, Thr, and Gln and the backbone methylene of Gly are known. Although base-specific hydrogen bonds usually predominate, recent examples have demonstrated that high specificity may also be achieved with mostly hydrophobic contacts.[27]

1.2.2. Engineering proteins with altered sequence selectivity. Significant research effort has been devoted to correlating alterations in the amino acid sequence of sequence-specific DNA binding proteins with alterations in the nucleotide sequence of the target. The "helix-swap" experiment of Wharton and Ptashne first demonstrated that the sequence selectivity of a DNA binding protein could be altered by mutation of amino acids in the recognition element.[28] Mutation of four amino acids in the DNA binding domain of the *434* repressor to residues found in the DNA binding domain of the structurally similar P_{22} repressor[29] conferred P_{22} repressor site selectivity on the *434* repressor.

More recently, zinc finger proteins have been the subject of similar studies. Zinc fingers contain a repeating motif of 30 amino acids containing two strictly conserved cysteine residues in the N-terminal region and two strictly conserved histidine residues in the C-terminal region.[30] The N-terminal region forms a β-sheet while the C-terminal region forms an α-helix folded around a zinc ion coordinated by the two cysteines and the two histidines.[31] Unlike other DNA binding proteins, which contain separate dimerization and recognition domains, zinc fingers proteins contain multiple, covalently linked zinc fingers and recognize DNA in a modular way.[32] Although there are at least ten structurally distinct families of zinc finger proteins, within a given family base-specific contacts are made by amino acids at highly predictable positions.[33]

Several groups have sought to develop rules relating the amino acid sequences of zinc finger proteins with their DNA targets. By systematically varying the amino acid

sequence at two of the three contact positions of the central zinc finger of Sp1, Desjarlais and Berg achieved recognition of sequences of the type 5'-GGGGN(G or T)GGG-3'.[34] From the correlation between the amino acid sequence of zinc fingers and the nucleotide sequences of the targets, a designed three-zinc-finger protein that targeted a specific DNA site with nanomolar affinity was developed. Additionally, Klug and coworkers used phage display methods to select zinc fingers derived from Zif268 that bound to specific DNA triplets,[35] and engineered a three-zinc-finger protein that bound to a specific fusion oncogene.[36] In contrast, rational modifications of the amino acid sequence of the zinc finger Krox-20 led to altered nucleotide selectivity not only at the positions contacted but also at adjacent positions.[37] Similar results were observed in mutants of the Sp1[38] and Adr1[39] zinc finger proteins. These results suggest that no simple set of rules exists for the prediction of the target sequence of a given DNA binding domain or the prediction of an amino acid sequence that will bind to a given DNA target.

1.2.3. DNA recognition by peptides. An alternative approach to studying protein-DNA recognition is to study the DNA binding properties of peptides corresponding to recognition domains of transcription factors. Although peptides corresponding to the recognition elements of DNA binding proteins generally lack sufficient nonspecific DNA affinity to afford sequence selective binding as monomers, examples of sequence selective DNA recognition by both covalent[40] and noncovalent[41] dimers of such peptides have been reported. In contrast to mutagenesis experiments with intact proteins, this approach permits factors beyond the amino acid sequence of the peptide, such as the relative orientation of DNA binding domains and the sequence specificity of appended DNA-binding small molecules, to be varied. However, in the absence of the full protein, control over the secondary and tertiary structure of the peptide containing the recognition elements can be problematic.

Both Schepartz and Kim have explored DNA recognition by dimeric peptides derived from the yeast transcription factor GCN4. GCN4 is a member of the bZIP family of DNA binding proteins, which share a common fold but differ in their ability to differentiate operator sequences that differ in half-site spacing.[42] Cuenoud and Schepartz found that a dimer of a 29-mer peptide consisting of the DNA binding domain of GCN4 recognized the GCN4 response element (GCRE) with a dissociation constant of 1.3 x 10^{-7} M as measured by gel mobility shift assay. Using iron(II) *bis*-terpyridyl complexes as dimerization domains, the relative orientation and spacing of the two DNA binding domains was systematically altered. Increasing the spacing or changing the angle between the domains caused changes of up to 4 kcal•mol^{-1} in the stability of the GCRE•peptide dimer complexes.[39a] Talanian *et al.* studied the effects of truncating the amino acid sequence of the DNA binding domain. Remarkably, dimers of peptides as short as 20 residues were identified that bound with similar sequence selectivity as the intact protein.[39b,c]

In an alternate approach for attaining the requisite nonspecific affinity for DNA, the Barton group has explored DNA recognition by oligopeptides tethered to phenanthrenequinone diimine (phi) complexes of rhodium(III).[43] The parent rhodium complexes bind with high nonspecific affinity by intercalation from the major groove (K_d < 10^{-6} M) and cleave DNA by abstraction of the ribose 3'-hydrogen upon photoactivation.[44] Tethering oligopeptides derived from the recognition domains of the zinc finger proteins Sp1 and Adr1 and the *434* repressor, a helix-turn-helix protein, conferred the part of the sequence selectivity of the parent proteins on the relatively sequence neutral metallointercalator. In contradistinction, tethering oligopeptides derived from the recognition domain of the P_{22} repressor resulted in recognition of the nonnatural site 5'-CCA-3'.

Part B of this thesis describes further investigations of DNA recognition by metallointercalator-peptide conjugates. These investigations were undertaken to explore the

diversity of sequence selectivity that could be achieved by single amino acid modification of the 5'-CCA-3' sequence selective metallointercalator-peptide conjugate $[Rh(phi)_2(phen')]^{3+}$-AANVAIAAWERAA-$CONH_2$, and to refine the model for sequence selective DNA recognition by the parent metallointercalator-peptide conjugate. The thermodynamic and structural basis of metallointercalator-peptide conjugate sequence selectivity is explored in Chapter 4. Modifications of the amino acid sequence of the peptide are described in Chapter 5. Systemic variation in the position of a critical glutamate residue led to the identification of new sequence-selective metallointercalator-peptide conjugate and the prediction of an additional residue of $[Rh(phi)_2(phen')]^{3+}$-AANVAIAAWERAA-$CONH_2$ that makes base-specific contacts. Confirmation of that prediction was obtained by making further sequence changes at that position; these changes led to additional sequence selectivity.

1.3. References and Notes

1. (a) Champoux, J. J. *DNA Topology and its Biological Effects*, Cold Spring Harbor Press, Cold Spring Harbor, NY: 1990, p 217. (b) Hsieh, T.-S. *DNA Topology and its Biological Effects*, Cold Spring Harbor Press, Cold Spring Harbor, NY: 1990, p. 243.
2. (a) Gellert, M. *Annu. Rev. Biochem.* **1981**, *50*, 879. (b) Liu, L. *CRC Crit. Rev. Biochem.* **1983**, *5*, 1.
3. (a) Brown, P. O.; Cozzarelli, N. R. *Science* **1979**, *206*, 1081. (b) Liu, L. F.; Liu, C.-C.; Alberts, B. M. *Cell* **1980**, *19*, 697. (c) Brown, P. O.; Cozzarelli, N. R. *Proc. Natl. Acad. Sci. U.S.A.* **1981**, *78*, 843.
4. (a) Ross, W. E. *Biochem. Pharmacol.* **1985**, *34*, 4191. (b) Zwelling, L. A. *Cancer Meras. Rev.* **1985**, *4*, 263. (c) D'Arpa, P.; Liu, L. F. *Biochim. Biophys. Acta*

1989, *989*, 163. (d) Liu, L. F. *Annu. Rev. Biochem.* **1989**, *58*, 351. (e) Schneider, E.; Hsiang, Y.-H.; Liu, F. *Adv. Pharmacol.* **1990**, *21*, 149.

5. (a) Hsiang, Y.-H.; Hertzberg, R.; Hecht, S. M.; Liu, L. F. *J. Biol. Chem.* **1985**, *260*, 14873. (b) Thomsen, B.; Mollerup, S.; Bonven, B. J.; Frank, R.; Blocker, H.; Nielson, O. F.; Westergaard, O. *EMBO J.* **1987**, *6*, 1817. (c) Hertzberg, R. P.; Caranfa, M. J.; Hecht, S. M. *Biochemistry* **1989**, *28*, 4629.
6. Berry, D. E.; MacKenzie, L.; Shultis, E. A.; Chan, J. A.; Hecht, S. M. *J. Org. Chem.* **1992**, *57*, 420.
7. For isolation and structure determination of chebulagic acid and related ellagitannins see: (a) Schmidt, O. T. *Fortschr. Chem. Org. Naturstoffe* **1956**, *13*, 70. (b) Haslam, E.; Uddin, M. *J. Chem. Soc. (C)* **1967**, 2381. (c) Jochims, J. C.; Taigel, G.; Schmidt, O. T. *Liebigs. Ann. Chem.* **1968**, *169*, 717. (d) Yoshida, T.; Okuda, T.; Koga, T.; Toh, N. *Chem. Pharm. Bull.* **1982**, *30*, 2655. (e) Yoshida, T.; Fujii, R.; Okuda, T. *Chem. Pharm. Bull.* **1980**, *28*, 3713.
8. For reviews of the synthetic applications of cyclobutanes, see: (a) Trost, B. M. *Top. Curr. Chem.* **1986**, *133*, 3. (b) Wong, H. N. C.; Lau, K.-L.; Tam, K.-F. *Top. Curr. Chem.* **1986**, *133*, 83. (c) Winterfeldt, E. *Kontakte (Darmstadt)* **1986**, *52*. For a review of the synthetic applications of cyclobutanones and cyclobutenones, see: (d) Bellus, D.; Ernst, B. *Angew. Chem. Int. Ed. Engl.* **1988**, *27*, 797.
9. This chemistry has been the subject of ongoing studies in the Carreira laboratory; see: (a) Shepard, M. S.; Carreira, E. M. *Tetrahedron* **1997**, *53*, 16253. (b) Dritz, J. H.; Carreira, E. M. *Tetrahedron Lett.* **1997**, *38*, 5579. (c) Shepard, M. S.; Carreira, E. M. *J. Am. Chem. Soc.* **1997**, *119*, 2597.
10. For additional examples of axial chirality transfer using a 1,3-disubstituted allene, see: (a) Urabe, H.; Takeda, T.; Hideura, D.; Sato, F. *J. Am. Chem. Soc.* **1997**, *119*, 11295. (b) Uang, B. J.; Po, S. Y.; Hung, S. C.; Liu, H. H.; Hsu, C. Y.; Lin, Y. S.;

Chang, J. W. *Pure Appl. Chem.* **1997**, *69*, 615. (c) Ikeda, I.; Honda, K.; Osawa, E.; Shiro, M.; Aso, M.; Kanematsu, K. *J. Org. Chem.* **1996**, *61*, 2031.

11. More recently, Shepard and Carreira have employed this chemistry to synthesize a protected form of the target: Carreira, E. M., personal communication.
12. For recent reviews, see: (a) Williams, D. H.; Westwell, M. S. *Chem. Soc. Rev.* **1998**, *27*, 57. (b) Nevinskii, G. A. *Mol. Biol.* **1995**, *29*, 6.
13. Throughout this thesis, the term "specificity" will be used to refer to the capacity of a ligand to discriminate among related substrates (for example, target and nontarget nucleotide sequences). Quantitatively, specificity is defined as the ratio of the association constant of the ligand for its target substrate to the association constant of the ligand for similar, nontarget substrates.
14. (a) Anderson, W. F.; Ohlendorf, D. H.; Takeda, Y.; Matthews, B. W. *Nature* **1981**, *290*, 754. (b) Ohlendorf, D. H.; Anderson, W. F.; Fisher, R. G.; Takeda, Y.; Matthews, B. W. *Nature* **1982**, *298*, 718. (c) McKay, D. B.; Steitz, T. A. *Nature* **1981**, *290*, 744. (d) Pabo, C. O.; Lewis, M. *Nature* **1982**, *298*, 443.
15. (a) Brennan, R. G.; Matthews, B. W. *J. Biol. Chem.* **1989**, *264*, 1903. (b) Harrison, S. C.; Aggarwal, A. K. *Ann. Rev. Biochem.* **1990**, *59*, 933.
16. (a) Jones, N. *Cell* **1990**, *61*, 9. (b) Davis, R. L.; Cheng, P.-F.; Lassar, A. B.; Weintraub, H. *Cell* **1990**, *60*, 733. (c) Anthony-Cahill, S. J.; Benfield, P. A.; Fairman, R.; Wasserman, Z. R.; Brenner, S. L.; Stafford, W. F., III; Altenbach, C.; Hubbell, W. L.; DeGrado, W. F. *Science* **1992**, *255*, 979.
17. (a) Gehring, W. J.; Muller, M.; Affolter, M.; Percival-Smith, A.; Billeter, M.; Qian, Y. Q.; Otting, G.; Wüthrich, K. *Trends Genet.* **1990**, *6*, 323. (b) Gehring, W. J.; Qian, Y. Q.; Billeter, M.; Furukubo-Tokunaga, K.; Schier, A. F.; Resendez-Perez, D.; Affolter, M.; Otting, G.; Wüthrich, K. *Cell* **1994**, *78*, 211. (c) Pomerantz, J. L.; Pabo, C. O.; Sharp, P. A. *Proc. Natl. Acad. Sci. U.S.A.* **1995**, *92*, 9752.

18. Kerppola, T. K. *Curr. Opin. Struct. Biol.* **1991**, *1*, 71.

19. (a) Berg, J. M. *Science* **1986**, *232*, 485. (b) Berg, J. M. *Ann. Rev. Biophys. Biophys. Chem.* **1990**, *19*, 405. (c) Vallee, B.L.; Coleman, J.E.; Auld, D.S. *Proc. Natl. Acad. Sci. U.S.A.* **1991**, *88*, 999. (d) Schwabe, J. W. R.; Klug, A. *Nature Struct. Biol.* **1994**, *1*, 345.

20. (a) Raumann, B. E.; Brown, B. M.; Sauer, R. T. *Curr. Opin. Struct. Biol.* **18994**, *4*, 36. (b) Phillips, S. E. V. *Ann. Rev. Biophys. Biomol. Struct.* **1994**, *23*, 671.

21. Blackwell, T. K.; Bowerman, B.; Priess, J. R.; Weintraub, H. *Science* **1994**, *266*, 621.

22. For a leading reference to a well-studied example, see: Wyman, C.; Rombel, I.; North, A. K.; Bustamante, C.; Kustu, S. *Science* **1997**, *275*, 1658.

23. For an example see: Wolberger, C.; Vershon, A. K.; Lui, B.; Johnson, A. D.; Pabo, C. O. *Cell* **1991**, *67*, 517.

24. Lündback, T.; Härd, T. *Proc. Natl. Acad. Sci. U.S.A.* **1996**, *93*, 4754.

25. (a) Aggarwal, A. K.; Rodgers, D. W.; Drottar, M.; Ptashne, M.; Harrison, S. C. *Science* **1988**, *242*, 899. (b) Shimon, L. J.; Harrison, S. C. *J. Mol. Biol.* **1993**, *232*, 826. (c) Rodgers, D. W.; Harrison, S. C. *Structure* **1993**, *1*, 227.

26. Adapted from Pabo, C. O.; Sauer, R. T. *Ann. Rev. Biochem.* **1992**, *61*, 1053 and Sardesai, N. Y. *Ph.D. Thesis*, California Institute of Technology, 1995.

27. (a) Omichinski, J. G.; Clore, G. M.; Schaad, O.; Felsenfeld, G.; Trainor, C.; Appella, E.; Stahl, S. J.; Gonenborn, A. M. *Science* **1993**, *261*, 438. (b) Puglisi, J. D.; Chen, L.; Frankel, A. D.; Williamson, J. R. *Proc. Natl. Acad. Sci. U.S.A.* **1993**, *90*, 3680. (c) Rould, M. A.; Perona, J. J.; Söll, D.; Steitz, T. A. *Science* **1989**, *246*, 1135.

28. Wharton, R. P.; Ptashne, M. *Nature* **1985**, *316*, 601.

29. (a) Sauer, R. T.; Pan, J.; Hopper, P.; Hehir, K.; Brown, J.; Poteete, A. R. *Biochemistry* **1981**, *20*, 3591. (b) Sauer, R. T.; Yocum, R. R.; Doolittle, R. F.; Lewis, M.; Pabo, C. O. *Nature* **1982**, *298*, 447. (c) Ptashne, M. *A Genetic Switch*, Cell Press and Blackwell Scientific Publications, Cambridge: 1986. (d) Sevilla-Sierra, P.; Otting, G.; Wüthrich, K. *J. Mol. Biol.* **1994**, *235*, 1003. (e) Harrison, S. C.; Anderson, J. E.; Koudelka, G. B.; Mondragón, A.; Subbiah, S.; Wharton, R. P.; Wolberger, C.; Ptashne, M. *Biophys. Chem.* **1988**, *29*, 31.

30. (a) Miller, J.; McLachlan, A. D.; Klug, A. *EMBO J.* **1985**, *4*, 1609. (b) Brown, R. S.; Sander, C.; Argos, P. *FEBS* **1985**, *186*, 271.

31. For the first solution structures of isolated zinc fingers, see: (a) Párraga, G.; Horvath, S. J.; Eisen, A.; Taylor, W. E.; Hood, L.; Young, E. T.; Klevit, R. E. *Science* **1988**, *241*, 1489. (b) Lee, M. S.; Gippert, G. P.; Soman, K. V.; Case, D. A.; Wright, P. E. *Science* **1989**, *245*, 635.

32. For the first cocrystal structure of a zinc finger protein with DNA, see: (a) Pavletich, N. P.; Pabo, C. O. *Science* **1991**, *252*, 809. (b) Pavletich, N. P.; Pabo, C. O. *Science* **1993**, *261*, 1701.

33. (a) Berg, J. M. *Acc. Chem. Res.* **1995**, *28*, 14. (b) Schmiedeskamp, M.; Klevit, R. E. *Curr. Opin. Struct. Biol.* **1994**, *4*, 28.

34. Desjarlais, J. R.; Berg, J. M. *Proc. Natl. Acad. Sci. U.S.A.* **1992**, *89*, 7345.

35. Choo, Y.; Klug, A. *Proc. Natl. Acad. Sci. U.S.A.* **1994**, *91*, 11168.

36. Choo, Y.; Sánchez-García, I.; Klug, A. *Nature* **1994**, *372*, 642.

37. Nardelli, J.; Gibson, T.; Charnay, P. *Nucl. Acids Res.* **1992**, *20*, 4137.

38. Desjarlais, J. R.; Berg, J. M. *Proteins* **1992**, *12*, 101.

39. Thukral, S. K.; Morrison, M. L.; Young, E. T. *Mol. Cell Biol.* **1992**, *12*, 2784.

40. (a) Cuenod, B.; Schepartz, A. *Science* **1993**, *259*, 510. (b) Talanian, R. V.; McKnight, C. J.; Kim, P. S. *Science* **1990**, *249*, 769. (c) Talanian, R. V.;

McKnight, C. J.; Rutkowski, R.; Kim, P. S. *Biochemistry* **1992**, *31*, 6871. (d) Morii, T.; Simomura, M.; Morimoto, S.; Saito, I. *J. Am. Chem. Soc.* **1993**, *115*, 1150. (e) Dervan, P. B. *Methods Enzymol.* **1991**, *208*, 497.

41. (a) O'Neil, K. T.; Hoess, R. H.; DeGrado, W. F. *Science* **1990**, *249*, 774. (b) Ueno, M.; Murakami, A.; Makino, K.; Morii, T. *J. Am. Chem. Soc.* **1993**, *115*, 12575.
42. Vinson, C. R.; Sigler, P. B.; McKnight, S. L. *Science* **1989**, *246*, 911.
43. (a) Lin, S. C. *Ph.D. Thesis*, California Institute of Technology, 1996. (b) Sardesai, N. Y.; Zimmerman, K.; Barton, J. K. *J. Am. Chem. Soc.* **1994**, *116*, 7502. (c) Sardesai, N. Y., Barton, J. K. *J. Biol. Inorg. Chem.* **1997**, *2*, 762.
44. Sitlani, A.; Long, E. C.; Pyle, A. M.; Barton, J. K. *J. Am. Chem. Soc.* **1992**, *114*, 2303.

Chapter 2: Studies Directed Toward the Total Synthesis of Chebulagic Acid I: The Asymmetric Intramolecular [2+2]-Photocycloaddition of Allenes with Enones and Enoates[1]

2.1. Introduction

2.1.1. Introduction. The intramolecular photocycloaddition of olefins with cyclic enones and enoates is a powerful reaction that renders complex, fused polycyclic frameworks readily accessible.[2] The conformational, steric, and stereoelectronic constraints that accompany ring formation allow control over the relative stereochemistry about the newly formed rings. Chiral centers adjacent to the reacting enones and enoates[3] and in the tether[4] have been used to control enone and olefin diastereofacial selectivity in these reactions. However, the diastereoselectivity of these photocycloadditions is highly substrate dependent and the diastereocontrolling center required in the photosubstrate may not be present in the synthetic target. In principle, the intramolecular [2+2]-photocycloaddition of optically active 1,3-disubstituted allenes with enones and enoates would provide a general method for the enantioselective synthesis of these systems. The *exo*-alkylidenecyclobutane adducts and the cyclobutanones[5] derived by oxidative cleavage of the exocyclic olefin of the photoproducts (Scheme 2.1) provide access to a wide variety of structures that are not otherwise readily accessible by synthesis. Together, asymmetric

Scheme 2.1. Synthetic equivalence of asymmetric [2+2]-photocycloaddition-exocyclic olefin oxidative cleavage and asymmetric ketene-enone cycloaddition.

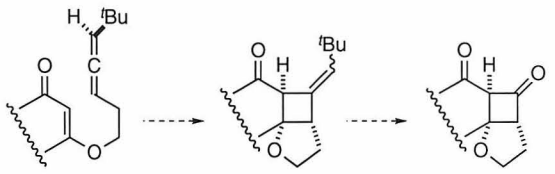

[2+2]-photocycloaddition and oxidative cleavage of the exocyclic olefin of the photoproduct represent the synthetic equivalent of an asymmetric ketene-enone cycloaddition.

2.1.2. Mechanistic aspects of photocycloadditions. The photocycloaddition of olefins and enones is generally accepted to proceed *via* an enone triplet that results from rapid intersystem crossing of the excited state singlet formed upon irradiation. Olefin trapping by Cβ(•) leads to biradical intermediate **1** (Scheme 2.2). Rotation of the C2'-C3' bond within the lifetime of **1** leads to a loss of olefin geometry. Intermediate **1** then partitions between collapse to cyclobutane products and collapse to starting material.[6] In principle, this mechanism provides a pathway for racemization of the allene substrate in an asymmetric [2+2]-photocycloaddition through successive addition, rotation, and reversion steps, leading to products of diminished enantiopurity.

Corey has demonstrated that when cyclohexenone is irradiated in the presence of either *cis*- or *trans*-2-butene, the same 1:1 mixture of diastereomeric cyclobutanes **2** and **3** is formed (Scheme 2.2).[7] Interruption of either reaction at partial completion indicated that less than 1% of the unreacted 2-butene had undergone *cis-trans* isomerization. Becker has demonstrated that initial bond formation in intramolecular alkene-enone photocycloadditions also occurs at Cβ(•).[8] Together, these results suggest that systems may be designed where reversion of biradical intermediates similar to **1** to starting material does not compete with collapse to products, and that allene and enone diastereofacial

Scheme 2.2. Mechanism of enone-olefin photocycloadditions.

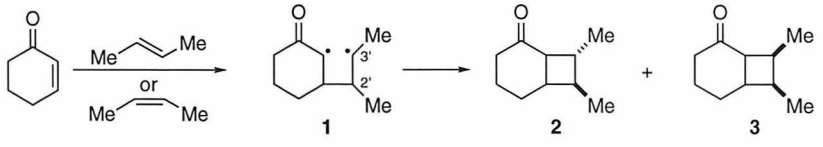

selectivity obtained in the initial C-C bond forming step may be preserved in the photoadducts.

2.1.3. Previous investigations of asymmetric photocycloadditions.

The enantioselective intramolecular photocycloaddition of 1,3-disubstituted allenes with enones and enoates has not been extensively investigated. In an isolated report Becker has documented the examples shown in Equations 2.1 and 2.2.[9] Irradiation of partially optically enriched **4** afforded olefin diastereomers **5** and **6**. Camphor-derived allene **7**, which was obtained as a mixture of allene diastereomers, afforded isomers **8** and **9** upon irradiation. Neither the levels of enantiomeric purity nor the relative nor absolute configuration of the photoproducts were determined. In addition, the optical purity of **4** was not known. Therefore, no conclusions regarding the feasibility of an enantioselective allene-enone [2+2]-photocycloaddition could be reached. Prior to this investigation, such a transformation had not been demonstrated.[10]

This chapter describes investigations aimed at demonstrating the feasibility and determining the scope and limitations of asymmetric intramolecular [2+2]-photocycloadditions of allenes with enones and enoates. The observation of asymmetric

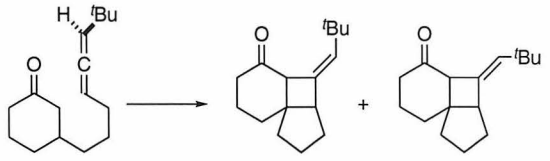

4 **5** **6** **(2.1)**

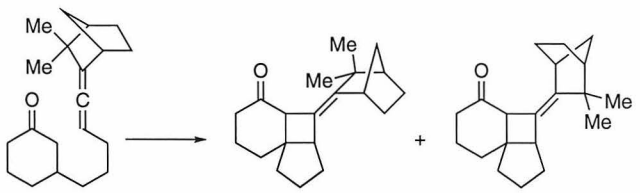

7 **8** **9** **(2.2)**

induction in intramolecular photocycloadditions of optically active 1,3-disubstituted allenes with enones and enoates is documented. The substrates examined in this study include allenes appended 1,3-cyclopentanedione, 1,3-cyclohexanedione, and 4-hydroxycoumarin. While photocycloaddition of the 1,3-cyclopentanedione and 1,3-cyclohexanedione derived substrates afforded mixtures of olefin diastereomers, photocycloaddition of the 4-hydroxycoumarin derived substrates afforded only one of the two possible olefin diastereomers. High levels of asymmetric induction (83-100%) were observed in all cases, establishing the viability of the asymmetric intramolecular [2+2]-photocycloaddition as a key transformation in synthetic schemes directed at the preparation of ellagitannin natural products in enantiomerically pure form. Finally, this chapter describes the establishment of the relative stereochemistry of the photoproducts through a combination of ^{1}H NMR NOE and x-ray crystallographic studies and the establishment of the absolute stereochemistry of the photoproducts through a photocycloaddition of an allene-enoate substrate containing an internal stereochemical label.

2.2. Experimental.

General procedures: All reagents were commercially obtained except where noted. When appropriate, reagents were purified prior to use. All non-aqueous reactions were performed using oven dried glassware under an atmosphere of dry nitrogen. Photoreactions were performed in Pyrex flasks (λ_{cutoff} = 293 nm) using a Hanovia 450 W Hg medium pressure UV lamp in a water cooled quartz immersion apparatus as the light source. Diethyl ether and tetrahydrofuran were distilled from sodium benzophenone ketyl prior to use. *N,N*-diisopropylethylamine, triethylamine, dichloromethane, and pyridine were distilled from calcium hydride prior to use. *N,N*-dimethylformamide was stood over 4 Å molecular sieves prior to use. Methanol was distilled from magnesium methoxide prior to use. Spectroscopy grade cyclohexane was used in photoreactions. Chromatographic

purification of products was accomplished using forced flow chromatography on Baker 7024-R silica gel according to the method of Still.[11] NMR spectra were recorded on a Bruker AM-500 operating at 500 and 126 MHz for ^{1}H and ^{13}C, respectively, a JEOL GSX-400 operating at 400 and 100 MHz for ^{1}H and ^{13}C, respectively, or a General Electric QE Plus operating at 300 and 75 MHz for ^{1}H and ^{13}C, respectively, and are referenced to internal solvent signals. Data for ^{1}H are reported as follows: chemical shift (δ ppm), integration, multiplicity (s = singlet, d = doublet, t = triplet, q = quartet, qn = quintet, m = multiplet), coupling constant (Hz), and assignment. ^{1}H NMR NOE difference spectra were recorded on degassed samples and were quantitated by integrating the difference spectra. The phase sensitive NOESY spectrum was recorded at 300 MHz on a degassed sample using the TPPI technique with a mixing time of 0.5 sec, a recycle delay of 2.0 sec, F2 and F1 spectral widths of 2717 Hz, and an initial matrix size of 256 x 1024 points which was transformed into a 512 x 512 matrix after symmetrization. IR spectra were recorded on a Perkin-Elmer 1600 Series spectrometer. Optical rotations were determined on a JASCO DIP-181 polarimeter operating at the sodium D line and are reported as follows: $[\alpha]_D^{23}$, concentration (g/100 mL), and solvent. High resolution mass spectrometry was performed by the Midwest Center for Mass Spectrometry at the University of Nebraska.

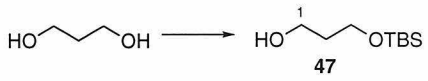

47

47: Triethylamine (7.37 mL, 53.1 mmol, 2.0 equiv), TBSCl (4.00 g, 26.6 mmol, 1.0 equiv), and 4-DMAP (324 mg, 2.65 mmol, 0.1 equiv) were added successively to a solution of 10.10 g (132.7 mmol, 5.0 equiv) 1,3-propandiol in 100 mL 1:1 DMF–CH_2Cl_2. The reaction mixture was stirred for 2 h at 23 °C, poured into 150 mL 1.0 M aqueous KH_2PO_4, and extracted with 300 mL Et_2O. The organic layer was washed with 2 x 50 mL saturated aqueous NaCl, dried over anhydrous $MgSO_4$, and concentrated *in vacuo*. The residue was purified by chromatography on silica gel (40 x 150 mm, 4:1 hexanes–EtOAc,

R_f 0.27) to afford 4.91 g (97%) of **47** as a clear, colorless oil. ^{1}H NMR (500 MHz, $CDCl_3$) δ 3.83 (2H, t, J = 5.6 Hz, C3H_2), 3.80 (2H, q, J = 5.5 Hz, C1H_2), 2.54 (1H, t, J = 5.3 Hz, OH), 1.78 (2H, qn, J = 5.6 Hz, C2H_2), 0.90 (9H, s, SiC(CH_3)$_3$), 0.07 (6H, s, Si(CH_3)$_2$) ppm; ^{13}C NMR (126 MHz, $CDCl_3$) δ 62.8, 62.4, 34.3, 25.9, 18.2, -5.5 ppm; IR (thin film) ν 3359, 2953, 2858, 1743, 1469, 1388, 1361, 1254, 1092, 1008, 963, 836, 777, 736, 662 cm^{-1}.

15

15: Celite (13.0 g), powdered 4 Å molecular sieves (13.0 g), and PDC (26.1 g, 69.5 mmol, 3.0 equiv) were added successively to a solution of 4.21 g (23.1 mmol, 1.0 equiv) of **47** in 100 mL CH_2Cl_2. The resulting slurry was stirred for 1 h at 23 °C and filtered through a pad (2 x 5 cm) of silica gel. The pad was washed with 3 x 100 mL Et_2O. The filtrate was concentrated *in vacuo* and the residue was purified by chromatography on silica gel (40 x 150 mm, 1.5:1 hexanes–CH_2Cl_2, R_f 0.22) to afford 2.90 g (66%) of **15** as a clear, colorless oil. ^{1}H NMR (500 MHz, $CDCl_3$) δ 9.80 (1H, t, J = 2.1 Hz, C1H), 3.99 (2H, t, J = 6.0 Hz, C3H_2), 2.60 (2H, dt, J = 6.0, 2.1 Hz, C2H_2), 0.88 (9H, s, SiC(CH_3)$_3$), 0.07 (6H, s, Si(CH_3)$_2$) ppm; ^{13}C NMR (126 MHz, $CDCl_3$) δ 201.9, 57.4, 46.5, 25.8, 18.2, -5.5 ppm; IR (thin film) ν 2929, 2858, 2725, 1727, 1654, 1466, 1388, 1255, 1102, 969, 836, 777 cm^{-1}.

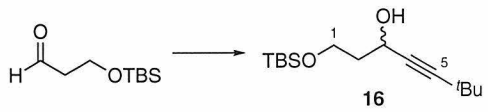

16

(±)-16: A 1.7 M solution of ^{t}BuLi in *n*-pentane (10.2 mL, 17.3 mmol, 1.3 equiv) was added dropwise to a solution of 2.45 mL (19.9 mmol, 1.5 equiv) *tert*-butylacetylene in 100 mL Et_2O at -78 °C. The resulting solution was stirred for 2 h, and a solution of **15** in 10 mL Et_2O was added dropwise. The reaction mixture was stirred at -78 °C for 1 h and allowed to warm to 23 °C thereafter. When warming was complete the reaction mixture

was poured into 100 mL 1.0 M aqueous KH_2PO_4. The aqueous layer was extracted with an additional 100 mL Et_2O, and the combined organic layers were washed with saturated aqueous NaCl, dried over anhydrous Na_2SO_4, and concentrated *in vacuo*. The residue was purified by chromatography on silica gel (30 x 150 mm, 10:1 hexanes–EtOAc, R_f 0.29) to afford 2.59 g (72%) of **(±)-16** as a clear, colorless oil. ^{1}H NMR (500 MHz, $CDCl_3$) δ 4.59 (1H, td, *J* = 6.2, 4.3 Hz, C3*H*), 4.02 (1H, ddd, *J* = 10.7, 7.7, 4.1 Hz, one of C1H_2), 3.81 (1H, ddd, *J* = 10.9, 7.5, 5.8 Hz, one of C1H_2), 3.19 (1H, d, *J* = 6.0 Hz, O*H*), 1.98-1.92 (1H, m, one of C2H_2), 1.86-1.80 (1H, m, one of C2H_2), 1.22 (9H, s, C6(CH_3)$_3$), 0.91 (9H, s, SiC(CH_3)$_3$), 0.09 (3H, s, one of Si(CH_3)$_2$), 0.08 (3H, s, one of Si(CH_3)$_2$) ppm; ^{13}C NMR (126 MHz, $CDCl_3$) δ 93.7, 79.1, 62.0, 61.2, 39.2, 31.0, 27.3, 25.9, 18.2, -5.52, -5.54 ppm; IR (thin film) ν 3407, 2956, 2930, 2859, 2235, 1470, 1390, 1326, 1257, 1204, 1097, 1021, 943, 834, 777, 733, 664 cm^{-1}.

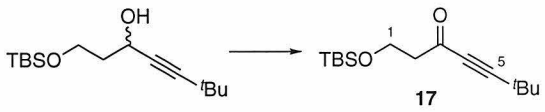

17

17: Dess-Martin periodinane (12.7 g, 29.9 mmol, 1.5 equiv), prepared according the literature procedure,[12] was added to a solution of 5.30 g (19.6 mmol, 1.0 equiv) of **(±)-16** in 100 mL CH_2Cl_2. The reaction mixture was stirred for 15 min at 23 °C and 300 mL Et_2O was added. The precipitates were removed by filtration through Celite and the filtrate was concentrated *in vacuo*. The residue was purified by chromatography on silica gel (30 x 100 mm, 10:1 hexanes–EtOAc, R_f 0.32) to afford 4.75 g (90%) of **64** as a clear, colorless oil. ^{1}H NMR (500 MHz, $CDCl_3$) δ 3.96 (2H, t, *J* = 6.4 Hz, C1H_2), 2.73 (2H, t, *J* = 6.4 Hz, C2H_2), 1.28 (9H, s, C6(CH_3)$_3$), 0.88 (9H, s, SiC(CH_3)$_3$), 0.06 (6H, s, Si(CH_3)$_2$) ppm; ^{13}C NMR (126 MHz, $CDCl_3$) δ 186.7, 101.8, 79.4, 58.7, 48.6, 30.1, 27.7, 25.8, 18.2, -5.4 ppm; IR (thin film) ν 2956, 2930, 2900, 2858, 2211, 1679, 1472, 1463, 1389, 1363, 1317, 1271, 1257, 1226, 1203, 1132, 1101, 1047, 1006, 984, 934, 897, 836, 811, 777,

726, 681, 660 cm^{-1}. HRMS (EI) calculated for $C_{15}H_{28}O_2Si$ 268.1858, calculated for $C_{14}H_{25}O_2Si$ (M^+ - CH_3) 253.1624, found 253.1620.

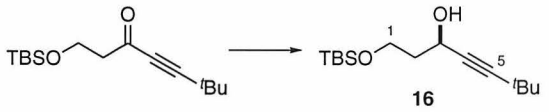

16

16: Neat (+)-β-isopinocampheyl-9-borabicyclo[3.3.1]nonane (1.68 g, 6.49 mmol, 2.0 equiv) was added to 0.871 g (3.24 mmol, 1.0 equiv) neat **17**, and the resulting yellow solution was stirred at 23 °C for 7 h. Et_2O (100 mL) and 6 M aqueous NaOH (100 mL) were added successively. The layers were separated and the aqueous layer was extracted with 2 x 50 mL Et_2O. The combined organic layers were washed with 50 mL 1.0 M aqueous KH_2PO_4 and 50 mL saturated aqueous NaCl, dried over anhydrous Na_2SO_4 and concentrated *in vacuo*. The residue was purified by chromatography on silica gel (30 x 150 mm, 10:1 hexanes–EtOAc, R_f 0.29) to afford 0.816 g (93%) of **16** as a clear, slightly yellow oil, spectroscopically and chromatographically identical to **(±)-16** except for optical rotation, $[\alpha]_D^{23}$ +17.6° (*c* = 1.87, CH_2Cl_2). A small portion was treated with 4-DMAP (5.0 equiv) and (*R*)-MTPACl (2.0 equiv) in CH_2Cl_2. Integration of the ^1H NMR (500 MHz, $CDCl_3$) resonances of the derived (*S*)-MTPA ester at δ 1.22 (major, C6(CH_3)$_3$) and δ 1.18 (minor, C6(CH_3)$_3$) ppm indicated a diastereomer ratio of 18.8:1.00 (90% ee).

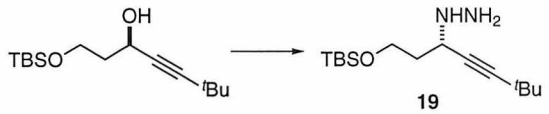

19

20: MsCl (258 μL, 3.33 mmol, 1.2 equiv) was added dropwise to a solution of 750 mg (2.77 mmol, 1.0 equiv) of **16** and 577 μL (4.16 mmol, 1.5 equiv) TEA in 20 mL CH_2Cl_2 at 0 °C at a rate such that the internal temperature was maintained below 5 °C. After stirring for 0.5 h the reaction mixture was transferred *via* cannula into 13 mL 1:1 MeOH–H_2NNH_2. The resulting solution was stirred at 23 °C for 36 h and poured into 120 mL water. The aqueous layer was extracted with 2 x 100 mL 95:5 CH_2Cl_2–MeOH. The organic layers

were combined, washed with 50 mL saturated aqueous NaCl, dried over anhydrous $MgSO_4$, and concentrated *in vacuo*. The residue was used without further purification.

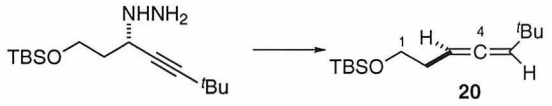

20

The residue was dissolved in 66 mL 1:1 Et_2O–CH_2Cl_2 and cooled to 0 °C. PTAD (986 mg, 5.63 mmol, 2.0 equiv) was added in one portion. When gas evolution was complete 65 mL *n*-pentane was added and the reaction mixture was filtered through a pad (2 x 5 cm) of silica gel. The pad was washed with 100 mL 4:1 *n*-pentane–CH_2Cl_2 and the filtrate was concentrated *in vacuo*. The residue was purified by chromatography on silica gel (20 x 80 mm, *n*-pentane, R_f 0.33) to afford 503 mg (71%) of **20** as a clear, colorless oil. ^{1}H NMR (500 MHz, $CDCl_3$) δ 5.14 (1H, q, J = 6.6 Hz, C3*H*), 5.11-5.05 (1H, m, C5*H*), 3.67 (2H, t, J = 7.0 Hz, C1H_2), 2.21 (2H, dq, J = 7.0, 3.9 Hz, C2H_2), 1.02 (9H, s, C6(CH_3)$_3$), 0.90 (9H, s, SiC(CH_3)$_3$), 0.06 (s, 6H, Si(CH_3)$_2$) ppm; ^{13}C NMR (126 MHz, $CDCl_3$) δ 201.7, 102.9, 89.1, 63.1, 32.9, 31.6, 30.2, 26.0, 18.4, -5.3 ppm; IR (thin film) ν 2960, 2901, 2859, 2738, 2710, 1962, 1472, 1462, 1408, 1387, 1361, 1327, 1254, 1206, 1191, 1103, 1006, 937, 873, 836, 811, 776, 736, 663 cm^{-1}; $[\alpha]_D^{23}$ +21.8° (*c* = 4.59, CH_2Cl_2). HRMS (EI) calculated for $C_{15}H_{28}OSi$ 254.2066, calculated for $C_{11}H_{19}OSi$ (M^+ - C4H_9) 197.1362, found 197.1360. Integration of the ^{1}H NMR (500 MHz, $CDCl_3$) resonances at δ 0.08 (major) and δ 0.06 (minor) ppm in the presence of 2.0 equiv Ag(fod) and 1.5 equiv (+)-Eu(hfc)$_3$ indicated a diastereomer ratio of greater than 20:1 (>90% ee).[13]

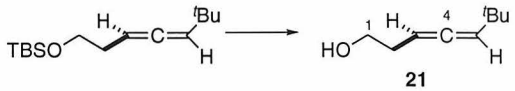

21

21: A 1.0 M solution of TBAF in THF (2.34 mL, 2.34 mmol, 1.2 equiv) was added to a solution of 495 mg (1.95 mmol, 1.0 equiv) of **20** in 8 mL THF. The resulting solution was stirred for 30 min at 23 °C and poured into 35 mL 1.0 M aqueous KH_2PO_4. The

aqueous layer was extracted with 50 mL Et_2O. The combined organic layers were washed with 20 mL 1.0 M aqueous KH_2PO_4, dried over anhydrous Na_2SO_4 and concentrated *in vacuo*. The residue was purified by chromatography on silica gel (20 x 80 mm, 2:1 *n*-pentane–Et_2O, R_f 0.48) to afford 221 mg (80%) of **21** as a clear, colorless oil. ^{1}H NMR (500 MHz, $CDCl_3$) δ 5.20-5.16 (2H, m, C3*H* and C5*H*), 3.72 (1H, dt, *J* = 7.9, 6.0, 1.7 Hz, C1H_2), 2.29-2.23 (2H, m, C2H_2), 1.53 (1H, t, *J* = 6.0 Hz, O*H*), 1.04 (9H, s, C6(CH_3)$_3$) ppm; ^{13}C NMR (126 MHz, $CDCl_3$) δ 201.9, 103.7, 89.0, 62.1, 32.5, 31.7, 30.1 ppm; IR (thin film) ν 3419, 2959, 2901, 2866, 1961, 1638, 1474, 1460, 1362, 1253, 1191, 1049, 874 cm^{-1}; $[\alpha]_D^{23}$ +74.1° (*c* = 1.43, CH_2Cl_2). HRMS (EI) calculated for C9H_{16}O 140.1201, found 140.1205.

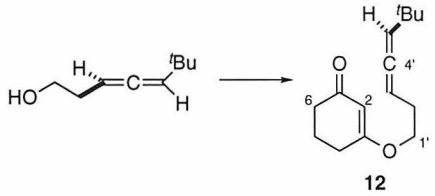

12

12: 1,3-Cyclohexanedione (106 mg, 0.942 mmol, 1.2 equiv) and DEAD (182 μL, 1.15 mmol, 1.5 equiv) were added to a solution of 108 mg (0.770 mmol, 1.0 equiv) of **21** and 246 mg (1.15 mmol, 1.5 equiv) Ph_3P in 8 mL THF, and the resulting orange solution was stirred for 15 min at 23 °C. The reaction mixture was concentrated *in vacuo* and the residue was purified by chromatography on silica gel (20 x 100 mm, 3:1 hexanes–EtOAc, R_f 0.25) to afford 101 mg (56%) of **12** as a clear, colorless oil. ^{1}H NMR (500 MHz, $CDCl_3$) δ 5.34 (1H, s, C2*H*), 5.18-5.14 (2H, m, C3'*H* and C5'*H*), 3.91-3.87 (2H, m, C1'H_2), 2.46-2.36 (4H, m, C4H_2 and C2'H_2), 2.33 (2H, t, *J* = 6.4 Hz, C6'H_2), 1.97 (2H, q, *J* = 6.4 Hz, C5H_2), 1.01 (9H, s, C6'(CH_3)$_3$) ppm; ^{13}C NMR (126 MHz, $CDCl_3$) δ 201.7, 199.7, 177.8, 104.2, 102.8, 88.2, 67.6, 36.8, 31.6, 30.1, 29.0, 28.2, 21.2 ppm; IR (thin film) ν 2956, 2900, 2867, 1961, 1653, 1604, 1460, 1428, 1395, 1365, 1327, 1219,

1181, 1135, 1058, 1009, 962, 928, 876, 826, 757 cm^{-1}; $[\alpha]_D^{23}$ +33.9° (*c* = 0.414, CH_2Cl_2). HRMS (EI) calculated for $C_{15}H_{22}O_2$ 234.1620, found 234.1630.

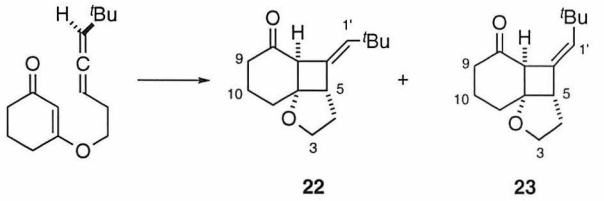

22 **23**

22, 23: A 200-mL Pyrex flask was charged with a solution of 130 mg of **12** of 89% ee in 120 mL cyclohexane. The solution was degassed by argon sparge for 10 min and irradiated at 23 °C for 4 h. The solvent was removed *in vacuo* and the residue was purified by chromatography on silica gel (20 x 100 mm, 4:1 hexanes–EtOAc, R_f 0.42 (**23**), 0.33 (**22**)) to afford 74 mg (57%) of **23** and 41 mg (32%) of **22** as clear, colorless oils. Data for **22**: ^{1}H NMR (500 MHz, C_6D_6) δ 5.52 (1H, t, *J* = 2.4 Hz, C1'*H*), 3.83 (1H, ddd, *J* = 9.3, 7.8, 1.7 Hz, one of C3H_2), 3.65 (1H, ddd, *J* = 10.4, 9.3, 5.6 Hz, one of C3H_2), 3.50 (1H, t, *J* = 2.8 Hz, C7*H*), 3.02 (1H, dt, *J* = 7.2, 2.6 Hz, C5*H*), 2.29 (1H, dt, *J* = 18.3, 3.7 Hz, one of C9H_2), 1.91-1.40 (7H, m, C4H_2, one of C9H_2, C10H_2, C11H_2), 0.93 (9H, s, C2'(CH_3)$_3$); ^{13}C NMR (126 MHz, $CDCl_3$) δ 208.2, 136.4, 127.6, 84.0, 67.4, 59.5, 50.5, 38.7, 33.8, 33.1, 31.1, 30.2, 19.1 ppm; IR (thin film) ν 2950, 2861, 1700, 1603, 1461, 1360, 1280, 1220, 1171, 1144, 1076, 995, 955, 918, 869, 835 cm^{-1}; $[\alpha]_D^{23}$ -106.7° (*c* = 0.150, CH_2Cl_2); Integration of the ^{1}H NMR (500 MHz, $CDCl_3$) resonances at δ 1.31 (major) and δ 1.26 (minor) ppm in the presence of 1.0 equiv Ag(fod) and 2.0 equiv (+)-Eu(hfc)$_3$ indicated an enantiomer ratio of 11.9:1.00 (85% ee). Data for **23**: ^{1}H NMR (500 MHz, $CDCl_3$) δ 5.40 (1H, t, *J* = 2.4 Hz, C1'*H*), 4.11 (1H, dd *J* = 8.9, 0.2 Hz, one of C3H_2), 3.98 (1H, ddd *J* = 11.2, 8.9, 5.3 Hz, one of C3H_2), 3.64 (1H, t, *J* = 2.8 Hz, C7*H*), 3.30 (1H, dt, *J* = 7.5, 2.6 Hz, C5*H*), 2.55 (1H, ddd, *J* = 16.6, 6.3, 3.2 Hz, one of C9H_2), 2.28 (1H, ddd, *J* = 16.8, 9.8, 7.6 Hz, one of C9H_2), 2.08-1.78 (6H, m, C4H_2, C10H_2, C11H_2), 1.04 (9H, s, C2'(CH_3)$_3$ ppm); ^{13}C NMR (126 MHz, $CDCl_3$) δ

209.4, 138.9, 130.0, 87.1, 67.8, 60.6, 51.0, 38.8, 33.4, 32.8, 30.8, 29.8, 19.7 ppm; IR (thin film) ν 2947, 2866, 1704, 1465, 1358, 1310, 1275, 1218, 1142, 1068, 992, 955, 905, 854 cm^{-1}; $[\alpha]_D^{23}$ +53.3° (*c* = 0.357, CH_2Cl_2); Integration of the ^1H NMR (500 MHz, $CDCl_3$) resonances at δ 1.25 (major) and δ 1.23 (minor) ppm in the presence of 1.0 equiv Ag(fod) and 2.0 equiv (+)-Eu(hfc)$_3$ indicated an enantiomer ratio of 14.7:1.00 (88% ee).

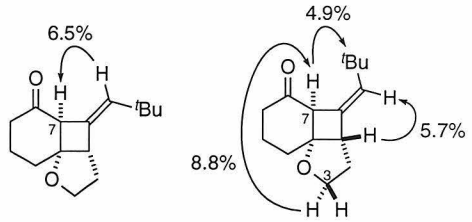

Selected ^1H NMR NOE difference data for **22** (300 MHz, C_6D_6, left) and **23** (300 MHz, $CDCl_3$, right)

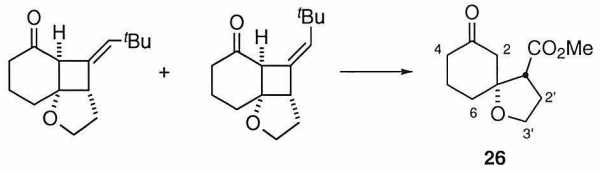

26: From **23**: A solution of 30 mg (0.13 mmol, 1.0 equiv) of **23** in 30 mL MeOH at -78 °C was treated with a dilute stream of ozone in oxygen for 1.5 min (0.8 mmol/min, 1.3 mmol, 10 equiv). Nitrogen was bubbled through the reaction mixture to remove excess ozone and 35 μL Bu_3P was added. The solution was stirred for 5 min at -78 °C and warmed to 23 °C thereafter. The volatiles were removed *in vacuo* and the residue was purified by chromatography on silica gel (1:1 hexanes–Et_2O, R_f 0.17) to afford 16 mg (77%) of **26** as a clear, colorless oil. ^1H NMR (400 MHz, C_6D_6) δ 3.69 (1H, td, *J* = 5.6, 4.9 Hz, one of C3'H_2), 3.34 (1H, q, *J* = 5.9, one of C3'H_2), 3.25 (3H, s, OCH_3), 2.48 (1H, dt, *J* = 13.9, 2.0, one of C1H_2), 2.40 (1H, t, *J* = 8.4, C1'*H*), 2.18 (1H, d, *J* = 14.0,

one of C1H_2), 2.17-2.06 (2H, m, C3H_2), 1.88-1.72 (2H, m, C5H_2), 1.62-1.37 (4H, m, C4H_2 and C2'H_2) ppm; ^{13}C NMR (100 MHz, C_6D_6) δ 205.8, 171.7, 86.0, 65.7, 53.2, 51.2, 48.2, 40.3, 35.9, 28.8, 21.3 ppm; IR (thin film) ν 2922, 2856, 1724, 1446, 1359, 1260, 1171, 1018 cm^{-1}; $[\alpha]_D^{23}$ -42.8° (*c* = 0.140, CH_2Cl_2). From **22**: 24 mg of **22** was similarly treated to afford 12 mg (72%) of **26**, $[\alpha]_D^{23}$ -38.1° (*c* = 0.105, CH_2Cl_2), identical in all other respects. The products of both ozonolyses were combined, and 10 mg (51 μmol, 1.0 equiv) was treated with 2.2 mg (56 μmol, 1.1 equiv) $NaBH_4$ in 3 mL MeOH at 0 °C. After stirring for 15 min at 0 °C the reaction mixture was poured into 2 mL 1.0 M aqueous KH_2PO_4, and extracted with 3 mL Et_2O. The organic layer was dried over anhydrous Na_2SO_4. Concentration *in vacuo* and chromatography on silica gel (4 x 20 mm, 1:1 hexanes–EtOAc, R_f 0.34) afforded 7 mg (70%) of the less polar diastereomeric alcohol, which was treated with 4-DMAP (5.0 equiv and (*R*)-MTPACl (2.0 equiv) in CH_2Cl_2. Integration of the ^{1}H NMR (500 MHz, C_6D_6) resonances of the derived (*S*)-MTPA ester at δ 3.53 (major, (*S*)-MTPA OCH_3) and δ 3.49 (minor, (*S*)-MTPA OCH_3) ppm indicated a diastereomer ratio of 11.5:1.00 (84% ee). HRMS (EI) calculated for $C_{11}H_{16}O_4$ 212.1048, found 212.1048.

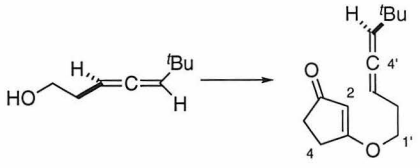

13

13: 1,3-Cyclopentanedione (91 mg, 0.94 mmol, 1.2 equiv) and DEAD (182 μL, 1.15 mmol, 1.5 equiv) were added to a solution of 108 mg (0.770 mmol, 1.0 equiv) of **21** and 246 mg (1.15 mmol, 1.5 equiv) Ph_3P in 5 mL THF, and the resulting orange solution was stirred for 15 min at 23 °C. The reaction mixture was concentrated *in vacuo* and the residue was purified by chromatography on silica gel (20 x 80 mm, 5:2 hexanes–EtOAc, R_f 0.25) to afford 121 mg (71%) of **13** as a clear, colorless oil. ^{1}H NMR (500 MHz, $CDCl_3$) δ

5.28 (1H, t, J = 1.1 Hz, C2H), 5.19-5.15 (2H, m, C3'H and C5'H), 4.02 (2H, m, C1'H_2), 2.62-2.59 (2H, m, C4H_2), 2.49-2.40 (4H, m, C5H_2 and C2'H_2), 0.86 (9H, s, C6'(CH_3)$_3$) ppm; ^{13}C NMR (126 MHz, $CDCl_3$) δ 205.8, 202.1, 190.1, 104.9, 104.6, 88.3, 71.1, 34.2, 31.9, 30.1, 28.6, 28.4 ppm; IR (thin film) ν 3093, 2958, 2865, 2358, 1962, 1705, 1680, 1592, 1462, 1439, 1413, 1389, 1344, 1288, 1248, 1222, 1180, 1008, 930, 879, 830 cm^{-1}; $[\alpha]_D^{23}$ +42.6° (c = 4.07, CH_2Cl_2). HRMS (EI) calculated for $C_{14}H_{20}O_2$ 220.1463, found 220.1466.

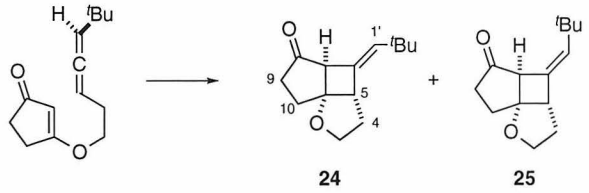

24 **25**

24, 25: A 200-mL Pyrex flask was charged with a solution of 130 mg of **13** of 89% ee in 125 mL cyclohexane. The solution was degassed by argon sparge for 10 min and irradiated at 23 °C for 6 h. The solvent was removed *in vacuo* and the residue was purified by chromatography on silica gel (20 x 100 mm, 5:1 hexanes–EtOAc, R_f 0.33 (**25**), 0.27 (**24**, and an unidentified side product) to afford 44 mg (34%) of **25** as a clear, colorless oil, and 46 mg (35%) of an inseparable mixture of two products, one of which was assigned as **24** on the basis of the ^{1}H NMR spectrum of the mixture, as a clear, colorless oil. Data for **24**: Integration of the ^{1}H NMR (500 MHz, $CDCl_3$) resonances at δ 1.19 (major) and δ 1.18 (minor) ppm in the presence of 1.0 equiv Ag(fod) and 2.0 equiv (+)-Eu(hfc)$_3$ indicated an enantiomer ratio of 7.94:1.00 (78% ee). Data for **25**: ^{1}H NMR (500 MHz, $CDCl_3$) δ 5.33 (1H, t, J = 1.8 Hz, C2'H), 4.18 (1H, t, J = 8.1, 7.9, 0.2 Hz, one of C3H_2), 3.92 (1H, ddd, J = 12.8, 7.7, 3.9 Hz, one of C3H_2), 3.36 (1H, δ, J = 1.9 Hz, C7H), 3.37-3.31 (1H, m, C5H), 2.66 (1H, ddd, J = 19.8, 9.4, 8.2 Hz, one of C9H_2), 2.53-2.45 (1H, m, one of C9H_2), 2.21-2.11 (2H, m, C10H_2), 2.04-1.98 (1H, m, one of C4H_2), 1.82 (1H, ddd, J = 12.2, 5.2, 0.2 Hz, one of C4H_2), 1.06 (9H, s,

C2'(CH_3)$_3$) ppm; ^{13}C NMR (126 MHz, $CDCl_3$) δ 212.7, 138.6, 118.2, 88.4, 68.9, 57.1, 52.1, 38.5, 33.7, 33.4, 30.6, 29.9 ppm; IR (thin film) ν 2950, 2864, 1737, 1469, 1413, 1360, 1314, 1264, 1199, 1138, 1068, 983, 912, 854 cm^{-1}; $[\alpha]_D^{23}$ +21.6° (*c* = 0.247, CH_2Cl_2); Integration of the ^{1}H NMR (500 MHz, $CDCl_3$) resonances at δ 1.37 (major) and δ 1.34 (minor) ppm in the presence of 1.0 equiv Ag(fod) and 2.0 equiv (+)-Eu(hfc)$_3$ indicated an enantiomer ratio of 6.68:1.00 (74% ee).

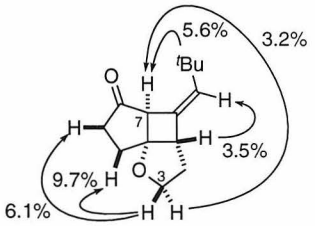

25

Selected ^{1}H NMR NOE difference data for **25** (300 MHz, C_6D_6)

Enantiomeric excess of unreacted 13 as a function of reaction time: A solution of 40 mg of **13** of 89% ee in 36 mL cyclohexane was degassed by argon sparge for 10 min. The solution was partitioned equally into three 25-mL Pyrex flasks and irradiated at 23 °C. The reaction was stopped at various intervals and the solvent was removed *in vacuo*. The extent of conversion of **13** to **24**, **25**, and an unidentified side product was determined by integration of the ^{1}H NMR (500 MHz, $CDCl_3$) resonances at δ 5.56-5.54 (unidentified side product), δ 5.39-5.39 (**24**), δ 5.34-5.33 (**25**), and δ 5.30-5.29 (**13**) ppm. The solvent was removed *in vacuo* and the crude reaction mixture was purified by chromatography on silica gel (10 x 80 mm, 5:1 hexanes–EtOAc, R_f 0.33) to isolate **25**. The enantiomeric excess of **25** was determined by integration of the ^{1}H NMR (500 MHz, $CDCl_3$) resonances at δ 1.37 (major) and δ 1.34 (minor) ppm in the presence of 1 equiv Ag(fod) and 2 equiv (+)-Eu(hfc)$_3$. When the reaction was stopped at 14% (20 min) and 38% (2 h) conversion, the enantiomeric excess of **25** was 88% and 82% respectively.

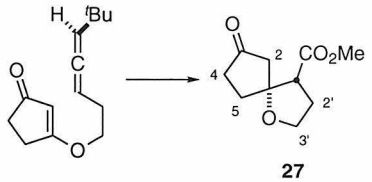

27

27: A 100-mL Pyrex flask was charged with a solution of 100 mg of **13** of 89% ee in 92 mL cyclohexane. The solution was degassed by argon sparge for 10 min and irradiated at 23 °C for 6 h. The solvent was removed *in vacuo*, and the residue was dissolved in 10 mL MeOH and cooled to -78 °C. A dilute stream of ozone in oxygen was bubbled through the reaction mixture for 5.5 min (0.8 mmol/min O_3, 4.4 mmol, 9.7 equiv). Nitrogen was bubbled through the reaction mixture to remove excess ozone and 136 μL (0.546 mmol, 1.2 equiv) Bu_3P was added. The reaction mixture was stirred for 5 min at -78 °C and warmed to 23 °C thereafter. The volatiles were removed *in vacuo* and the residue was purified by chromatography on silica gel (20 x 80 mm, 1:1.2 hexanes–EtOAc, Rf 0.18) to afford 61 mg (72%) of **27** as a clear, colorless oil. ^{1}HMR (500 MHz, C_6D_6) δ 3.59-3.54 (1H, m, one of C3'*H*), 3.38-3.34 (1H, m, one of C3'*H*), 3.18 (3H, s, OCH_3), 2.47 (1H, t, *J* = 8.1 Hz, C1'*H*), 2.29-2.21 (2H, m, one of C2H_2 and one of C4H_2), 2.11-1.98 (3H, m, one of C2*H*, one of C4*H*, and one of C2'*H*), 1.74-1.62 (2H, m, one of C5H_2 and one of C2'H_2), 1.61-1.53 (1H, m, one of C5*H*) ppm; ^{13}C NMR (126 MHz, C_6D_6) δ 213.1, 172.0, 88.2, 65.6, 51.3, 51.1, 46.5, 36.8, 34.8, 29.2 ppm; IR (thin film) ν 2956, 2924, 2853, 1742, 1662, 1376, 1320, 1260, 1161, 1026, 954 cm^{-1}; $[\alpha]_D^{23}$ -20.5° (c = 0.221, CH_2Cl_2). A solution of 9 mg (55 μM, 1.0 equiv) of **27** in 3 mL MeOH at 0 °C was treated with 2.1 mg (54 μmol, 1.2 equiv) $NaBH_4$. After stirring for 30 min at 0 °C the reaction mixture was poured into 4 mL 1.0 M aqueous KH_2PO_4, and extracted with 6 mL Et_2O. The organic layer was dried over anhydrous Na_2SO_4. Concentration *in vacuo* and chromatography on silica gel (10 x 40 mm, 1:1 hexanes–EtOAc, R_f 0.27) afforded 7 mg (64%) of the less polar diastereomeric alcohol, which was treated with 4-DMAP (5.0 equiv

and (*R*)-MTPACl (2.0 equiv) in CH_2Cl_2. Integration of the ^1H NMR (500 MHz, C_6D_6) resonances of the derived (*S*)-MTPA ester at δ 3.48 (minor, (*S*)-MTPA OCH_3) and δ 3.44 (major, (*S*)-MTPA OCH_3) ppm indicated a diastereomer ratio of 5.33:1.00 (68% ee). HRMS (EI) calculated for $C_{10}H_{14}O_4$ 198.0892, found 198.0888.

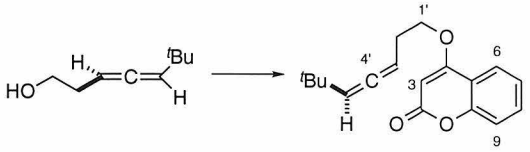

14

14: 4-Hydroxycoumarin (150 mg, 0.927 mmol, 1.25 equiv) and DEAD (146 μL, 0.927 mmol, 1.25 equiv) were added to a solution of 104 mg (0.741 mmol, 1.0 equiv) of **21** and 242 mg (1.11 mmol, 1.5 equiv) Ph_3P in 8 mL THF, and the resulting orange solution was stirred for 15 min at 23 °C. The reaction mixture was concentrated *in vacuo* and the residue was purified by chromatography on silica gel (20 x 100 mm, 5:1 hexanes–EtOAc, R_f 0.21) to afford 120 mg (57%) of **14** as a white solid. ^1H NMR (500 MHz, $CDCl_3$) δ 7.79 (1H, dd, *J* = 7.9, 1.6, C5*H* or C8*H*), 7.51 (1H, dd, *J* = 8.6, 7.0, 1.6, C6*H* or C7*H*), 7.27 (1H, dd, *J* = 8.5, 0.7, C5*H* or C8*H*), 7.23 (1H, ddd, *J* = 8.5, 7.1, 1.1, C6*H* or C7*H*), 5.64 (1H, s, C3*H*), 5.25 (1H, q, *J* = 6.4, C5'*H*), 5.18-5.15 (1H, m, C3'*H*), 4.17 (2H, t, *J* = 6.6, C1'H_2), 2.61-2.54 (2H, m, C2'H_2), 0.99 (9H, s, C6'(CH_3)$_3$) ppm; ^{13}C NMR (126 MHz, $CDCl_3$) δ 201.8, 165.5, 162.8, 153.3, 132.2, 123.7, 123.0, 116.6, 115.6, 104.4, 90.4, 87.8, 68.4, 31.6, 30.0, 28.1 ppm; IR (thin film) ν 3093, 3044, 2957, 2864, 1963, 1826, 1743, 1610, 1567, 1495, 1473, 1459, 1415, 1369, 1328, 1279, 1239, 1205, 1184, 1158, 1147, 1107, 1081, 1033, 997, 933, 912, 894, 874, 827, 769, 750, 734, 684, 646 cm^{-1}; $[\alpha]_D^{23}$ +45.0° (*c* = 4.00, CH_2Cl_2). HRMS (EI) calculated for $C_{18}H_{20}O_3$ 284.1412, calculated for $C_{18}H_{19}O_3$ (M^+ - H) 283.1334, found 283.1338.

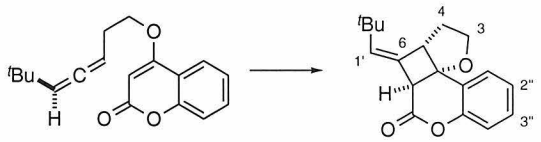

28

28: A 100-mL Pyrex flask was charged with 120 mg of **14** of 92% ee in 90 mL cyclohexane. The solution was degassed by argon sparge for 10 min and irradiated at 23 °C for 2 h. The solvent was removed *in vacuo* and the residue was purified by chromatography on silica gel (20 x 100 mm, 5:1 hexanes–EtOAc, R_f 0.34) to afford 107 mg (89%) of **28** as a white solid. ^{1}H NMR (500 MHz, $CDCl_3$) δ 7.44 (1H, ddd, *J* = 8.1, 1.1, 0.3 Hz, C1"*H* or C4"*H*); 7.35 (1H, ddd, *J* = 8.3, 7.4, 1.7 Hz, C2"*H* or C3"*H*), 7.22 (1H, td, *J* = 7.4, 1.1 Hz, C2"*H* or C3"*H*), 7.10 (1H, ddd, *J* =7.4, 1.7, 0.2 Hz, C1"*H* or C4"*H*), 5.78 (1H, t, *J* = 2.4 Hz, C1'*H*), 4.45 (1H, ddd, *J* = 8.7, 1.7, 1.6 Hz, one of C3H_2), 4.18 (1H, ddd, *J* = 10.9, 9.3, 5.8, one of C3H_2), 4.01 (1H, t, *J* = 3.0 Hz, C7*H*), 3.70-3.67 (1H, m, C5*H*), 2.40-2.32 (1H, m, one of C4*H*), 2.18-2.14 (1H, m, one of C4*H*), 1.09 (9H, s, C2'(CH_3)$_3$) ppm; ^{13}C NMR (126 MHz, $CDCl_3$) δ 165.1, 150.4, 138.9, 130.0, 126.7, 126.0, 125.1, 121.7, 117.3, 79.7, 68.6, 57.9, 49.8, 34.0, 33.7, 30.1 ppm; IR (thin film) ν 2956, 2867, 1761, 1616, 1588, 1490, 1474, 1455, 1363, 1328, 1260, 1203, 1186, 1167, 1115, 1087, 1069, 1034, 999, 955, 927, 758 cm^{-1}; $[\alpha]_D^{23}$ +162° (*c* = 0.363, CH_2Cl_2); A solution of 11 mg (37 μM, 1.0 equiv) of **28** in 1 mL THF at 0 °C was treated with 40 μL (80 μM, 2.2 equiv) of a 2.0 M solution of $LiBH_4$ in THF. The reaction mixture was stirred at 0 °C for 30 min, poured into 2 mL 1.0 M aqueous KH_2PO_4, and extracted with 3 mL Et_2O. The organic layer was dried over anhydrous Na_2SO_4. Concentration *in vacuo* and chromatography on silica gel (4 x 20 mm, 2:1 hexanes–EtOAc, R_f 0.36) afforded 4 mg (80%) of a diol that was treated with 4-DMAP (10 equiv) and (*R*)-MTPACl (4.0 equiv) in CH_2Cl_2. Integration of the ^{1}H NMR (500 MHz, $CDCl_3$) resonances of the derived (*S*)-MTPA ester at δ 1.04 (minor, C2'(CH_3)$_3$) and δ 1.02 (major, C2'(CH_3)$_3$) ppm indicated a diastereomer ratio of 22.9:1.00 (92% ee).

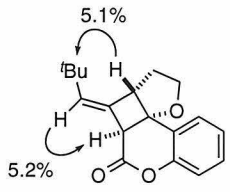

Selected ^{1}H NMR NOE difference data for **28** (300 MHz, $CDCl_3$)

Irradiation of 14 in the presence of a triplet sensitizer: A solution of 31 mg of **14** and 286 mg of benzophenone in 1 mL benzene was irradiated through a uranium glass filter (λ_{cutoff} = 350 nm) for 2 hr. The volatiles were removed *in vacuo*. Analysis of the residue by ^{1}H NMR (500 MHz, $CDCl_3$) indicated that only **28** was formed during the reaction.

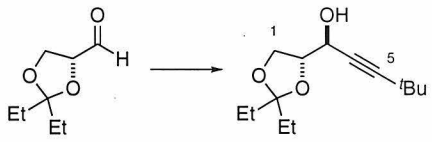

30

30: A 1.6 M solution of ^{t}BuLi in pentane (3.32 mL, 5.31 mmol, 1.5 equiv) was added dropwise to a solution of 693 μL (5.68 mmol, 1.6 equiv) of *tert*-butylacetylene in 5 mL THF at -78 °C. The resulting solution was stirred for 30 min at -78 °C, and a solution of 550 mg (3.48 mmol, 1.0 equiv) D-glyceraldehyde diethyl ketal, prepared according to the literature procedure,[14] in 5 mL THF was added dropwise. The transfer was quantitated with an additional 2 mL THF. The reaction mixture was warmed to 23 °C. When warming was complete the reaction mixture was poured into 20 mL 1.0 M aqueous KH_2PO_4 and 25 mL Et_2O. The aqueous layer was extracted with an additional 3 x 20 mL Et_2O, and the combined organic layers were washed with saturated aqueous NaCl, dried over anhydrous Na_2SO_4, and concentrated *in vacuo*. The residue was purified by chromatography on silica gel (20 x 350 mm, 4:1 hexanes–Et_2O, R_f 0.25) to afford 210 mg (25%) of **30** as a clear, colorless oil. ^{1}H NMR (500 MHz, $CDCl_3$) δ 4.57-4.53 (1H, m, C3*H*), 4.21 (1H, td, *J* = 7.1, 3.5, C2*H*), 4.06 (1H, dd, *J* = 8.2, 6.7, one of C1H_2), 3.98 (1H, t, *J* = 8.1, one of

C1H_2), 2.23-2.20 (1H, br s, O*H*), 1.76-1.62 (4H, m, both of diethyl ketal CH_2), 1.21 (9H, s, C6(CH_3)$_3$), 0.94 (3H, t, J = 7.3, one of diethyl ketal CH_3), 0.90 (3H, t, J = 7.5, one of diethyl ketal CH_3) ppm; ^{13}C NMR (126 MHz, $CDCl_3$) δ 113.8, 95.4, 78.2, 75.2, 65.3, 62.1, 30.8, 29.8, 28.9, 27.4, 8.1 ppm; IR (thin film) ν 3444, 2969, 2240, 1836, 1463, 1378, 1362, 1263, 1202, 1173, 1124, 1082, 1060, 1040, 978, 941, 919, 870, 831, 767, 709, 676 cm^{-1}; $[\alpha]_D^{23}$ +47.1° (c = 0.170, CH_2Cl_2).

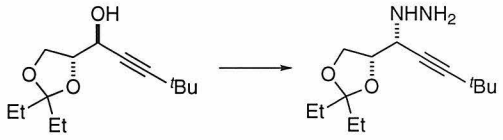

32

32: MsCl (225 μL, 2.90 mmol, 1.2 equiv) was added dropwise to a solution of 581 mg (2.42 mmol, 1.0 equiv) of **30** and 503 μL (3.63 mmol, 1.5 equiv) TEA in 5 mL CH_2Cl_2 at 0 °C at a rate such that the internal temperature was maintained below 5 °C. After stirring for 0.5 h, the reaction mixture was transferred *via* cannula into a solution of 10 mL MeOH and 10 mL anhydrous H_2NNH_2. The reaction mixture was stirred at 23 °C for 144 h and poured into 100 mL water. The aqueous layer was extracted with 2 x 40 mL 95:5 CH_2Cl_2–MeOH. The organic layers were combined, dried over anhydrous Na_2SO_4, and concentrated *in vacuo*. The residue was used without further purification.

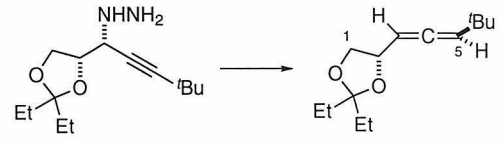

33

33: The residue was dissolved in 20 mL 1:1 Et_2O–CH_2Cl_2 and cooled to 0 °C. PTAD (848 mg, 4.84 mmol, 2.0 equiv) was added in one portion. When gas evolution was complete, 20 mL *n*-pentane was added and the reaction mixture was filtered through a pad (1 x 2 cm) of silica gel. The pad was washed with 20 mL 4:1 *n*-pentane–CH_2Cl_2 and the filtrate was concentrated *in vacuo*. The residue was purified by chromatography on silica gel (20 x 80

mm, 1:1 *n*-pentane–CH_2Cl_2, R_f 0.19) to afford 348 mg (64%) of **33** as a clear, colorless oil. ^{1}H NMR (500 MHz, $CDCl_3$) δ 5.30 (1H, dd, *J* = 6.2, 1.5 Hz, C5*H*), 5.24 (1H, dd, *J* = 7.3, 6.3 Hz, C3*H*), 4.53 (1H, dddd, *J* = 7.9, 7.4, 6.1, 1.5 Hz, C2*H*), 4.08 (1H, dd, *J* = 8.0, 6.1 Hz, one of C1H_2), 3.66 (1H, t, *J* = 7.9 Hz, one of C1H_2), 1.69-1.62 (4H, m, both of diethyl ketal CH_2), 1.03 (9H, s, C6(CH_3)$_3$), 0.93-0.89 (6H, m, both of diethyl ketal CH_3) ppm; ^{13}C NMR (126 MHz, $CDCl_3$) δ 202.0, 113.3, 105.1, 92.3, 75.3, 69.9, 31.6, 30.1, 30.0, 29.8, 8.1, 8.0 ppm; IR (thin film) ν 2964, 2881, 1964, 1463, 1390, 1362, 1336, 1310, 1272, 1250, 1232, 1198, 1173, 1132, 1078, 1038, 961, 918, 875, 748 cm^{-1}; $[\alpha]_D^{23}$ -25.1° (*c* = 2.47, CH_2Cl_2).

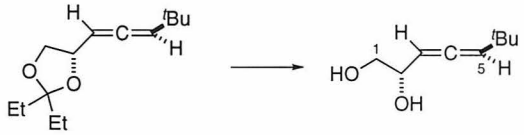

34

34: Oxalic acid (20 mg, 0.222 mmol, 0.17 equiv) was added to a solution of 300 mg (1.34 mmol, 1.0 equiv) of **33** in 13 mL MeOH. The resulting solution was stirred for 48 h at 23 °C, concentrated *in vacuo*, and the residue was purified by chromatography on silica gel (20 x 100 mm, 1.5:1 hexanes–EtOAc, R_f 0.23) to afford 136 mg (65%) of **34** as a clear, colorless oil. ^{1}H NMR (500 MHz, $CDCl_3$) δ 5.35 (1H, dd, *J* = 6.3, 2.4, C5*H*), 5.28 (1H, t, *J* = 6.2, C3*H*), 4.26-4.22 (1H, m, C2*H*), 3.68 (1H, dd, *J* = 11.2, 3.5, one of C1H_2), 3.54 (1H, dd, *J* = 11.3, 7.2, one of C1H_2), 2.32-2.06 (2H, br s, C1O*H* and C2O*H*), 1.04 (9H, s, C6(CH_3)$_3$) ppm; ^{13}C NMR (126 MHz, $CDCl_3$) δ 200.3, 106.5, 93.5, 70.4, 66.7, 31.8, 30.1 ppm; IR (thin film) ν 3358, 2959, 2865, 1962, 1647, 1472, 1458, 1395, 1362, 1317, 1253, 1205, 1190, 1123, 1080, 871 cm^{-1}; $[\alpha]_D^{23}$ -62.6° (*c* = 0.303, CH_2Cl_2).

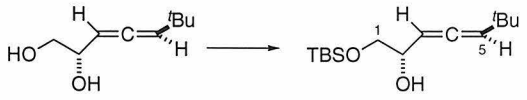

35

35: TEA (181 μL, 1.31 mmol, 1.5 equiv), TBSCl (131 mg, 0.871 mmol, 1.0 equiv), and 4-DMAP (11 mg, 0.087 mmol, 0.1 equiv) were added successively to a solution of 136 mg (0.871 mmol, 1.0 equiv) of **34** in 15 mL CH_2Cl_2. The resulting solution was stirred for 16 h at 23 °C, poured into 20 mL 1.0 M aqueous KH_2PO_4, and extracted with 2 x 20 mL Et_2O. The combined organic layers were dried over anhydrous Na_2SO_4 and concentrated *in vacuo*. The residue was purified by chromatography on silica gel (20 x 60 mm, 1:1 hexanes–CH_2Cl_2, R_f 0.26) to afford 120 mg (54%) of **35** as a clear, colorless oil. ^{1}H NMR (500 MHz, $CDCl_3$) δ 5.29 (1H, dd, J = 6.3, 2.2, C5*H*), 5.24 (1H, t, J = 6.3 Hz, C3*H*), 4.20-4.14 (1H, m, C2*H*), 3.66 (1H, dd, J = 10.0, 3.9 Hz, one of C1H_2), 3.52 (1H, dd, J = 10.0, 7.4 Hz, one of C1H_2), 2.48 (1H, d, J = 2.0, O*H*), 1.04 (9H, s, C6(CH_3)$_3$), 0.91 (9H, s, SiC(CH_3)$_3$), 0.81 (6H, s, Si(CH_3)$_2$) ppm; ^{13}C NMR (126 MHz, $CDCl_3$) δ 200.6, 105.4, 93.2, 70.6, 67.4, 31.7, 30.1, 25.9, 18.3, -5.4 ppm; IR (thin film) ν 3566, 3441, 2958, 2929, 2902, 2859, 1964, 1732, 1473, 1463, 1390, 1362, 1318, 1254, 1218, 1190, 1109, 1073, 1006, 938, 837, 815, 728, 668 cm^{-1}; $[\alpha]_D^{23}$ +4.0° (c = 3.02, CH_2Cl_2).

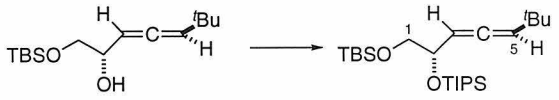

36

36: TEA (103 μL, 0.739 mmol, 2.0 equiv) and TIPSOTf (129 μL, 0.4812 mmol, 1.3 equiv) were added successively to a solution of 100 mg (0.370 mmol, 1.0 equiv) of **35** in 12 mL CH_2Cl_2. The resulting solution was stirred at 23 °C for 2 h, poured into 20 mL 1.0 M aqueous KH_2PO_4, and extracted with 2 x 15 mL Et_2O. The organic layers were dried over anhydrous Na_2SO_4 and concentrated *in vacuo*. The residue was purified by

chromatography on silica gel (20 x 80 mm, hexanes, R_f 0.19) to afford 154 mg (97%) of **36** as a clear, colorless oil. ^{1}H NMR (400 MHz, $CDCl_3$) δ 5.16-5.14 (2H, m, C3*H* and C5*H*), 4.28-4.22 (1H, m, C2*H*), 3.64 (1H, dd, *J* = 9.9, 6.2, one of C1H_2), 3.54 (1H, dd, *J* = 10.0, 5.5, one of C1H_2), 1.26-0.98 (30H, m, C6(CH_3)$_3$ and C2OSi(^{i}*Pr*)$_3$), 0.88 (9H, s, C1OSiC(CH_3)$_3$), 0.05 (6H, s, C1OSi(CH_3)$_2$) ppm; ^{13}C NMR (100 MHz, $CDCl_3$) δ 200.9, 103.9, 95.3, 73.5, 68.8, 31.6, 30.2, 36.1, 22.7, 18.1, 18.0, 12.4, -5.3 ppm; IR (thin film) ν 2958, 2866, 2714, 1963, 1463, 1408, 1388, 1362, 1255, 1195, 1126, 1070, 998, 967, 939, 919, 883, 836, 777, 740, 680 cm^{-1}; $[\alpha]_D^{23}$ -27.3° (*c* = 3.96, CH_2Cl_2).

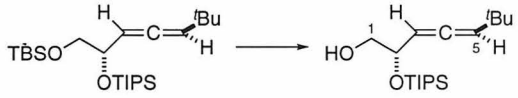

29

29: A solution of 152 mg of **36** in HF•pyridine in pyridine–THF, prepared according to the procedure of Trost,[15] was stirred at 23 °C for 6 h, poured into 20 mL 1.0 M aqueous KH_2PO_4, and extracted with 20 mL Et_2O. The organic layer was washed with 2 x 10 mL saturated aqueous $CuSO_4$ solution, dried over anhydrous Na_2SO_4, and concentrated *in vacuo*. The residue was purified by chromatography on silica gel (20 x 80 mm, 2:1 hexanes–CH_2Cl_2, R_f 0.20) to afford 89 mg (79%) of **29** as a clear, colorless oil. ^{1}H NMR (500 MHz, $CDCl_3$) δ 5.22 (1H, dd, *J* = 6.3, 1.4 Hz, C5*H*), 5.19 (1H, t, *J* = 6.4 Hz, C3*H*), 4.33-4.30 (1H, m, C2*H*), 3.60 (1H, dd, *J* = 10.9, 4.4, one of C1H_2), 3.54 (1H, dd, *J* = 10.9, 6.6, one of C1H_2), 2.14-1.90 (1H, br s, O*H*), 1.13-1.05 (21H, m, C2OSi(^{i}*Pr*)$_3$), 1.03 (9H, s, C6(CH_3)$_3$) ppm; ^{13}C NMR (126 MHz, $CDCl_3$) δ 200.8, 104.4, 94.1, 73.0, 67.7, 31.6, 30.1, 18.0, 17.9, 12.3 ppm; IR (thin film) ν 3584, 3453, 2960, 2866, 1963, 1463, 1387, 1363, 1325, 1253, 1205, 1188, 1099, 1062, 1015, 997, 946, 920, 882, 825, 747, 680 cm^{-1}; $[\alpha]_D^{23}$ -25.6° (*c* = 2.97, CH_2Cl_2).

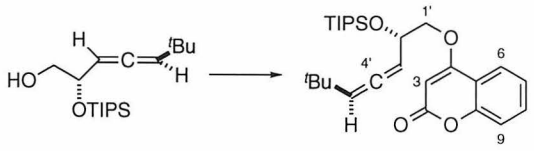

37

37: 4-Hydroxycoumarin (68 mg, 0.422 mmol, 1.5 equiv), DEAD (66 μL, 0.422 mmol, 1.5 equiv), and Ph_3P (126 mg, 0.479 mmol, 1.7 equiv) were added to a solution of 88 mg (0.282 mmol, 1.0 equiv) of **29** in 6.5 mL THF. The resulting orange solution was stirred for 30 min at 23 °C. The reaction mixture was concentrated *in vacuo* and the residue was purified by chromatography on silica gel (20 x 80 mm, 6:1 hexanes–Et_2O, R_f 0.19) to afford 73 mg (57%) of **37** as a clear, colorless oil. ^{1}H NMR (500 MHz, CDCl3) δ 7.86 (1H, dd, *J* = 7.9, 1.2 Hz, C6*H* or C9*H*), 7.56 (1H, ddd, *J* = 10.4, 7.8, 1.2 Hz, C7*H* or C8*H*), 7.32 (1H, d, *J* = 10.4 Hz, C6*H* or C9*H*), 7.26 (1H, t, *J* = 7.8 Hz, C7*H* or C8*H*), 5.72 (1H, s, C3*H*), 5.34-5.30 (2H, m, C3'*H* and C5'*H*), 4.77-4.74 (1H, m, C2'*H*), 4.18 (1H, dd, *J* = 9.8, 6.5 Hz, one of C1'H_2), 4.12 (1H, dd, *J* = 9.8, 4.5 Hz, one of C1'H_2), 1.22-1.06 (30H, m, C6'(CH_3)$_3$ and C2'OSi(^{i}*Pr*)$_3$) ppm; ^{13}C NMR (126 MHz, $CDCl_3$) δ 200.9, 165.6, 162.8, 153.3, 132.3, 123.7, 123.1, 116.7, 115.6, 105.2, 93.9, 90.7, 73.8, 70.2, 31.7, 30.0, 18.0, 17.9, 12.3 ppm; IR (thin film) ν 3089, 2947, 2867, 1963, 1732, 1715, 1622, 1568, 1494, 1453, 1410, 1372, 1326, 1274, 1239, 1184, 1159, 1141, 1106, 1068, 1030, 998, 970, 928, 883, 820, 764, 752, 682, 594 cm^{-1}; $[\alpha]_D^{23}$ +8.3° (*c* = 2.04, CH_2Cl_2).

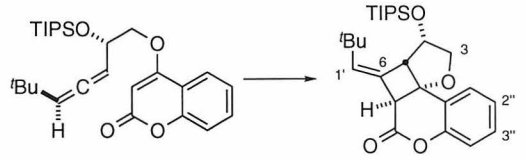

44

44: A 100-mL Pyrex flask was charged with 68 mg of **37** in 68 mL cyclohexane. The solution was degassed by argon sparge for 10 min, and irradiated at 23 °C for 4 h. The solvent was removed *in vacuo* and the residue was purified by chromatography on silica

gel (20 x 80 mm, 5:1 hexanes–Et_2O, R_f 0.31) to afford 61 mg (90%) of **44** as a clear, colorless oil that solidified on standing. ^1H NMR (500 MHz, $CDCl_3$) δ 7.36-7.30 (2H, m, C1"*H* or C4"*H* and C2"*H* or C3"*H*), 7.18 (1H, td, *J* = 7.6, 1.2 Hz, C2"*H* or C3"*H*), 7.04 (1H, dd, *J* = 8.2, 1.1, one of C1"*H* or C4"*H*), 5.70 (1H, t, *J* = 2.4 Hz, C1'*H*), 4.84 (1H, dt, *J* = 7.6, 5.1 Hz, C4*H*), 4.36 (1H, dd, *J* = 9.6, 4.9 Hz, one of C3H_2), 4.18 (1H, t, *J* = 2.8, C7*H*), 4.05 (1H, dd, *J* = 9.5, 5.4 Hz, one of C3H_2), 3.75 (1H, dt, *J* = 7.5, 2.5 Hz, C5*H*), 1.16-1.04 (21H, m, C4OSi(^iPr)$_3$), 1.02 (9H, s, C2'(CH_3)$_3$) ppm; ^{13}C NMR (126 MHz, $CDCl_3$) δ 164.6, 150.5, 139.1, 130.3, 127.0, 125.1, 121.8, 119.6, 117.5, 80.0, 76.3, 74.6, 62.7, 51.6, 34.1, 29.9, 18.3, 18.1, 12.9 ppm; IR (thin film) ν 2952, 2866, 1760, 1588, 1491, 1451, 1392, 1364, 1341, 1304, 1201, 1117, 1066, 1040, 1015, 998, 950, 909, 883, 836, 763 cm^{-1}; $[\alpha]_D^{23}$ -6.7° (*c* = 0.300, CH_2Cl_2).

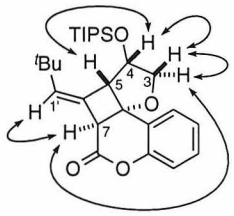

Selected ^1H NMR NOESY correlations for **44** (300 MHz, $CDCl_3$)

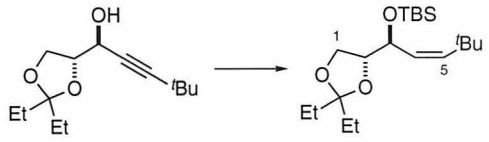

39

39: DIEA (320 μL, 1.83 mmol, 2.0 equiv) was added to a solution of 222 mg (0.916 mmol, 1.0 equiv) of **30** in 10 mL CH_2Cl_2. The resulting solution was cooled to -78 °C and 315 μL (1.37 mmol, 1.5 equiv) TBSOTf was added dropwise. The solution was allowed to warm to 0 °C and stirred for 1 h at 0 °C. The reaction mixture was poured into 10 mL 1.0 M aqueous KH_2PO_4 and extracted with 3 x 20 mL Et_2O. The combined organic layers

were washed with saturated aqueous NaCl, dried over anhydrous Na_2SO_4, and concentrated *in vacuo*. The residue was dissolved in 10 mL pyridine and 100 mg 5% palladium on carbon was added. The resulting slurry was stirred under 1 atm H_2 for 8 h and filtered through a plug of Celite. The plug was washed with *n*-heptane and the filtrate was concentrated *in vacuo*. The residue was purified by chromatography on silica gel (20 x 150, 20:1 hexanes–Et_2O) to afford 244 mg (75%) of **39** as a clear, colorless oil. ^1H NMR (300 MHz, $CDCl_3$) δ 5.37 (1H, d, J = 12.5 Hz, C5*H*), 5.04 (1H, dd, J = 12.5, 9.2 Hz, C4*H*), 4.86 (1H, dd, J = 9.2, 5.1, C3*H*), 4.03 (1H, t, J = 7.1 Hz, one of C1H_2), 3.94 (1H, dd, J = 7.1, 5.1 Hz, C2*H*), 3.85 (1H, t, J = 7.1 Hz, one of C1H_2), 1.69-1.61 (4H, m, both of diethyl ketal CH_2), 1.15 (9H, s, C6(CH_3)$_3$), 0.89-0.86 (15H, m, SiC(CH_3)$_3$ and both of diethyl ketal CH_3), 0.09 (3H, s, one of SiCH_3), 0.08 (3H, s, one of SiCH_3) ppm; ^{13}C NMR (75 MHz, $CDCl_3$) δ 140.9, 128.3, 113.1, 79.8, 69.1, 66.6, 34.5, 31.1, 29.9, 29.8, 28.8, 18.1, 8.5, 8.2, -3.9, -4.4 ppm; IR (thin film) ν 2931, 2872, 1467, 1360, 1249, 1196, 1173, 1126, 1085, 1002, 920, 838, 773, 679 cm^{-1};

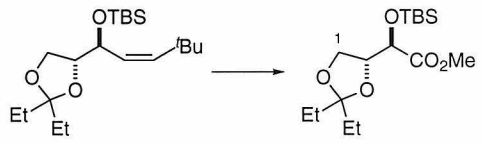

42

42: A solution of 214 mg (0.600 mmol, 1.0 equiv) of **39** in 10 mL CH_2Cl_2 was cooled to -78 °C and treated with a dilute stream of ozone in oxygen for 7.5 min (0.8 mmol/min, 6.00 mmol, 10 equiv). Nitrogen was bubbled through the reaction mixture to remove excess ozone and 2 mL Me_2S was added. The solution was allowed to slowly warm to 23 °C and stirred at 23 °C for 2 h. The volatiles were removed *in vacuo* and the residue was dissolved in 5 mL ^{t}BuOH and 5 mL 1.25 M pH 7 aqueous phosphate buffer. The solution was cooled to 0 °C and 2 mL 0.4 M aqueous $KMnO_4$ solution was added. The reaction mixture was stirred for 6 h at 23 °C. Saturated aqueous Na_2SO_3 was added until the purple color discharged. The reaction mixture was filtered through Celite. The aqueous layers

were treated with 10 mL 1.0 M aqueous KH_2PO_4 and extracted with 3 x 10 mL EtOAc. The combined organic layers were washed with saturated aqueous NaCl, dried over anhydrous Na_2SO_4, and concentrated *in vacuo*. The residue was dissolved in 5 mL Et_2O and treated with an ethereal solution of diazomethane until a yellow color persisted. Excess diazomethane was quenched by dropwise addition of AcOH. The reaction mixture was washed with 5 mL saturated aqueous NaCl, dried over anhydrous Na_2SO_4, and concentrated *in vacuo*. The residue was purified by chromatography on silica gel (20 x 100, 2:1 hexanes–EtOAc, R_f 0.30) to afford 77 mg (39%) of **42** as a clear, colorless oil. ^{1}H NMR (300 MHz, C_6D_6) δ 4.43-4.33 (2H, m, C3*H* and C2*H*), 4.04 (1H, dd, J = 8.4, 5.8 Hz, one of C1H_2), 3.90 (1H, dd, J = 8.4, 6.2 Hz, one of C1H_2), 3.31 (3H, s, OCH_3), 1.77-1.69 (2H, m, one of diethyl ketal CH_2), 1.55 (2H, q, J = 7.5 Hz, one of diethyl ketal CH_2), 1.02-0.87 (15H, m, both of diethyl ketal CH_3 and OSiC(CH_3)$_3$), 0.08 (3H, s, one of SiCH_3), 0.04 (3H, s, one of SiCH_3) ppm; ^{13}C NMR (75 MHz, $CDCl_3$) δ 171.9, 113.6, 77.1, 72.9, 66.2, 66.0, 29.7, 28.7, 25.6, 18.1, 8.1, -5.3 ppm; IR (thin film) ν 2930, 2884, 2858, 2711, 1752, 1459, 1438, 1389, 1361, 1255, 1198, 1160, 1086, 1059, 1005, 916, 870, 855, 838, 780, 675 cm^{-1}; $[\alpha]_D^{23}$ +18.8° (c = 2.57, CH_2Cl_2).

43

43: Concentrated aqueous HCl (100 μL) was added to a solution of 10 mg (0.030 mmol, 1.0 equiv) of **42** in 2 mL MeOH. The resulting solution was stirred at 23 °C for 30 min and concentrated to afford 3.4 mg (97%) of **43**, spectroscopically identical with an authentic sample.[16]

X-ray crystallography of (±)-15: **Data Collection:**[17] A clear, colorless crystal of molecular formula $C_{18}H_{20}O_3$ with approximate dimensions of 0.13 x 0.25 x 0.48 mm obtained by crystallization from acetone at 23 °C by slow evaporation was mounted on a glass fiber and placed in a goniometer head on an Enraf-Nonius CAD4 computer controlled kappa axis diffractometer equipped with a graphite monochromator using MoKα radiation (λ = 0.71073 Å). Unit cell parameters and an orientation matrix for data collection were obtained by auto-indexing and least-squares refinement of 22 reflections in the range $2° < \Theta < 14°$. The crystal system was monoclinic with cell constants and calculated volume of: a = 11.388(3) Å, b = 10.536(2) Å, c = 13.154(4) Å, β = 105.99(2)°, V = 1511(1) Å^3. From space group required extinctions and subsequent least squares refinement, the space group was determined to be $P2_1/c$ (# 14). A total of 3014 unique reflections was collected at a temperature of 25±1 °C using the Ω-2Θ scan technique to a maximum 2Θ angle of 50.0°.

Data Reduction: As a check on crystal and electronic stability, two representative reflections were measured every 60 minutes. A linear decay correction was applied to the data. Lorentz, polarization, and no absorption corrections were made.

Structure Solution and Refinement: The structure was solved with SHELX-86[18] using direct methods, which revealed the positions of 21 atoms. HYDRO[19] was employed to locate the remaining hydrogens. Hydrogen atoms were included in the refinement but restrained to ride on the atom to which they were bonded. Anomalous dispersion effects were included in F_c;[20] the values for $\Delta f'$ and $\Delta f''$ were those of Cromer.[21] Only 1620 reflections having F_o greater than 3.0 times $\sigma(F_o)$ were used in the refinements. The final cycle of least-squares included 190 variable parameters and converged with a maximum parameter shift of 0.00 times its esd, and unweighted and weighted agreement factors of 0.0746 and 0.0748, respectively. The standard deviation of an observation of unit weight

was 0.53. The largest peak in the final difference Fourier has a height of 0.31 e/Å^3 with an estimated error based on ΔF^{22} of 0.07; Plots of $\Sigma w(|F_o|- |F_c|)^2$ versus $|F_o|$ reflection order in data collection, $\sin\Theta/\lambda$, and various classes of indices showed no unusual trends. Scattering factors were taken from Cromer and Waber.[23] All calculations were performed on a MicroVAX computer using MolEN.[19,24]

2.3. Results

2.3.1. Synthesis of photosubstrates. The intramolecular [2+2]-photocycloadditions of olefins and allenes with enones and enoates are powerful tools for the construction of complex polycyclic structures with control over the relative configuration of three new stereocenters. In principle, employing chiral 1,3-disubstituted allenes in [2+2]-photocycloadditions with enones and enoates would afford an asymmetric variant of these reactions, and several attempts at developing such a scheme have been described. Becker has reported that irradiation of **10** affords **11** as a single diastereomer (Equation 2.3).[4] Based on this precedent the enantioselective photocycloaddition model substrates **12**, **13**, and **14** were chosen for synthesis. These photosubstrates differ from **10** in two respects: (1) the allene moiety is substituted at the 3'-terminus with a bulky *tert*-butyl group which was anticipated to preclude addition of an enone or enoate triplet to one of the diastereofaces of the allene; and (2) a heteroatom substitution which facilitates coupling of the enone and allenyl alcohol fragments using the Mitsunobu condensation is present.[25]

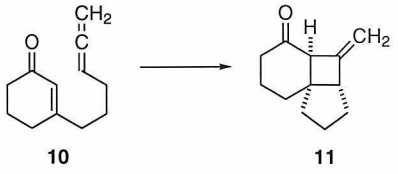

10 **11** **(2.3)**

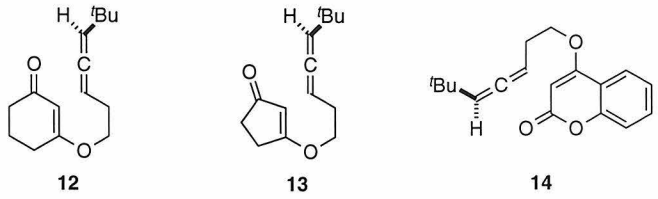

Figure 2.1. Model substrates for enantioselective photocycloadditions.

The allene fragment common to **12**, **13**, and **14** was synthesized in enantioenriched form as shown in Scheme 2.3. Addition of lithium *tert*-butylacetylide to aldehyde **15** afforded **(±)-16**, which was oxidized using the Dess-Martin periodinane[26] and reduced with (*S*)-Alpine-Borane[27] (Aldrich) to afford **16** in 89-92% enantiomeric excess, as determined by ^{1}H NMR analysis of its (*S*)-MTPA ester derivative.[28] Alkynol **16** was converted to allene **20** in 71% overall yield (3 steps) using the conditions described

Scheme 2.3. Synthesis of photocycloaddition model substrates.

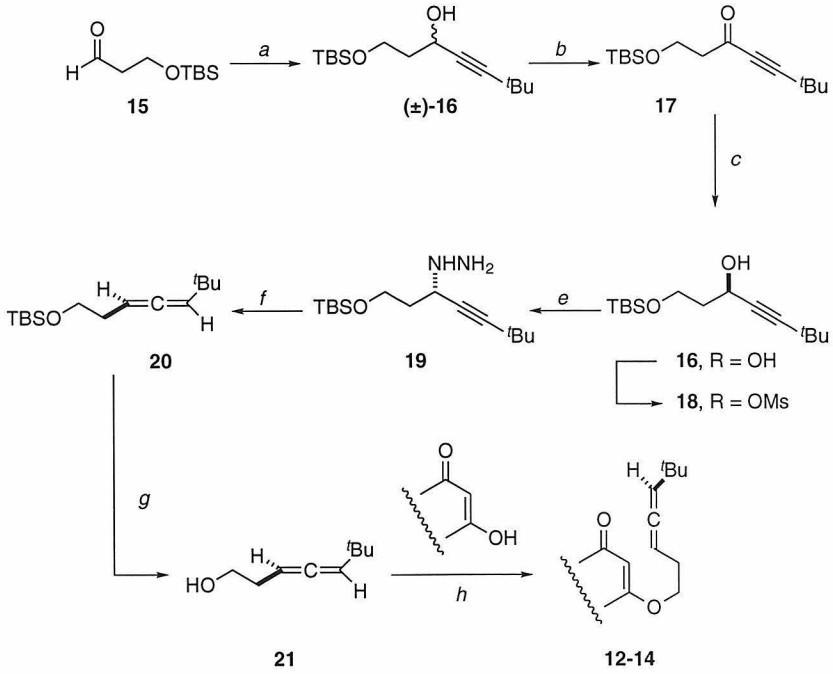

(a) lithium *tert*-butylacetylide, Et_2O, -78 °C, 2 h (72%). (b) Dess-Martin periodinane, CH_2Cl_2, 23 °C, 15 min (90%). (c) (*S*)-Alpine Borane, 23 °C, 7 h (93%, 90% ee). (d) MsCl, TEA, CH_2Cl_2, 0 °C, 30 min. (e) 1:1 MeOH–H_2NNH_2, 23 °C, 36 h. (f) PTAD, 1:1 CH_2Cl_2–Et_2O, 0 °C, 5 min (71%, 3 steps). (g) TBAF, THF, 23 °C, 30 min (80%). (h) Ph_3P, DEAD, THF, 23 °C, 15 min (56-71%).

by Myers for the preparation of eneyne allenes.[29] The transfer of asymmetry from the propargyl alcohol **16** to the allene **20** was found to be quantitative as determined by ^{1}H NMR analysis of **20** (89-92% ee) in the presence of the chiral shift reagents Ag(fod) and (+)-Eu(hfc)$_3$.[30] Desilylation of **20** with tetrabutylammonium fluoride afforded allenic alcohol **21**, which was coupled with 1,3-cyclohexanedione, 1,3-cyclopentanedione, and 4-hydroxycoumarin under Mitsunobu conditions[24] to afford photosubstrates **12**, **13**, and **14** in 56%, 71%, and 57% yield respectively.

2.3.2. Photocycloadditions of 1,3-cyclopentanedione and 1,3-cyclohexanedione derived substrates. The photocycloadditions of **12**, **13**, and **14** were performed at 23 °C in cyclohexane in Pyrex vessels (λ_{cutoff} = 293 nm) as described by Becker.[2c] Irradiation of **12** afforded the diastereomeric *exo*-alkylidenecyclobutanes **22** and **23** in a 1.2:1 mixture that was readily separable by chromatography on silica gel (Equation 2.4). The overall yield of photocycloaddition products was 89%. The enantiomeric excesses of **22** and **23** were determined by ^{1}H NMR analysis in the presence of 2.0 equivalents (+)-Eu(hfc)$_3$ and 1.0 equivalent Ag(fod) (Figure 2.2).[31] For both **22** and **23** the enantiomeric excess was found to equal, within experimental error, that of the photosubstrate.

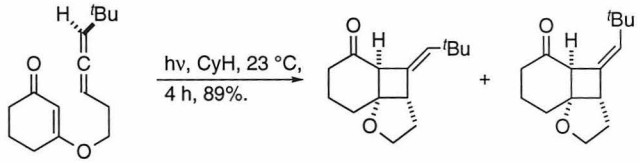

12 *(89% ee)* **22** *(85% ee)* **23** *(88% ee)*

Asymmetric Induction *96%* *99%*

(2.4)

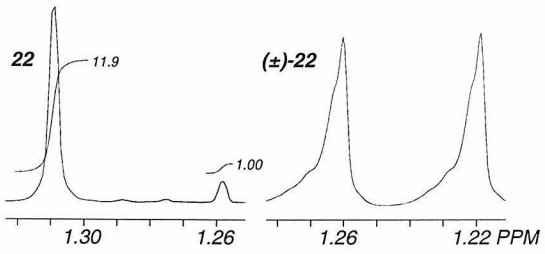

*Partial ^{1}HNMR Spectra (500 MHz, $CDCl_3$) of **22** and **(±)-22** in the presence of Ag(fod) and (+)-Eu(hfc)$_3$ showing the signal for the* tert*-butyl group.*

Figure 2.2. Enantiomeric excess determination of photoproducts derived from 1,3-cyclopentanedione and 1,3-cyclohexanedione.

Irradiation of **13** (Equation 2.5) afforded the diastereomeric *exo*-alkylidenecyclobutanes **24** and **25** in 69% overall yield upon irradiation under identical conditions. Irradiation also resulted in the formation of an unidentifiable side product that was inseparable from **24**. This side product may arise from poor regioselectivity rather than poor diastereoselection in the initial bond forming step of the photocycloaddition. This hypothesis is supported by the observation that ozonolysis of the crude photoproducts affords both **27** and an unidentified product whose ^{1}H NMR spectrum contains a signal for the *tert*-butyl group. Determination of the enantiomeric excesses of **24** and **25** by ^{1}H NMR analysis in the presence of 1.0 equivalent Ag(fod) and 2.0 equivalents (+)-Eu(hfc)$_3$ indicated that some racemization had occurred.[32]

The relative stereochemistry of **22**, **23**, and **25** was determined by ^{1}H NMR NOE difference experiments (Figure 2.3). The olefin geometry of **22** was assigned based on an enhancement of C7*H* upon irradiation of the vinylic signal. The olefin geometries of **23**

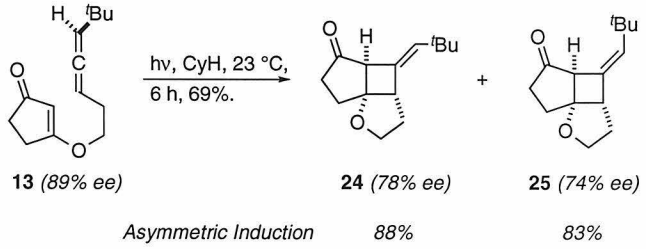

13 *(89% ee)* **24** *(78% ee)* **25** *(74% ee)*

Asymmetric Induction *88%* *83%*

(2.5)

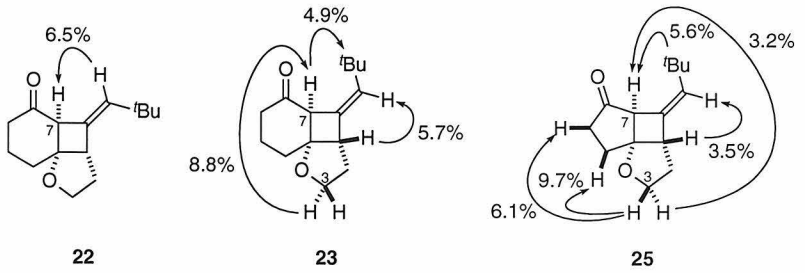

Figure 2.3. Selected ^{1}H NMR NOE difference data for photoproducts derived from 1,3-cyclopentanedione and 1,3-cyclohexanedione.

and **25** were assigned based on an enhancement of the vinylic signal upon irradiation of C5*H*. These assignments were supported by the observation of an enhancement of the *tert*-butyl signal of **23** upon irradiation of C7*H* and an enhancement of the C7*H* signal of **25** upon irradiation of the *tert*-butyl signal. The strong enhancement of C7*H* upon irradiation of one of the two diastereomeric C3*H* signals in **23** and **25** allowed assignment of the relative stereochemistry about the cyclobutane ring.

In order to demonstrate the synthetic equivalence of the asymmetric [2+2]-photocycloaddition to a chiral ketene-olefin cycloaddition and to verify that the photoadducts **22** and **23** differed only in olefin stereochemistry and possessed the same absolute configuration, **22** and **23** were ozonolyzed independently in methanol to afford the same keto ester **26** after retro-Claisen fragmentation of the intermediate β-diketone (Equation 2.6). Reduction of **26** with sodium borohydride in methanol afforded a mixture of diastereomeric cyclohexanols. A ^{1}H NMR analysis of the (*S*)-MTPA ester derived from the major diastereomer indicated an enantiomeric excess of 84%,[33] confirming the

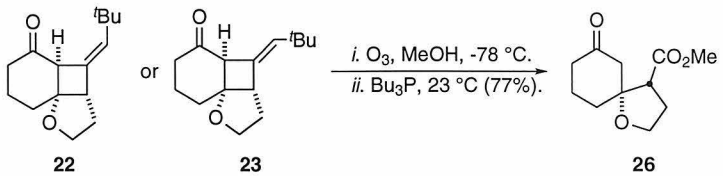

(2.6)

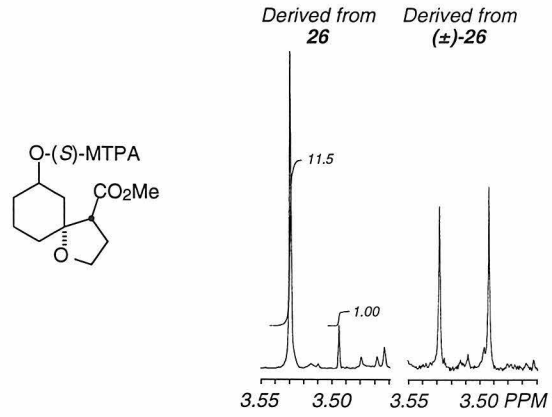

Partial ^{1}HNMR Spectra (500 MHz, $CDCl_3$) of the (S)-MTPA esters derived from the major $NaBH_4$ reduction products of ***26*** *and* ***(±)-26*** *showing the signal for the MTPA OMe group.*

Figure 2.4. Confirmation of asymmetric induction in photocycloaddition of 1,3-cyclopentanedione and 1,3-cyclohexanedione derived substrates by conversion to a cycloalkanol and (*S*)-MTPA ester derivatization.

enantiomeric excess data obtained by ^{1}H NMR analysis of **22** and **23** in the presence of chiral shift reagents (Figure 2.4).

Because **24** could not be isolated in pure form, the cycloaddition products obtained upon irradiation of **13** were ozonolyzed directly to afford keto ester **27** (Equation 2.7). Reduction of **27** with sodium borohydride afforded a mixture of diastereomeric cyclopentanols. A ^{1}H NMR analysis of the (*S*)-MTPA ester of the major diastereomeric cyclopentanol indicated an enantiomeric excess of 68%,[34] supporting the enantiomeric excess data obtained by ^{1}H NMR analysis of **22** and **23** in the presence of chiral shift reagents. The discrepancy between the enantiomeric excesses determined by ^{1}H NMR analysis of the (*S*)-MTPA esters of the cycloalkanols obtained by reduction of **26** and **27**

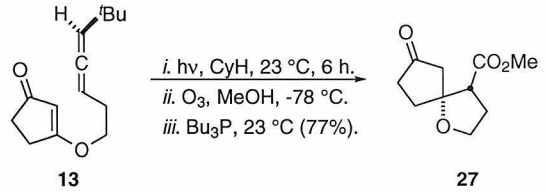

13 **27** **(2.7)**

and those determined by ^{1}H NMR analysis of the photoproducts in the presence of chiral shift reagents may be attributed to partial racemization of **26** and **27** through a β-elimination-Michael addition sequence.

2.3.3. Photocycloaddition of 4-hydroxycoumarin-derived substrate.

In contrast to the 1,3-cyclohexanedione and 1,3-cyclopentanedione derived substrates, the 4-hydroxycoumarin derived substrate **14** afforded **28** in 89% yield and greater than 90% olefin diastereoselection upon irradiation in cyclohexane (Equation 2.8). The enantiomeric excess of **28**, determined by reduction with lithium borohydride to the primary alcohol-phenol and ^{1}H NMR analysis of the derived bis-(*S*)-MTPA ester,[35] was identical to that of

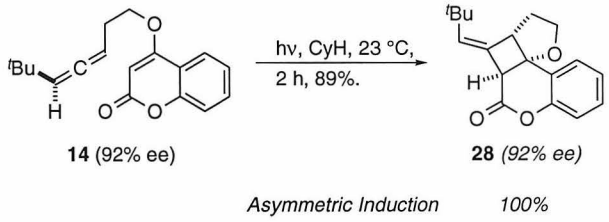

14 (92% ee) **28** *(92% ee)*

Asymmetric Induction *100%*

(2.8)

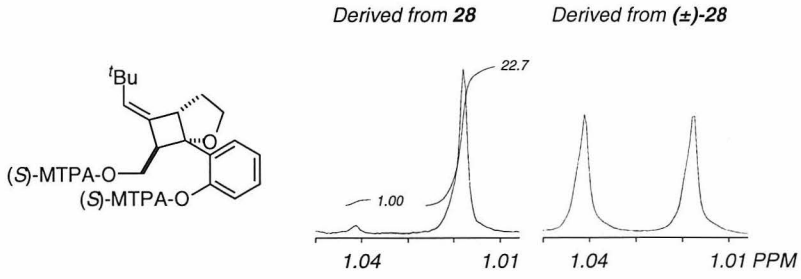

Partial ^{1}HNMR Spectra (500 MHz, $CDCl_3$) of the bis-(S)-MTPA esters derived from the $LiBH_4$ reduction products of ***28*** *and* ***(±)-86*** *showing the signal for the* tert-*butyl group.*

Figure 2.5. Enantiomeric excess determination of photoproduct derived from 4-hydroxycoumarin.

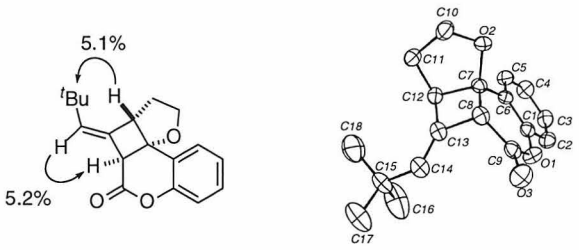

Selected ^{1}HNMR NOE Data

X-ray Crystal Structure of (±)-28

Figure 2.6. Determination of relative stereochemistry of photoproduct derived from 4-hydroxycoumarin.

the photosubstrate **14** (Figure 2.5). The relative stereochemistry was determined by ^{1}H NMR difference NOE experiments and confirmed by single crystal x-ray analysis of **(±)-28** (Figure 2.6).[17]

In order to probe the origin of the high olefin diastereoselectivity in the conversion of **14** to **28**, **14** was irradiated through a uranium glass filter in the presence of benzophenone, a triplet sensitizer. Using these conditions,[36] which preclude the possibility of a concerted reaction proceeding through an enoate singlet excited state, only **28** was formed, indicating that the marked change in the ratio of diastereomeric *exo*-alkylidenecyclobutane photoproducts could not be attributed to a change of mechanism.

2.3.4. Determination of sense of stereochemical induction in photocycloadditions. In order to determine the sense of stereochemical induction in these reactions allene **29** containing an internal stereochemical label of known absolute and relative configuration was prepared as shown in Scheme 2.4. Addition of lithiated *tert*-butylacetylene to the diethyl ketal of D-glyceraldehyde[25] afforded a separable mixture of diastereomeric alkynols. The major diastereomer **30** was subjected to the Myers allene synthesis sequence[39] previously described to afford allene **33** in 64% yield from **30**. The diethyl ketal was removed and the primary alcohol was selectively protected as its *tert*-

Scheme 2.4. Synthesis of photocycloaddition substrate containing an internal stereochemical label.

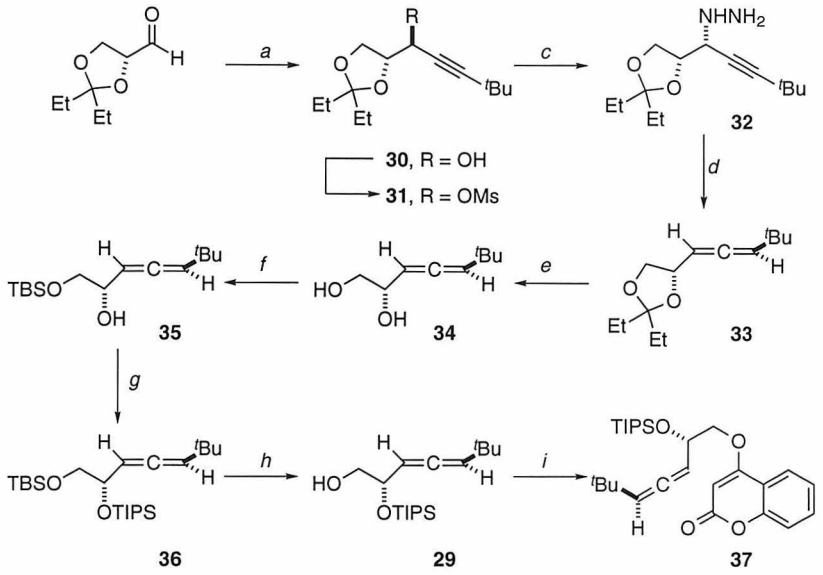

(a) lithium *tert*-butylacetylide, THF, -78 °C, 1 h (25%). (b) MsCl, TEA, CH_2Cl_2, 0 °C, 30 min. (c) 1:1 MeOH–H_2NNH_2, 23 °C, 144 h. (d) PTAD, 1:1 CH_2Cl_2–Et_2O, 0 °C, 5 min (64%, 3 steps). (e) $H_2C_2O_4$, MeOH, 23 °C, 48 h (65%). (f) TBSCl, TEA, 4-DMAP, CH_2Cl_2, 23 °C, 16 h (54%). (g) TIPSOTf, TEA, CH_2Cl_2, 23 °C, 2 h (97%). (h) HF•pyr, pyr–THF, 23 °C, 6 h (79%). (i) Ph_3P, DEAD, 4-hydroxycoumarin, THF, 23 °C, 30 min (57%).

butyldimethylsilyl ether. Silylation of the secondary alcohol with triisopropylsilyl trifluoromethanesulfonate followed by removal of the *tert*-butyldimethylsilyl group under the conditions of Trost[26] afforded **29**, which was coupled to 4-hydroxycoumarin by Mitsunobu condensation to afford photosubstrate **37**.

The stereochemistry of the newly formed carbinol stereocenter of **30** was determined by conversion to the known lactone *cis*-diol **43** (Scheme 2.5).[37] Successive silylation and semihydrogenation[38] of **30** afforded alkene **39**. Ozonolysis followed by permanganate oxidation[39] produced acid **41**, which was isolated as its methyl ester **42** following treatment with diazomethane. Treatment of **42** with methanolic HCl afforded **43**, which was identical by ^{1}H NMR[40] to an authentic sample,[16] confirming the *trans* stereochemical relationship of the vicinal alcohol stereocenters of **30**.

Scheme 2.5. Determination of relative stereochemistry of allene containing an internal stereochemical label.

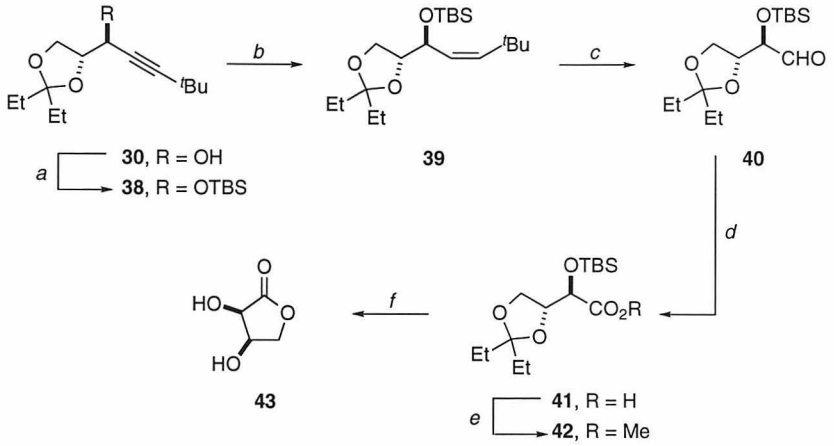

(a) DIEA, TBSOTf, CH_2Cl_2, 0 °C, 1 h. (b) Pd/C, pyr, H_2, 23 °C, 8 h (75%). (c) O_3, CH_2Cl_2, -78 °C, then Me_2S, 23 °C, 2 h. (d) $KMnO_4$, pH 7, 23 °C, 6 h. (e) CH_2N_2, Et_2O, 23 °C (39%). (f) HCl, MeOH, 23 °C, 30 min (97%).

Irradiation of **37** in cyclohexane at 23 °C afforded **44** in excellent yield as a single diastereomer by ^{1}H NMR analysis (Equation 2.9). The stereochemical assignments were determined by analysis of the vicinal coupling constants and phase-sensitive NOESY data (Figure 2.7). In particular, the observed 7.5 Hz coupling constant between C4H and C5H, which is compatible with the dihedral angle between $C4H_\beta$ and C5H (17°) but not the dihedral angle between $C4H_\alpha$ and C5H (117°) in the x-ray crystal structure of **(±)-28**,[41] and a strong cross peak correlating C4H and C5H in the ^{1}H NMR NOESY spectrum[42] support a *cis* stereochemical assignment.

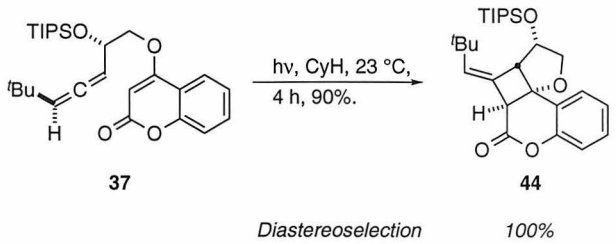

(2.9)

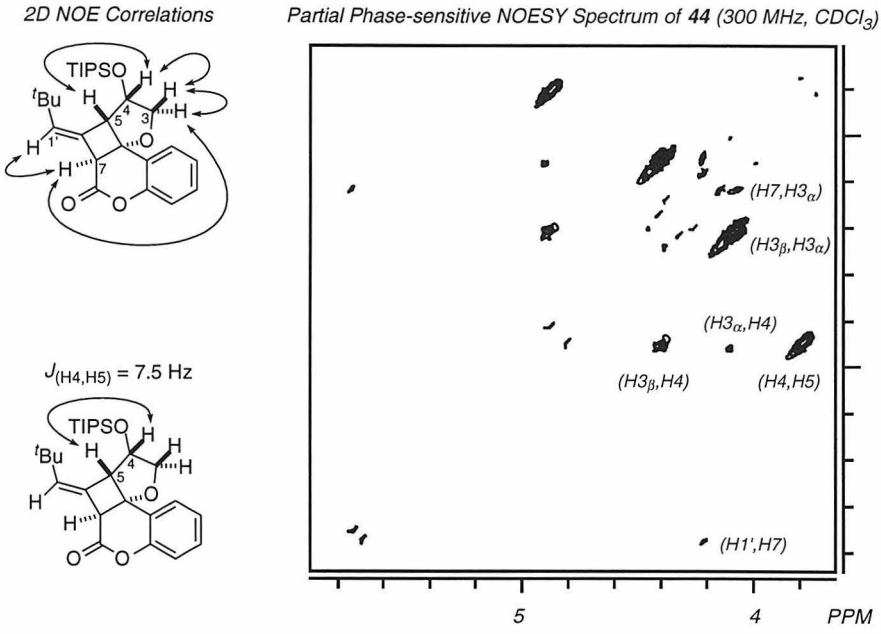

Figure 2.7. Determination of relative stereochemistry of photoproduct containing an internal stereochemical label.

2.4. Discussion

From the stereochemical outcome of the photocycloaddition of **37**, it is possible to derive the allene diastereoface selectivity in the enantioselective [2+2]-photocycloadditions documented in this chapter and construct a transition state model which accounts for the diastereoselectivity and enantioselectivity in the formation of **44** and, by analogy, in the formation of **22**, **23**, **24**, **25** and **28**. In this model, shown in Scheme 2.6, Cβ(•) of the triplet biradical formed upon irradiation of the enone or enoate adds to the less hindered end of the allene on the diastereoface opposite the large *tert*-butyl substituent to give intermediate **45**.[43] The regiochemistry of initial bond formation is consistent with Hammond's "Rule of Five"[44] and the observed diastereoselection is accommodated by an approach of the allene in which C3'H and not C2' resides over the ring. Rapid interconversion of the diastereomeric vinylic radicals causes loss of olefin geometry (**45** ↔ **45'**). Rotation of the *tert*-butylvinyl fragment in the appropriate direction to align the

Scheme 2.6. Model for diastereofacial selectivity in allene-enone and allene-enoate enantioselective photocycloadditions.

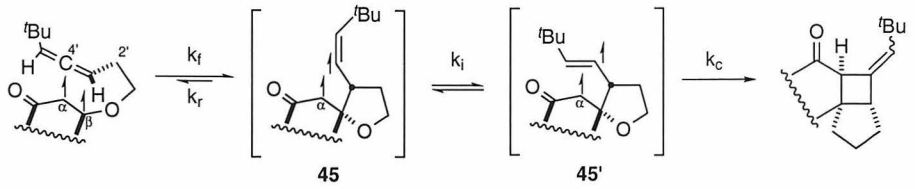

biradical orbitals results in collapse of **45** and **45'** to the *exo*-alkylidenecyclobutane products.

The formation of mixtures of olefin diastereomers upon photocycloaddition of **12** and **13** indicates that interconversion of the vinylic radicals **45** and **45'** is rapid relative to ring closure ($k_i > k_c$) in the 1,3-cyclopentanedione and 1,3-cyclohexanedione derived systems, while the observation of high levels of stereochemical induction in the photocycloadditions of **12**, **14**, and **37** indicates that the rate of reversion of the biradical intermediate to starting material is not competitive with the rate of ring closure ($k_c >> k_r$) in systems containing a six-membered cyclic enone or enoate. The diminished levels of stereochemical induction obtained upon photocycloaddition of **13** may be rationalized by a mechanism involving *cis-trans* isomerization of the initially formed *tert*-butylvinyl radical[45] and a rate of reversion to starting material that is competitive with that of ring closure. This hypothesis is supported by the observation that the enantiomeric excess of the photoproduct **25** diminishes as the reaction progresses.

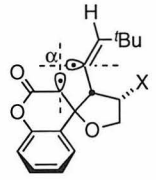

46

Figure 2.8. Proposed transition state geometry leading to diastereoselective product formation in photocycloadditions of 4-hydroxycoumarin derived substrates.

The formation of a single *exo*-alkylidenecyclobutane in the photocycloadditions of the 4-hydroxycoumarin derived allene-enoates **14** and **37** may be rationalized by the presence of memory effects in the 1,4-biradical intermediate as it undergoes intersystem crossing and collapse to cyclic products (Figure 2.8).[46] Investigation of these effects by Griesbeck in the context of the Paterno-Buchi cycloaddition reaction suggests that diastereoselective product formation may occur when the 1,4-biradical intermediates both possess short singlet lifetimes and exist in the optimal configuration for triplet-to-singlet intersystem crossing due to the spatial arrangements of their substituents. The rate of intersystem crossing of a 1,4-biradical through a mechanism involving spin-orbit coupling is a function of the spatial orientation and electronic character of the orbitals of the biradical. The Salem-Rowland rules define the spatial orientation of the biradical orbitals which results in the maximum efficiency of spin-orbit coupling: (1) the efficiency of spin-orbit coupling increases as the distance between the radical centers decreases; (2) the efficiency of spin-orbit coupling is proportional to the ionic character of the radicals; and (3) the efficiency of spin-orbit coupling is maximized when the orbitals are orthogonal. According to these rules, the putative 1,4-biradical intermediates formed upon irradiation of **14** and **37** are ideal candidates for rapid intersystem crossing. The fused ring systems formed upon intramolecular cycloaddition of **14** and **37** are highly conformationally restricted. Examination of models suggests that the orbitals of the 1,4-biradical formed upon addition of the enoate triplet Cβ(•) to the proximal terminus of the allene are favorably disposed for intersystem crossing (α approximately 90°, **46**, Figure 2.8) and collapse to cyclobutane products. As a result of the rapid rates of intersystem crossing and ring closure, the initial orientation of the *tert*-butylvinyl substituent in the 1,4-biradical intermediates formed upon irradiation of **14** and **37** is preserved in the photoadducts, resulting in the formation of only one of the two possible olefin diastereomers in each case.

2.5. Conclusions

These investigations demonstrate the feasibility of employing a chiral, 1,3-disubstituted allene as the source of asymmetry in intramolecular [2+2]-photocycloadditions and quantify the extent of asymmetric induction that may be expected in these reactions. High levels of asymmetric induction in the photoadducts were observed in all cases. While the photocycloadditions of allenes appended to 1,3-pentanedione and 1,3-hexanedione at C3 afforded *exo*-alkylidenecyclobutane products as mixtures of olefin diastereomers, the photocycloadditions of allenes appended to 4-hydroxycoumarin at C4 afforded *exo*-alkylidenecyclobutane products as single olefin diastereomers. Transition state models that accommodate these observations have been suggested. The asymmetric intramolecular [2+2]-photocycloaddition can provide access to optically active, fused polycyclic structures that are not readily available using current enantioselective synthetic methodology.

2.6. References and Notes

1. Adapted from Carreira, E. M.; Hastings, C. A.; Shepard, M. S.; Yerkey, L. A.; Millward, D. B. *J. Am. Chem. Soc.* **1994**, *116*, 6622.
2. (a) Baker, W. R.; Senter, P. D.; Coates, R. M. *J. Chem. Soc. Chem. Comm.* **1980**, 1011. (b) Becker, D.; Harel, Z.; Birnbaum, D. *J. Chem. Soc. Chem. Comm.* **1975**, 375. (c) Becker, D.; Harel, Z.; Nagler, M.; Gillon, A. *J. Org. Chem.* **1982**, *47*, 3297. (d) Crimmins, M. T. *Chem. Rev.* **1988**, *88*, 1453-1473. (e) Crimmins, M. T.; Reinhold, T. L. *Organic Reactions*; Wiley: New York, 1993; Vol. 44. p. 297. (f) Schreiber, S. L. *Science* **1985**, *227*, 857. (g) Dauben, W. G.; Shapiro, G.; Luders, L. *Tetrahedron Lett.* **1985**, *26*, 1429. (h) Dauben, W. G.; Shapiro, G. *Tetrahedron Lett.* **1985**, *26*, 989.
3. Dauben, W. G.; Shapiro, G. *J. Org. Chem.* **1984**, *49*, 4252.

4. (a) Crimmins, M. T.; Jung, D. K.; Gray, J. L. *J. Am. Chem. Soc.* **1993**, *115*, 3146-3155. (b) Crimmins, M. T.; Watson, P. S. *Tetrahedron Lett.* **1993**, *34*, 199-202. (c) Crimmins, M. T.; King, B. W.; Watson, P. S.; Guise, L. E. *Tetrahedron* **1997**, *53*, 8963-8974. (d) Tanaka, M.; Tomioka, K.; Koga, K. *Tetrahedron* **1994**, *50*, 12829-12842. (e) Tenaglia, A.; Barille, D. *Synlett* **1995**, 776-778.
5. Bellus, D.; Ernst, B. *Angew. Chem. Int. Ed. Engl.* **1988**, *27*, 797.
6. Schuster, D. I.; Lem, G.; Kaprinidis, N. A. *Chem. Rev.* **1993**, *93*, 3.
7. Corey, E. J.; Bass, J. D.; LeMahieu, R.; Mitra, R. B. A. *J. Am. Chem. Soc.* **1964**, *86*, 5570.
8. Becker, D.; Nagler, M.; Sahali, Y.; Haddad, N. *J. Org. Chem.* **1991**, *56*, 4537.
9. Becker, D.; Nagler, M.; Harel, Z.; Gillon, A. *J. Org. Chem.* **1983**, *48*, 2584.
10. For a leading reference on the thermal cycloaddition of an enantioenriched allene, see: Pasto, D. J.; Brophy, J. *J. Phys. Org. Chem.* **1993**, *6*, 95.
11. Still, W. C.; Kahn, M.; Mitra, A. *J. Org. Chem.* **1978**, *43*, 2923.
12. Ireland, R. E.; Liu, L. B. *J. Org. Chem.* **1993**, *58*, 2899.
13. The enantiomeric excess varied from batch to batch but was reproducibly 89-92%.
14. Schmid, C. R.; Bradley, D. A. *Synthesis* **1982**, 587.
15. Trost, B. M.; Caldwell, C. G.; Murayama, E.; Heissler, D. *J. Org. Chem.* **1983**, *48*, 3252.
16. Cohen, N.; Banner, B. L.; Lopresti, R. J.; Wong, F.; Rosenberger, M.; Liu, Y.-Y.; Thom, E.; Liebmann, A. A. *J. Am. Chem. Soc.* **1983**, *105*, 3661. Sample courtesy of Dr. Justin Du Bois.
17. I am grateful to Prof. Kenneth I. Hardcastle (California State University, Northridge) for x-ray crystallographic data collection and structure solution of **(±)-28**.
18. Sheldrick, G. M., "SHELXS-86, Program for Crystal Structure Solution," University of Gottingen, Gottingen, Germany, 1986.

19. Fair, C. K., "MolEN, An Interactive Structure Solution Procedure," Enraf-Nonius, Delft, The Netherlands, 1990.

20. Ibers, J. A.; Hamilton, W. C. *Acta Crystallogr.* **1964**, *17*, 781.

21. Cromer, D. T.; Waber, J. T. *International Tables for X-Ray Crystallography*; Knyoch: Birmingham, England, 1974; Vol. IV. Table 2.3.1.

22. Cruickshank, D. W. J. *Acta Crystallogr.* **1949**, *2*, 154.

23. Cromer, D. T.; Waber, J. T. *International Tables for X-Ray Crystallography*; Knyoch: Birmingham, England, 1974.

24. Tables of crystallographic data, positional parameters, and general displacement parameters are given in Appendix I.

25. Mitsunobu, O. *Synthesis* **1981**, 1.

26. Dess, D. B.; Martin, J. C. *J. Org. Chem.* **1983**, *48*, 4156.

27. Midland, M. M.; Tramontano, A.; Zderic, S. A. *J. Am. Chem. Soc.* **1977**, *99*, 5211.

28. Integration of the ^{1}H NMR (500 MHz, $CDCl_3$) resonances for the *tert*-butyl group at δ 1.22 (major) and δ 1.18 (minor) ppm indicated a diastereomer ratio of 18.8:1.00 (90% ee).

29. Myers, A. G.; Finney, N. S.; Kuo, E. Y. *Tetrahedron Lett.* **1989**, *30*, 5747.

30. Integration of the ^{1}H NMR (500 MHz, $CDCl_3$) resonances for the silyl-bound *tert*-butyl group at δ 0.08 (major) and δ 0.06 (minor) ppm in the presence of 2.0 equiv Ag(fod) and 1.5 equiv (+)-Eu(hfc)$_3$ indicated a diastereomer ratio of greater than 20:1 (>90% ee). This combination of reagents has been reported by Myers for the resolution of allene enantiomers (see reference 28).

31. For **22**, integration of the ^{1}H NMR (500 MHz, $CDCl_3$) resonances for the *tert*-butyl group at δ 1.25 (major) and δ 1.23 (minor) ppm in the presence of 1.0 equiv Ag(fod) and 2.0 equiv (+)-Eu(hfc)$_3$ indicated an enantiomer ratio of 14.7:1.00 (88% ee). For **23**, integration of the ^{1}H NMR (500 MHz, $CDCl_3$) resonances for the *tert*-butyl group

at δ 1.31 (major) and δ 1.26 (minor) ppm in the presence of 1.0 equiv Ag(fod) and 2.0 equiv (+)-Eu(hfc)$_3$ indicated an enantiomer ratio of 11.9:1.00 (85% ee).

32. For **24**, integration of the ^{1}H NMR (500 MHz, $CDCl_3$) resonances for the *tert*-butyl group at δ 1.37 (major) and δ 1.34 (minor) ppm in the presence of 1.0 equiv Ag(fod) and 2.0 equiv (+)-Eu(hfc)$_3$ indicated an enantiomer ratio of 6.68:1.00 (74% ee). For **25**, integration of the ^{1}H NMR (500 MHz, $CDCl_3$) resonances for the *tert*-butyl group at δ 1.19 (major) and δ 1.18 (minor) ppm in the presence of 1.0 equiv Ag(fod) and 2.0 equiv (+)-Eu(hfc)$_3$ indicated an enantiomer ratio of 7.94:1.00 (78% ee).
33. Integration of the ^{1}H NMR (500 MHz, C_6D_6) resonances for the (*S*)-MTPA methoxy group at δ 3.53 (major) and δ 3.49 (minor) ppm indicated a diastereomer ratio of 11.5:1.00 (84.0% ee).
34. Integration of the ^{1}H NMR (500 MHz, C_6D_6) resonances for the (*S*)-MTPA methoxy group at δ 3.48 (minor) and δ 3.44 (major) ppm indicated a diastereomer ratio of 5.33:1.00 (68% ee).
35. Integration of the ^{1}H NMR (500 MHz, $CDCl_3$) resonances for the *tert*-butyl group at δ 1.04 (minor) and δ 1.02 (major) ppm indicated a diastereomer ratio of 22.9:1.00 (92% ee).
36. Wells, P. P.; Morrison, H. *J. Am. Chem. Soc.* **1975**, *97*, 154.
37. These experiments were performed by Prof. Erick. M. Carreira.
38. This reagent combination allows highly reproducible semihydrogenation of alkynes: B. E. Ledford and E. M. Carreira, unpublished results.
39. Abiko, A.; Roberts, J. C.; Takesawa, T.; Masamune, S. *Tetrahedron Lett.* **1986**, *27*, 4537.
40. Measured at 300 MHz in D_2O for both authentic material and material derived from **30**.

41. The predicted ^{1}H-^{1}H coupling constant between C4H$_\alpha$ and C5H is 2-3 Hz. The actual coupling constant could not be determined from the ^{1}H NMR spectrum of **28** due to overlapping signals. For a discussion of the relationship between ^{1}H-^{1}H coupling constants and the dihedral angle, see Jackman, L. M.; Sternhell, S. *Applications of NMR Spectroscopy in Organic Chemistry*, Pergamon: Oxford, 1969; p. 281.

42. The cross peak between C4H and C5H was 42% as intense as the cross peak between C3H$_\alpha$ and C3H$_\beta$, which is in better agreement with the C4H$_\beta$, C5H distance of 2.285 Å (predicted NOE intensity 32% of the C3H$_\beta$, C3H$_\alpha$ NOE) than the C4H$_\alpha$, C5H distance of 2.876 Å (predicted NOE intensity 8.1% of the C3H$_\alpha$, C3H$_\beta$ NOE) in the crystal structure of **(±)-28** (The C3H$_\alpha$, C3H$_\beta$ distance is 1.892 Å). For a discussion of the use of NOE difference data to determine stereochemistry, see: Derome, A. E. *Modern NMR Techniques for Chemistry Research*, Pergamon, Oxford: 1987; p. 129.

43. Becker has documented results supporting the premise that initial bond formation occurs at Cβ; see: Becker, D.; Nagler, M.; Harel, Z.; Gillon, A. *J. Org. Chem.* **1983**, *48*, 2584.

44. Liu, R. S. H.; Hammond, G. S. *J. Am. Chem. Soc.* **1967**, *89*, 4936.

45. The energy barrier to interconversion of vinyl radical has been estimated at about 2 kcal/mole and the lifetime has been estimated at 3 x 10^{-8} to 3 x 10^{-10} sec.; see: Simamura, O. in *Top. Stereochem.* **1969**, *4*, 1. The lifetime of 3,6-dimethyloctane-3,6-diradical has been estimated at 1 x 10^{-6} sec.; see: Bartlett, P. D.; Porter, N. A. *J. Am. Chem. Soc.* **1968**, *90*, 5318.

46. (a) Griesbeck, A. G.; Mauder, H.; Stadtmuller, S. *Acc. Chem. Res.* **1994**, *27*, 70. (b) Griesbeck, A. G.; Stadtmuller, S. *J. Am. Chem. Soc.* **1991**, *113*, 6923. (c) Griesbeck, A. G.; Stadtmuller, S. *J. Am. Chem. Soc.* **1990**, *112*, 1281.

Chapter 3: Studies Directed Toward the Total Synthesis of Chebulagic Acid II: Synthesis of an Advanced Intermediate Containing All Stereocenters of Chebulic Acid

3.1. Introduction

3.1.1. Introduction. Chebulagic acid **1**, isolated from the dried fruits of *Terminalia chebula*,[1] is a representative member of the ellagitannin class of natural products, many of which have shown potent biological activity in a variety of pharmacological assays.[2] Chebulagic acid is a nanomolar inhibitor of both calf thymus and human adenocarcinoma topoisomerase I.[3] Both type I and type II topoisomerases have been implicated in regulating transcription by altering the linking number of superhelical DNA. Because it is a potent inhibitor of topoisomerase I, chebulagic acid could be a useful tool in the study of topoisomerase-mediated cellular processes.

3.1.2. Structure of chebulic and chebulagic acids. Chebulagic acid contains a highly acylated glucose core locked in a $^1C_4$ conformation by dicarboxylate substituents at C2-C4 and C3-C5. Both of these substituents are ubiquitous in ellagitannin natural products. The C2-C4 substituent occurs in two tautomeric forms, both of which are present in carpinusnin **3**.[4] The tricarboxylate tautomer chebulic acid **2** also occurs in *Terminalia chebula* extracts.[1c,5] Together, the glucose core of chebulagic acid and the anomeric trihydroxybenzoyl and C3-C5-hexahydroxydiphenoyl substituents comprise the natural product corilagin.[6]

The chebulic acid component of these natural products is highly oxygenated and contains a challenging array of three contiguous stereocenters. Because of the biological relevance of chebulagic acid and the many synthetic challenges it poses, we have initiated studies directed toward its total synthesis. This chapter describes efforts directed toward

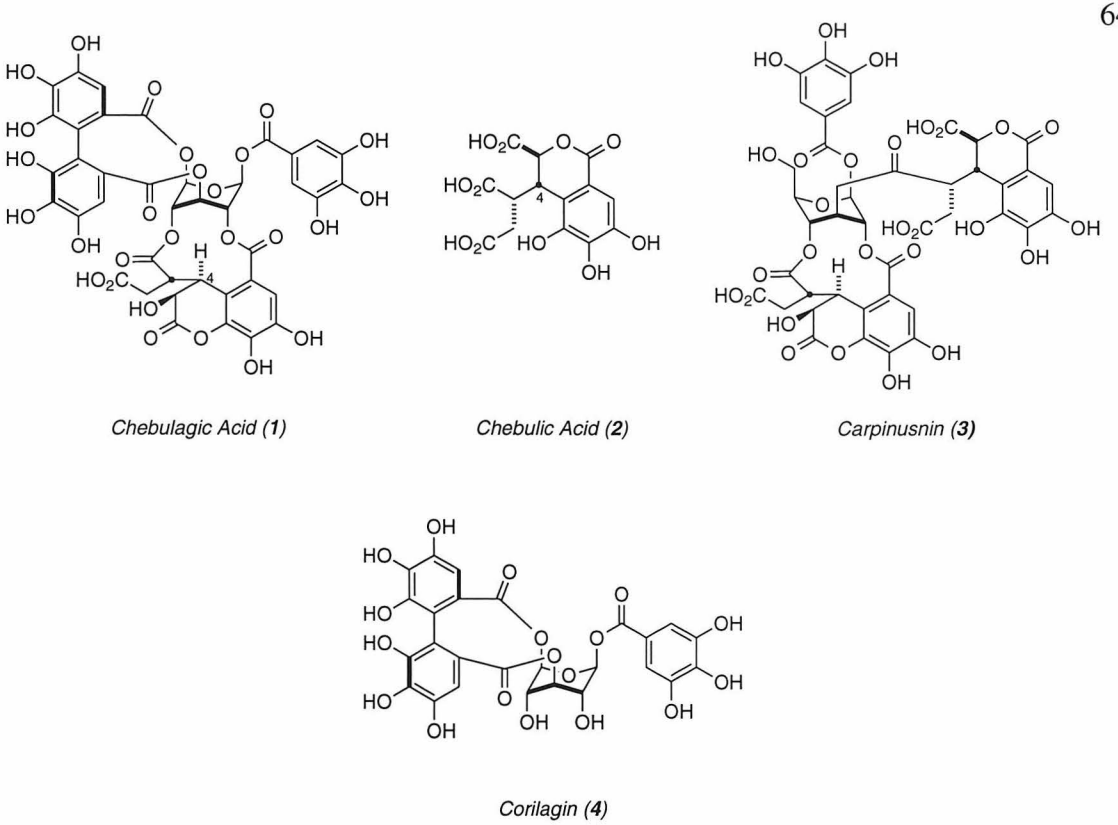

Figure 3.1. Ellagitannin synthesis targets: chebulagic acid (**1**); chebulic acid (**2**); carpinusnin (**3**); corilagin (**4**).

the synthesis of chebulic acid that have culminated in the preparation of an advanced intermediate containing all stereochemical information present in chebulic acid.

3.1.3. Retrosynthetic analysis of chebulic acid. A critical issue in a synthetic program directed at preparation of ellagitannin natural products is the preparation of chebulic acid. The enantioselective [2+2]-photocycloaddition chemistry described in Chapter 2 of this thesis, which provides access to fused polycyclic products in high enantiomeric excess, directly addresses the synthetic challenge posed by the C4 stereocenter of **2**. It was envisioned that intramolecular photocycloaddition of **7** would afford an intermediate such as **6** with the correct relative and absolute stereochemistry at C4. Cleavage of the exocyclic olefin of the photoproduct, ring expansion of the

Scheme 3.1. Retrosynthetic design for chebulic acid employing [2+2]-intramolecular photocycloaddition.

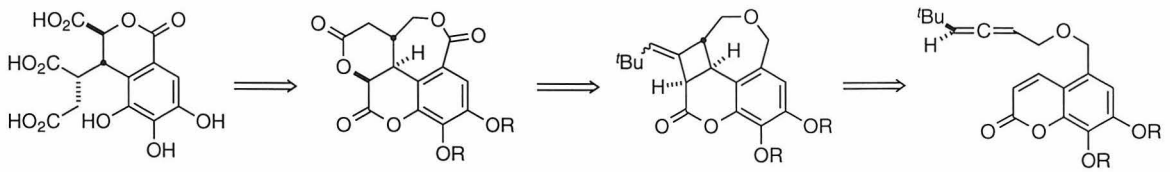

cyclobutanone, and oxidation to the tricarboxylate would afford a **5**, a protected form of **2** suitable for the synthesis of chebulagic acid **1**.

3.2. Experimental

General procedures: All reagents were commercially obtained except where noted. When appropriate, reagents were purified prior to use. All nonaqueous reactions were performed using oven dried glassware under an atmosphere of dry nitrogen. Photoreactions were performed in Pyrex flasks (λ_{cutoff} = 293 nm) using a Hanovia 450 W Hg medium pressure UV lamp in a water cooled quartz immersion apparatus as the light source. Diethyl ether and tetrahydrofuran were distilled from sodium benzophenone ketyl prior to use. *N,N*-diisopropylethylamine, diisopropylamine, triethylamine, dichloromethane, and pyridine were distilled from calcium hydride prior to use. *N,N*-dimethylformamide was stood over 4 Å molecular sieves prior to use. Hexanes were rendered olefin-free and distilled from sodium prior to use. Methanol was distilled from magnesium methoxide prior to use. Chromatographic purification of products was accomplished using forced flow chromatography on Baker 7024-R silica gel according to the method of Still.[7] NMR spectra were recorded on a Bruker AM-500 operating at 500, 471, 126, and 77 MHz for ^{1}H, ^{19}F, ^{13}C, and ^{2}H respectively, a JEOL GSX-400 operating at 400 and 100 MHz for ^{1}H and ^{13}C, respectively, or a General Electric QE Plus operating at 300 and 75 MHz for ^{1}H and ^{13}C, respectively. ^{1}H NMR, ^{2}H NMR, and ^{13}C NMR

spectra are referenced to internal solvent signals. ^{19}FNMR spectra are referenced to external C_6H_5F. Data for ^{1}H are reported as follows: chemical shift (δ ppm), integration, multiplicity (s = singlet, d = doublet, t = triplet, q = quartet, m = multiplet), coupling constant (Hz), and assignment. The phase sensitive NOESY spectra of ***d*-28** and **52** were recorded at 300 MHz on degassed samples using the TPPI technique with mixing times of 2.0 sec, recycle delays of 0.9 sec, F2 spectral widths of 2173 Hz and F1 spectral widths of 2164 Hz, and initial matrix sizes of 256 x 1024 points which were transformed into a 512 x 512 matrices after symmetrization. The phase sensitive NOESY spectrum of **61** was recorded at 500 MHz on a degassed sample using the TPPI technique with a mixing time of 0.5 sec, a recycle delay of 2.0 sec, F2 and F1 spectral widths of 3597 Hz, and initial and final matrix sizes of 2048 x 2048 points and was symmetrized. IR spectra were recorded on a Perkin-Elmer 1600 Series spectrometer. Optical rotations were determined on a JASCO DIP-181 polarimeter operating at the sodium D line and are reported as follows: $[\alpha]_D^{23}$, concentration (g/100 mL), and solvent. Elemental analyses were performed by the Elemental Analysis Facility, Department of Chemistry, California Institute of Technology. Molecular mechanics simulations were performed with MacroModel[8] running on a Silicon Graphics Indigo[2] R10000 High Impact workstation.

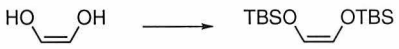

70

70: TEA (4.05 mL, 29.1 mmol, 2.4 equiv), TBSCl (4.39 g, 29.1 mmol, 2.4 equiv), and 4-DMAP (148 mg, 1.2 mmol, 0.1 equiv) were added to a solution of 1.00 mL (12.1 mmol, 1.0 equiv) *cis*-2-butene-1,4-diol in 10 mL CH_2Cl_2 at 0 °C. The resulting solution was stirred for 2 h at 23 °C, poured into 20 mL 1.0 M aqueous KH_2PO_4, and extracted with 3 x 10 mL Et_2O. The combined organic layers were dried over anhydrous $MgSO_4$ and concentrated *in vacuo*. The residue was purified by chromatography on silica gel (40 x 100 mm, 10:1 hexanes–Et_2O, R_f 0.30) to afford 2.91 g (76%) of **70** as a clear, colorless oil.

8

8: A solution of 9.31 g (16.4 mmol, 1.0 equiv) of **70** and 90 mg of Sudan Red III in 90 mL CH_2Cl_2 at -78 °C was treated with a dilute stream of ozone in oxygen until the red color discharged (3.6 h). Nitrogen was bubbled through the reaction mixture to remove excess ozone and 18 mL Me_2S was added. The solution was stirred for 1 h at -78 °C and warmed to 23 °C. The reaction mixture was stirred for 2 h at 23 °C and concentrated *in vacuo*. The residue was purified by distillation (500 mTorr, 47 °C) to afford 3.3 g (58%) of **8** as a clear, colorless oil. ^{1}H NMR (300 MHz, $CDCl_3$) δ 9.72 (1H, t, *J* = 2.0 Hz, C*H*O), 4.11 (2H, d, *J* = 2.1 Hz, CH_2), 0.96 (9H, s, Si(CH_3)$_3$), 0.08 (6H, s, Si(CH_3)$_2$) ppm.

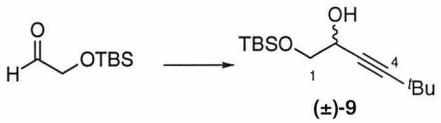

(±)-9

(±)-9: A 1.7 M solution of ^{t}BuLi in *n*-pentane (18.7 mL, 31.8 mmol, 1.72 equiv) was added dropwise *via* cannula to a solution of 3.94 mL (32.0 mmol, 1.73 equiv) *tert*-butylacetylene in 175 mL Et_2O at -78 °C. The resulting solution was stirred at -78 °C for 2.5 h, and 5.85 g (18.5 mmol, 1.0 equiv) of **8** was added. The reaction mixture was allowed to warm to 23 °C and poured into 100 mL H_2O. The aqueous layer was extracted with 2 x 50 mL Et_2O and the combined organic layers were dried over anhydrous $MgSO_4$ and concentrated *in vacuo*. The residue was purified by chromatography on silica gel (40 x 100 mm, 8:1 hexanes–EtOAc, R_f 0.31) to afford 4.74 g (56%) of **(±)-9** as a clear, colorless oil. ^{1}H NMR (300 MHz, $CDCl_3$) δ 4.38 (1H, dt, *J* = 7.6, 3.8 Hz, C2*H*), 3.72 (1H, dd, *J* = 13.9, 3.9 Hz, one of C1H_2), 3.58 (1H, dd, *J* = 13.7, 7.7 Hz, one of C1H_2), 2.54 (1H, d, *J* = 3.7 Hz, O*H*), 1.22 (9H, s, C5(CH_3)$_3$), 0.91 (9H, s, Si(CH_3)$_3$), 0.09 (3H, s, one of SiCH_3), 0.08 (3H, s, one of SiCH_3) ppm.

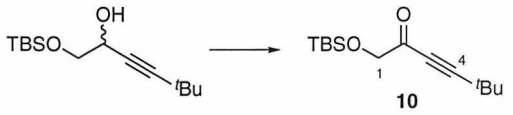

10

10: Dess-Martin periodinane (2.08 g, 4.89 mmol, 2.5 equiv), prepared according to the literature procedure,[9] was added to a solution of 500 mg (1.96 mmol, 1.0 equiv) of **(±)-9** in 10 mL CH_2Cl_2. The resulting solution was stirred at 23 °C for 1 h. Et_2O (10 mL) was added and the precipitate was removed by filtration through Celite. The filtrate was concentrated *in vacuo* and the residue was purified by chromatography on silica gel (20 x 80 mm, 8:1 hexanes–EtOAc, R_f 0.45) to afford 470 mg (95%) of **10** as a clear, colorless oil. ^{1}H NMR (400 MHz, $CDCl_3$) δ 4.28 (2H, s, C1H_2), 1.28 (9H, s, C5(CH_3)$_3$), 0.93 (9H, s, Si(CH_3)$_3$), 0.10 (6H, s, Si(CH_3)$_2$) ppm.

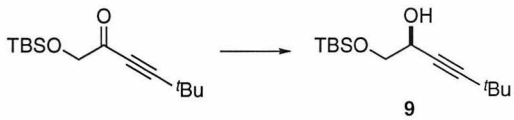

9

9: Neat (+)-β-isopinocampheyl-9-borabicyclo[3.3.1]nonane (403 mg, 1.56 mmol, 2.0 equiv) was added to 197 mg (0.777 mmol, 1.0 equiv) of neat **10**, and the resulting yellow solution was stirred at 23 °C for 12 h. Acetaldehyde (1 mL) was added to the reaction mixture. The resulting solution was stirred for 1 h at 23 °C. The volatiles were removed *in vacuo* at 500 mTorr. The residue was dissolved in 1 mL THF and 3 M aqueous NaOH (0.5 mL) and 30% aqueous H_2O_2 (0.5 mL) were added successively. The reaction mixture was stirred for 2 h and extracted with 3 x 5 mL Et_2O. The combined organic layers were dried over anhydrous Na_2SO_4 and concentrated *in vacuo*. The residue was purified by chromatography on silica gel (20 x 100 mm, 8:1 hexanes–EtOAc, R_f 0.31) to afford 106 mg (53%) of **9** as a clear, colorless oil, spectroscopically and chromatographically identical to **(±)-9**. 4-DMAP (5.0 equiv) and (*R*)-MTPACl (2.0 equiv) were added to 2 mg of **9** in CH_2Cl_2. Integration of the ^{1}H NMR (300 MHz, $CDCl_3$) resonances of the derived (*S*)-

MTPA ester at δ 1.21 (major, C6(CH_3)$_3$) and δ 1.18 (minor, C6(CH_3)$_3$) ppm indicated a diastereomer ratio of 11.9:1.00 (84% ee).

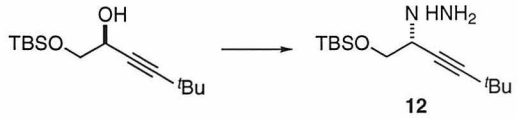

12

13: MsCl (34 μL, 0.444 mmol, 1.1 equiv) was added dropwise to a solution of 103 mg (0.403 mmol, 1.0 equiv) of **9** and 84 μL (0.605 mmol, 1.5 equiv) TEA in 3 mL CH_2Cl_2 at 0 °C. After stirring for 0.5 h, the reaction mixture was transferred *via* cannula into a solution of 2 mL 1:1 MeOH–H_2NNH_2. The reaction mixture was stirred at 23 °C for 18 h and poured into 20 mL water. The aqueous layer was extracted with 2 x 20 mL 95:5 CH_2Cl_2–MeOH. The organic layers were combined, washed with 5 mL saturated aqueous NaCl solution, dried over anhydrous $MgSO_4$, and concentrated *in vacuo*. The residue was used without further purification.

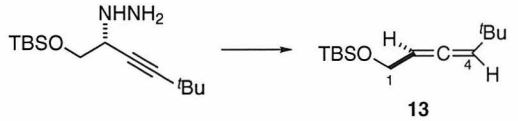

13

The residue was dissolved in 10 mL 1:1 Et_2O–CH_2Cl_2 and cooled to 0 °C. PTAD (141 mg, 0.806 mmol, 2.0 equiv) was added in one portion. When gas evolution was complete, the reaction mixture was washed successively with 1 mL H_2O and 1 mL saturated aqueous NaCl, dried over anhydrous Na_2SO_4, and concentrated *in vacuo*. The residue was purified by chromatography on silica gel (20 x 80 mm, 4:1 *n*-pentane–CH_2Cl_2, R_f 0.48) to afford 68 mg (70%) of **13** as a clear, colorless oil. ^{1}H NMR (500 MHz, $CDCl_3$) δ 5.27 (1H, q, J = 6.3 Hz, C2*H*), 5.20 (1H, dt, J = 6.3, 2.6 Hz, C4*H*), 4.21-4.13 (2H, m, C1H_2), 1.04 (9H, s, C5(CH_3)$_3$), 0.90 (9H, s, SiC(CH_3)$_3$), 0.08 (6H, s, Si(CH_3)$_2$) ppm; ^{13}C NMR (126 MHz, $CDCl_3$) δ 200.7, 104.3, 93.5, 62.2, 31.8, 30.2, 25.9, 18.4, -5.1 ppm; IR (thin film) ν 2960, 2931, 2901, 2857, 1962, 1473, 1463, 1411, 1389, 1362, 1255, 1205, 1190, 1143, 1086, 1048, 1006, 938, 925, 887, 837, 814, 776, 717, 678, 664 cm^{-1}.

14

14: A 1.0 M solution of TBAF in THF (339 μL, 339 mmol, 1.2 equiv) was added to a solution of 68 mg (0.28 mmol, 1.0 equiv) of **13** in 2 mL THF. The resulting solution was stirred for 30 min at 23 °C, diluted with 8 mL Et_2O, and washed with 15 mL H_2O. The aqueous layer was extracted with 5 mL Et_2O and the combined organic layers were dried over anhydrous Na_2SO_4 and concentrated *in vacuo*. The residue was purified by chromatography on silica gel (10 x 60 mm, 4:1 hexanes–EtOAc, R_f 0.27) to afford 31 mg (89%) of **14** as a clear, colorless oil. ^{1}H NMR (500 MHz, $CDCl_3$) δ 5.40 (1H, q, J = 5.9 Hz, C2*H*), 5.32 (1H, dt, J = 6.2, 2.9 Hz, C4*H*), 4.12-4.10 (2H, m, C1H_2), 2.04 (1H, br s, O*H*), 1.05 (9H, s, C5(CH_3)$_3$) ppm; ^{13}C NMR (126 MHz, $CDCl_3$) δ 200.3, 106.1, 93.6, 60.9, 31.8, 30.1 ppm; IR (thin film) ν 3332, 2960, 2903, 2866, 1961, 1742, 1727, 1475, 1462, 1412, 1389, 1363, 1253, 1206, 1190, 1119, 1049, 1013, 941, 870, 740, 692 cm^{-1}.

15

15: MsCl (265 μL, 3.42 mmol, 1.2 equiv) was added dropwise *via* syringe to a solution of 600 μL (4.32 mmol, 1.5 equiv) TEA and 361 mg (2.86 mmol, 1.0 equiv) of **14** in 6 mL 1:1 hexanes–CH_2Cl_2 at 0 °C. The reaction mixture was stirred at 0 °C for 15 min, filtered, and concentrated *in vacuo*. The residue was purified by chromatography on silica gel (20 x 30 mm, 2:1 hexanes–CH_2Cl_2 with 2% v/v TEA) to afford 453 mg (78%) of **15** as a clear, colorless oil that was used immediately.

16

16: TBSCl (28.2 g, 0.187 mol, 1.05 equiv) was added to a solution of 37.1 mL (0.267 mol, 1.5 equiv) TEA and 10.0 g (0.178 mol, 1.0 equiv) propargyl alcohol in 230 mL CH_2Cl_2 at 0 °C. After addition was complete the resulting solution was stirred for 15 min at 0 °C and poured into 100 mL 1.0 M aqueous KH_2PO_4. The aqueous layer was extracted with 2 x 50 mL Et_2O. The organic layers were combined, dried over anhydrous $MgSO_4$, and concentrated *in vacuo*. The residue was purified by distillation (20 Torr, 97 °C) to afford 18.5 g (61%) of **16** as a clear, colorless oil. ^{1}H NMR (300 MHz, C_6D_6) δ 4.06 (2H, d, J = 2.3 Hz, C3H_2), 1.99 (1H, t, J = 2.3 Hz, C1H), 0.93 (9H, s, SiC(CH_3)$_3$), 0.04 (6H, s, Si(CH_3)$_2$) ppm; ^{13}C NMR (75 MHz, C_6D_6) δ 83.7, 74.1, 52.5, 26.9, 19.3, -4.1 ppm; IR (thin film) ν 3313, 2956, 2930, 2886, 2858, 2122, 1472, 1390, 1362, 1257, 1099, 1006, 939, 923, 837, 778, 725, 667 cm^{-1}.

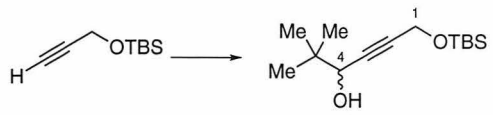

17

17: A solution of 3.45 g (20.3 mmol, 2.2 equiv) of **16** in 40 mL THF was cooled to -78 °C, and 5.94 mL (18.4 mmol, 2.0 equiv) of a 3.1 M solution of MeMgBr in Et_2O was added dropwise *via* syringe, resulting in the formation of a white precipitate. When addition was complete the reaction mixture was allowed to warm to 23 °C, whereupon the precipitate dissolved. After stirring for 2.5 h at 23 °C the reaction mixture was cooled to -78 °C and 1.0 mL (9.2 mmol, 1.0 equiv) trimethylacetaldehyde was added in one portion. The reaction mixture was allowed to warm to 23 °C. When warming was complete 40 mL saturated aqueous NH_4Cl solution was added and the layers were separated. The organic layer was diluted with 20 mL hexanes and washed with 20 mL saturated aqueous NaCl solution. The aqueous layers were combined and extracted with 3 x 60 mL Et_2O. The

combined organic layers were dried over anhydrous Na_2SO_4 and concentrated *in vacuo*. The residue was purified by chromatography on silica gel (40 x 90 mm, 8:1 hexanes–EtOAc, R_f 0.35) to afford 2.06 g (87%) of **17** as a clear, colorless oil. ^{1}H NMR (500 MHz, $CDCl_3$) δ 4.36 (2H, d, J = 1.8 Hz, C1H_2), 4.04 (1H, t, J = 1.7 Hz, C4H), 1.66 (1H, br s, OH), 0.99 (9H, s, C5(CH_3)$_3$), 0.91 (9H, s, SiC(CH_3)$_3$), 0.12 (6H, s, Si(CH_3)$_2$) ppm; ^{13}C NMR (126 MHz, $CDCl_3$) δ 84.5, 84.4, 71.5, 51.7, 35.8, 25.8, 25.3, 18.8, -5.1 ppm; IR (thin film) ν 3440, 2955, 2930, 2859, 1472, 1463, 1391, 1364, 1322, 1256, 1221, 1190, 1130, 1085, 1041, 1007, 938, 898, 837, 814, 778, 724, 666 cm^{-1}.

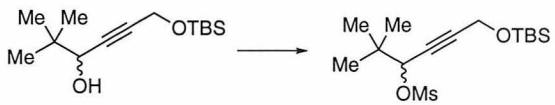

18

19: MsCl (1.12 mL, 14.5 mmol, 1.2 equiv) was added dropwise *via* syringe to a solution of 2.51 mL (18.1 mmol, 1.5 equiv) TEA and 2.06 g (12.1 mmol, 1.0 equiv) of **17** in 100 mL CH_2Cl_2 at 0 °C. The resulting solution was stirred for 35 min at 0 °C and poured into 50 mL 1.0 M aqueous KH_2PO_4. The aqueous layer was extracted with 3 x 20 mL Et_2O. The combined organic layers were dried over anhydrous Na_2SO_4 and concentrated *in vacuo*. The residue was used without further purification.

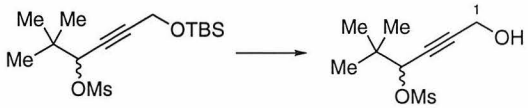

19

The residue was dissolved in 9 mL of a previously prepared solution of 7% concentrated aqueous HF in 63:1 CH_3CN:H_2O. The reaction mixture was stirred at 23 °C for 45 min and poured into 100 mL H_2O. The aqueous layer was extracted with 3 x 50 mL Et_2O. The combined organic layers were washed with 100 mL saturated aqueous $NaHCO_3$, dried over anhydrous Na_2SO_4, and concentrated *in vacuo*. The residue was purified by chromatography on silica gel (40 x 90 mm, 1.3:1 hexanes–EtOAc, R_f 0.20) to afford 1.53

g (93%) of **19** as a clear, colorless oil. ^{1}H NMR (400 MHz, $CDCl_3$) δ 4.87 (1H, t, J = 1.8 Hz, C4*H*), 4.35 (2H, d, J = 1.8 Hz, C1H_2), 3.12 (3H, s, SCH_3), 2.00 (1H, br s, O*H*), 1.05 (9H, s, C5(CH_3)$_3$) ppm; ^{13}C NMR (100 MHz, $CDCl_3$) δ 87.6, 80.2, 79.7, 50.8, 39.1, 35.9, 25.4 ppm; IR (thin film) ν 3520, 3028, 2972, 2939, 2874, 1732, 1713, 1482, 1466, 1416, 1398, 1360, 1252, 1226, 1196, 1173, 1138, 1034, 1019, 976, 944, 920, 904, 853, 779, 754 cm^{-1}.

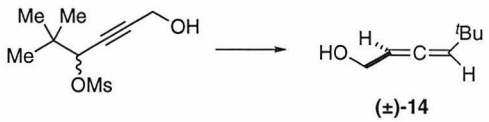

(±)-14

(±)-14: A 1.0 M solution of $LiAlH_4$ in THF (13.9 mL, 13.9 mmol, 2.0 equiv) was added *via* cannula to a solution of 1.53 g (6.95 mmol, 1.0 equiv) of **19** in 90 mL Et_2O at -78 °C. The resulting solution was stirred at 0 °C for 2 h, poured into 45 mL saturated aqueous NH_4Cl which had been cooled to 0 °C, and extracted with 5 x 20 mL Et_2O. The combined organic layers were dried over anhydrous Na_2SO_4, and the residue was purified by chromatography on silica gel (20 x 40 mm, 40:1 CH_2Cl_2–Et_2O, R_f 0.45) to afford 715 mg (82%) **(±)-14** as a clear, colorless oil, spectroscopically and chromatographically identical to **14**.

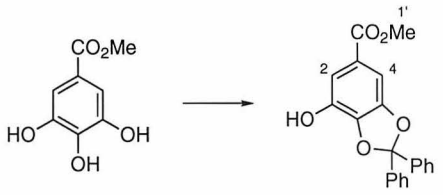

20

20: Ketal **20** was prepared using a modification of the literature procedure.[10] Methyl gallate hydrate (71.5 g, 0.384 mol, 1.0 equiv) was added to 91.6 g (0.384 mol, 1.0 equiv) freshly distilled neat dichlorodiphenylmethane and the resulting slurry was heated to 180 °C with stirring. When gas evolution ceased the reaction was cooled to 23 °C under nitrogen and the resulting glassy solid dissolved in the minimum amount of Et_2O (600 mL). The

solution was washed with 100 mL saturated aqueous $NaHCO_3$ solution, filtered through a pad (2 cm x 5 cm) of silica gel, concentrated to 200 mL *in vacuo*, diluted with 100 mL hexanes, and cooled to 0 °C. The product was collected by filtration. Recrystallization (2:1 hexanes–EtOAc, 60 °C to -20 °C) afforded 100.1 g (74%) of **20** as a white, crystalline solid. ^{1}H NMR (300 MHz, $CDCl_3$) δ 7.59-7.55 (4H, m, four of diphenyl ketal H_{arom}), 7.40-7.37 (6H, m, six of diphenyl ketal H_{arom}), 7.33 (1H, d, J = 1.5 Hz, C2*H* or C6H), 7.22 (1H, d, J = 1.5 Hz, C2*H* or C6H), 5.19 (1H, s, O*H*), 3.86 (3H, s, C1'H_3) ppm; ^{13}C NMR (75 MHz, $CDCl_3$) δ 166.9, 148.3, 139.4, 139.1, 138.2, 129.3, 128.3, 126.3, 124.1, 118.7, 114.2, 103.2, 52.3 ppm; IR (thin film) ν 3316, 2951, 1691, 1638, 1574, 1557, 1540, 1509, 1439, 1384, 1330, 1248, 1207, 1093, 1076, 1041, 1016, 946, 914, 872, 845, 823, 765, 695 cm^{-1}.

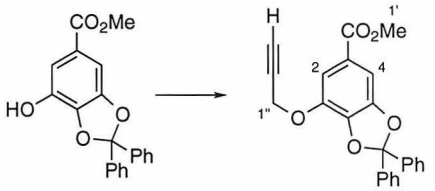

21

21: A solution of 266.2 g (764 mmol, 1.0 equiv) of **20**, 116.2 g K_2CO_3 (841 mmol, 1.1 equiv), and 125 g (841 mmol, 1.1 equiv) of an 80% solution of propargyl bromide in toluene in 1.53 L acetone was stirred at reflux for 11 h, cooled to 23 °C, filtered through Celite, concentrated to 600 mL, and filtered through Celite again. The volatiles were removed *in vacuo*. Recrystallization from hexanes–EtOAc afforded 242.2 g (82%) of **21** as a white, crystalline solid, mp 94-95 °C. ^{1}H NMR (300 MHz, $CDCl_3$) δ 7.60-7.57 (4H, m, four of diphenyl ketal H_{arom}), 7.43 (1H, d, J = 1.4 Hz, C2*H* or C6H), 7.40-7.37 (6H, m, six of diphenyl ketal H_{arom}), 7.32 (1H, d, J = 1.4 Hz, C2*H* or C6H), 4.85 (2H, d, J = 2.4 Hz, C$^{1"}H_2$), 3.87 (3H, s, C1'H_3), 2.53 (1H, t, J = 2.4 Hz, C$^{3"}H$) ppm; ^{13}C NMR (75 MHz, $CDCl_3$) δ 165.8, 148.3, 140.6, 139.7, 139.2, 129.1, 128.0, 126.0, 124.1, 118.5, 112.3, 104.4, 77.8, 76.2, 57.1, 51.8 ppm; IR (thin film) ν 3290, 3062, 3032, 2950,

2123, 1715, 1633, 1606, 1586, 1506, 1435, 1381, 1320, 1266, 1244, 1205, 1181, 1159, 1114, 1044, 1021, 1001, 981, 948, 917, 868, 825, 764, 733, 698, 642 cm^{-1}. Elemental analysis calculated for $C_{24}H_{18}O_5$ C 74.60%, H 4.70%, found C 74.36%, H 4.56%.

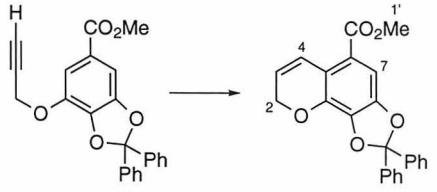

22

22: A solution of 46.5 g (0.120 mol) of **21** in 500 mL *N,N*-dimethylaniline was refluxed for 24 h. The solvent was removed by distillation *in vacuo* and the residue was purified by chromatography on silica gel (80 x 300 mm, 1.5:1 hexanes–CH_2Cl_2, R_f 0.22) to afford 29.2 g (63%) of **22** as a white solid. ^{1}H NMR (300 MHz, $CDCl_3$) δ 7.60-7.56 (4H, m, four of diphenyl ketal H_{arom}), 7.40-7.35 (7H, m, six of diphenyl ketal H_{arom} and C4*H*), 7.15 (1H, s, C7*H*), 5.86 (1H, dt, J = 10.3, 3.8 Hz, C3*H*), 4.81 (2H, dd, J = 3.8, 1.9 Hz, C4*H*), 3.85 (3H, s, C1'H_3) ppm; ^{13}C NMR (75 MHz, $CDCl_3$) δ 166.6, 147.6, 139.4, 137.8, 137.3, 129.3, 128.3, 126.3, 123.1, 121.6, 120.7, 119.9, 118.7, 104.1, 65.0, 52.0 ppm; IR (thin film) ν 3031, 3062, 2950, 2846, 1715, 1632, 1601 cm^{-1}. Elemental analysis calculated for $C_{24}H_{18}O_5$ C 74.60%, H 4.70%, found C 74.50%, H 4.53%.

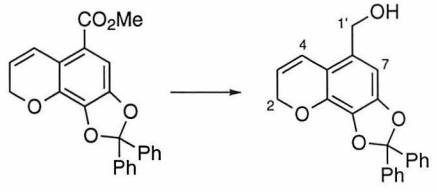

23

23: $LiAlH_4$ (12.2 g, 322 mmol, 1.0 equiv) was added to a mechanically stirred solution of 124.4 g (322 mmol, 1.0 equiv) of **22** in 600 mL Et_2O at 0 °C at a rate such that the internal temperature was maintained below 10 °C. The reaction mixture was stirred for 5 min and 12.2 mL H_2O was added dropwise at a rate such that the internal temperature was maintained below 10 °C. The reaction mixture was stirred for 15 min and 12.2 mL 15%

NaOH was added. The resulting slurry was stirred for 1 h and filtered through Celite. The filtrate was washed with 200 mL Et_2O and the combined eluents were concentrated *in vacuo*. Recrystallization from hexanes–EtOAc afforded 91.9 g (79%) of **23** as a white, crystalline solid, mp 120-121 °C. ^{1}H NMR (500 MHz, $CDCl_3$) δ 7.61-7.58 (4H, m, four of diphenyl ketal H_{arom}), 7.39-7.31 (6H, m, six of diphenyl ketal H_{arom}), 6.67 (1H, dt, J = 10.2, 1.9 Hz, C4*H*), 6.53 (1H, s, C7*H*), 5.75 (1H, dt, J = 10.2, 3.8 Hz, C3*H*), 4.81 (2H, dd, J = 3.8, 1.9 Hz, C2H_2), 4.58 (1H, br s, C1'H_2) ppm; ^{13}C NMR (126 MHz, $CDCl_3$) δ 139.9, 137.8, 133.7, 130.0, 129.1, 128.2, 126.4, 121.3, 120.1, 117.8, 116.4, 102.3, 65.3, 62.6, 62.5 ppm; IR (thin film) ν 3415, 1633, 1490, 1450, 1398, 1291, 1239, 1208, 1129, 1055, 1018, 948, 908, 838, 732, 698, 641 cm^{-1}. Elemental analysis calculated for $C_{23}H_{18}O_4$ C 77.08%, H 5.06%, found C 76.76%, H 4.93%.

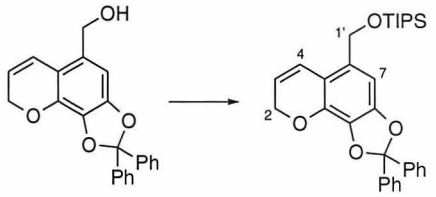

24

24: TEA (53.4 mL, 385 mmol, 1.5 equiv), 4-DMAP (6.3 g, 51 mmol, 0.2 equiv), and TIPSOTf (78.1 g, 256 mmol, 1.0 equiv) were added successively to a solution of 91.9 g (256 mmol, 1.0 equiv) of **23** in 763 mL CH_2Cl_2 at 0 °C. The resulting solution was stirred at 23 °C for 12 h and poured into 500 mL 1.0 M aqueous KH_2PO_4. The aqueous layer was extracted with 2 x 500 mL Et_2O. The organic layers were combined, dried over anhydrous Na_2SO_4, and concentrated *in vacuo*. The residue was purified by chromatography on silica gel (60 x 200 mm, 6:1 hexanes–CH_2Cl_2, R_f 0.25) to afford 127.5 g (97%) of **24** as a clear, colorless oil. ^{1}H NMR (500 MHz, $CDCl_3$) δ 7.61-7.59 (4H, m, four of diphenyl ketal H_{arom}), 7.38-7.33 (6H, m, six of diphenyl ketal H_{arom}), 6.67 (1H, s, C7*H*), 6.55 (1H, dt, J = 10.2, 0.3 Hz, C4*H*), 5.70 (1H, dt, J = 10.1, 3.6 Hz, C3*H*), 4.79 (2H, dd, J = 3.6, 0.3 Hz, C2H_2), 4.73 (1H, s, C1'H_2), 1.17 (3H, septuplet, J = 6.8 Hz, Si(C*H*$(CH_3)_2)_3$), 1.08

(18H, d, J = 6.8 Hz, Si(CH(CH_3)$_2$)$_3$) ppm; ^{13}C NMR (126 MHz, $CDCl_3$) δ 148.3, 140.2, 137.4, 132.7, 131.0, 129.0, 128.1, 126.4, 121.3, 119.2, 117.4, 115.0, 100.8, 65.1, 62.5, 18.1, 17.7, 12.1 ppm; IR (thin film) ν 3424, 2942, 2864, 1636, 1490, 1462, 1450, 1399, 1294, 1235, 1209, 1180, 1129, 1055, 1019, 948, 916, 882, 842, 798, 777, 760, 697, 642 cm^{-1}. Elemental analysis calculated for $C_{32}H_{38}O_4Si$ C 74.67%, H 7.44%, found C 74.67%, H 7.81%.

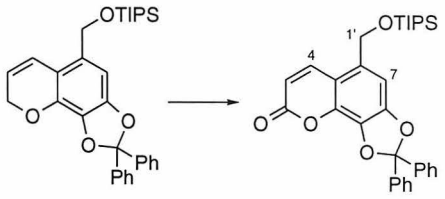

25

25: Celite (103 g), 4 Å molecular sieves (103 g), and PDC (140 g, 371 mmol, 3.0 equiv) were added to a solution of 63.7 g (124 mmol, 1.0 equiv) of **24** in 560 mL CH_2Cl_2. The resulting slurry was stirred at 23 °C for 16 h, poured into 3 L 1:1 *n*-pentane–Et_2O, and filtered. The filtrate was washed with 200 mL Et_2O. The eluents were combined and concentrated *in vacuo*. The residue was purified by recrystallization from hexanes–Et_2O to afford 65.0 g (50%) of **25** as a white, crystalline solid, mp 137-138 °C. ^{1}H NMR (500 MHz, $CDCl_3$) δ 7.89 (1H, d, J = 9.9 Hz, C3H), 7.63-7.61 (4H, m, four of diphenyl ketal H_{arom}), 7.41-7.37 (6H, m, six of diphenyl ketal H_{arom}), 6.98 (1H, s, C7H), 6.23 (1H, d, J = 9.9 Hz, C4H_2), 4.90 (1H, s, C1'H_2), 1.17 (3H, septuplet, J = 6.8 Hz, Si(CH(CH$_3$)$_2$)$_3$), 1.08 (18H, d, J = 6.8 Hz, Si(CH(CH_3)$_2$)$_3$) ppm; ^{13}C NMR (126 MHz, $CDCl_3$) δ 159.8, 150.3, 140.5, 139.4, 138.8, 133.5, 132.5, 129.4, 128.3, 126.2, 119.5, 112.9, 112.2, 104.9, 62.7, 18.0, 12.0 ppm; IR (thin film) ν 3440, 2943, 2865, 1743, 1634, 1494, 1462, 1451, 1409, 1327, 1267, 1209, 1134, 1059, 1021 cm^{-1}. Elemental analysis calculated for $C_{32}H_{36}O_5Si$ C 72.70%, H 6.86%, found C 72.65%, H 6.77%.

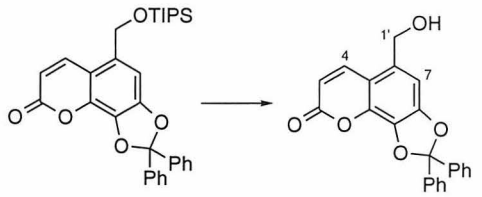

26

26: A 1.0 M solution of TBAF in THF (141 mL, 141 mmol, 1.2 equiv) was added to 62.0 g (117 mmol, 1.0 equiv) of **25** in 540 mL THF. The resulting solution was stirred for 2 h at 23 °C and 1.4 L Et_2O and 500 mL 1.0 M aqueous KH_2PO_4 was added. The aqueous layer was extracted with 2 x 200 mL Et_2O. The organic layers were combined, dried over anhydrous Na_2SO_4, and concentrated *in vacuo*. The residue was purified by recrystallization from hexanes–$CHCl_3$ to afford 42.7 g (98%) of **26** as a white solid. ^{1}H NMR (500 MHz, $CDCl_3$) δ 7.96 (1H, d, J = 9.9 Hz, C3*H*), 7.62–7.60 (4H, m, four of diphenyl ketal H_{arom}), 7.40–7.38 (6H, m, six of diphenyl ketal H_{arom}), 6.92 (1H, s, C7*H*), 6.27 (1H, d, J = 9.9 Hz, C4*H*), 4.81 (2H, br s, C1'H_2), 1.61–1.50 (1H, br s, O*H*) ppm; IR (thin film) ν 3421, 2959, 2924, 2854, 1737, 1718, 1707, 1687, 1654, 1636, 1570, 1561, 1544, 1524, 1492, 1458, 1450, 1407, 1325, 1266, 1207, 1182, 1138, 1106, 1078, 1048, 1018, 950, 916, 866, 823, 769, 730, 697 cm^{-1}. Elemental analysis calculated for $C_{23}H_{16}O_5$ C 74.19%, H 4.33%, found C 74.00%, H 4.39%.

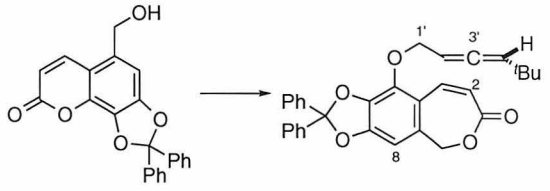

27

27: A 25 mL round-bottom flask was charged with 76 mg (2.5 mmol, 1.2 equiv) of an 80% dispersion of NaH in mineral oil. The dispersion was washed 3 times with anhydrous hexanes, and dried briefly under *in vacuo*. A nitrogen atmosphere was reestablished and 5 mL DMF was added. The solution was cooled to 0 °C, and 786 mg (2.1 mmol, 1.0 equiv) of **26** was added as a solution in 1 mL DMF *via* cannula. Fifteen

minutes after gas evolution ceased 450 mg (2.2 mmol, 1.1 equiv) of **15** was added, and the mixture stirred at 23 °C for 12 hours. The reaction mixture was diluted with 20 mL H_2O, and extracted 3 x 10 mL Et_2O. The organic layers were combined, washed with 10 mL saturated aqueous NaCl, dried over anhydrous $MgSO_4$, and concentrated *in vacuo*. The residue was purified by chromatography on silica gel (60 x 250 mm, 1.8:1 hexanes–Et_2O, R_f 0.23) to afford 560 mg (55%) of **27** as a clear, colorless oil. ^{1}H NMR (500 MHz, $CDCl_3$) δ 7.58-7.53 (4H, m, four of diphenyl ketal H_{arom}), 7.48 (1H, d, J = 12.3 Hz, C2*H*), 7.42-7.36 (6H, m, six of diphenyl ketal H_{arom}), 6.70 (1H, s, C8*H*), 6.22 (1H, d, J = 12.3 Hz, C3*H*), 5.40 (1H, q, J = 6.5 Hz, C2'*H*), 5.17 (1H, dt, J = 6.2, 2.2 Hz, C4'*H*), 4.91-4.82 (4H, m, C10H_2 and C1'H_2), 0.92 (9H, s, C5'(CH_3)$_3$) ppm; ^{13}C NMR (126 MHz, $CDCl_3$) δ 203.0, 168.2, 150.1, 140.1, 139.3, 137.1, 135.7, 131.2, 129.5, 128.4, 126.3, 123.1, 119.8, 118.5, 104.8, 103.7, 89.3, 70.9, 68.5, 31.7, 29.9 ppm; IR (thin film) ν 3062, 2959, 2926, 2862, 1963, 1713, 1622, 1614, 1592, 1488, 1453, 1383, 1304, 123.8, 1209, 1116, 1086, 1045, 1021, 949, 818, 762, 699 cm^{-1}.

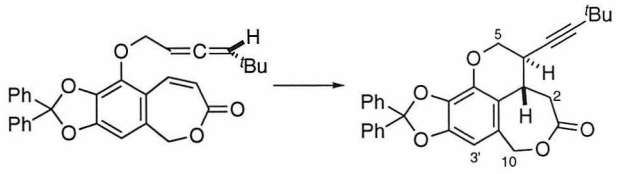

28

28: A 250-mL Pyrex flask equipped with a Teflon valve was charged with a solution of 250 mg of **27** in 167 mL CH_2Cl_2. The solution was degassed by freeze-pump-thaw to an overpressure of 10 mTorr and irradiated with a Hanovia 450 W Hg medium pressure lamp at 0 °C for 4 h. The volatiles were removed *in vacuo* and the residue was purified by chromatography on silica gel (20 x 100 mm, 3:1 hexanes–EtOAc, R_f 0.33) to afford 146 mg (58%) of **28** as a white solid. ^{1}H NMR (500 MHz, C_6D_6) δ 7.70-7.61 (4H, m, four of diphenyl ketal H_{arom}), 7.08-6.97 (6H, m, six of diphenyl ketal H_{arom}), 6.07 (1H, s, C3'*H*), 4.52 (1H, d, J = 14.0, one of C10H_2), 4.43 (1H, d, J = 14.0 Hz, one of C10H_2), 3.69

(1H, dd, J = 10.6, 5.5 Hz, one of C5H_2), 3.65 (1H, dd, J = 10.6, 3.4 Hz, one of C5H_2), 2.84 (1H, dd, J = 15.4, 12.3 Hz, one of C2H_2), 2.76 (1H, dd, J = 15.5, 4.0 Hz, one of C2H_2), 2.71 (1H, dt, J = 12.2, 4.0 Hz, C3H), 2.30-2.27 (1H, m, C4H), 0.97 (9H, s, C(CH_3)$_3$) ppm; ^{13}C NMR (126 MHz, C_6D_6) δ 171.3, 147.2, 140.8, 140.7, 139.1, 135.3, 129.3, 129.2, 128.5, 128.4, 126.7, 118.2, 117.7, 102.3, 94.3, 74.4, 68.8, 67.7, 38.3, 33.2, 31.3, 30.9, 27.4 ppm; IR (thin film) ν 3063, 3032, 2967, 2927, 2900, 2866, 2280, 2268, 1746, 1732, 1716, 1637, 1496, 1471, 1450, 1392, 1372, 1337, 1315, 1286, 1262, 1240, 1209, 1181, 1128, 1113, 1095, 1083, 1045, 1020, 1002, 949, 921, 906, 834, 812, 778, 764, 700, 676, 660, 642, 629, 616 cm^{-1}; The above reaction was similarly performed on 12 mg of **27** of 85% ee, affording 6.0 mg (50%) of **28**, which was dissolved in 1.5 mL THF and cooled to 0 °C. A 2.0 M solution of $LiBH_4$ in THF (13.2 μL, 26.4 μM, 2.1 equiv) was added to the solution. The reaction mixture was stirred at 0 °C for 30 min, poured into 2 mL 1.0 M aqueous KH_2PO_4, and extracted with 5 mL Et_2O. Concentration *in vacuo* and chromatography on silica gel (4 x 20 mm, 1:1 hexanes–EtOAc, R_f 0.19) afforded 4 mg (80%) of a diol, **30**, which was treated with 4-DMAP (10 equiv) and (*R*)-MTPACl (4.0 equiv) in CH_2Cl_2. Integration of the ^{1}H NMR (500 MHz, $CDCl_3$) resonances of the derived (*S*)-MTPA ester **31** at δ 5.17 (major, one of C10H_2) and δ 5.12 (minor, one of C10H_2) ppm indicated a diastereomer ratio of 16.1:1.00 (88% ee).

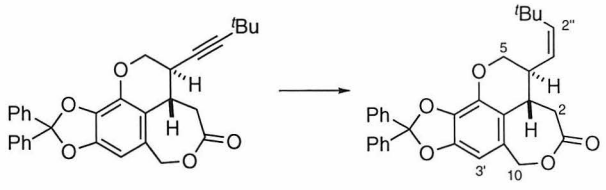

29

29: A slurry of 90 mg (0.187 mmol, 1.0 equiv) of **28** in 9 mL pyridine and 90 mg of 5% palladium on carbon was stirred at 23 °C under 1 atm of H_2 for 2 h. The reaction mixture was filtered through Celite, and the filtrate concentrated *in vacuo*. The residue was dissolved in 10 mL *n*-heptane and concentrated *in vacuo* to remove residual pyridine. The

residue was purified by chromatography on silica gel (20 x 100 mm, 1:1 hexanes–Et_2O, R_f 0.32) to afford 85 mg (94%) of **29** as a white solid. ^{1}H NMR (500 MHz, C_6D_6) δ 7.79-7.69 (4H, m, four of diphenyl ketal H_{arom}), 7.08-6.98 (6H, m, six of diphenyl ketal H_{arom}), 6.01 (1H, s, C3'*H*), 5.28 (1H, d, *J* = 12.2 Hz, C2"*H*), 4.81 (1H, t, *J* = 11.8 Hz, C1"*H*), 4.58 (1H, d, *J* = 14.4 Hz, one of C10H_2), 4.31 (1H, d, *J* = 14.5, one of C10H_2), 3.78 (1H, dd, *J* = 12.0, 3.5 Hz, one of C5H_2), 3.68 (1H, dd, *J* = 10.6, 3.0 Hz, one of C5H_2), 2.93-2.90 (1H, m, C3*H*), 2.67 (1H, t, *J* = 13.6 Hz, one of C2H_2), 2.59-2.56 (1H, m, C4*H*), 2.40 (1H, dd, *J* = 14.4, 3.0 Hz, one of C2H_2), 0.88 (9H, s, C3"(CH_3)$_3$) ppm; ^{13}C NMR (100 MHz, $CDCl_3$) δ 173.4, 146.7, 144.9, 139.8, 139.7, 138.7, 133.8, 130.2, 129.8, 129.2, 128.2, 127.4, 126.4, 126.3, 122.2, 116.8, 102.3, 70.0, 69.6, 37.4, 35.8, 33.7, 33.6, 31.4 ppm; IR (thin film) ν 3440, 2960, 1732, 1635, 1496, 1470, 1450, 1388, 1365, 1336, 1288, 1236, 1209, 1114, 1044, 1020, 949, 920, 752, 699 cm^{-1}.

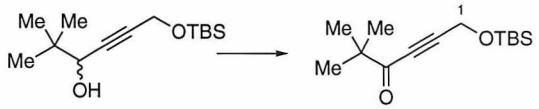

32

32: Dess-Martin periodinane (1.91 g, 4.5 mmol, 1.5 equiv), prepared according to the literature procedure,[9] was added to a solution of 662 mg (3.0 mmol, 1.0 equiv) in 13 mL CH_2Cl_2. The resulting solution was stirred at 23 °C for 20 min and 40 mL Et_2O was added. The mixture was filtered and the eluent was concentrated *in vacuo*. The residue was purified by chromatography on silica gel (20 x 100 mm, 8:1 hexanes–EtOAc, R_f 0.45) to afford 530 mg (70%) of **32** as a clear, colorless oil. ^{1}H NMR (500 MHz, $CDCl_3$) δ 4.49 (2H, s, C1H_2), 1.20 (9H, s, C5(**C**H_3)$_3$), 0.91 (9H, s, SiC(**C**H_3)$_3$), 0.13 (6H, s, Si(**C**H_3)$_2$) ppm; ^{13}C NMR (126 MHz, $CDCl_3$) δ 193.6, 91.9, 82.0, 51.5, 44.7, 25.9, 25.7, 18.2, -5.2 ppm; IR (thin film) ν 2970, 2901, 2859, 2281, 2211, 1675, 1476, 1461, 1392, 1364, 1255, 1139, 1098, 1006, 932, 836, 780, 744, 670 cm^{-1}.

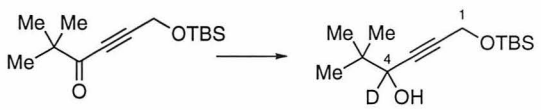

***d*-17**

***d*-17:** A solution of 200 mg (0.786 mmol, 1.0 equiv) of **32** and 49.4 mg (1.18 mmol, 1.5 equiv) $NaBD_4$ in 10 mL MeOH was stirred for 10 min at 23 °C and poured into 50 mL 1.0 M aqueous KH_2PO_4, and extracted with 3 x 50 mL Et_2O. The organic layers were combined and dried over anhydrous Na_2SO_4. Concentration *in vacuo* and chromatography on silica gel (20 x 100 mm, 8:1 hexanes–EtOAc, R_f 0.35) afforded 190 mg (94%) of ***d*-17** as a clear, colorless oil. ^{1}H NMR (500 MHz, $CDCl_3$) δ 4.36 (2H, s, C1H_2), 0.99 (9H, s, C5(CH_3)$_3$), 0.91 (9H, s, SiC(CH_3)$_3$), 0.12 (6H, s, Si(CH_3)$_2$) ppm; ^{2}H NMR (77 MHz, $CDCl_3$) δ 4.04 ppm; ^{13}C NMR (126 MHz, $CDCl_3$) δ 84.4, 84.3, 51.7, 35.7, 25.8, 25.2, 18.3, -5.1 ppm; IR (thin film) ν 3448, 2956, 2930, 2859, 2740, 1473, 1463, 1390, 1364, 1255, 1158, 1093, 1061, 1028, 1011, 981, 936, 836, 814, 778, 736, 666 cm^{-1}.

***d*-18**

***d*-14:** MsCl (69 μL, 0.89 mmol, 1.2 equiv) was added dropwise to a solution of 190 mg (0.74 mmol, 1.0 equiv) of ***d*-17** and 154 μL (1.1 mmol, 1.5 equiv) TEA in 10 mL CH_2Cl_2 at 0 °C. The reaction mixture was stirred at 0 °C for 30 min, poured into 25 mL 1.0 M aqueous KH_2PO_4, and extracted with 3 x 20 mL Et_2O. The organic layers were combined, dried over anhydrous Na_2SO_4, and concentrated *in vacuo*. The residue was used without further purification.

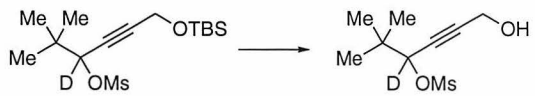

***d*-19**

The residue was dissolved in 2 mL of a previously prepared solution of 7% concentrated aqueous HF in 63:1 CH_3CN:H_2O. The reaction mixture was stirred at 23 °C for 20 min,

poured into 25 mL saturated aqueous $NaHCO_3$, and extracted with 3 x 20 mL Et_2O. The combined organic layers were dried over anhydrous Na_2SO_4 and concentrated *in vacuo*. The residue was dissolved in 10 mL C_6H_6 and concentrated *in vacuo* to effect azeotropic removal of water. The residue was used without further purification.

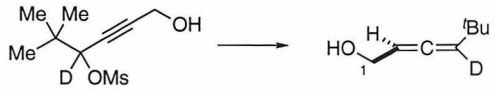

***d*-14**

The residue was dissolved in 10 mL Et_2O, cooled to -78 °C, and1.48 mL (1.48 mmol, 2.0 equiv) of a 1.0 M ethereal solution of $LiAlH_4$ was added. The resulting solution was stirred for 30 min at 0 °C, poured into 45 mL saturated aqueous NH_4Cl which had been cooled to 0 °C, and extracted with 5 x 20 mL Et_2O. The combined organic layers were dried over anhydrous Na_2SO_4, and the residue was purified by chromatography on silica gel (20 x 40 mm, 40:1 CH_2Cl_2–Et_2O, R_f 0.45) to afford 75 mg (88%) of ***d*-14** as a clear, colorless oil. ^{1}H NMR (500 MHz, $CDCl_3$) δ 5.40 (1H, tt, J = 5.8, 0.7 Hz, C2*H*), 4.11 (2H, d, J = 6.2 Hz, C1H_2), 1.05 (9H, s, C5(CH_3)$_3$) ppm; ^{2}H NMR (77 MHz, $CDCl_3$) δ 5.36 ppm; ^{13}C NMR (126 MHz, $CDCl_3$) δ 200.3, 93.7, 60.9, 31.7, 30.1 ppm; IR (thin film) ν 3332, 2960, 2930, 2903, 2866, 1955, 1461, 1363, 1255, 1207, 1157, 1061, 1014, 964, 803 cm^{-1}. Integration of the ^{1}H NMR (500 MHz, $CDCl_3$) resonances at δ 5.40 (C2*H*) and δ 5.32 (residual C4*H*) ppm indicated that the deuteroallene was 96% isotopically pure.

***d*-15**

***d*-15:** MsCl (60 μL, 0.78 mmol, 1.2 equiv) was added dropwise to a solution of 75 mg (0.65 mmol, 1.0 equiv) of ***d*-14** and 140 μL (0.98 mmol, 1.5 equiv) TEA in CH_2Cl_2 at 0 °C. The resulting solution was stirred at 0 °C for 30 min and purified by chromatography

on silica gel (20 x 30 mm, 2:1 hexanes–CH_2Cl_2 with 2% v/v TEA) to afford 130 mg (98%) of ***d*-15** as a clear, colorless oil that was used immediately.

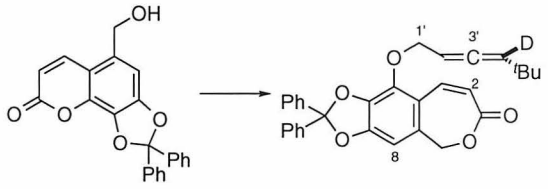

***d*-27**

***d*-27:** A 25 mL round-bottom flask was charged with 28 mg (0.71 mmol, 1.2 equiv) of an 80% dispersion of NaH in mineral oil. The dispersion was washed 3 times with anhydrous hexanes and dried briefly *in vacuo*. A nitrogen atmosphere was reestablished and 9 mL DMF was added. The solution was cooled to 0 °C, and 221 mg (0.59 mmol, 1.0 equiv) of **26** was added as a solution in 1 mL DMF *via* cannula. Fifteen minutes after gas evolution ceased 130 mg (0.65 mmol, 1.1 equiv) of ***d*-15** was added, and the mixture was stirred at 23 °C for 12 hours. The reaction mixture was diluted with 20 mL H_2O, and extracted 3 x 10 mL Et_2O. The organic layers were combined, washed with 10 mL saturated aqueous NaCl, dried over anhydrous $MgSO_4$, and concentrated *in vacuo*. The residue was purified by chromatography on silica gel (20 x 120 mm, 1.8:1 hexanes–Et_2O, R_f 0.23) to afford 80 mg (28%) of ***d*-27** as a clear, colorless oil. ^{1}H NMR (500 MHz, $CDCl_3$) δ 7.58-7.53 (4H, m, four of diphenyl ketal H_{arom}), 7.48 (1H, d, J = 12.3 Hz, C3*H*), 7.42-7.36 (6H, m, six of diphenyl ketal H_{arom}), 6.70 (1H, s, C7*H*), 6.22 (1H, d, J = 12.3 Hz, C4*H*), 5.40 (1H, t, J = 6.5 Hz, C4'*H*), 4.91-4.82 (4H, m, C1'H_2 and C3'H_2), 0.92 (9H, s, C7'(CH_3)$_3$) ppm; ^{2}H NMR (77 MHz, $CDCl_3$) δ 5.23 ppm; ^{13}C NMR (100 MHz, $CDCl_3$) δ 203.0, 168.1, 150.0, 140.0, 139.3, 137.0, 135.6, 131.2, 129.5, 128.3, 126.3, 126.2, 123.1, 119.8, 118.5, 104.8, 103.6, 89.4, 70.9, 68.5, 31.5, 29.8 ppm; IR (thin film) ν 3062, 2960, 2901, 2865, 1953, 1714, 1621, 1592, 1487, 1462, 1452, 1384, 1303, 1266, 1238, 1209, 1182, 1160, 1117, 1088, 1045, 1020, 949, 856, 819, 762, 699, 642 cm^{-1}.

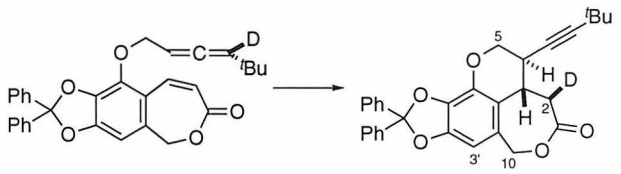

d-28

***d*-28:** A 250-mL Pyrex flask equipped with a Teflon valve was charged with a solution of 50 mg of **27** in 50 mL CH_2Cl_2. The solution was degassed by freeze-pump-thaw to an overpressure of 10 mTorr and irradiated with a Hanovia 450 W Hg medium pressure lamp at 0 °C for 3 h. The volatiles were removed *in vacuo* and the residue was purified by chromatography on silica gel (20 x 100 mm, 3:1 hexanes–EtOAc, R_f 0.33) to afford 25 mg (50%) of **28** as a white solid. ^{1}H NMR (500 MHz, C_6D_6) δ 7.70-7.61 (4H, m, four of diphenyl ketal H_{arom}), 7.08-6.97 (6H, m, six of diphenyl ketal H_{arom}), 6.07 (1H, s, C3'*H*), 4.52 (1H, d, *J* = 14.0, one of C10H_2), 4.43 (1H, d, *J* = 14.0 Hz, one of C10H_2), 3.69 (1H, dd, *J* = 10.6, 5.5 Hz, one of C5H_2), 3.65 (1H, dd, *J* = 10.6, 3.4 Hz, one of C5H_2), 2.84 (1H, d, *J* = 12.3 Hz, one of C2H_2), 2.71 (1H, dd, *J* = 12.2, 4.0 Hz, C3*H*), 2.30-2.27 (1H, m, C4*H*), 0.97 (9H, s, C(CH_3)$_3$) ppm; ^{13}C NMR (126 MHz, C_6D_6) δ 171.3, 147.2, 140.8, 140.7, 139.1, 135.3, 129.3, 129.2, 128.5, 128.4, 126.7, 118.2, 117.7, 102.3, 94.3, 74.4, 68.8, 67.7, 38.3, 33.2, 31.3, 30.9, 27.4 ppm.

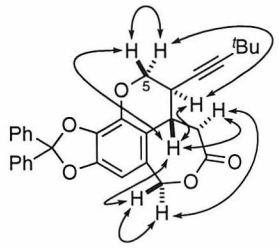

Selected ^{1}H NMR NOESY correlations for ***d*-28** (300 MHz, C_6D_6)

Stereoselectivity of deuterium incorporation upon D$^+$-quenching of enolate derived from 28: A 0.7 M solution of LDA in hexanes–THF (314 μL, 0.22 mmol, 2.0

equiv), prepared by dropwise addition of 448 μL of a 1.6 M solution of ^{n}BuLi in hexanes to 100 μL ^{i}Pr$_2$NH in 354 μL THF at -78 °C, was added dropwise to a solution of 54 mg (0.11 mmol, 1.0 equiv) of **28** in 2 mL THF at -78 °C. The resulting solution was stirred at -78 °C for 1 h and 500 μL D_2O was added. The solution was allowed to warm to 23 °C, poured into 5 mL of 1.0 M aqueous KH_2PO_4, and extracted with 10 mL Et_2O. The organic layer was dried over anhydrous Na_2SO_4 and concentrated *in vacuo*. The residue was dissolved in 10 mL C_6H_6 and concentrated *in vacuo* to effect azeotropic removal of water. The residue was dissolved in 3 mL CH_2Cl_2 and 10 mg trichloroacetic acid was added. The resulting solution was stirred for 5 min and poured into 5 mL saturated aqueous $NaHCO_3$. The organic layer was separated, dried over anhydrous Na_2SO_4, and concentrated *in vacuo*. The residue was purified by chromatography on silica gel (20 x 100 mm, 3:1 hexanes–EtOAc, R_f 0.33) to afford 30 mg (55%) of ***d*-27** as a white solid. Integration of the ^{1}H NMR (500 MHz, C_6D_6) resonances at δ 2.75 ppm (C2H_β), δ 2.80 ppm (C2H_α), and δ 2.66 ppm (C3*H*) with correction for internal return indicated a C2H_α:C2H_β ratio of 1.6:1.

Irradiation of *d*-27 in protic solvent: A 100-mL Pyrex flask equipped with a Teflon valve was charged with a solution of 250 mg ***d*-27** of 96% isotopic purity in 167 mL CH_2Cl_2. The solution was degassed by freeze-pump-thaw to an overpressure of 10 mTorr and irradiated at 0 °C with a Hanovia 450 W Hg medium pressure lamp for 3 h. The volatiles were removed *in vacuo* and the residue was purified by chromatography on silica gel (20 x 100 mm, 3:1 hexanes–EtOAc, R_f 0.33) to afford 20 mg (52%) of ***d*-28** as a white solid. Integration of the ^{1}H NMR (500 MHz, C_6D_6) resonances at δ 2.80 (C2H_α) and δ 2.75 (C2H_β) ppm indicated that the isotopic purity at C2H_β was 93%.

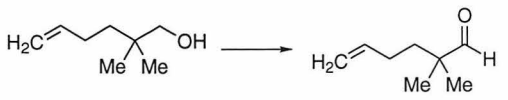

40

40: Oxalyl chloride (5.4 mL, 62 mmol, 2.0 equiv) was added dropwise *via* cannula to a solution of 8.8 mL (124 mmol, 4.0 equiv) DMSO in 75 mL CH_2Cl_2 at -78 °C at a rate such that the internal temperature did not rise above -65 °C. The resulting solution was stirred for 5 min at -78 °C and a solution of 4.0 g (31 mmol, 1.0 equiv) of 2,2-dimethyl-5-hexen-1-ol, prepared according to the literature procedure,[11] in 25 mL CH_2Cl_2 was added dropwise *via* cannula at a rate such that the internal temperature did not rise above -65 °C. The resulting solution was stirred for 30 min at -78 °C and 21.5 mL (155 mmol, 5.0 equiv) TEA was added dropwise *via* cannula at a rate such that the internal temperature did not rise above -65 °C. The reaction mixture was allowed to warm to 0 °C, poured into 200 mL 1.0 M aqueous KH_2PO_4, and extracted with 2 x 100 mL CH_2Cl_2. The organic layers were combined, dried over anhydrous Na_2SO_4, and concentrated *in vacuo*. The residue was purified by distillation (20 Torr, 63 °C) to afford 3.78 g (96%) of **40** as a clear, colorless oil, spectroscopically identical with reported values.[11]

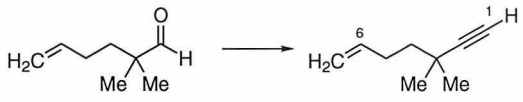

42

42: A solution of 22.5 g (200 mmol, 1.57 equiv) of ^{t}BuOK in 400 mL THF was cooled to -78 °C and 22.0 g (147 mmol, 1.00 equiv) of **41**, prepared according to the literature procedure,[12] and 30.0 g (237 mmol, 1.61 equiv) of **40** were added dropwise *via* cannula successively. The resulting solution was stirred and allowed to warm to 23 °C. After 1 h the reaction mixture was poured into 600 mL water and extracted with 1 L *n*-pentane. The organic layer was dried over anhydrous Na_2SO_4. The solvents were removed by distillation at 760 Torr after which the product was isolated by distillation *in vacuo* (25

Torr, 41 °C), affording 14.9 g (68%) of **42** as a clear, colorless oil. ^{1}H NMR (500 MHz, $CDCl_3$) δ 5.89-5.81 (1H, m, C6*H*), 5.06-5.01 (1H, m, one of C7H_2), 4.96-4.93 (1H, m, one of C7H_2), 2.24-2.19 (2H, m, C5H_2), 2.09 (1H, s, C1*H*), 1.51-1.47 (2H, m, C4H_2), 1.22 (6H, s, C3(CH_3)$_2$) ppm; ^{13}C NMR (126 MHz, $CDCl_3$) δ 138.8, 114.2, 91.5, 68.0, 42.2, 30.9, 29.7, 29.1 ppm; IR (thin film) ν 3307, 3079, 2972, 2938, 2870, 2852, 2109, 1826, 1715, 1642, 1469, 1453, 1434, 1417, 1385, 1364, 1310, 1249, 1205, 996, 912, 809, 769, 715, 630 cm^{-1}.

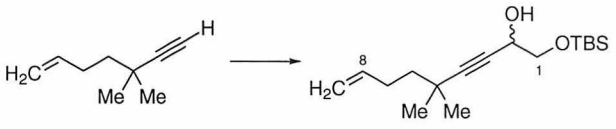

(±)-43

(±)-43: A 1.44 M solution of ^{n}BuLi in hexanes (78.7 mL, 113 mmol, 1.00 equiv) was added dropwise *via* cannula to a solution of 14.3 g (117 mmol, 1.03 equiv) of **42** in 670 mL Et_2O at -78 °C. The resulting solution was stirred for 30 min at -78 °C and a solution of 23.3 g (147 mmol, 1.30 equiv) of **8** in 70 mL Et_2O was added dropwise *via* cannula. The resulting solution was stirred and allowed to warm to 23 °C. After 30 min the reaction mixture was poured into 500 mL water. The aqueous layer was extracted with 2 x 100 mL Et_2O. The organic layers were combined and dried over anhydrous Na_2SO_4. Concentration *in vacuo* and chromatography on silica gel (60 x 220 mm, 10:1 hexanes–Et_2O, R_f 0.20) afforded 26.4 g (83%) of **(±)-43** as a clear, colorless oil. ^{1}H NMR (500 MHz, $CDCl_3$) δ 5.88-5.80 (1H, m, C8*H*), 5.04-4.99 (1H, m, one of C9H_2), 4.95-4.92 (1H, m, one of C9H_2), 4.40-4.36 (1H, m, C2*H*), 3.73-3.70 (1H, m, one of C1H_2), 3.60-3.56 (1H, m, one of C1H_2), 2.53-2.52 (1H, m, O*H*), 2.21-2.16 (2H, m, C7H_2), 1.49-1.45 (2H, m, C6H_2), 1.194 (3H, s, one of C5(CH_3)$_2$), 1.191 (3H, s, one of C5(CH_3)$_2$), 0.91 (9H, s, SiC(CH_3)$_3$), 0.10 (3H, s, one of Si(CH_3)$_2$), 0.09 (3H, s, one of Si(CH_3)$_2$) ppm; ^{13}C NMR (126 MHz, $CDCl_3$) δ 138.9, 114.1, 92.7, 78.0, 67.3, 63.3, 63.1, 42.3, 30.9, 29.7, 29.1, 25.8, 18.3, -5.3 ppm; IR (thin film) ν 3424, 2958, 2929, 2858, 2240,

1642, 1472, 1385, 1362, 1312, 1255, 1123, 1062, 1031, 1006, 908, 837, 778 cm^{-1}. Elemental analysis calculated for $C_{17}H_{32}O_2Si$ C 68.86%, H 10.88%, found C 69.02%, H 11.24%.

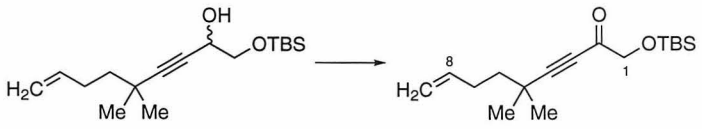

44

44: Oxalyl chloride (15.6 mL, 179 mmol, 2.0 equiv) was added dropwise *via* cannula to a solution of 25.4 mL (358 mmol, 4.0 equiv) DMSO in 220 mL CH_2Cl_2 at -78 °C at a rate such that the internal temperature did not rise above -65 °C. The resulting solution was stirred for 5 min at -78 °C and a solution of 25.1 g (89.5 mmol, 1.0 equiv) of **(±)-43** in 20 mL CH_2Cl_2 was added dropwise *via* cannula at a rate such that the internal temperature did not rise above -65 °C. The resulting solution was stirred for 30 min at -78 °C and 62 mL (447 mmol, 5.0 equiv) TEA was added dropwise *via* cannula at a rate such that the internal temperature did not rise above -65 °C. The reaction mixture was allowed to warm to 0 °C, poured into 200 mL 1.0 M aqueous KH_2PO_4, and extracted with 2 x 100 mL Et_2O. The organic layers were combined, dried over anhydrous Na_2SO_4, and concentrated *in vacuo*. The residue was purified by chromatography on silica gel (60 x 200 mm, 20:1 hexanes–Et_2O, R_f 0.20) to afford 23.3 g (93%) of **44** as a clear, colorless oil. ^{1}H NMR (500 MHz, $CDCl_3$) δ 5.86-5.78 (1H, m, C8*H*), 5.05-5.01 (1H, m, one of C9H_2), 4.98-4.95 (1H, m, one of C9H_2), 4.29 (2H, s, C1H_2), 2.20-2.16 (2H, m, C7H_2), 1.59-1.54 (2H, m, C6H_2), 1.27 (6H, s, C5(CH_3)$_2$), 0.92 (9H, s, SiC(CH_3)$_3$), 0.10 (6H, s, Si(CH_3)$_2$) ppm; ^{13}C NMR (126 MHz, $CDCl_3$) δ 186.8, 138.1, 114.7, 103.1, 78.7, 70.4, 41.7, 31.6, 29.6, 28.3, 25.7, 18.4, -5.4 ppm; IR (thin film) ν 2930, 2858, 2211, 1699, 1676, 1472, 1256, 1108, 914, 839, 779 cm^{-1}. Elemental analysis calculated for $C_{17}H_{30}O_2Si$ C 69.33%, H 10.27%, found C 69.50%, H 10.55%.

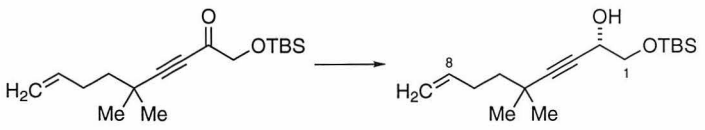

43

43: Neat (+)-β-isopinocampheyl-9-borabicyclo[3.3.1]nonane (23.25 g, 90 mmol, 1.08 equiv) was added to 23.2 g (83.3 mmol, 1.0 equiv) neat **44**, and the resulting yellow solution was stirred at 23 °C for 16 h. Acetaldehyde (5 mL) was added to the reaction mixture. The reaction mixture was stirred for 1 h at 23 °C. The volatiles were removed *in vacuo* at 500 mTorr. THF (300 mL) and 5 mM aqueous pH 7 phosphate buffer (31 mL) were added to the residue. The mixture was cooled to 0 °C and 31 mL 30% aqueous H_2O_2 was added. The reaction mixture was stirred for 3 h at 23 °C and extracted with 2 x 200 mL Et_2O. The combined organic layers were dried over anhydrous Na_2SO_4 and concentrated *in vacuo*. The residue was purified by chromatography on silica gel (60 x 250 mm, 10:1 hexanes–Et_2O, R_f 0.20) to afford 13.0 g (56%) of **43** as a clear, colorless oil, spectroscopically and chromatographically identical to **(±)-43** except for optical rotation, $[\alpha]_D^{23}$ -50.0 ° (*c*= 0.770, CH_2Cl_2). To 2 mg of **9** were added 4-DMAP (5.0 equiv) and (*R*)-MTPACl (2.0 equiv) in CH_2Cl_2. Integration of the ^{19}FNMR (471 MHz, $CDCl_3$) resonances of the derived (*S*)-MTPA ester at δ -71.638 (major) and δ -71.472 (minor) ppm indicated a diastereomer ratio of 27.6:1.00 (93% ee).

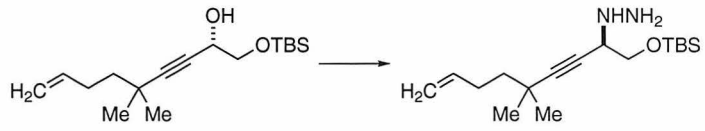

46

47: MsCl (153 μL, 2.0 mmol, 1.1 equiv) was added dropwise to a solution of 500 mg (1.8 mmol, 1.0 equiv) of **43** and 375 μL (2.7 mmol, 1.5 equiv) TEA in 14 mL CH_2Cl_2 at 0 °C. After stirring for 0.5 h the reaction mixture was transferred *via* cannula into a solution of 9 mL 1:1 MeOH–H_2NNH_2. The reaction mixture was stirred at 23 °C for 36 h and poured into 60 mL water. The aqueous layer was extracted with 2 x 50 mL 95:5

CH_2Cl_2–MeOH. The organic layers were combined, washed with 15 mL saturated aqueous NaCl solution, dried over anhydrous $MgSO_4$, and concentrated *in vacuo*. The residue was used without further purification.

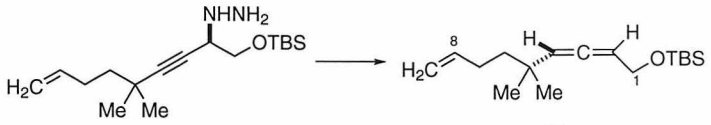

47

The residue was dissolved in 17 mL 1:1 Et_2O–CH_2Cl_2 and cooled to 0 °C. PTAD (630 mg, 3.6 mmol, 2.0 equiv) was added in one portion. When gas evolution was complete 32 mL *n*-pentane was added and the reaction mixture was filtered through a 2 cm pad of silica gel. The pad was washed successively with 60 mL 2:1 *n*-pentane–CH_2Cl_2 and 45 mL 2:1 *n*-pentane–Et_2O. The eluents were combined and concentrated *in vacuo* to afford 251 mg (53%) of **47** as a clear, colorless oil. ^{1}H NMR (500 MHz, $CDCl_3$) δ 5.85-5.77 (1H, m, C8*H*), 5.30-5.25 (1H, m, C2*H* or C4*H*), 5.12-5.10 (1H, m, C2*H* or C4*H*), 5.02-4.97 (1H, m, one of C9H_2), 4.93-4.90 (1H, m, one of C9H_2), 4.21-4.13 (2H, m, C1H_2), 2.05-2.00 (2H, m, C7H_2), 1.40-1.37 (2H, m, C6H_2), 1.01 (6H, s, C5(CH_3)$_2$), 0.90 (9H, s, SiC(CH_3)$_3$), 0.08 (6H, s, Si(CH_3)$_2$) ppm; ^{13}C NMR (126 MHz, $CDCl_3$) δ 201.5, 139.4, 113.9, 102.6, 93.4, 62.2, 42.3, 34.7, 29.2, 27.9, 27.8, 26.0, 18.4, -5.07, -5.11 ppm; IR (thin film) ν 3078, 2958, 2929, 2858, 1962, 1641, 1472, 1384, 1362, 1255, 1142, 1088, 1048, 1006, 909, 837, 776, 716 cm^{-1}; $[\alpha]_D^{23}$ +199 ° (*c*= 0.415, CH_2Cl_2). Elemental analysis calculated for $C_{17}H_{32}OSi$ C 72.79%, H 11.50%, found C 73.11%, H 11.79%.

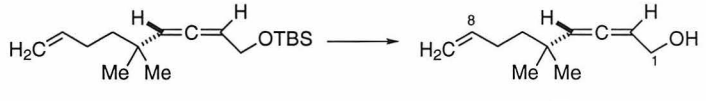

48

48: A 1.0 M solution of TBAF in THF (32.1 mL, 32.1 mmol, 1.2 equiv) was added to a solution of 7.50 g (26.7 mmol, 1.0 equiv) of **47** in 100 mL THF. The resulting solution

was stirred for 5 min at 23 °C, poured into 200 mL 1.0 M aqueous KH_2PO_4, and extracted successively with 130 mL *n*-pentane and 200 mL Et_2O. The organic layers were combined, dried over anhydrous Na_2SO_4, and concentrated *in vacuo*. The residue was purified by chromatography on silica gel (40 x 150 mm, 2:1 *n*-pentane–Et_2O, R_f 0.35) to afford 4.21 g (95%) of **48** as a clear, colorless oil. ^{1}H NMR (500 MHz, $CDCl_3$) δ 5.85-5.77 (1H, m, C8*H*), 5.42-5.38 (1H, m, C2*H* or C4*H*), 5.24-5.22 (1H, m, C2*H* or C4*H*), 5.02-4.98 (1H, m, one of C9H_2), 4.94-4.91 (1H, m, one of C9H_2), 4.13-4.10 (2H, m, C1H_2), 2.06-2.01 (2H, m, C7H_2), 1.44-1.38 (2H, m, C6H_2), 1.02 (6H, s, C5(CH_3)$_2$) ppm; ^{13}C NMR (126 MHz, $CDCl_3$) δ 201.1, 139.2, 114.0, 104.3, 93.5, 60.9, 42.2, 34.7, 29.1, 27.84, 27.81 ppm; IR (thin film) ν 3329, 3077, 2960, 2926, 2867, 1961, 1641, 1469, 1383, 1364, 1312, 1253, 1195, 1119, 1051, 1012, 909, 873, 744, 738 cm^{-1}; $[\alpha]_D^{23}$ +432 ° (*c*= 0.520, CH_2Cl_2).

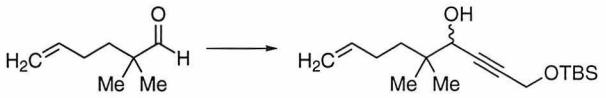

49

(±)-48: A 3.1 M solution of MeMgBr in Et_2O (10.5 mL, 32.7 mmol, 1.1 equiv) was added to a solution of 6.07 g (35.7 mmol, 1.2 equiv) of **16** in 70 mL THF at -78 °C. The cooling bath was removed and the reaction mixture was stirred for 2.5 h while warming to 23 °C. Gas evolution was observed. The reaction mixture was cooled to -78 °C and 3.75 g (29.7 mmol, 1.0 equiv) of **40** was added. The cooling bath was removed and the reaction mixture was stirred for 30 min while warming to 23 °C. The reaction mixture was poured into 300 mL 1.0 M aqueous KH_2PO_4 and extracted successively with 2 x 150 mL Et_2O. The organic layers were combined, dried over anhydrous Na_2SO_4, and concentrated *in vacuo*. The residue was used without further purification.

50

TEA (708 μL, 5.1 mmol, 1.5 equiv) and MsCl (316 μL, 4.0 mmol, 1.2 equiv) were added successively to a solution of 1.00 g of the residue in 10 mL CH_2Cl_2 at 0 °C. The reaction mixture was stirred for 30 min at 0 °C. The reaction mixture was poured into 50 mL 1.0 M aqueous KH_2PO_4 and extracted successively with 3 x 50 mL Et_2O. The organic layers were combined, dried over anhydrous Na_2SO_4, and concentrated *in vacuo*. The residue was used without further purification.

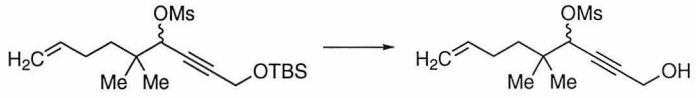

51

The residue was dissolved in 4 mL of a previously prepared solution of 7% concentrated aqueous HF in 63:1 CH_3CN:H_2O. The resulting solution was stirred at 23 °C for 30 min and poured into 25 mL saturated aqueous $NaHCO_3$. The aqueous layer was extracted with 3 x 25 mL Et_2O. The combined organic layers were combined, dried over anhydrous Na_2SO_4, and concentrated *in vacuo*. The residue was dissolved in 10 mL C_6H_6 and concentrated *in vacuo* to effect azeotropic removal of water.

(±)-48

The residue was dissolved in 20 mL Et_2O and cooled to 0 °C and 5.1 mL (5.1 mmol, 1.5 equiv) of a 1.0 M solution of $LiAlH_4$ in THF was added *via* cannula. The resulting solution was stirred at 0 °C for 15 min and 200 μL H_2O was added dropwise *via* syringe. The reaction mixture was stirred for 5 min and 600 μL 15% aqueous NaOH was added. The reaction mixture was stirred for 15 min and 200 μL H_2O was added. The mixture was

filtered and the eluents were concentrated *in vacuo*. The residue was purified by chromatography on silica gel (20 x 40 mm, 2:1 hexanes–Et_2O, R_f 0.19) to afford 470 mg (53%, 4 steps) **(±)-48** as a clear, colorless oil, spectroscopically and chromatographically identical to **48**.

52

52: MsCl (2.35 mL, 30.4 mmol, 1.2 equiv) was added dropwise to a solution of 4.21 g (25.3 mmol, 1.0 equiv) of **48** and 5.27 mL (38.0 mmol, 1.5 equiv) TEA in 26 mL CH_2Cl_2 and 26 mL hexanes at a rate such that the internal temperature did not rise above 10 °C. The resulting solution was stirred for 15 min and filtered. The filtrate was washed with 15 mL hexanes. The combined eluents were concentrated *in vacuo* and the residue was purified by chromatography on silica gel (40 x 100 mm, 2:1 hexanes–Et_2O with 2% v/v TEA, R_f 0.40) to afford 5.63 g (91%) of **52** as a clear, colorless oil. ^{1}H NMR (500 MHz, $CDCl_3$) δ 5.84-5.76 (1H, m, C8*H*), 5.39-5.35 (1H, m, C2*H* or C4*H*), 5.29-5.27 (1H, m, C2*H* or C4*H*), 5.02-4.97 (1H, m, one of C9H_2), 4.94-4.91 (1H, m, one of C9H_2), 4.71-4.69 (2H, m, C1H_2), 3.02 (3H, s, SCH_3), 2.04-2.00 (2H, m, C7H_2), 1.42-1.37 (2H, m, C6H_2), 1.03 (6H, s, C5(CH_3)$_2$) ppm; ^{13}C NMR (126 MHz, $CDCl_3$) δ 204.8, 139.0, 114.2, 104.0, 87.5, 68.8, 42.1, 38.3, 34.9, 29.1, 27.7 ppm; IR (thin film) ν 3076, 2962, 2869, 1963, 1640, 1469, 1416, 1359, 1246, 1174, 1124, 1041, 920, 815, 763, 714 cm^{-1}; $[\alpha]_D^{23}$ +422 ° (*c*= 0.406, CH_2Cl_2). Elemental analysis calculated for $C_{12}H_{20}O_3S$ C 58.99%, H 8.25%, found C 59.10%, H 8.50%.

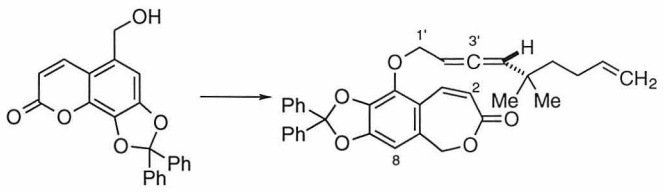

53

53: A 25 mL round-bottom flask was charged with 1.28 g (32.1 mmol, 1.4 equiv) of an 80% dispersion of NaH in mineral oil. The dispersion was washed 3 times with anhydrous hexanes, and dried briefly under *in vacuo*. A nitrogen atmosphere was reestablished and 90 mL DMF was added. The solution was cooled to 0 °C, and 11.9 g (32.1 mmol, 1.4 equiv) of **26** was added as a solid. After gas evolution ceased the mixture was transferred *via* cannula into a flask containing 5.60 g (22.9 mmol, 1.0 equiv) of **52** and stirred at 23 °C for 1.5 hours. The reaction mixture was diluted with 300 mL H_2O, and extracted 3 x 100 mL Et_2O. The organic layers were combined, dried over anhydrous $MgSO_4$, and concentrated *in vacuo*. The residue was purified by chromatography on silica gel (60 x 150 mm, 2:1 hexanes–Et_2O, R_f 0.18) to afford 6.48 g (54%) of **53** as a clear, colorless oil. ^{1}H NMR (500 MHz, $CDCl_3$) δ 7.56-7.53 (4H, m, four of diphenyl ketal H_{arom}), 7.47 (1H, d, J = 12.3 Hz, C2*H*), 7.40-7.38 (6H, m, six of diphenyl ketal H_{arom}), 6.70 (1H, s, C8*H*), 6.22 (1H, d, J = 12.3 Hz, C3*H*), 5.80-5.72 (1H, m, C8'*H*), 5.43-5.39 (1H, m, C2'*H* or C4'*H*), 5.12-5.10 (1H, m, C2'*H* or C4'*H*), 4.99-4.83 (6H, m, C10H_2, C1'H_2, and C9'H_2), 1.98-1.94 (2H, m, C7'H_2), 1.34-1.31 (2H, m, C6'H_2), 0.90 (6H, s, C5'(CH_3)$_2$) ppm; ^{13}C NMR (126 MHz, $CDCl_3$) δ 203.7, 168.2, 150.1, 140.1, 139.3, 139.1, 137.0, 135.6, 131.2, 129.5, 128.4, 126.29, 126.27, 123.0, 119.8, 118.5, 114.0, 103.7, 103.2, 89.3, 70.9, 68.5, 65.1, 42.1, 34.6, 29.1, 27.7, 27.4 ppm; IR (thin film) ν 3062, 2959, 5925, 1960, 1708, 1640, 1611, 1591, 1488, 1450, 1381, 1303, 1236, 1206, 1116, 1086, 1045, 1020, 948, 907, 862, 849, 818, 762, 698 cm^{-1}; $[\alpha]_D^{23}$ +153 ° (*c*= 2.44, CH_2Cl_2). Elemental analysis calculated for $C_{35}H_{32}O_5$ C 78.44%, H 6.19%, found C 77.66%, H 6.32%.

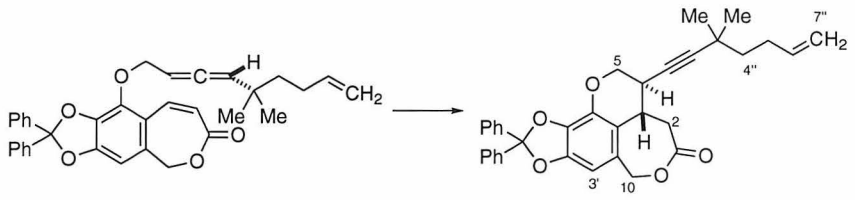

54

54: A 1-L Pyrex flask equipped with a Teflon valve was charged with a solution of 1.0 g of **53** in 770 mL CH_2Cl_2. The solution was degassed by freeze-pump-thaw to an overpressure of 10 mTorr and irradiated with a Hanovia 450 W Hg medium pressure lamp at 0 °C for 5 h. The volatiles were removed *in vacuo* and the residue was purified by chromatography on silica gel (40 x 200 mm, 5:1 hexanes–EtOAc, R_f 0.17) to afford 550 mg (55%) of **54** as a white, crystalline solid, mp 55-57 °C. ^{1}H NMR (500 MHz, $CDCl_3$) δ 7.60-7.55 (4H, m, four of diphenyl ketal H_{arom}), 7.39-7.34 (6H, m, six of diphenyl ketal H_{arom}), 6.46 (1H, s, C3'*H*), 5.73-5.65 (1H, m, C6"*H*), 5.13 (1H, d, *J* = 13.8 Hz, one of C10H_2), 5.08 (1H, d, *J* = 13.8 Hz, one of C10H_2), 4.93-4.85 (2H, m, C7"H_2), 4.27 (1H, dd, *J* = 10.7, 3.3 Hz, one of C5H_2), 4.13 (1H, dd, *J* = 10.7, 3.3 Hz, one of C5H_2), 3.40 (1H, dt, *J* = 11.7, 4.9 Hz, C3*H*), 3.12-3.01 (3H, m, C2H_2 and C4*H*), 1.96-1.91 (2H, m, C5"H_2), 1.36-1.29 (2H, m, C4"H_2), 1.09 (3H, s, one of C5'(CH_3)$_2$), 1.08 (3H, s, one of C5'(CH_3)$_2$) ppm; ^{13}C NMR (126 MHz, $CDCl_3$) δ 172.4, 146.8, 139.71, 139.67, 138.6, 138.4, 134.9, 129.2, 128.23, 128.20, 127.5, 126.4, 126.3, 118.2, 117.2, 114.2, 102.5, 93.3, 75.0, 69.3, 67.6, 42.2, 38.3, 32.7, 31.14, 31.05, 29.6, 29.2, 29.1, 14.1 ppm; IR (thin film) ν 3063, 2967, 2922, 1744, 1638, 1497, 1470, 1450, 1368, 1285, 1256, 1240, 1209, 1112, 1044, 1020, 948, 908, 845, 778, 764, 699, 668, 642 cm^{-1}; $[\alpha]_D^{23}$ +61 ° (*c*= 0.814, CH_2Cl_2). Elemental analysis calculated for $C_{35}H_{32}O_5$ C 78.44%, H 6.19%, found C 78.02%, H 6.30%.

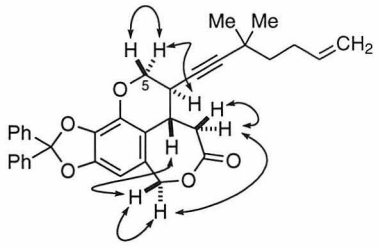

Selected ^{1}H NMR NOESY correlations for **54** (300 MHz, C_6D_6)

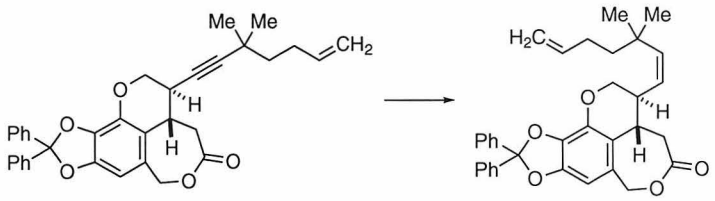

55

56: A slurry of 700 mg (1.34 mmol, 1.0 equiv) of **54** and 156 mg of 5% palladium on carbon in 62.5 mL pyridine and 19.1 mL 3,3-dimethyl-1-butene was stirred at 23 °C under 1 atm of H_2 for 4 h. An additional 10 mL 3,3-dimethyl-1-butene was added and the slurry was stirred for 2 h. The reaction mixture was filtered through Celite, and the filtrate was concentrated *in vacuo*. The residue was dissolved in 10 mL *n*-heptane and concentrated *in vacuo* to remove residual pyridine. The residue was purified by chromatography on silica gel (20 x 100 mm, 1:1 hexanes–Et_2O, R_f 0.32) to afford 424 mg (50%) of a mixture of the desired product (85%) and the product of alkyne semihydrogenation and terminal olefin hydrogenation (15%) as a white solid, and 251 mg of starting material which was recycled.

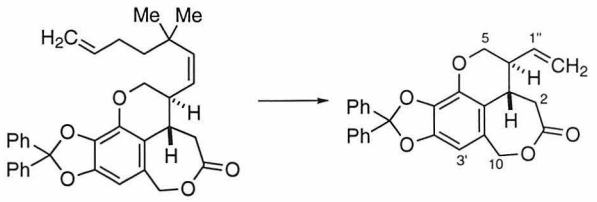

56

A solution of 170 mg (0.325 mmol, 1.0 equiv) of **55** in 464 mL CH_2Cl_2 in a flask equipped with a Teflon valve was degassed by freeze-pump-thaw to an overpressure of 10 mTorr, and a solution of 15 mg (0.016 mmol, 0.05 equiv) of ruthenium catalyst **33**, prepared according to the literature procedure,[13] in 10 mL CH_2Cl_2 was added *via* syringe. The flask was sealed and the reaction mixture was stirred at 40 °C for 36 h (*Caution:* use blast shield). Ethyl vinyl ether (0.5 mL) was added and the reaction mixture was stirred at 40 °C for 1 h. The volatiles were removed *in vacuo* and the residue was purified by chromatography on silica gel (40 x 200 mm, 2:1 hexanes–EtOAc, R_f 0.26) to afford 81 mg (58%) of **56** as a white, crystalline solid, mp 90-91 °C. ^{1}H NMR (500 MHz, $CDCl_3$) δ 7.59-7.57 (4H, m, four of diphenyl ketal H_{arom}), 7.39-7.35 (6H, m, six of diphenyl ketal H_{arom}), 6.39 (1H, s, C3'*H*), 5.75 (1H, ddd, *J* = 18.2, 9.3, 7.9 Hz, C1"*H*), 5.21-5.11 (3H, m, C2"H_2 and one of C10H_2), 4.99 (1H, d, *J* = 14.4 Hz, one of C10H_2), 4.36 (1H, dd, *J* = 10.9, 3.0 Hz, one of C5H_2), 4.28 (1H, dd, *J* = 10.9, 4.3 Hz, one of C5H_2), 3.46-3.44 (1H, m, C3*H*), 3.05 (1H, dd, *J* = 15.0, 12.9, one of C2H_2), 2.74-2.69 (2H, m, one of C2H_2 and C4*H*) ppm; ^{13}C NMR (126 MHz, $CDCl_3$) δ 173.5, 146.7, 139.8, 139.7, 134.8, 133.2, 129.21, 129.19, 128.2, 127.1, 126.34, 126.27, 125.2, 119.2, 118.2, 116.5, 102.2, 69.8, 69.5, 42.2, 37.4, 33.8, 31.9 ppm; IR (thin film) ν 3064, 3032, 2957, 2925, 2856, 2522, 1745, 1634, 1496, 1470, 1450, 1395, 1379, 1338, 1287, 1254, 1208, 1131, 1099, 1045, 1020, 948, 910, 831, 779, 734, 699, 642 cm^{-1}; $[\alpha]_D^{23}$ +29 ° (*c*= 0.200, CH_2Cl_2).

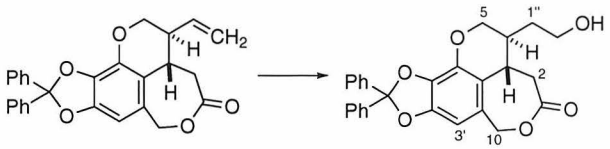

57

57: $ClRh(PPh_3)_3$ (11 mg, 0.12 mmol, 0.1 equiv) and a 1.0 M solution of catecholborane in THF (468 μL, 0.468 mmol, 4.0 equiv) were added to a solution of 50 mg (0.117 mmol, 1.0 equiv) of **56** in 6.7 mL THF. The resulting solution was stirred at 23 °C for 30 min. The reaction mixture was cooled to 0 °C and 400 μL EtOH, 400 μL 10 mM pH 7.0 phosphate buffer, and 400 μL 15% H_2O_2 were added successively. The resulting solution was stirred for 3 h at 23 °C, poured into 10 mL 1.0 M aqueous KH_2PO_4 and extracted with 5 x 15 mL 1:1 hexanes;Et_2O. The organic layers were combined, dried over anhydrous Na_2SO_4, and concentrated *in vacuo*. The residue was purified by chromatography on silica gel (20 x 120 mm, 1:1 EtOAc–CH_2Cl_2, R_f 0.31) to afford 45 mg (86%) of **57** as a white solid. ^{1}H NMR (500 MHz, $CDCl_3$) δ 7.58-7.53 (4H, m, four of diphenyl ketal H_{arom}), 7.39-7.33 (6H, m, six of diphenyl ketal H_{arom}), 6.42 (1H, s, C3'*H*), 5.11 (2H, s, C10H_2), 4.24-4.23 (2H, m, C5H_2), 3.84-3.77 (2H, m, C2"H_2), 3.48 (1H, dt, *J* = 11.2, 4.5 Hz, C3*H*), 3.04 (1H, dd, *J* = 15.1, 11.3, one of C2H_2), 2.89 (1H, dd, *J* = 15.1, 4.5 Hz, one of C2H_2), 2.32-2.27 (1H, m, C4*H*), 1.65-1.53 (2H, m, C1"H_2) ppm; ^{13}C NMR (126 MHz, $CDCl_3$) δ 173.1, 146.6, 139.8, 139.6, 138.7, 134.8, 132.1, 132.0, 129.23, 129.18, 128.5, 128.4, 128.2, 127.4, 126.4, 126.3, 118.1, 117.1, 102.4, 69.8, 68.0, 60.3, 37.0, 34.1, 33.5, 28.1 ppm; IR (thin film) ν 3392, 3061, 2932, 2882, 1738, 1634, 1496, 1470, 1450, 1396, 1372, 1289, 1256, 1209, 1179, 1120, 1095, 1044, 1019, 948, 908, 937, 778, 725, 696, 642 cm^{-1}; $[\alpha]_D^{23}$ -10.8 ° (*c*= 1.00, CH_2Cl_2). To 2 mg of **9** were added 4-DMAP (5.0 equiv) and (*R*)-MTPACl (2.0 equiv) in CH_2Cl_2. Integration of the ^{1}H NMR (500 MHz, $CDCl_3$) resonances of the derived (*S*)-MTPA ester at δ 3.53 (major, (*S*)-MTPA OCH_3) and δ 3.61 (minor, (*S*)-MTPA OCH_3) ppm indicated a diastereomer ratio of 40.8:1.00 (95% ee).

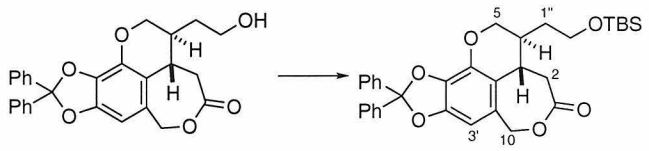

58

58: A solution of 221 mg (0.497 mmol, 1 equiv) of **57**, 103 μL (0.746 mmol, 1.5 equiv) TEA, 90 mg (0.596 mmol, 1.2 equiv) TBSCl, and 6.1 mg (0.05 mmol, 0.1 equiv) 4-DMAP in 37 mL CH_2Cl_2 was stirred at 23 °C for 14 h and partitioned between 50 mL 1.0 M aqueous KH_2PO_4 and 100 mL Et_2O. The organic layer was dried over anhydrous Na_2SO_4 and concentrated *in vacuo*. The residue was purified by chromatography on silica gel (20 x 150 mm, 4:1 hexanes–EtOAc, R_f 0.26) to afford 241 mg (87%) of **58** as a white solid. ^{1}H NMR (500 MHz, $CDCl_3$) δ 7.59-7.56 (4H, m, four of diphenyl ketal H_{arom}), 7.39-7.34 (6H, m, six of diphenyl ketal H_{arom}), 6.42 (1H, s, C3'*H*), 5.14 (1H, d, *J* = 14.0 Hz, one of C10H_2), 5.09 (1H, d, *J* = 14.0 Hz, one of C10H_2), 4.24 (1H, dd, *J* = 11.2, 2.9 Hz, one of C5H_2), 4.19 (1H, dd, *J* = 11.2, 5.3 Hz, one of C5H_2), 3.78-3.71 (2H, m, C2"H_2), 3.47 (1H, dt, *J* = 12.1, 4.3 Hz, C3*H*), 3.03 (1H, dd, *J* = 15.1, 12.1, one of C2H_2), 2.85 (1H, dd, *J* = 15.1, 4.3 Hz, one of C2H_2), 2.32-2.26 (1H, m, C4*H*), 1.60-1.51 (2H, m, C1"H_2), 0.89 (9H, s, SiC(CH_3)$_3$), 0.05 (6H, s, Si(CH_3)$_2$) ppm; ^{13}C NMR (126 MHz, $CDCl_3$) δ 173.1, 146.6, 139.8, 139.7, 138.8, 134.8, 129.2, 129.17, 128.2, 127.4, 126.4, 126.3, 117.4, 102.2, 69.7, 67.8, 60.6, 37.1, 34.0, 33.4, 28.3, 25.9, 25.6, 18.2, -3.6, -5.4 ppm; IR (thin film) ν 3064, 3034, 2929, 2857, 1744, 1636, 1497, 1471, 1450, 1395, 1374, 1290, 1254, 1210, 1181, 1127, 1098, 1044, 1020, 949, 918, 835, 777, 734, 699, 642 cm^{-1}; $[\alpha]_D^{23}$ +60.0 ° (*c*= 2.96, CH_2Cl_2).

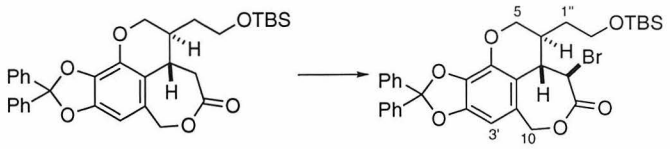

59

59: A 0.714 M solution of LDA in hexanes–THF[14] (707 μL, 0.585 mmol, 2.0 equiv) was added to a solution of 141 mg (0.252 mmol, 1.0 equiv) of **58** in 8.2 mL THF at -78 °C. The resulting solution was stirred for 1.5 h at -78 °C and a solution of 251 mg (0.757 mmol, 3.0 equiv) CBr_4 in 2 mL of toluene was added dropwise *via* cannula. The resulting solution was stirred for 30 min at -78 °C and quenched by dropwise addition of 29 μL AcOH. The reaction mixture was warmed to 23 °C and partitioned between 50 mL Et_2O and 50 mL 1.0 M aqueous KH_2PO_4. The organic layer was dried over anhydrous Na_2SO_4 and concentrated *in vacuo*. The residue was purified by chromatography on silica gel (20 x 150 mm, 5:1 hexanes–EtOAc, R_f 0.20) to afford 115 mg (71%) of **59** as a white solid. ^{1}H NMR (500 MHz, $CDCl_3$) δ 7.59-7.54 (4H, m, four of diphenyl ketal H_{arom}), 7.38-7.36 (6H, m, six of diphenyl ketal H_{arom}), 6.59 (1H, s, C3'*H*), 5.47 (1H, d, *J* = 12.9 Hz, one of C10H_2), 4.95 (1H, d, *J* = 12.9 Hz, one of C10H_2), 4.71-4.67 (1H, m, C2*H*), 4.37 (1H, dd, *J* = 7.9, 1.7 Hz, one of C5H_2), 3.96-3.92 (1H, m, C3*H*), 3.82-3.77 (2H, m, C2"H_2), 3.67 (1H, dd, *J* = 7.9, 5.2 Hz, one of C5H_2), 2.58-2.53 (1H, m, C4*H*), 2.08-2.02 (2H, m, C1"H_2), 0.91 (9H, s, SiC(CH_3)$_3$), 0.08 (6H, s, Si(CH_3)$_2$) ppm; ^{13}C NMR (126 MHz, $CDCl_3$) δ 168.0, 147.3, 139.7, 139.4, 135.2, 129.3, 129.2, 128.8, 128.28, 128.25, 128.17, 126.43, 126.35, 126.27, 118.6, 115.2, 103.4, 68.9, 66.9, 60.8, 47.5, 42.3, 34.5, 26.0, 18.3, -5.33, -5.37 ppm; IR (thin film) ν 2954, 2927, 2855, 1731, 1634, 1497, 1469, 1451, 1397, 1368, 1296, 1256, 1208, 1182, 1132, 1076, 1046, 1019, 948, 918, 836, 808, 777, 697 cm^{-1}.

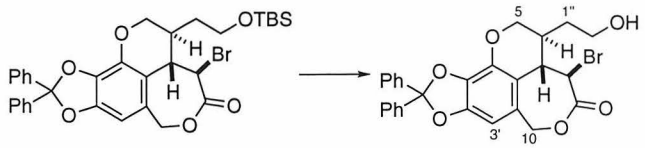

60

60: A solution of 155 mg of **59** in 30 mL of a previously prepared solution of 7% concentrated aqueous HF in 63:1 CH_3CN:H_2O was stirred at 0 °C for 30 min and poured into 50 mL 1.0 M aqueous KH_2PO_4 and 125 mL Et_2O. The aqueous layer was extracted with 3 x 50 mL Et_2O. The combined organic layers were washed with 50 mL saturated aqueous $NaHCO_3$, dried over anhydrous Na_2SO_4, and concentrated *in vacuo*. The residue was purified by chromatography on silica gel (20 x 150 mm, 12:1 CH_2Cl_2–Et_2O, R_f 0.22) to afford 107 mg (84%) of **60** as a white, crystalline solid, mp 45-47 °C. ^{1}H NMR (500 MHz, $CDCl_3$) δ 7.59-7.54 (4H, m, four of diphenyl ketal H_{arom}), 7.38-7.36 (6H, m, six of diphenyl ketal H_{arom}), 6.58 (1H, s, C3'*H*), 5.46 (1H, d, *J* = 13.0 Hz, one of C10H_2), 4.96 (1H, d, *J* = 13.0 Hz, one of C10H_2), 4.71 (1H, br d, *J* = 4.7 Hz, C2*H*), 4.34 (1H, dd, *J* = 11.3, 2.1 Hz, one of C5H_2), 4.01-3.97 (1H, m, C3*H*), 3.86-3.82 (2H, m, C2"H_2), 3.70 (1H, dd, *J* = 11.3, 5.0 Hz, one of C5H_2), 2.61-2.54 (1H, m, C4*H*), 2.09-2.03 (2H, m, C1"H_2) ppm; ^{13}C NMR (126 MHz, $CDCl_3$) δ 168.0, 147.4, 139.7, 139.6, 139.4, 135.2, 129.4, 129.3, 128.31, 128.28, 126.4, 118.6, 115.0, 103.5, 69.0, 67.0, 60.5, 47.4, 42.2, 34.2, 28.7 ppm; IR (thin film) ν 3420, 3032, 2925, 1725, 1657, 1497, 1450, 1367, 1314, 1262, 1234, 1208, 1129, 1074, 1046, 1018, 948, 926, 764 cm^{-1}; $[\alpha]_D^{23}$ +122 ° (*c*= 0.600, CH_2Cl_2).

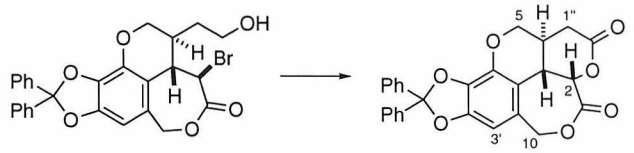

61

61: Dess-Martin periodinane (112 mg, 0.264 mmol, 1.2 equiv), prepared according to the literature procedure,[9] was added to a solution of 115 mg (0.220 mmol, 1.0 equiv) of **60** in

15.5 mL CH_2Cl_2. The resulting solution was stirred at 23 °C for 45 min and 45 mL Et_2O was added. The reaction mixture was stirred for 5 min, filtered through Celite, and concentrated *in vacuo*. The residue was dissolved in 9.2 mL ^{t}BuOH and 4.6 mL 1.25 mM aqueous pH 5.0 phosphate buffer and 736 μL 0.3 M aqueous $KMnO_4$ solution were added successively. After 1 h an additional 736 μL 0.3 M aqueous $KMnO_4$ solution was added. After 2.5 h saturated aqueous $NaHSO_3$ was added until the purple color discharged. The reaction mixture was poured into 150 mL 1.0 M aqueous KH_2PO_4 and 15 mL Et_2O. The aqueous layer was acidified to pH 2 with 1.0 M aqueous HCl and extracted with 3 x 15 mL Et_2O. The organic layers were combined, dried over anhydrous Na_2SO_4, and concentrated *in vacuo*. A thick-walled glass bomb was charged with a solution of the residue in 15 mL CH_2Cl_2 and 50 μL TEA. The flask was sealed and heated to 35 °C for 3 h. The reaction mixture was partitioned between 100 mL 1.0 M aqueous KH_2PO_4 and 4 x 80 mL Et_2O. The organic layers were combined, dried over anhydrous Na_2SO_4, and concentrated *in vacuo*. The residue was purified by chromatography on silica gel (20 x 120 mm, 1:1.5 hexanes–EtOAc, R_f 0.18) to afford 80 mg (77%) of **61** as a white solid. ^{1}H NMR (500 MHz, $CDCl_3$) δ 7.58-7.54 (4H, m, four of diphenyl ketal H_{arom}), 7.40-7.36 (6H, m, six of diphenyl ketal H_{arom}), 6.63 (1H, s, C3'*H*), 5.74 (1H, d, *J* = 11.3 Hz, C2*H*), 5.14 (1H, d, *J* = 12.9 Hz, one of C10H_2), 4.84 (1H, d, *J* = 12.9 Hz, one of C10H_2), 4.24 (2H, s, C5H_2), 4.04-4.01 (1H, m, C3*H*), 2.69-2.59 (3H, m, C4*H* and C1"H_2) ppm; ^{13}C NMR (126 MHz, $CDCl_3$) δ 170.6, 148.0, 139.5, 139.1, 129.4, 129.3, 128.3, 126.4, 113.4, 104.9, 68.8, 67.2, 32.7, 32.5, 30.8 ppm.

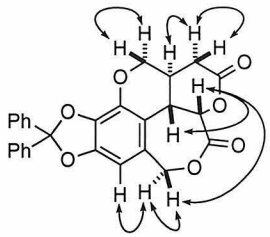

Selected ^{1}H NMR NOESY correlations for **61** (500 MHz, C_6D_6)

3.3. Results

3.3.1. Synthesis of the chebulic acid core: synthesis of the allene component of the chebulic acid precursor photosubstrate in enantioenriched form. The allene component of retrosynthetic intermediate **7** was synthesized in enantioenriched form as shown in Scheme 3.2. Addition of lithium *tert*-butylacetylide to

Scheme 3.2. Preparation of allene component for chebulic acid synthesis in enantioenriched form.

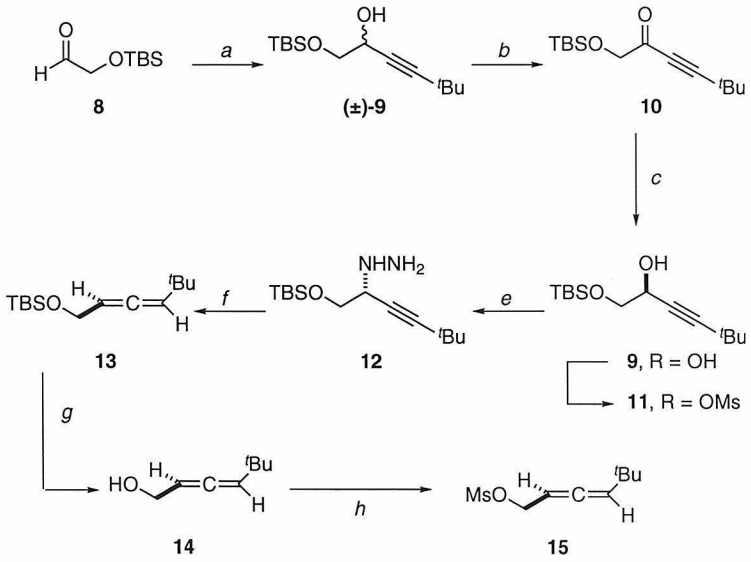

(a) lithium *tert*-butylacetylide, Et_2O, -78 °C, 2.5 h (56%). (b) Dess-Martin periodinane, CH_2Cl_2, 23 °C, 1 h, (95%). (c) (*S*)-Alpine Borane, 23 °C, 12 h (53%, 85% ee). (d) MsCl, TEA, CH_2Cl_2, 0 °C, 30 min. (e) 1:1 MeOH–H_2NNH_2, 23 °C, 18 h. (f) PTAD, 1:1 CH_2Cl_2–Et_2O, 0 °C, 5 min (70%). (g) TBAF, THF, 23 °C, 30 min (89%). (h) MsCl, TEA, CH_2Cl_2, 0 °C, 1 h (78%).

aldehyde **8** afforded **(±)-9**, which was oxidized to alkynone **10** with the Dess-Martin periodinane.[15] Reduction of **10** with (*S*)-Alpine-Borane[16] afforded **7** in 85% enantiomeric excess,[17] as determined by ^{1}H NMR analysis of its (*S*)-MTPA ester,[18] and modest yield. Alkynol **9** was converted to allene **13** in 70% overall yield for 3 steps using the conditions described by Myers for the preparation of eneyne allenes.[19] The steps that convert **9** into **13** have been shown to be completely stereospecific. Therefore, the enantiopurity of the allene component of the intramolecular photocycloaddition that establishes the stereochemistry at C4 in the synthetic target is limited only by the enantiopurity of the precursor propargyl alcohol.

3.3.2. Synthesis of the chebulic acid core: synthesis of the allene component of the chebulic acid precursor photosubstrate in racemic form.

Because of the large quantities of material required to investigate elaboration of intramolecular photocycloaddition products to chebulic acid, racemic **14** was prepared as shown in Scheme 3.3.[20] Addition of the bromomagnesium acetylide derived from silylated

Scheme 3.3. Preparation of allene component for chebulic acid synthesis in racemic form.

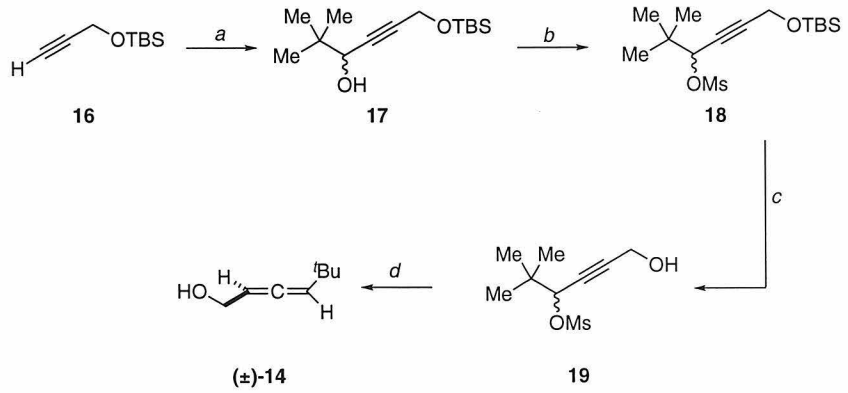

(a) *i*. MeMgBr, THF, -78 → 23 °C, 2.5 h; *ii*. ^{t}BuCHO, -78 °C → 23 °C, 30 min (87%). (b) MsCl, TEA, CH_2Cl_2, 0 °C, 15 min. (c) HF, CH_3CN, H_2O, 23 °C, 45 min (93%). (d) $LiAlH_4$, Et_2O, 0 °C, 2 h (82%).

propargyl alcohol **16** to trimethylacetaldehyde afforded **17**. Methanesulfonylation of **17** followed by desilylation afforded **19**, which underwent conjugate reduction upon treatment with lithium aluminum hydride in diethyl ether to furnish **(±)-14**. This sequence was routinely performed on multigram scale.

3.3.3. Synthesis of the chebulic acid core: synthesis of the chebulic acid precursor photosubstrate. The coumarin component of retrosynthetic intermediate **7** was synthesized as shown in Scheme 3.4. Protection of methyl gallate with neat dichlorodiphenylmethane afforded **20**.[10] Alkylation of **20** with propargyl bromide

Scheme 3.4. Preparation of the photosubstrate for chebulic acid synthesis.

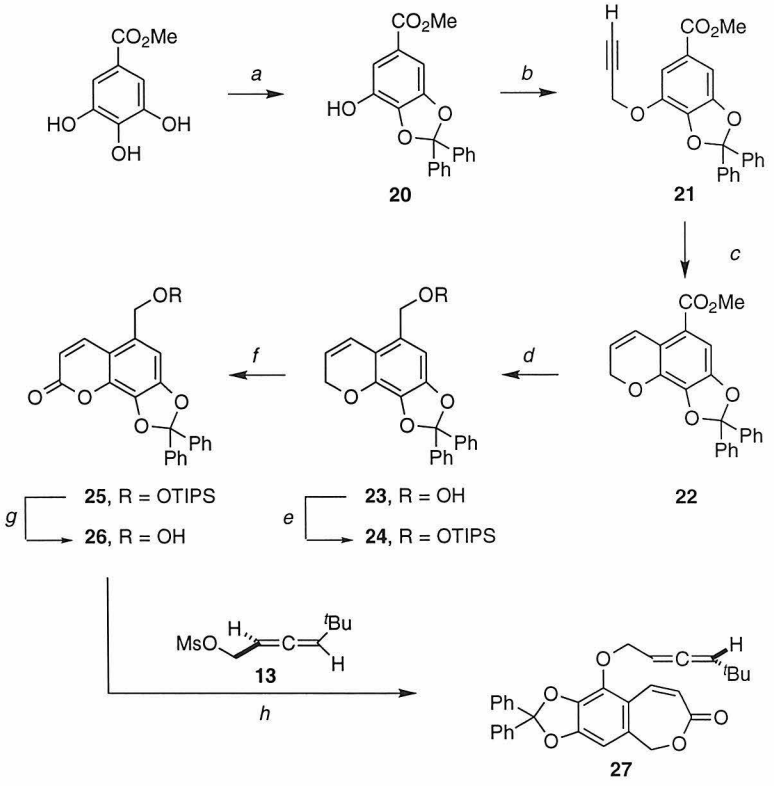

(a) Ph_2CCl_2, 180 °C, 15 min (74%). (b) propargyl bromide, K_2CO_3, acetone, reflux, 11 h (82%). (c) *N*,*N*-dimethylaniline, reflux, 24 h (63%). (d) $LiAlH_4$, Et_2O, 0 °C (79%). (e) TIPSOTf, TEA, 4-DMAP, CH_2Cl_2, 23 °C, 12 h (97%). (f) PDC, Celite, 4 Å molecular sieves, CH_2Cl_2, 23 °C, 16 h (50%). (g) TBAF, THF, 23 °C, 2 h (98%). (h) NaH, DMF, 0 °C $\rightarrow$ 23 °C, 12 h (55%).

afforded **21**, which rearranged to **22** upon prolonged heating in *N,N*-dimethylaniline. Lithium aluminum hydride reduction of **22** afforded **23**, which was protected with triisopropylsilyl trifluoromethanesulfonate to afford **24**. Treatment of **24** with pyridinium dichromate effected selective oxidation at C2 to afford coumarin **25**. Deprotonation of **25** with sodium hydride in the presence of allenyl methanesulfonate **15** resulted in clean formation of 7-membered lactone phenyl ether **27**. Although **27** was not part of the retrosynthetic plan, the photocycloaddition chemistry of **27** was investigated to probe the function of the photocycloaddition reaction in the context of a complex intermediate.

3.3.4. Synthesis of the chebulic acid core: formation of an unexpected photoproduct. Analysis of the ^{1}H NMR and ^{13}C NMR spectrum of the product formed upon irradiation of **27** in CH_2Cl_2 at 0 °C suggested that alkyne **28** had been formed instead of the expected tetracyclic photoadduct (Equation 3.1). This assignment was supported by the presence of characteristic ^{1}H NMR signals at 2.84 and 2.76 ppm corresponding to the protons at C2 and ^{13}C NMR[21] signals 94.3 and 74.4 ppm corresponding to the alkyne quaternary carbons. The presence of an alkyne was confirmed

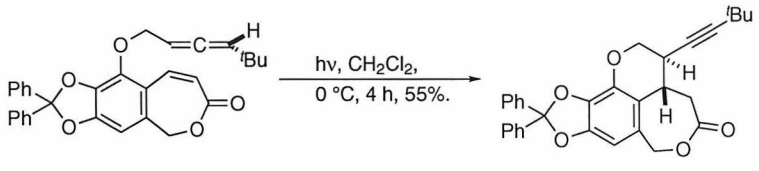

27 *(85% ee)* **28** *(85% ee)*

Asymmetric Induction *100%*

(3.1)

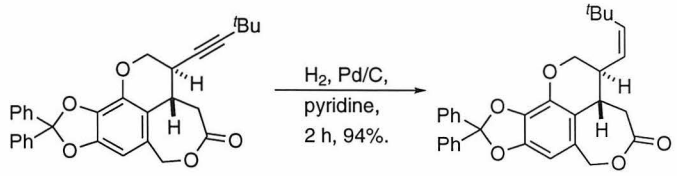

28 **29**

(3.2)

Scheme 3.5. Derivitization of alkyne photoproduct for enantiomeric excess determination.

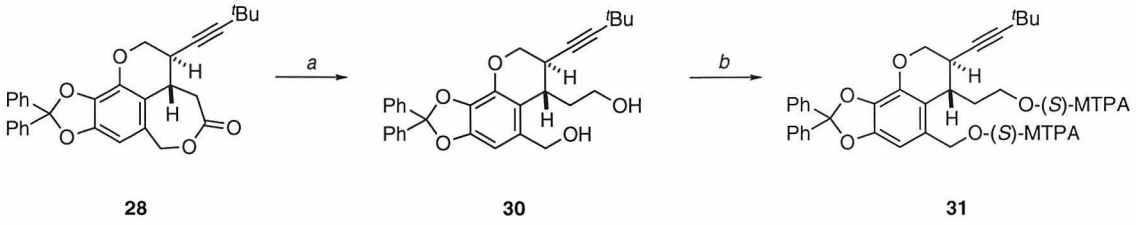

(a) $LiBH_4$, THF, 0 °C, 30 min (80%). (b) (*R*)-MTPACl, 4-DMAP, CH_2Cl_2, 23 °C, 5 min (100%).

by semihydrogenation of **28** with palladium on carbon in pyridine to the *cis*-olefin **29** (Equation 3.2). The relative stereochemistry of alkyne **28** was tentatively assigned based on the transition-state model for enantioselective photocycloadditions previously described.[22] The unexpected product may form by a 1,5-hydrogen shift in a biradical intermediate resulting from the initial C-C bond forming step. Alternatively, the initial [2+2]-photocycloaddition product may undergo strain-induced retro-Conia fragmentation to give an enol that tautomerizes to **28**. Studies undertaken to distinguish these mechanistic alternatives are described below.

To determine the extent of enantiomeric induction in the photocyclization of **27**, lactone **28** was reduced to diol **30**, which was derivitized as the bis-(*S*)-MTPA ester **31** (Scheme 3.5). Analysis of the ^1H NMR spectrum of **31** indicated that the enantiomeric excess of **28** was identical, within experimental error, to that of the precursor allene **14**.[23]

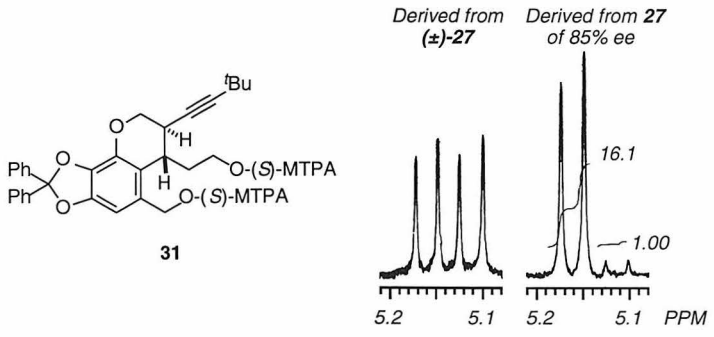

Figure 3.2. Enantiomeric excess determination of alkyne photoproduct.

Scheme 3.6. Synthesis of deuterium-labeled photosubstrate.

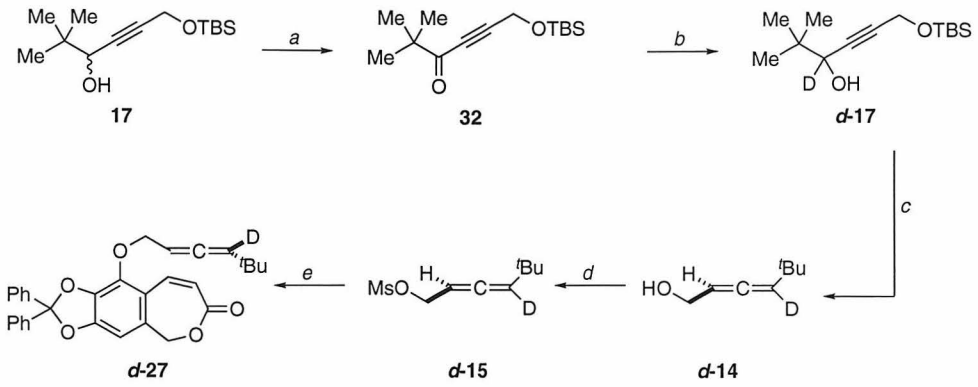

(a) Dess-Martin periodinane, CH_2Cl_2, 0 °C, 20 min (70%). (b) $NaBD_4$, MeOH, 23 °C, 10 min (94%) (c) *i.* MsCl, Et_3N, CH_2Cl_2, 0 °C; *ii.* HF, CH_3CN, H_2O, 23 °C, 20 min; *iii.* $LiAlH_4$, Et_2O, -78 °C (88%, three steps). (d) MsCl, Et_3N, CH_2Cl_2, 0 °C (98%). (e) NaH, DMF, 0 °C→23 °C, 12 h (28%).

Therefore, the photocyclization of **27** occurred with complete enantioselection. A comparison of partial ^1H NMR spectra of **31** derived from racemic **27** and from **27** of 85% enantiomeric excess is shown in Figure 3.2.

3.3.5. Mechanistic study of stereospecific 1,5-hydrogen atom transfer in the formation of an unusual allene/enoate photoproduct.[24] To scrutinize the mechanism responsible for the formation of **28**, photosubstrate **27** was deuterium-labeled at the distal terminus of the allene as shown in Scheme 3.6. Oxidation of **17** using the Dess-Martin periodinane[15] followed by reduction with sodium borodeuteride afforded ***d*-17**, which was converted to labeled allene ***d*-14** as previously described. Analysis of the ^1H NMR and ^2H NMR spectra of ***d*-17** indicated that the isotopic purity at the labeled position was 96%.

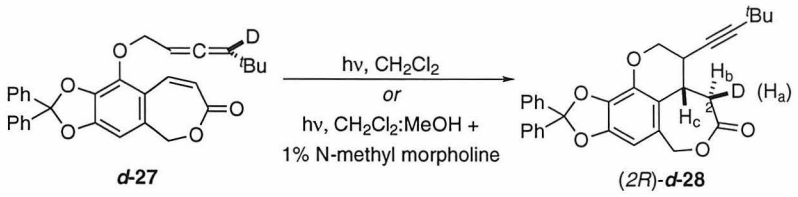

(3.3)

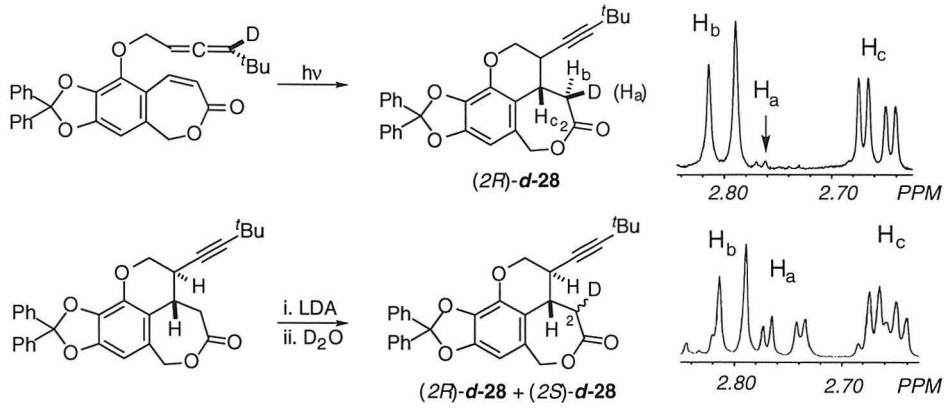

Partial ^{1}HNMR (500 MHz, C_6D_6) spectra of **d-26** *formed upon irradiation of* **d-25** *and upon enolization of* **26** *and quenching with D_2O.*

Figure 3.3. Comparison of diastereoselection in deuterium incorporation at C^2 upon enolate tautomerization and upon photocycloaddition.

Irradiation of ***d*-27** in CH_2Cl_2 afforded the deuterium-labeled acetylenic product ***d*-28** (Equation 3.3). Analysis of the ^{1}H NMR spectrum of ***d*-28** revealed that the deuterium label had been transferred to C2 with greater than 20:1 diastereoselectivity (Figure 3.3). Analysis of the phase sensitive NOESY spectrum of ***d*-28** confirmed the stereochemical assignment of **28** and indicated that the (*2R*) isomer had been preferentially formed (Figure 3.4). Because the deuterium-labeled photosubstrate was 96% isotopically pure as determined by analysis of its ^{1}H NMR spectrum, the diastereoselectivity in the formation of ***d*-28** measured by ^{1}H NMR analysis represents a lower limit for the stereoselectivity in the 1,5-hydrogen atom transfer reaction that affords **28**.

To exclude the possibility that ***d*-28** was formed through retro-Conia fragmentation of a transient tetracyclic photoadduct followed by stereospecific tautomerization of the

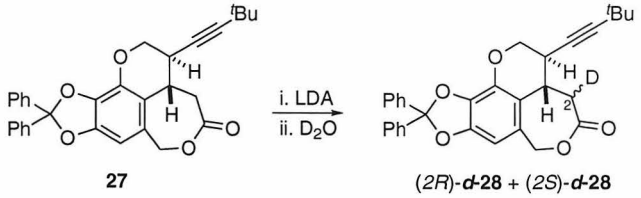

(3.4)

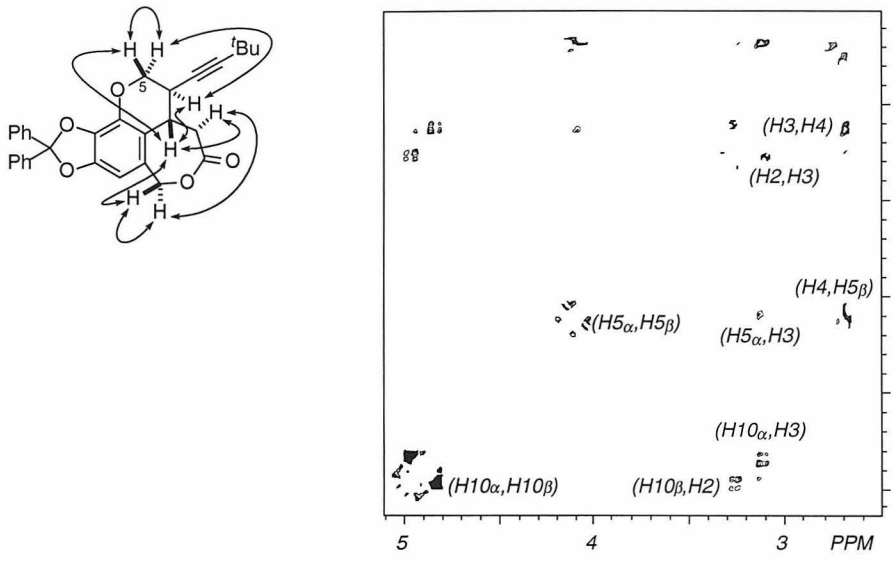

Figure 3.4. Determination of stereoselectivity of 1,5-hydrogen atom transfer in the formation of alkyne photoproduct.

intermediate enol, ***d*-27** was irradiated in 19:1 CH_2Cl_2–MeOH + 1% N-methyl morpholine. The same labeled product ***d*-28** was formed stereospecifically (Equation 3.3). Analysis of the ^1H NMR spectrum of the product indicated that less than 3% incorporation of protium had occurred at C2. Additionally, when the lithium enolate of **28** was generated and quenched at -78 °C with D_2O, the two diastereomers (2*R*)-***d*-28** and (2*S*)-***d*-28** were formed in a 2.2:1 ratio (Equation 3.4) as determined by analysis of the ^1H NMR spectrum (Figure 3.3).[25,26]

3.3.6. Synthesis and photocycloaddition of allene containing a pendant olefin. Because **28** possessed the correct relative stereochemistry at the two established stereocenters and because the photocyclization reaction afforded complete transfer of asymmetry from the starting allene to the alkyne product, the elaboration of **28** to chebulic acid was attempted. The critical aspects of the synthetic plan for converting **28** to chebulic acid were (1) conversion of the alkyne substituent to a hydroxyethyl

substituent, a masked form of the carboxylate present in **2**; (2) oxidation of the lithium enolate of the 7-membered lactone with electrophilic bromine followed by unmasking of the carboxylate derived from the alkyne substituent; (3) nucleophilic displacement of the α-bromolactone by the carboxylate anion to afford a dilactone containing all three stereocenters of chebulic acid in the correct relative configuration; and (4) oxidation of the cyclic ether to a cyclic lactone, installing the final carboxylate of chebulic acid. However, **28** proved unsuitable for this plan when all attempts to remove the *tert*-butyl substituent were unsuccessful. Although olefin **29** was readily cleaved upon treatment with osmium tetroxide/sodium periodate, the derived α-branched aldehyde was stereochemically unstable and proved intractable to Wittig olefination conditions.

Because of the difficulties encountered in converting the *tert*-butylalkynyl substituent of **29** to the carboxyethyl substituent present in the synthetic target, a strategy was developed for removal of the exocyclic olefin alkyl substituent derived from the allene 3'-substituent. Grubbs has described a ruthenium(II) olefin metathesis catalyst, **33**, that possesses extraordinary tolerance for oxygen functionality in the substrate.[27] A number of elegant applications of this catalyst have been reported, including cycloalkene synthesis *via* ring-closing metathesis.[28] In this reaction (**34**→**35**, Scheme 3.7), an acyclic olefin byproduct is also formed, which comprises the desired terminal olefin in the strategy

Scheme 3.7. Olefin metathesis strategy for stereocontrolling auxiliary removal.

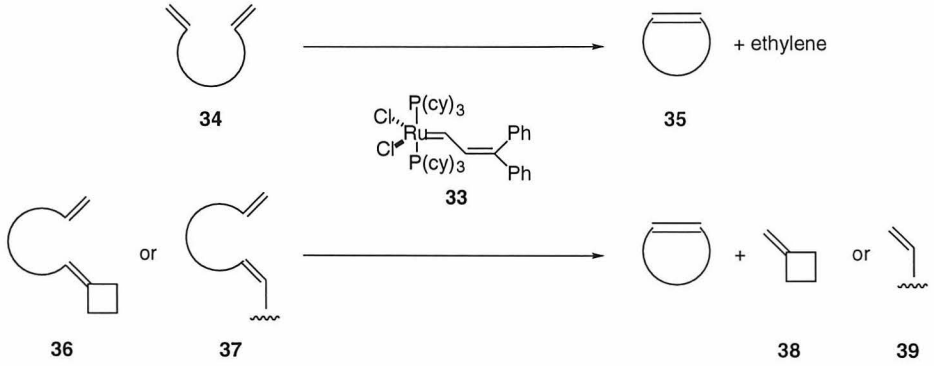

outlined in Scheme 3.7.[29] In principle this strategy is applicable both to *exo*-alkylidenecyclobutane photocycloaddition products (**36**→**38**), and to alkyne photocyclization products following semihydrogenation (**37**→**39**).

Scheme 3.8. Synthesis and photochemistry of dimethylpentenyl-substituted allene in enantiomerically enriched form.

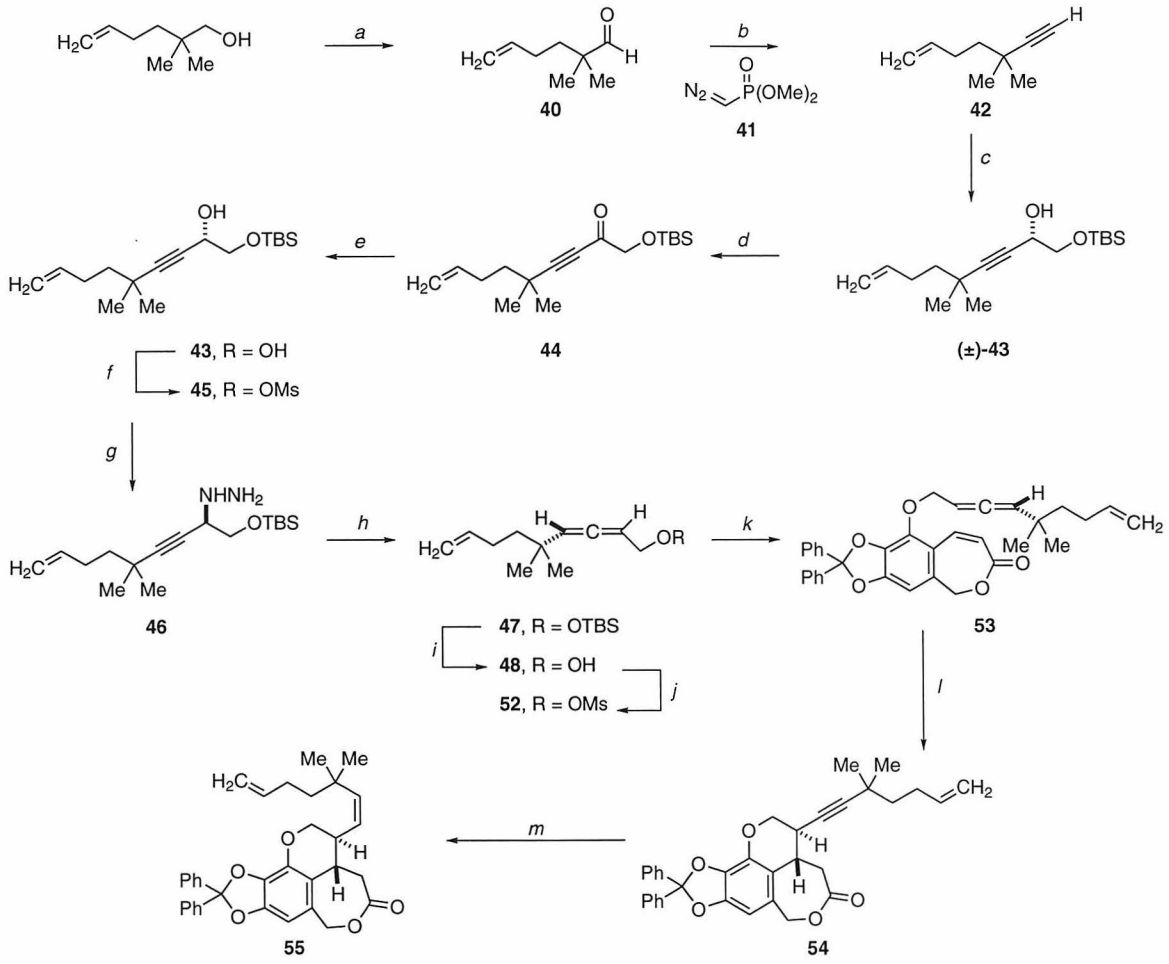

(a) DMSO, oxalyl chloride, CH_2Cl_2, then 2,2-dimethyl-5-hexen-1-ol, then TEA, -78 °C→0 °C, 30 min (96%). (b) ^{t}BuOK, **41**, THF, -78 °C, then **42**, -78 °C→0 °C, 1 h (68 °C). (c) ^{n}BuLi, Et_2O, -78 °C, then **8**, 30 min (83%). (d) DMSO, oxalyl chloride, CH_2Cl_2, **(±)-43**, then TEA, -78 °C→0 °C, 30 min (93%). (e) (*S*)-Alpine Borane, 23 °C, 16 h (56%, 93% ee). (f) MsCl, TEA, CH_2Cl_2, 0 °C, 30 min. (g) 1:1 MeOH– H_2NNH_2, 23 °C, 36 h. (h) PTAD, 1:1 CH_2Cl_2–Et_2O, 0 °C, 5 min (53%). (i) TBAF, THF, 23 °C, 5 min (95%). (j) MsCl, TEA, CH_2Cl_2, 0 °C, 15 min (91%). (k) NaH, DMF, 0 °C→23 °C, 1.5 h (54%). (l) hν, CH_2Cl_2, 0 °C, 5 h (55%). (m) Pd/C, H_2, 3,3-dimethyl-1-butene, pyridine, 23 °C, 6 h (50% plus 36% recovered **54**).

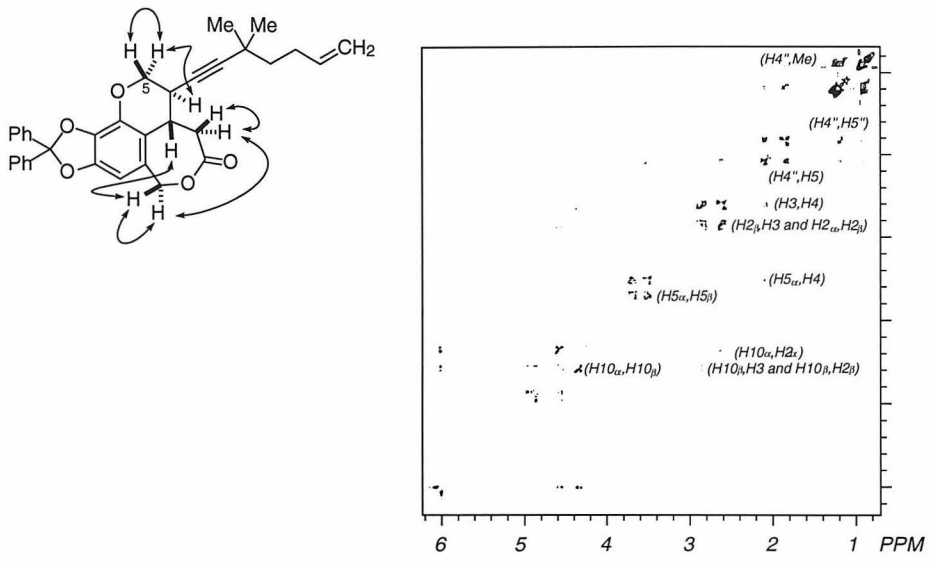

Figure 3.5. Determination of relative stereochemistry of photoproduct derived from dimethylpentenyl allene.

An allene containing a dimethylpentenyl substituent at the 3'-terminus was prepared in enantioenriched form as shown in Scheme 3.8. The known aldehyde **40**,[11] prepared by Swern oxidation of 2,2-dimethyl-5-hexen-1-ol, was olefinated with phosphonate **41**.[12] *In Situ* decomposition of the diazoalkene product followed by rearrangement of the derived carbene afforded alkyne **42**,[30] which was converted to allene **48**, coupled to coumarin **26**, and photolyzed as described for the preparation of **28**. Comparison of the phase sensitive NOESY spectrum of **54** with that of ***d*-28** indicated that the stereochemical outcome of the photocyclization of **53** was not affected by the presence of the pendant olefin (Figure 3.5). Semihydrogenation of the alkyne functionality of **48** was accomplished using 10% palladium on carbon in pyridine. The selectivity of this reagent combination for the internal alkyne over the terminal alkene was improved by the inclusion of 3,3-dimethyl-1-butene as a competing substrate for reduction.

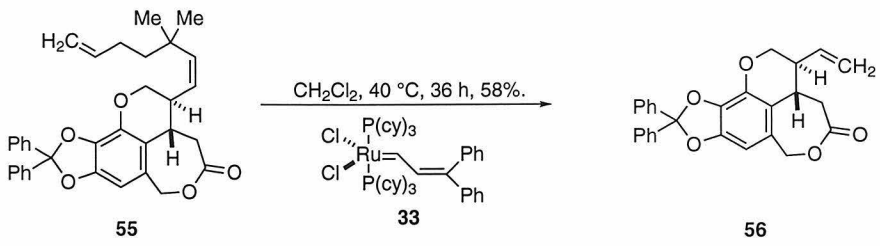

(3.5)

3.3.7. Removal of photocycloaddition stereocontrolling group by ring-closing metathesis. Treatment of **55** with 5 mol% ruthenium catalyst **33** in dilute, degassed CH_2Cl_2 solution in a sealed vessel at 40 °C afforded terminal olefin **56** (Equation 3.5) in 58% yield. Conducting the metathesis reaction under these conditions was important in mitigating loss of product due to dimerization. Despite the lengthy reaction times and elevated temperatures, no decomposition products derived from olefination of the lactone carbonyl were observed.

3.3.8. Attempted elaboration of metathesis product to chebulic acid. The carboxyethyl moiety of chebulic acid was revealed and the C3 stereocenter was installed as shown in Scheme 3.9. Rhodium-catalyzed hydroboration of **56** using the conditions of Evans afforded **57**,[31] which was protected with TBSCl to afford **58**. Oxidation of the lithium enolate of **58** with carbon tetrabromide at -78 °C afforded **59** as a single diastereomer by ^{1}H NMR. The silyl ether protecting group of **59** was removed and the primary hydroxyl group oxidized with the Dess-Martin periodinane[15] followed by buffered permanganate.[32] Lactonization of the derived carboxylate, which was not isolated, afforded dilactone **61**.

Scheme 3.9. Installation of the C^3 stereocenter of chebulic acid.

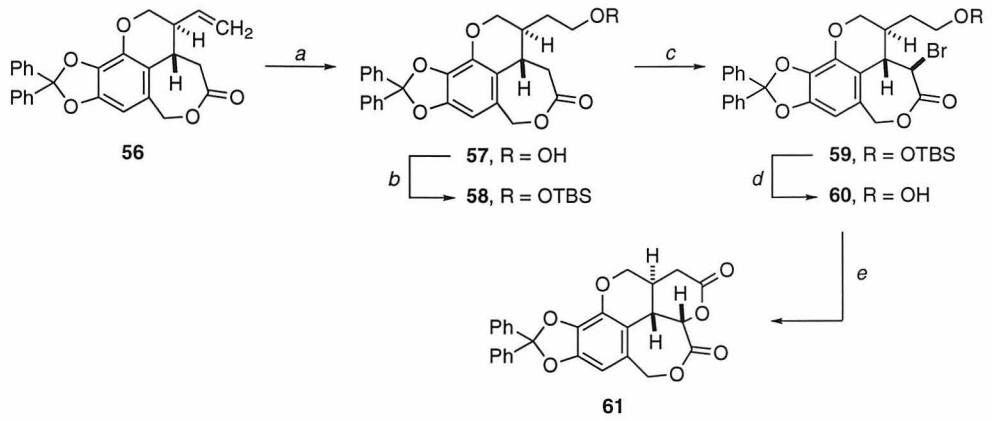

(a) catecholborane, $ClRh(PPh_3)_3$, THF, 23 °C, 30 min, then H_2O_2, 23 °C, 3 h (86%). (b) TBSCl, TEA, 4-DMAP, CH_2Cl_2, 23 °C, 14 h (87%). (c) LDA, THF, -78 °C, 1.5 h, then CBr_4, 30 min (71%). (d) HF, CH_3CN, H_2O, 0 °C, 30 min (84%). (e) *i.* Dess-Martin periodinane, CH_2Cl_2, 23 °C, 45 min. *ii.* $KMnO_4$, pH 5.0, 23 °C 2.5 h (77%).

The enantiomeric induction in the photocyclization of **54** was determined by ^1H NMR analysis of the (*S*)-MTPA ester derived from **57** (Figure 3.6).[33] The observed 40.8:1.00 diastereomer ratio, corresponding to 95% enantiomeric excess, indicated that the presence of the dimethylpentenyl substituent had not affected the stereoselectivity of the photocyclization. The relative stereochemistry of the three stereocenters of **61** was determined by analysis of the phase-sensitive NOESY spectrum shown in Figure 3.7. In particular the strong NOE cross peak correlation between C2*H* and C3*H*, and a much

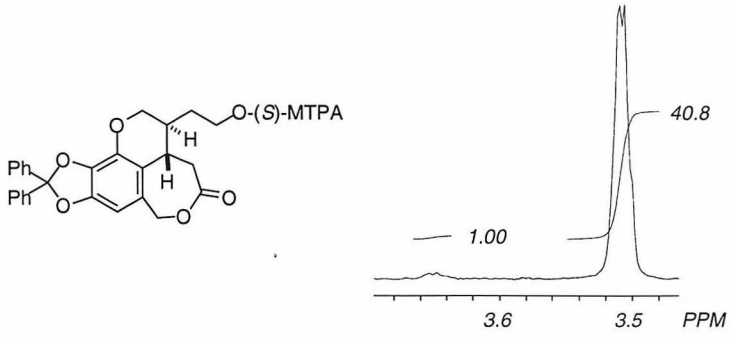

Figure 3.6. Determination of enantiomeric excess of photoproduct derived from dimethylpentenylallene.

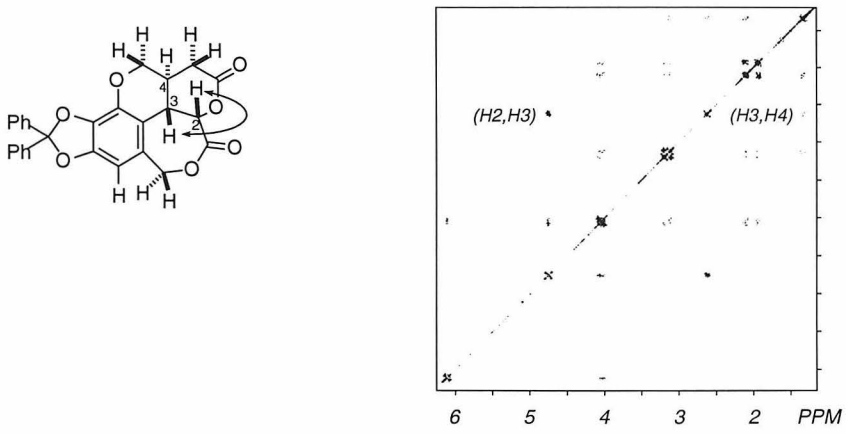

Figure 3.7. Confirmation of correct relative stereochemistry of advanced intermediate containing all stereocenters of chebulic acid.

weaker cross peak between C3*H* and C4*H*, supports a 2,3-*cis*, 3-4-*trans* stereochemical assignment.

Elaboration of **61**, which possesses the correct relative and absolute configuration of the three adjacent stereocenters, to chebulic acid was unsuccessful. Treatment of **61** with ruthenium tetroxide in acetonitrile[34] effected clean conversion of the benzylic methine to the tertiary alcohol, and attempts to oxidize the cyclic ether to the hemiacetal under free radical conditions led to extensive decomposition of the substrate. Accordingly, studies directed toward the conversion of alkyne photoproduct **54** to chebulic acid **2** were abandoned.

3.4. Discussion.

3.4.1. Preparation of an advanced intermediate for the synthesis of chebulic acid. The asymmetric intramolecular allene-enone and allene-enoate photocycloadditions are powerful transformations that permit rapid assembly of complex, fused, polycyclic structures in enantiomerically pure form. A number of elegant syntheses employing diastereoselective photocycloadditions in which the stereochemical bias arises

from asymmetric centers in the tether connecting the reacting partners[35] or adjacent to the reacting enone or enoate[36] have been reported. In all of these photocycloadditions the stereocontrolling center is preserved in the photoadduct. However, in the photocycloadditions of chiral, 1,3-disubstituted allenes with enones and enoates previously reported,[22] the axial chirality of the allene is the source of asymmetry and the stereocontrolling group is absent in the photoproduct.[37] In order to demonstrate the synthetic utility of the allene-enoate asymmetric photocycloaddition its application to the synthesis of chebulic acid **2** has been investigated.

In the context of the synthesis of chebulic acid, the asymmetric [2+2]-photocycloaddition permitted rapid access to **28**, an intermediate containing both methine stereocenters of the target, in enantiomerically pure form. Difficulty in converting the *tert*-butylalkyne moiety of **28** to the carboxyethyl moiety present in the target motivated the development general strategies for removing alkyl groups in the photoproducts derived from 3'-substituents of the allene reactants.[38] Two aspects of the olefin-metathesis based strategy described in this chapter are noteworthy: (1) the pendant olefin does not undergo intramolecular addition by the intermediate biradical to form a polycyclic product; and (2) the extraordinary functional group tolerance of the metathesis catalyst **33**, demonstrated by the conversion of highly oxygenated substrate **55** to **56**, permits this strategy to be employed with complex synthetic intermediates. Formally, asymmetric photocycloaddition or asymmetric photocyclization-semihydrogenation followed by metathetic excision of the alkyl substituent is equivalent to asymmetric photocycloaddition of an achiral, monosubstituted allene.

There were two possibilities for the installation of the C3 stereocenter of chebulic acid: (1) bromination of the lithium enolate of **58** followed by oxidation of the hydroxyl group to the carboxylate and intramolecular displacement to afford **61** with net inversion; and (2) oxidation of the hydroxyl group to the carboxylate followed by selective enolization

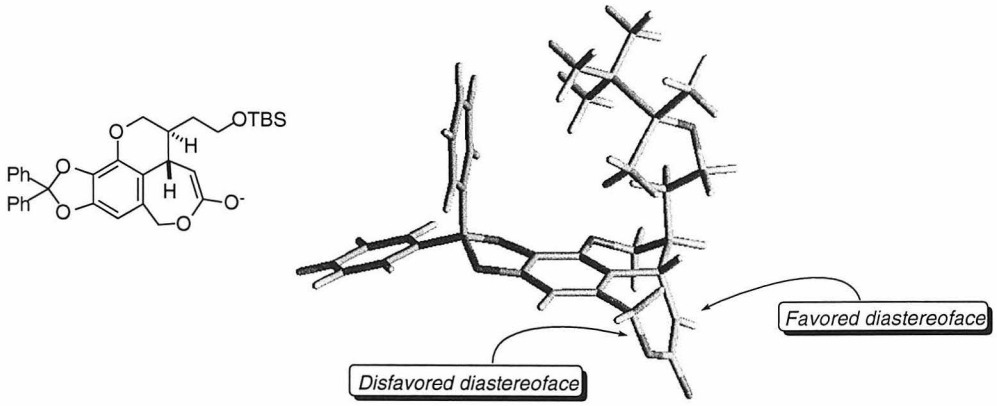

Figure 3.8. Conformational basis for stereoselectivity in installation of the C3 stereocenter of chebulic acid.

and oxidation of the lactone to afford an α-hydroxylactone that would cyclize to **61** with net retention. Accordingly, a preference for either diastereomer upon oxidation of the lithium enolate of **58** would have been synthetically acceptable. Molecular mechanics minimization (MM2*) of the naked enolate derived from **58** revealed a conformational preference for oxidation of the *pro-S* face (Figure 3.8).[39] Accordingly, the lithium enolate of **58** was oxidized with carbon tetrabromide, affording a single diastereomer as judged by analysis of the ^{1}H NMR spectrum of the product. Analysis of the NOESY spectrum of **61** indicated that the correct relative configuration of the three stereocenters of chebulic acid had been established, confirming the predicted sense of asymmetric induction in the bromination of the lithium enolate of **58**.

3.4.2. Formation of an unexpected photoproduct arising from 1,5-hydrogen atom transfer. In principle two mechanistic pathways that account for the formation of **28** upon irradiation of **27** may be envisioned (Scheme 3.10). Irradiation of **27** generates an enoate triplet that adds to the proximal terminus of the allene to give an intermediate 1,4-biradical **62**. In principle this biradical has three fates following intersystem crossing to the singlet state: (1) ring closure to give *exo*-alkylidene cyclobutane

Scheme 3.10. Mechanistic possibilities for the formation of alkyne photoproduct.

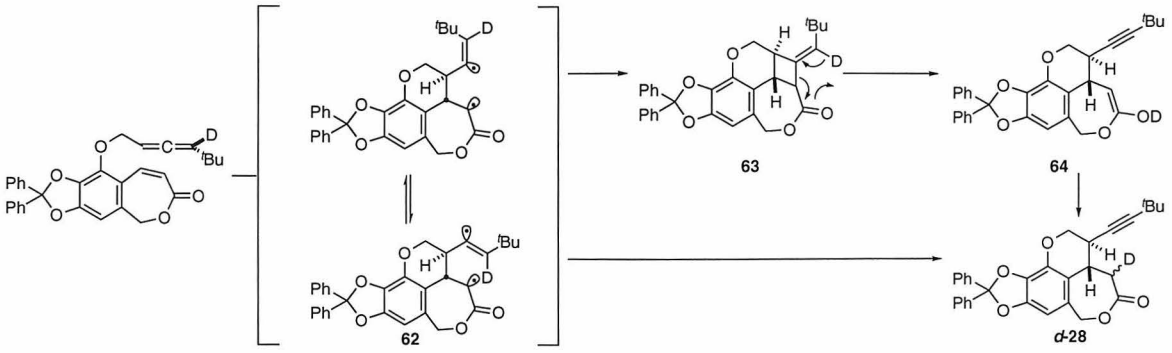

63; (2) 1,5-hydrogen transfer to give alkyne **28** directly; and (3) reversion to starting material. Tetracyclic photocycloaddition products were uniformly not observed upon irradiation of substrates that afford alkyne adducts. Nonetheless, **63** could form transiently, decomposing *via* a strain-induced retro-Conia fragmentation[40] that affords enol **64**, which would tautomerize to afford **28**.

To distinguish these mechanistic alternatives, deuterium-labeled allene-enoate ***d*-27** was prepared. The diastereoselectivity at C2 upon irradiation of ***d*-27** is dependent on the pathway by which **28** is formed. If **28** is formed by retro-Conia fragmentation of **63** followed by tautomerization of **64** to **28**, then the stereochemistry at C2 of the product would be determined by the tautomerization step, leading to a diastereomeric mixture of deuterium-labeled products (*2R*)- and (*2S*)-***d*-28**. Additionally, if enol **64** is an intermediate in the formation of **28**, irradiation of ***d*-27** in protic solvent should result in exchange of the enolic proton during the lifetime of **64**, leading to unlabeled **28**. However, if **28** is formed by direct 1,5-hydrogen atom transfer, then the diastereoselectivity of product formation should be controlled by the conformation of **62**. Analysis of Dreiding models of **62** and molecular mechanics minimization (MM2*) of alkene **65** revealed a conformational preference that would favor hydrogen atom transfer to the β-face (Figure 3.9).[41] Additionally, conducting the reaction in MeOH should not lead to loss of the deuterium label under the neutral conditions of the reaction if enol **64** is not

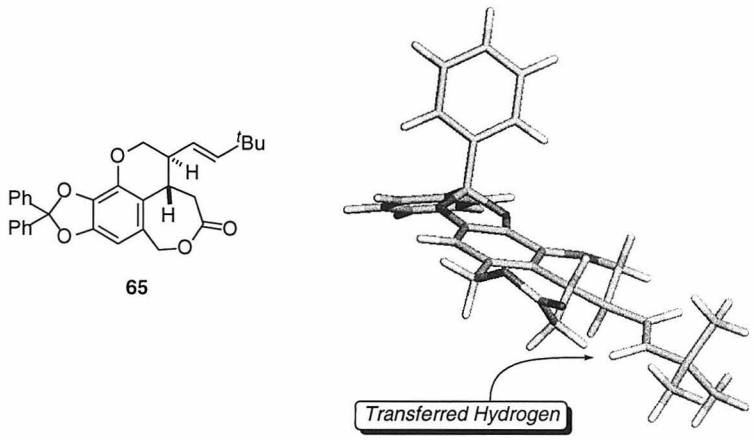

Figure 3.9. Conformational basis for stereoselectivity in 1,5-hydrogen atom transfer.

an intermediate in the formation of **28**. When ***d*-27** was irradiated in CH_2Cl_2 at 0 °C, a single C2 diastereomer (*2R*)-***d*-28** was formed. Moreover, no diminution in isotopic purity was observed when ***d*-27** was irradiated in a dichloromethane–methanol mixture. Collectively these results can only be accommodated by a mechanistic pathway involving biradical intermediate **62**, which undergoes a stereospecific 1,5-deuterium shift.

A working model that accounts for the high levels of asymmetric induction in photocycloadditions of optically active allenes with cyclic enones and enoates to form cyclobutanes has been described (Scheme 3.11).[22] The observation of high optical activity in the photoproducts suggests a mechanism in which the stereochemistry of the products is established kinetically upon addition of the enone excited state to the least hindered allene face (**66** $\rightarrow$ **67** $\rightarrow$ **68**). Importantly, within the lifetime of the putative 1,4-biradical intermediate **68/68'**, allylic C-C single bond rotation and inversion of the vinyl radical occur (**68** $\rightleftarrows$ **68'**)[42] with consequent loss of olefin geometry.[43,44] The observation of asymmetric induction in the photocyclization that leads to alkyne formation is consistent with a mechanism in which hydrogen atom transfer by the putative 1,4-biradical **68'** is faster than retroaddition, k_t (**68'** $\rightarrow$ **69**) >> k_r (**68/68'** $\rightarrow$ **67**).[45] Although the structural features of **27** that result in the formation of an alkynyl adduct rather than a cyclobutyl

Scheme 3.11. Origin of enantioselectivity in the formation of alkyne [2+2]-photocycloaddition products.

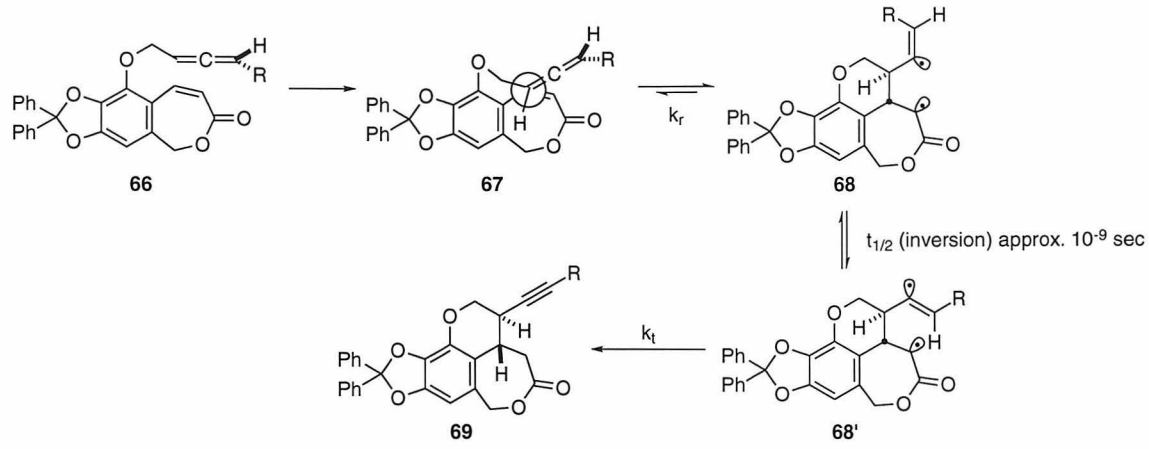

adduct have not been delineated, the strain associated with the formation of the putative tetracyclic adduct **63** may preclude its formation, resulting in the observed preference for 1,5-hydrogen shift. These results demonstrate that high optical induction can be expected in [2+2]-photocycloadditions not only when the biradical can cyclize to a four-membered ring product, but also when other processes are available to this high-energy intermediate that are faster than ring closure, such as 1,5-hydrogen atom transfer.

3.5. Conclusions

These investigations demonstrate that asymmetric [2+2]-photocycloadditions employing chiral 1,3-disubstituted allenes are useful methods for the construction of complex, highly functionalized, polycyclic structures with absolute stereocontrol. Employing asymmetric photocycloaddition methodology an advanced synthetic intermediate **61** containing all stereocenters of chebulic acid has been prepared in high enantiomeric enrichment. During the preparation of **61**, a ring-closing-metathesis based strategy for excision of the stereocontrolling 3'-substituent was developed, and an unusual allene/enoate photocyclization was identified. Isotopic labeling experiments conducted to

investigate the mechanism of the unusual photocycloaddition support a transition state model advanced in Chapter 2 that describes the origins of enantioselectivity in asymmetric photocycloadditions.

3.6. References and Notes

1. (a) Schmidt, O. T. *Fortschr. Chem. Org. Naturstoffe* **1956**, *13*, 70. (b) Haslam, E.; Uddin, M. *J. Chem. Soc. (C)* **1967**, 2381. (c) Jochims, J. C.; Taigel, G.; Schmidt, O. T. *Liebigs. Ann. Chem.* **1968**, *169*, 717. (d) Yoshida, T.; Okuda, T.; Koga, T.; Toh, N. *Chem. Pharm. Bull.* **1982**, *30*, 2655. (e) Yoshida, T.; Fujii, R.; Okuda, T. *Chem. Pharm. Bull.* **1980**, *28*, 3713.
2. Kashiwada, Y.; Nanaka, G.; Nishioka, I.; Chang, J.-J.; Lee, K. H. *J. Nat. Prod.* **1992**, *55*, 1033.
3. Berry, D. E.; MacKenzie, L.; Shultis, E. A.; Chan, J. A.; Hecht, S. M. *J. Org. Chem.* **1992**, *57*, 420.
4. Nanaka, G.; Akazawa, M.; Nishioka, I. *Heterocycles* **1992**, *33*, 597.
5. For an x–ray crystal structure of chebulic acid triethyl ester see: Schilling, G.; Schweiger, R.; Weis, G.; Mayer, W.; Weiss, J.; Siegel, R. *Liebigs Ann. Chem.* **1981**, *182*, 603.
6. (a) Yoshida, T.; Okuda, T. *Heterocycles* **1980**, *14*, 1743. (b) Okuda, T.; Yoshida, T.; Nayeshiro, H. *Chem. Pharm. Bull.* **1977**, *25*, 1862.
7. Still, W. C.; Kahn, M.; Mitra, A. *J. Org. Chem.* **1978**, *43*, 2923.
8. Mohamadi, F.; Richards, N. G. J.; Guida, W. C.; Liskamp, R.; Lipton, M.; Caufield, C.; Chang, G.; Hendrickson, T.; Still, W. C. *J. Comput. Chem.* **1990**, *11*, 1990.
9. Ireland, R. E.; Lu, L. *J. Org. Chem.* **1993**, *58*, 2899.
10. Jurd, L. *J. Am. Chem. Soc.* **1959**, *81*, 4606.

11. Beckwith, A. L. J.; Lawrence, T. *J. Chem. Soc. Perkin II* **1979**, 1535.

12. Seyferth, D.; Marmor, R. S.; Hilbert, P. *J. Org. Chem.* **1971**, *36*, 1379.

13. Nguyen, S. T.; Grubbs, R. H. *J. Am. Chem. Soc.* **1993**, *115*, 9856.

14. Prepared as described for enolization and quench of **28**.

15. Dess, D. B.; Martin, J. C. *J. Org. Chem.* **1983**, *48*, 4156.

16. Midland, M. M.; Tramontano, A.; Zderic, S. A. *J. Am. Chem. Soc.* **1977**, *99*, 5211.

17. Derivitization of **27** as its (*S*)–MTPA ester and integration of the ^{1}H NMR (300 MHz, $CDCl_3$) resonances at δ 1.21 (major, $C_6(C\mathbf{H}_3)_3$) and δ 1.18 (minor, $C_6(C\mathbf{H}_3)_3$) ppm indicated a diastereomer ratio of 11.9:1.00 (84% ee).

18. Dale, J. A.; Dull, D. L.; Mosher, H. S. *J. Org. Chem.* **1969**, *34*, 2453.

19. Myers, A. G.; Finney, N. S.; Kuo, E. Y. *Tetrahedron Lett.* **1989**, *30*, 5747.

20. Chemistry developed by Mrs. Mary S. Shepard.

21. Determined at 500 MHz (^{1}H) and 126 MHz (^{13}C) in C_6D_6.

22. Carreira, E. M.; Hastings, C. A.; Shepard, M. S.; Yerkey, L. A.; Millward, D. B. *J. Am. Chem. Soc.* **1994**, *116*, 6622. See also Chapter 2 of this thesis.

23. Integration of the ^{1}H NMR (500 MHz, C_6D_6) resonances at δ 5.17 (major, one of C1'H_2) and δ 5.12 (minor, one of C1'H_2) ppm indicated a diastereomer ratio of 14.3:1.00 (87% ee).

24. Adapted from Hastings, C. A.; Ringgenberg, J. D.; Carreira, E. M. *Tetrahedron Lett.* **1997**, *38*, 8789.

25. (a) The observed ratio of H_b/H_a is 1.6:1 which, after correction for internal return, affords the indicated 2.2:1 ratio. The correction is necessary since it is known that enolates generated with LDA suffer reprotonation by the diisopropylamine which is generated in the course of the reaction and remains associated with the enolate (Seebach, D. *Angew. Chem., Int. Ed. Engl.* **1988**, *27*, 1624-1654). The extent of internal return was quantified by comparison of the integrals of H_a and H_b with the

integral of H_c. Thus, if the integrals of H_a, H_b, and H_c are I_a, I_b, and I_c, respectively, then % internal return = $(I_a + I_b - I_c)/I_c$, or 26%. The ratio of the two diastereomers (*R*)-**7**/(*S*)-**7** = $(I_c - I_a)/(I_c - I_b)$ = 2.2:1.

26. The protonation of lithium enolates has been suggested to occur by rapid protonation at oxygen followed by a slow tautomerization; see: Keefe, J. R.; Kresge, A. J. In *The Chemistry of Enols*; Rappoport, Z., Ed.; Wiley: Chichester, 1990; Chapter 7, pp 399-480.
27. Dias, E. L.; Nguyen, S. T.; Grubbs, R. H. *J. Am. Chem. Soc.* **1997**, *119*, 3887 and references therein.
28. For a review of synthetic application of ring closing metathesis, see: Grubbs, R. H.; Miller, S. J.; Fu, G. C. *Acc. Chem. Res.* **1995**, 446.
29. I am grateful to Prof. R. H. Grubbs and Prof. G. C. Fu for helpful discussions.
30. Gilbert, J. C.; Weerasooriya, U. *J. Org. Chem.* **1982**, *47*, 1837.
31. Evans, D. A.; Fu, G. C.; Hoveyda, A. H. *J. Am. Chem. Soc.* **1988**, *110*, 6917.
32. Abiko, A.; Roberts, J. C.; Takesawa, T.; Masamune, S. *Tetrahedron Lett.* **1986**, *27*, 4537.
33. Integration of the ^{1}H NMR (500 MHz, $CDCl_3$) resonances of the derived (*S*)-MTPA ester at δ 3.53 (major, (*S*)-MTPA OC**H**$_3$) and δ 3.61 (minor, (*S*)-MTPA OC**H**$_3$) ppm indicated a diastereomer ratio of 40.8:1.00 (95% ee).
34. Smith, A. B.; Scarborough, R. M. *Syn. Comm.* **1980**, *10*, 205.
35. (a) Crimmins, M. T.; Jung, D. K.; Gray, J. L. *J. Am. Chem. Soc.* **1993**, *115*, 3146-3155. (b) Crimmins, M. T.; Watson, P. S. *Tetrahedron Lett.* **1993**, *34*, 199-202. (c) Crimmins, M. T.; King, B. W.; Watson, P. S.; Guise, L. E. *Tetrahedron* **1997**, *53*, 8963-8974. (d) Tanaka, M.; Tomioka, K.; Koga, K. *Tetrahedron* **1994**, *50*, 12829-12842. (e) Tenaglia, A.; Barille, D. *Synlett* **1995**, 776-778.
36. Dauben, W. G.; Shapiro, G. *J. Org. Chem.* **1984**, *49*, 4252.

37. Mislow has termed this type of chirality transfer "self-immolative," see: Mislow, K. *Introduction to Stereochemistry*, Benjamin: New York, 1965; p. 131.

38. For a similar two-step transformation involving asymmetric intramolecular photocycloaddition of an allenylsilane followed by protodesilylation, see: Shepard, M. S.; Carreira, E. M. *J. Am. Chem. Soc.* **1997**, *119*, 2597.

39. A Monte Carlo conformer search (50 conformers evaluated) identified the conformer shown in Figure 3.8 as the global minimum.

40. (a) Rouessac, F.; Conia, J.-M. *Tetrahedron Lett.* **1965**, *7*, 3319. (b) Rouessac, F.; Conia, J.-M. *Tetrahedron Lett.* **1965**, *7*, 3313.

41. A Monte Carlo conformer search (50 conformers evaluated) identified the conformer shown in Figure 3.9 as the global minimum. In order to illustrate the stereochemical preference for 1,5-hydrogen atom transfer to the β-face arising from the ring conformation shown, the exocyclic alkene substituent has been rotated in order to place the transferred hydrogen in proximity to the acceptor radical.

42. (a) Kochi, J. K. *Adv. Free Rad. Chem.* **1975**, *5*, 189. (b) Fessenden, R. W.; Schuler, R. H. *J. Chem. Phys.* **1963**, *39*, 2147.

43. For a [2+2]-photocycloaddition reaction of an alkene with an enone which intercepts the 1,4-biradical, see: Becker, D.; Morlender, N.; Haddad, N. *Tetrahedron Lett.* **1995**, *36*, 1921-1924.

44. For mechanistic investigations of alkene-enone photocycloadditions, see: (a) Andrew, D.; Weedon, A. C. *J. Am. Chem. Soc.* **1995**, *117*, 5647-5663. (b) Maradyn, D. J.; Weedon, A. C. *J. Am. Chem. Soc.* **1995**, *117*, 5359-5360. (c) Haddad, N.; Abramovich, Z. *J. Org. Chem.* **1995**, *60*, 6883-6887. For computational studies, see: (d) Broeker, J. L.; Eksterowicz, J. E.; Belk, A. J.; Houk, K. N. *J. Am. Chem. Soc.* **1995**, *117*, 1847-1848.

45. For examples in which retroaddition competes with ring closure, see: (a) McCullough, J. J.; Ramachandran, B. R.; Snyder, F. F.; Taylor, G. N. *J. Am. Chem. Soc.* **1975**, *97*, 6767-6776. (b) Hastings, D. J.; Weedon, A. C. *J. Am. Chem. Soc.* **1991**, *113*, 8525-8527. (c) Maradyn, D. J.; Sydnes, L. K.; Weedon, A. C. *Tetrahedron Lett.* **1993**, *34*, 2413-2416. (d) Rudolph, A.; Weedon, A. C. *Can. J. Chem.* **1990**, *68*, 1590-1597.

Chapter 4: Probing the Origins of the DNA 5'-CCA-3' Sequence Selectivity of the Metallointercalator-Peptide Conjugate $[Rh(phi)_2(phen')]^{3+}$-AANVAIAAWERAA-$CONH_2$: Implications for Design

4.1. Introduction

4.1.1. Introduction. Nucleic acid binding proteins play important roles in the fundamental cellular processes of replication, transcription, translation, and repair, and there is significant interest in the molecular basis of their sequence specificity. Structural studies of transcription factors have identified a number of common folds; examples include the helix-turn-helix,[1] helix-loop-helix,[2] homeodomain,[3] basic region-leucine zipper,[4] and zinc finger motifs.[5] In all of these protein classes, the DNA recognition elements are contained in a single α-helix that makes base-specific contacts in the major groove, and with one exception[6] all the transcription factors characterized to date bind to DNA as dimers or linked multimers. Although peptides corresponding to the recognition elements of DNA binding proteins generally lack sufficient nonspecific DNA affinity to afford sequence selective binding as monomers, examples of sequence selective DNA recognition by both covalent[7] and noncovalent[8] dimers of such peptides have been reported.

4.1.2. DNA binding and cleavage by phenanthrenequinone diimine complexes of rhodium(III). Barton has developed a family of coordinatively saturated phenanthrenequinone diimine (phi) complexes of rhodium(III) that bind to double helical DNA by intercalation from the major groove.[9] These complexes bind with high nonspecific affinity ($K_d < 10^{-6}$ M) and cleave DNA by abstraction of the ribose 3'-hydrogen upon photoactivation.[10] Variation of the ancillary ligands affords complexes that recognize specific nucleotide sequences.[11] NMR structural studies of Δ-α-[Rh[(*R,R*)-Me_2trien]phi]$^{3+}$

(Me_2trien = 2,9-diamino-4,7-diazadecane) bound to an oligonucleotide containing its target sequence 5'-TGCA-3' have indicated that intercalation of the phi ligand results in localized, minimal distortion of B-form DNA (Figure 4.1).[12,13] This family of structurally well-characterized metal complexes targets a variety discrete nucleotide sequences with high affinity and specificity from the major groove. Consequently, these complexes are ideal anchors for appending peptides containing recognition elements from DNA binding proteins to explore the factors governing sequence selectivity in protein-DNA recognition.

4.1.3. Recognition of DNA by metallointercalator-peptide conjugates. The P_{22} and *434* repressors are structurally similar helix-turn-helix proteins that bind as dimers to specific operator sites (Figure 4.2).[14] Ptashne demonstrated that a single α-helix is responsible for the DNA sequence selectivity of these proteins by conferring P_{22} repressor site selectivity on the *434* repressor by mutation of four amino acids in the DNA binding domain of the *434* repressor to residues found in the DNA binding domain of the P_{22} repressor.[15] Three of these residues reside in a single α-helix, which was labeled the "recognition α-helix." The consensus operator half site sequence of the *434* repressor is 5'-ACAATAT-3', and the 5'-ACAA-3' subsequence is strictly conserved in 11 of the 12 naturally occurring *434* repressor operator sites. Tethering oligopeptides derived from the recognition α-helix of the *434* repressor to $[Rh(phi)_2(phen')]^{3+}$ (phen' = (5-amidoglutaryl)-1,10-phenanthroline) conferred selectivity for 5'-ACAA-3' sequences on the relatively sequence neutral metallointercalator.[16] Tethering oligopeptides derived from the DNA binding domains of the zinc finger transcription factors Sp1 and Adr1 to $[Rh(phi)_2(bpy')]^{3+}$ (bpy' = 4-(4-carboxybutyl),4'-methyl-2,2'-bipyridine) also conferred the sequence selectivity of the parent proteins on the metallointercalator.[17] Together, these results demonstrate that metallointercalator-peptide conjugates are excellent model systems for studying protein-DNA recognition.

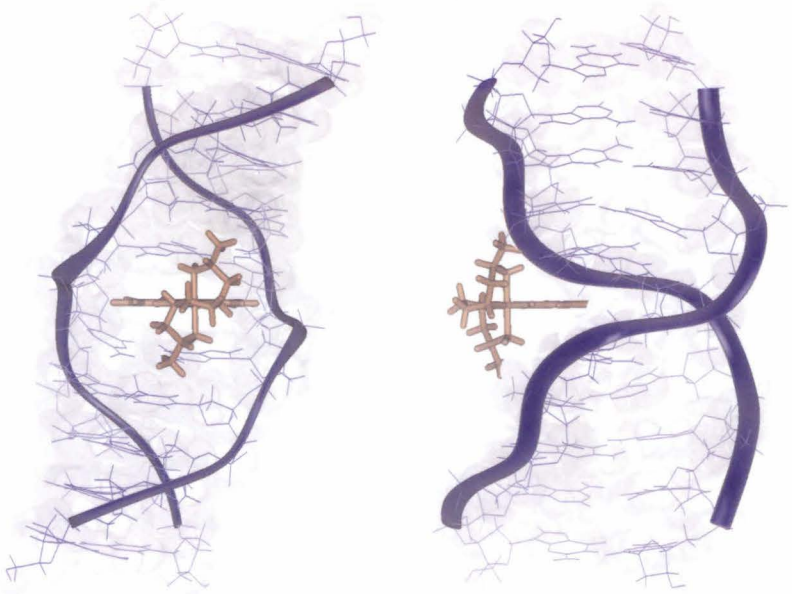

Figure 4.1. Solution structure of a rhodium(III) phi complex bound to DNA by intercalation from the major groove.

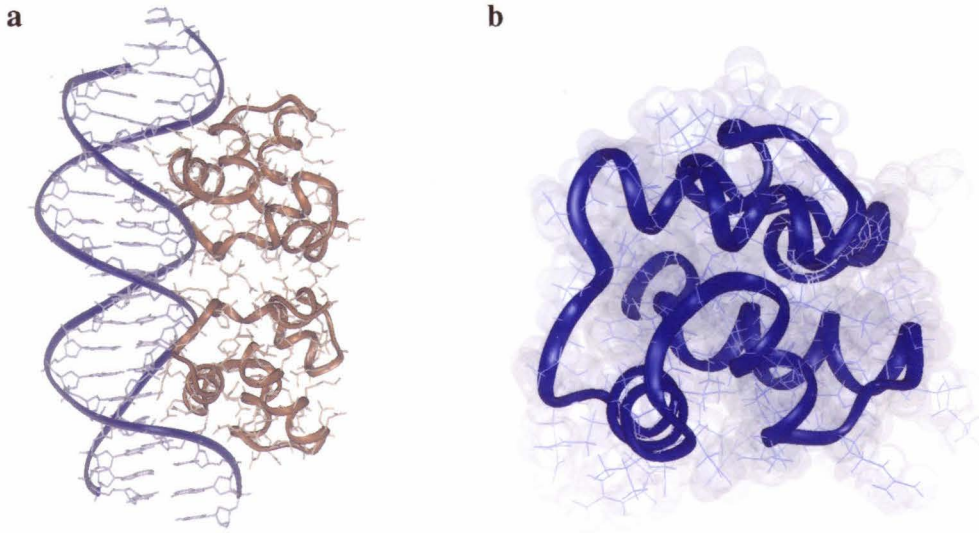

Figure 4.2. Helix-turn-helix DNA binding proteins used as sources of DNA recognition α-helices. (a) Crystal structure of the *434* repressor dimer bound to a synthetic 20 base pair operator at 2.5 Å resolution. (b) Representative NMR structure of the P_{22} repressor. Recognition α-helix is at lower left.

Table 4.1.[a] DNA recognition by P_{22}-repressor derived peptide conjugates of $[Rh(phi)_2(phen')]^{3+}$.

Peptide Sequence[b]	DNA Recognition Site[c]
$[Rh(phi)_2(phen')]^{3+}$-AANVAISQWERAA-$CONH_2$	5'-CC**A**-3'
$[Rh(phi)_2(phen')]^{3+}$-AAAVAISQWERAA-$CONH_2$	5'-CC**A**-3'
$[Rh(phi)_2(phen')]^{3+}$-AANVAISQWEAAA-$CONH_2$	5'-CC**A**-3'
$[Rh(phi)_2(phen')]^{3+}$-AANVAISQWE^{OMe}RAA-$CONH_2$	
$[Rh(phi)_2(phen')]^{3+}$-AANVAIAAWERAA-$CONH_2$	5'-CC**A**-3'
$[Rh(phi)_2(phen')]^{3+}$-AAKVAISQKQRAA-$CONH_2$	
$[Rh(phi)_2(phen')]^{3+}$-AANVAISQWKRAA-$CONH_2$	5'-CC**A**-3'
$[Rh(phi)_2(phen')]^{3+}$-AAKVAISQKERAA-$CONH_2$	
$[Rh(phi)_2(phen')]^{3+}$-AANVAIAAWDRAA-$CONH_2$	

[a]Reproduced from reference 18.

[b]E^{OMe} = glutamate ε-methyl ester.

[c]The primary photocleavage site is indicated in bold.

Unlike metallointercalator conjugates of peptides containing DNA recognition elements from Sp1, Adr1, and the *434* repressor, metallointercalator conjugates of P_{22} repressor derived peptides do not recognize the same nucleotide sequences as the parent protein.[18] While the consensus operator half site sequence of the P_{22} repressor is 5'-ANTNAAG-3', conjugates of $[Rh(phi)_2(phen')]^{3+}$ with oligopeptides derived from the recognition α-helix of the P_{22} repressor recognize the three base pair site 5'-CCA-3' (Table 4.1), cleaving with 5'-asymmetry upon photoactivation. Optimal selectivity was observed at 55 °C in the presence of 5 mM Mn^{2+} or Mg^{2+}. The origins of this change in sequence selectivity were explored by mutating amino acids to alanine individually and pairwise. Mutation of Ser^7 and Gln^8 to alanine did not affect the sequence selectivity of the metallointercalator-peptide conjugate, but mutation of Glu^{10} resulted in a loss of sequence selectivity. In the parent P_{22} protein the residues corresponding to Ser^7 and Gln^8 are

exposed to solvent while the residue corresponding to Glu^{10} is buried in the interior, suggesting that a change in the face of the α-helix that contacts the DNA is responsible for the observed change in sequence selectivity. The role of Glu^{10} was examined by mutation to glutamine, alanine, and aspartate. The extremely conservative Glu to Gln and Glu to Asp mutations resulted in complete loss of sequence selectivity and a significant drop in the helical content of the peptide. Mutation of Glu^{10} to Ala also resulted in a loss of sequence selectivity but an increase in the helical content of the peptide. From these results Sardesai *et al.* proposed that Glu^{10} contacts the 4-amino group of the 5'-terminal cytosine of the 5'-CCA-3' site.

This chapter describes investigations of the structural and thermodynamic basis of the 5'-CCA-3' sequence selectivity of $[Rh(phi)_2(phen')]^{3+}$-AANVAIAAWERAA-$CONH_2$ ([Rh]-E10).[19] A protocol for measuring thermodynamic dissociation constants of phi complexes of rhodium by DNA cleavage titration was developed. Comparison of the dissociation constants of [Rh]-E10 for the sequence 5'-CCA-3' at 23 °C and 55 °C and the bulk intercalative dissociation constant of $[Rh(phi)_2(phen')]^{3+}$ permitted the energetics of sequence-selective binding to be determined. Conformational changes associated with DNA binding by [Rh]-E10 were investigated by CD spectroscopy. Finally, Δ-$[Rh(phi)_2(phen')]^{3+}$-AANVAIAAWERAA-$CONH_2$ ([Δ-Rh]-E10) was synthesized and the structure of [Δ-Rh]-E10 in aqueous solution was examined using multidimensional NMR.

4.2. Experimental

4.2.1. Materials and Methods. All reagents were commercially obtained except where noted. When appropriate, reagents were purified prior to use. All non-aqueous reactions were performed using oven dried glassware under an atmosphere of dry argon. Tetrahydrofuran and 1,4-dioxane were distilled from sodium benzophenone ketyl and stored over 4 Å molecular sieves prior to use. Triethylamine, diisopropylamine, *N*-

methylpyrrolidine, and dichloromethane were distilled from calcium hydride prior to use. *N,N*-dimethylformamide was dried over 4 Å molecular sieves prior to use. Purification of organic products was accomplished using forced flow chromatography on Baker 7024-R silica gel or Merck LiChroprep RP-18 reverse phase silica gel.[20] Purification of metal complexes was accomplished by chromatography on Sephadex SP-C25 or SP-C50 cation-exchange resins that had been equilibrated with KCl and washed with three column volumes of Milli-Q H_2O. The concentration of solutions of peptide conjugates of $[Rh(phi)_2(phen')]^{3+}$ was determined by UV-visible spectroscopy using ε_{350} (isosbestic) = 23,600 $M^{-1}cm^{-1}$.[18] The concentration of solutions of hairpin oligonucleotides was determined by UV-visible spectroscopy using estimated extinction coefficients derived from values per base-paired base of 7300 (A), 8200 (G), 5800 (C), and 7100 (T) $cm^{-1}M^{-1}$ and a value for non-base-paired thymine bases of 8400 $cm^{-1}M^{-1}$. The concentration of solutions of sonicated calf thymus DNA was determined by UV-visible spectroscopy using ε_{260} = 6600 (nucleotides, $M)^{-1}cm^{-1}$.

4.2.2. Instrumentation. Nucleic acids and metallointercalator-peptide conjugates were purified on a Waters 600 multisolvent delivery system equipped with a 996 PDA detector, Vydac 218TP510 (metallointercalator-peptide conjugates) or Rainin Dynamax 300-Å (DNA) semipreparative C_{18} columns, and Millennium chromatography manager software. Products were detected at 260 nm (DNA), or 360 nm (metallointercalator-peptide conjugates). NMR spectra were recorded on a Varian Unity Plus operating at 600 MHz for ^1H, a Bruker AMX-500 operating at 500 MHz for ^1H, or a Bruker AM-500 operating at 500 MHz for ^1H. The phase-sensitive COSY spectrum of Δ-[Rh]-E10 was recorded at 500 MHz using the TPPI technique[21] with F2 and F1 spectral widths of 5000 Hz, an initial matrix size of 512 x 1024 points and a final matrix size of 1024 x 1024 points. The phase-sensitive TOCSY spectrum of Δ-[Rh]-E10 was recorded at

600 MHz using the States[22] technique with F2 and F1 spectral widths of 8000 Hz, an initial matrix size of 512 x 2048 points and a final matrix size of 1024 x 2048 points. The phase-sensitive NOESY spectrum of Δ-[Rh]-E10 was recorded at 600 MHz using the States technique with a mixing time of 0.2 sec, F2 and F1 spectral widths of 12000 Hz, an initial matrix size of 512 x 2048 points, and a final matrix size of 2048 x 2048 points. NMR data were processed with Felix[23] running on a Silicon Graphics Indigo^2 R10000 High Impact workstation. Two-dimensional NMR spectra were apodized in F1 and F2 using skewed sine bell squared windows. Solvent signals were attenuated using convolution-based methods.[24] CD spectra were recorded on a Jasco J-500 or J-600 spectrometer using 1 cm path length cells. UV-visible spectra were recorded on an HP-8452A diode array spectrometer. Photocleavage experiments were performed with an Oriel model 6140 1000 W Hg/Xe lamp fitted with a monochromator and a 300 nm cutoff filter. Gel electrophoresis experiments were quantified using a Molecular Dynamics Phosphorimager and ImageQuant software. Simulations of dissociation constant determinations by photocleavage titration were performed using Mathematica[25] running on a Sun Sparcstation 4+. Dissociation constants were determined by fitting photocleavage titration data to Equation 4.7 by nonlinear regression using SigmaPlot.

4.2.3. Synthesis of oligonucleotides. Oligonucleotides were synthesized by the phosphoramidite method[26] using 1.0 μmol columns on an Applied Biosystems ABI392 DNA/RNA synthesizer. Prior to detritylation, oligonucleotides were purified by HPLC using a linear gradient of 13%→30% MeCN in 100 mM aqueous NH_4OAc pH 7.0 over 25 min followed by isocratic elution at 30% MeCN in 100 mM aqueous NH_4OAc pH 7.0, at a flow rate of 4.0 mL/min. Following detritylation, oligonucleotides were purified by HPLC using a linear gradient of 5%→15% MeCN in 100 mM aqueous NH_4OAc pH

7.0 over 37 min followed by isocratic elution at 15% MeCN in 100 mM aqueous NH_4OAc pH 7.0, at a flow rate of 4.0 mL/min.

4.2.4. Synthesis of peptides. Automated peptide synthesis was accomplished on an ABI430 peptide synthesizer using PAM resins and *N*-^{t}BOC protected amino acids.[27] The following side chain protecting groups were employed: Arg (MTS or TOS); Glu (OBzl or O^{t}Bu); Trp (CHO).

4.2.5. Synthesis of $[Rh(phi)_2(phen')]^{3+}$. $[Rh(phi)_2(phen')]Cl_3$ was synthesized according to the literature procedure.[28] Following completion of the coordination step, the reaction mixture was cooled to 23 °C and diluted with 100 mL H_2O and 1 mL 1.0 M aqueous KCl. The precipitate was removed by filtration and the residue was purified by cation-exchange chromatography on Sephadex SP-C50 cation-exchange resin (25 x 400 mm, stepped gradient 0.1 →0.3 M aqueous KCl). The product eluted as a yellow-orange solution at 0.3 M KCl. Fractions containing the product were applied to a reverse phase silica gel column (25 x 80 mm). The column was washed with 500 mL Milli-Q H_2O and eluted with 3:1 0.1% aqueous TFA–MeCN. Lyophilization afforded a mixture of the chloride and trifluoroacetate salts of $[Rh(phi)_2(phen')]^{3+}$ as an orange powder, spectroscopically identical to reported values.

4.2.6. Enantiomer separation of $[Rh(phi)_2(phen')]^{3+}$. A solution of 600 mg of racemic $[Rh(phi)_2(phen')]^{3+}$ in 50 mL Milli-Q H_2O was stirred with the minimum amount of Sephadex SP-C25 cation-exchange resin required for complete adsorption of the metal complex. The cation-exchange resin bearing the $[Rh(phi)_2(phen')]^{3+}$ was isolated by filtration, washed with 100 mL Milli-Q H_2O, and applied to the top of a 2.5 x 600 mm column of Sephadex SP-C25 cation-exchange resin. The column was eluted with

recirculated 60 mM $K_3[Co(l\text{-cysu})_3]$[29] at a flow rate of 1.5 mL/min for 160 h with protection from light. The bands corresponding to Δ-$[Rh(phi)_2(phen')]^{3+}$ (higher R_f) and Λ-$[Rh(phi)_2(phen')]^{3+}$ (lower R_f) were physically separated and the metal complex was eluted from the cation-exchange resin with 1:1 0.2 M aqueous HCl–MeCN. The volatiles were removed *in vacuo*. The residue was dissolved in 100 mL Milli-Q H_2O and applied to a reverse phase silica gel column (25 x 80 mm). The column was washed with 500 mL Milli-Q H_2O and eluted with 3:1 0.1% aqueous TFA–MeCN. Lyophilization afforded a mixture of the chloride and trifluoroacetate salts of Δ-$[Rh(phi)_2(phen')]^{3+}$ as an orange powder, spectroscopically identical to reported values. The enantiomeric excess of the separated enantiomers, determined by comparison of CD spectra with reported values ($\Delta\varepsilon_{280}$ = -26 $M^{-1}\bullet cm^{-1}$, $\Delta\varepsilon_{450}$ = -10 $M^{-1}\bullet cm^{-1}$),[17] was >95%.

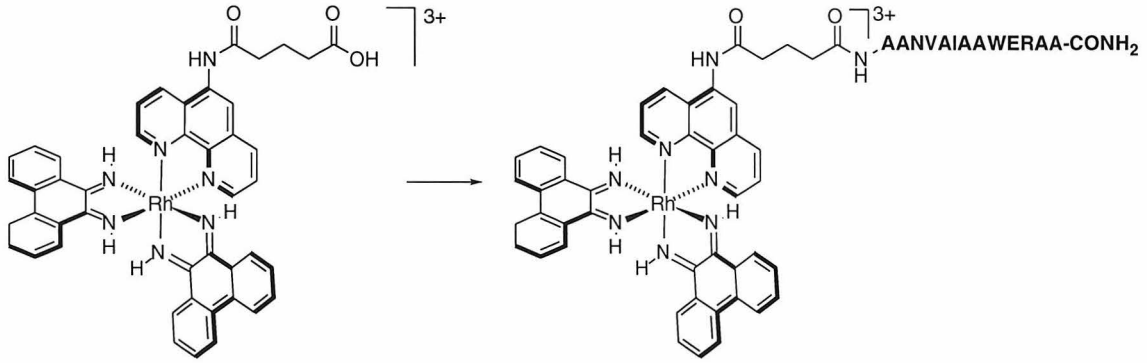

4.2.7. Synthesis of [Rh]-E10. [Rh]-E10 was synthesized using a modification of the reported procedure.[26] The resin-bound peptide (77.6 μmol, 1.0 equiv) was successively washed with CH_2Cl_2, stirred for 10 min in 65% TFA in CH_2Cl_2, washed with CH_2Cl_2, washed with 10% DIEA in CH_2Cl_2, and washed with CH_2Cl_2 to remove the N-terminal ^{t}BOC protecting group. After drying *in vacuo*, the resin-bound peptide was successively stirred for 30 min in 6% 2-aminoethanol in 95% aqueous DMF, washed with DMF, stirred for 30 min in 6% 2-aminoethanol in 95% aqueous DMF, washed with DMF,

washed with CH_2Cl_2, washed with 1:1 CH_2Cl_2–MeOH, and washed with EtOH to remove the Trp CHO protecting group. The resin-bound peptide was dried *in vacuo*.

HOBT (10.5 mg, 77.6 μmol, 1.8 equiv) and DCC (16.0 mg, 77.6 μmol, 1.8 equiv) were added to a solution of 73.5 mg (77.6 μmol, 1.8 equiv) of $[Rh(phi)_2(phen')]Cl_3$ in 1 mL NMP. The resulting solution was stirred at 23 °C for 15 min with protection from light. The dried resin-bound peptide was added to the solution and the resulting slurry was stirred at 23 °C for 48 h with protection from light. The resin-bound metallointercalator-peptide conjugate was isolated by filtration and successively washed with NMP, DMF, CH_2Cl_2, 1:1 CH_2Cl_2–MeOH, and EtOH. The resin-bound peptide was dried *in vacuo*. The metallointercalator-peptide conjugate was cleaved from the resin and the remaining protecting groups were removed by treatment with anhydrous HF following standard protocols.[25,30] The metallointercalator-peptide conjugate was purified by HPLC using a linear gradient of 15%→40% 0.1% TFA in MeCN in 0.1% aqueous TFA over 19 min followed by isocratic elution at 40% 0.1% TFA in MeCN in 0.1% aqueous TFA, at a flow rate of 4.5 mL/min (t_{ret} = 18.5 min). The product was characterized by HPLC coinjection with an authentic sample.[31]

4.2.8. Synthesis of [Δ-Rh]-E10. [Δ-Rh]-E10 was synthesized and purified according to the protocol described for the synthesis of [Rh]-E10, using 1.0 equiv of HOBT, DCC, and Δ-$[Rh(phi)_2(phen')]Cl_3$. The product was characterized by ^1H NMR (*vide supra*) and by HPLC coinjection with an authentic sample.[32]

4.2.9. Model of dissociation constant determination by photocleavage titration. The association constant of a ligand *L* at a given site *i* is defined as:

$$K_{B,i} = \frac{[L \cdot DNA]_i}{[L]_f [DNA]_{f,i}} \quad \textbf{(4.1)}$$

where $K_{B,i}$ is the association constant of ligand L at site i, $[L{\bullet}DNA]_i$ is the concentration of ligand–DNA complex at site i, $[L]_f$ is the concentration of unbound ligand, and $[DNA]_{f,i}$ is the concentration of oligonucleotides unoccupied at site i. Equation 4.1 can be solved and generalized for an oligonucleotide of s binding sites as follows:

$$[L \cdot DNA]_i = \frac{K_{B,i}[L]_f [DNA]_t}{\left(1 + K_{B,i}[L]_f\right)} \quad \textbf{(4.2)}$$

$$[L]_t = [L]_f + \sum_{i=1}^{s} [L \cdot DNA]_i \quad \textbf{(4.3)}$$

$$[L]_t = [L]_f + \sum_{i=1}^{s} \frac{K_{B,i}[L]_f [DNA]_t}{\left(1 + K_{B,i}[L]_f\right)} \quad \textbf{(4.4)}$$

where $[DNA]_t$ is the total DNA concentration in duplexes, and $[L]_t$ is the total ligand concentration. Assuming that the oligonucleotide contains only one site of interest of association constant K_1 and n additional sites of association constant K_2, Equation 4.4 may be expressed as:

$$[L]_t = [L]_f + \frac{K_1[L]_f [DNA]_t}{\left(1 + K_1[L]_f\right)} + \frac{n \cdot K_2[L]_f [DNA]_t}{\left(1 + K_2[L]_f\right)} \quad \textbf{(4.5)}$$

Equation 4.5 may be solved for $[L]_f$. Substitution of the real root[32] into Equation 4.1 permits the calculation of the fraction of a given site that is occupied by ligand. If γ is the fraction of bound complexes at a given site that produce strand scission under the conditions of the experiment, the observed fraction cleaved at a given site ($F_{c,obs}$) may be described as:

$$F_{c,obs} = \left(\left(1 - \left(\gamma \bullet \frac{[L \cdot DNA]_2}{[DNA]_t}\right)\right)^x\right)\left(\gamma \bullet \frac{[L \cdot DNA]_1}{[DNA]_t}\right) \quad \textbf{(4.6)}$$

where $[L{\bullet}DNA]_1$ is the concentration of sites of association constant K_1 occupied by ligand, $[L{\bullet}DNA]_2$ is the concentration of sites of association constant K_2 occupied by ligand, and x is the number of sites of association constant K_2 between the site of association constant K_1 and the radiolabel. Using Mathematica plots of the ratio of $F_{c,obs}$ in the presence (Equation 4.6, x = 10) and absence (Equation 4.6, x = 0) of 10 sites not of interest were constructed. Simulated $F_{c,obs}$ data for a system with ($K_1 = 10^8$, $K_2 = 10^6$, γ = 1.0) was fit with SigmaPlot using Equation 4.7, which describes a system with one high-affinity binding site. Deviations between the input and output values of K_1 were acceptable (<25%) at ligand–DNA ratios below 1:3.[33]

$$F_c = \frac{\gamma \bullet \left([DNA]_t + [L]_t + K_d - \left(([DNA]_t + [L]_t + K_d)^2 - 4 \bullet [DNA]_t \bullet [L]_t\right)^{1/2}\right)}{2 \bullet [DNA]_t} \quad \textbf{(4.7)}$$

4.2.10. Dissociation constant determination of sequence-selective metallointercalator-peptide conjugates by photocleavage titration. Hairpin oligonucleotides were 5'-endlabeled with T4 polynucleotide kinase and [γ-^{32}P]-ATP.[34] Photocleavage reactions were performed in 20 μL total volume contained in 1.7 mL presiliconized Eppendorf tubes. The reaction mixtures contained ~200,000 cpm labeled hairpin oligonucleotide, metallointercalator-peptide conjugate and unlabeled hairpin oligonucleotide in a 1:3 ratio, 5 mM $MnCl_2$, and 50 mM pH 7.0 sodium cacodylate buffer. Metallointercalator-peptide conjugate concentrations ranged from 7.2 x 10^{-6} M to 7.2 x 10^{-11} M. The reaction mixtures were incubated at 23 °C or 55 °C for 5 min, and irradiated with 313 nm light at 23 °C or 55 °C, respectively, for 10 min. Control reactions lacking metallointercalator were irradiated under identical conditions, and control reactions

containing metallointercalator were incubated at 23 °C or 55 °C without irradiation. Following irradiation the reaction mixtures were concentrated *in vacuo* and resuspended in 5 μL 80% formamide sequencing loading buffer. Approximately 50,000 cpm of each sample, and Maxam-Gilbert A+T and C+G sequencing reactions[35] were loaded on a 20% denaturing polyacrylamide gel and electrophoresed at 1200 V for 2.5 h. The gel was transferred to film prior to autoradiography. The experimental dissociation constants were determined by fitting $F_{c,obs}$ at the site of interest as a function of DNA and metallointercalator-peptide conjugate concentration to Equation 4.7.

4.2.11. Bulk dissociation constant determination of non-sequence-selective metallointercalators by photocleavage titration. Hairpin oligonucleotides were endlabeled and irradiated in the presence of $[Rh(phi)_2(phen')]^{3+}$ as described for determination of dissociation constants of sequence-selective metallointercalator-peptide conjugates. The experimental dissociation constants were determined by fitting $F_{c,obs}$ over all intercalation sites as a function of DNA and metallointercalator-peptide conjugate concentration to Equation 4.7, using the concentration of hairpin oligonucleotide intercalation sites (base pairs - 1) as the concentration of DNA.

4.3. Results

4.3.1. Synthesis of [Rh]-E10 and [Δ-Rh]-E10. [Rh]-E10 was synthesized by coupling the resin-bound E10 peptide, synthesized on PAM resin using *N*-^{t}BOC protected amino acids, with the 1.8 equiv of the HOBT ester of $[Rh(phi)_2(phen')]^{3+}$ in N-methylpyrrolidine as described by Sardesai *et al.* (Scheme 4.1).[36] Because of the instability of $[Rh(phi)_2(phen')]^{3+}$ to aqueous base, the formyl protecting group was removed from the tryptophan residue before coupling. [Δ-Rh]-E10 was synthesized by the coupling resin-bound peptide with 1.0 equiv of the HOBT ester of Δ-$[Rh(phi)_2(phen')]Cl_3$,

Scheme 4.1. Synthesis of [Rh]-E10 and [Δ-Rh]-E10.

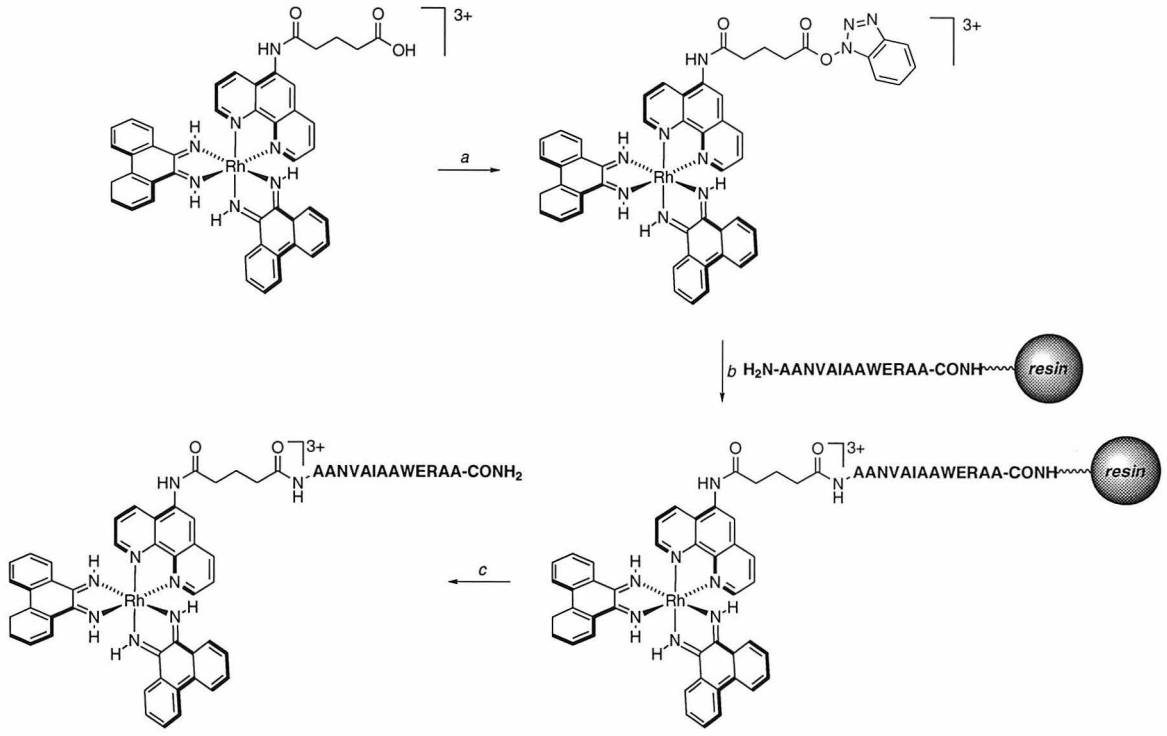

(a) DCC, HOBT, NMP, 23 °C, 15 min. (b) resin-bound peptide, 23 °C, 48 h. (c) anhydrous HF deprotection (2-3%).

which was obtained by enantiomer separation on Sephadex SP-C25 cation-exchange resin using $K_3[Co(l\text{-cysu})_3]$ as the eluent. Following coupling, the acid-labile protecting groups were removed and the peptide was cleaved from the resin with anhydrous HF. Purification by HPLC afforded the conjugates in 2-3% yield as determined by UV-visible spectroscopy, based on 100% yield for the synthesis of the resin-bound peptide.

4.3.2. NMR study of a metallointercalator-peptide conjugate. The 500 MHz ^{1}H NMR spectrum of [Δ-Rh]-E10 in D_2O at 23 °C (not buffered, pH ~5.0) is shown in Figure 4.3. Individual spin systems were identified by analysis of the 500 MHz COSY spectrum in D_2O and the 600 MHz TOCSY spectrum in 90:10 H_2O–D_2O.[37] Sequential assignments for the seven alanine residues were obtained by analysis of the

Table 4.2. ^{1}H NMR (600 MHz, 90:10 H_2O–D_2O) chemical shifts for Δ-[Rh]-E10.

Residue	H_N	H_α	H_β	other
phi_1[a]				H_1 8.03; H_2 7.42; H_3 7.72; H_4 8.19
phi_2[a]				H_1 8.35; H_2 7.58; H_3 7.82; H_4 8.22
phen'[b]				$H_{1 \text{ or } 3}$ 8.87; H_2 8.03; $H_{1 \text{ or } 3}$ 8.82; $H_{1' \text{ and } 3'}$ 8.91; $H_{2'}$ 8.06
linker[c]				1' 2.69; 2' 2.04; 3' 2.41
Ala[1]	8.30	4.28	1.38	
Ala[2]	8.34	4.24	1.32	
Asn[3]	8.29	4.58	2.74	
Val[4]	7.82	4.02	2.02	Me 0.88
Ala[5]	8.19	4.24	1.27	
Ile[6]	7.83	3.91	1.67	$H_{\gamma 1}$ 0.98; $H_{\gamma 2}$ 1.30; Me_γ 0.74; Me_δ 0.66
Ala[7]	8.07	4.11	1.10	
Ala[8]	8.16	4.07	1.35	
Trp[9]	7.65	4.49	3.14, 3.23	$H_{\text{arom } 2}$ 7.16; $H_{\text{arom } 4}$ 7.30; $H_{\text{arom } 5}$ 6.83; $H_{\text{arom } 6}$ 6.98; $H_{\text{arom } 7}$ 7.26; $H_{\text{arom NH}}$ 10.11
Glu[10]	7.64	4.00	1.71	$H_{\gamma 1}$ 1.82; $H_{\gamma 2}$ 1.92
Arg[11]	7.83	4.12	1.73, 1.79	H_γ 1.58; H_δ 3.17; H_{guan} 7.16
Ala[12]	8.06	4.19	1.31	
Ala[13]	8.07	4.22	1.34	

[a]There are two pairs of accidentally isochronous phi spin systems which are labeled phi_1 and phi_2.

[b]Phen' H_2-H_4 and H_7-H_9 spin systems were not distinguished and are labeled H_1-H_3 and $H_{1'}$-$H_{3'}$.

[c]Linker methylene protons are labeled 1' through 3' with 1' adjacent to the phen' carboxamide.

interresidue NOE's between $H_{\alpha,i}$ and $H_{N,i+1}$ and confirmed by analysis of other interresidue NOEs in the 600 MHz NOESY spectrum in 90:10 H_2O–D_2O (Figure 4.4). Chemical shift values for amino acid resonances (Table 4.2) differed little from median values,[38] and chemical shift values for the metallointercalator differed little from those for free $[Rh(phi)_2(phen')]^{3+}$. An expansion of the H_N-H_α region showing the sequential assignment

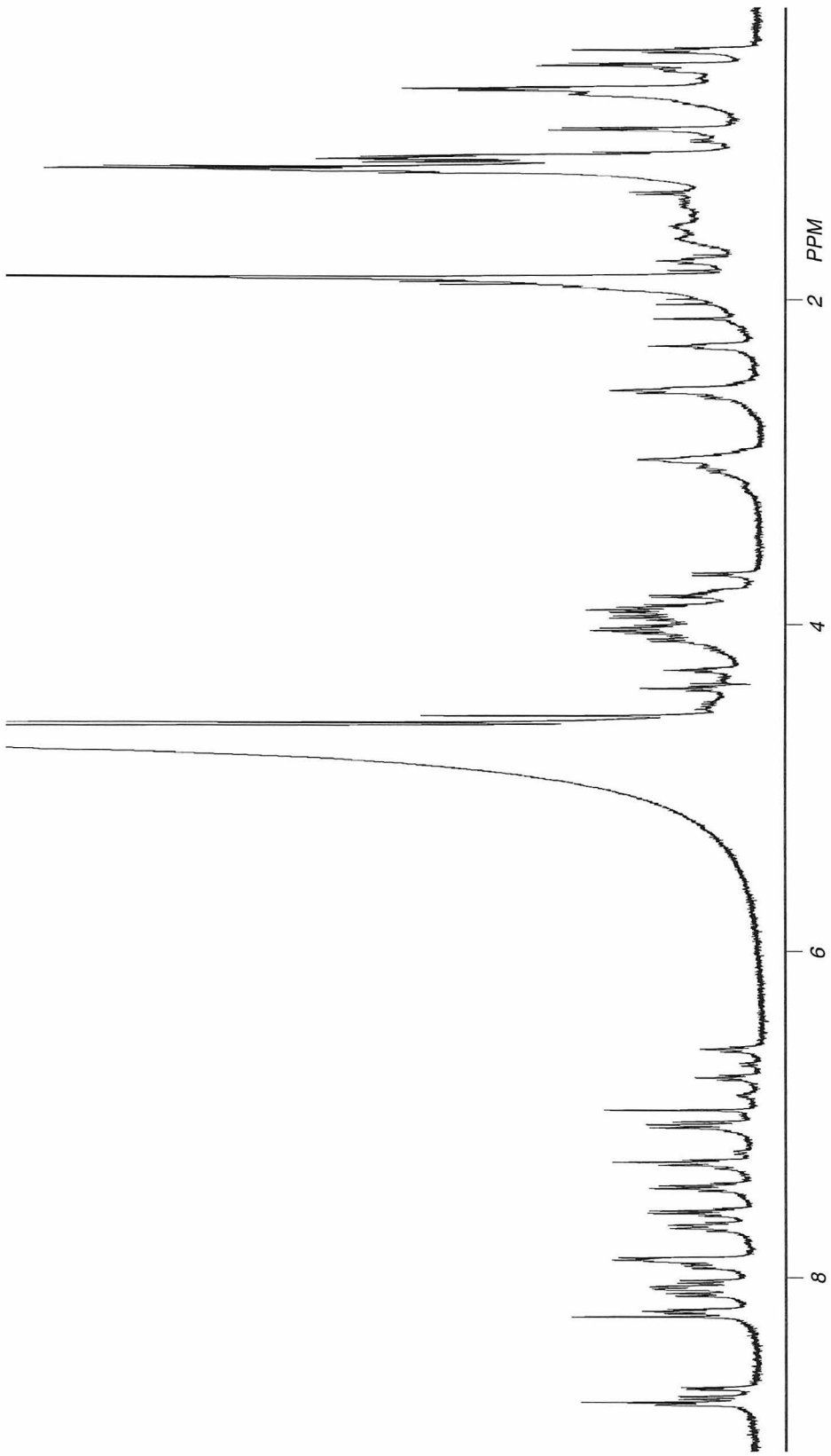

Figure 4.3. ^{1}H NMR spectrum of [Δ-Rh]-E10 (500 MHz, D_2O).

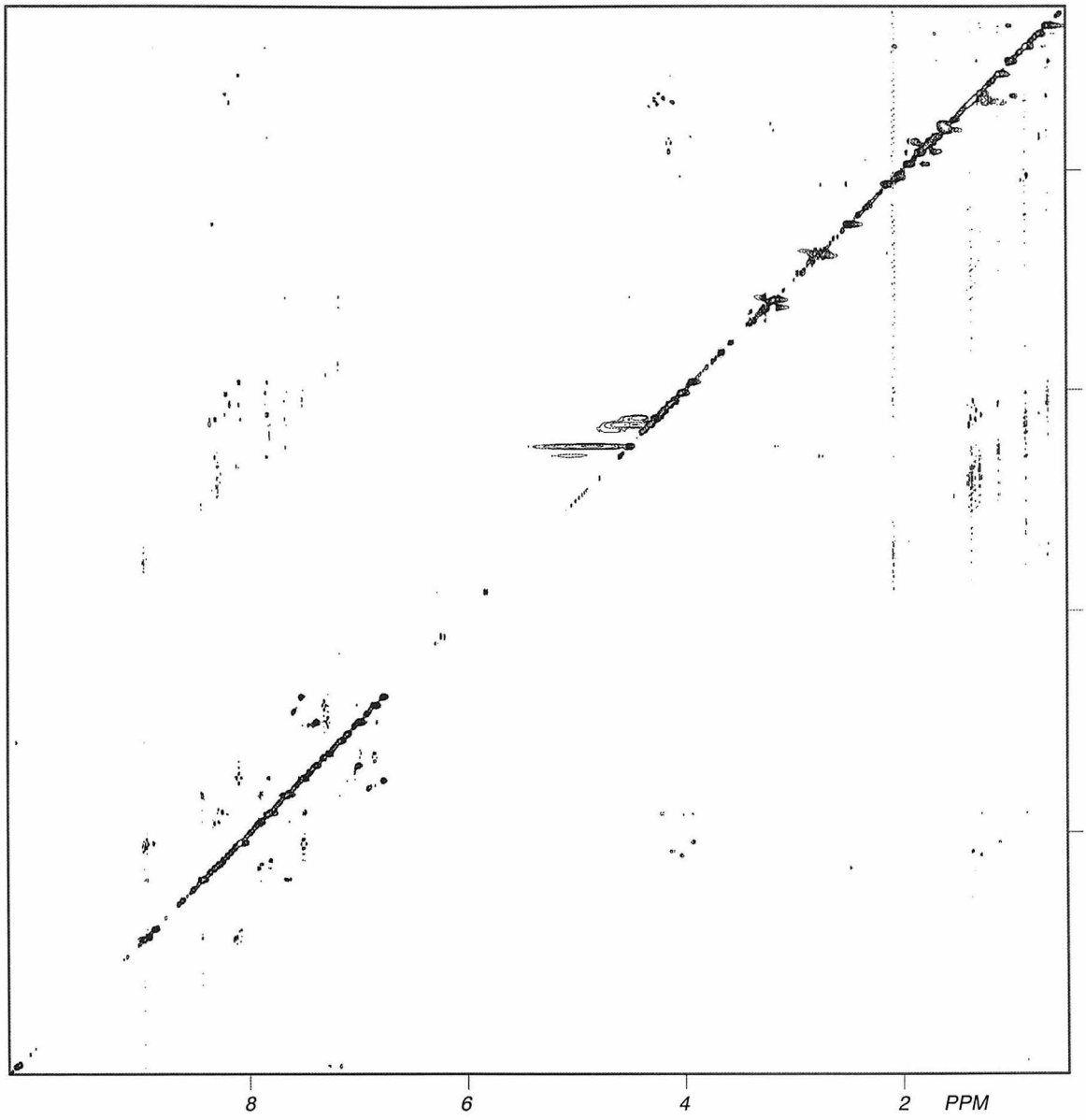

Figure 4.4. NOESY spectrum of [Δ-Rh]-E10 (600 MHz, 90:10 H_2O–D_2O).

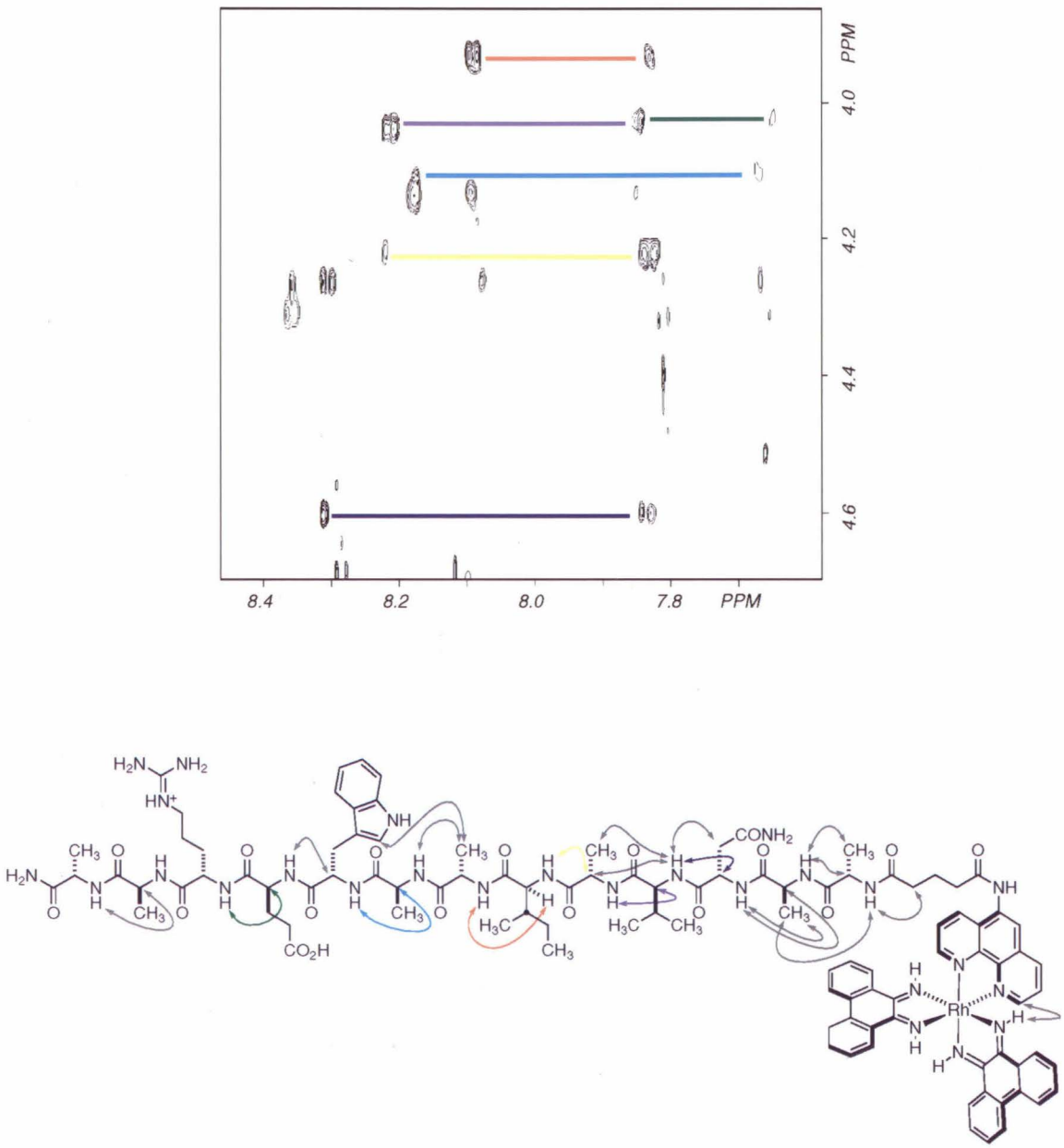

Figure 4.5. Sequential assignment process for [Δ-Rh]-E10 showing H_N-H_α region. *Top*: Partial ^{1}HNMR NOESY spectrum showing H_N-H_α region. *Bottom*: Diagram of intraresidue NOEs. NOEs indicated in spectrum above are color coded. Other NOEs are gray. For clarity, most hydrogens are omitted and NOEs involving omitted hydrogens are indicated by an arrow pointing to the carbon to which they are bound.

process and a summary of intraresidue NOEs are shown in Figure 4.5. Few intraresidue NOEs between nonadjacent residues were observed, indicating a largely random-coil conformation of the peptide and little association between the peptide and the metal center.

4.3.3. Modeling of dissociation constant determination experiments.[39] Selection of experimental conditions for accurate measurement of dissociation constants by photocleavage titration must account for the effects of lower-affinity intercalation sites on the oligonucleotide containing the sequence of interest. Accordingly, a mathematical description of a generalized experiment to measure dissociation constants that employed an oligonucleotide with *n* binding sites of dissociation constant K_1 between the radiolabel and a binding site of interest of dissociation constant K_2 (Figure 4.6) was developed. Using Equation 4.6, which describes the fraction cleaved at the site of interest as a function of the DNA concentration, the association constants at the high affinity site of interest and the additional, lower-affinity sites, the ligand–DNA ratio,

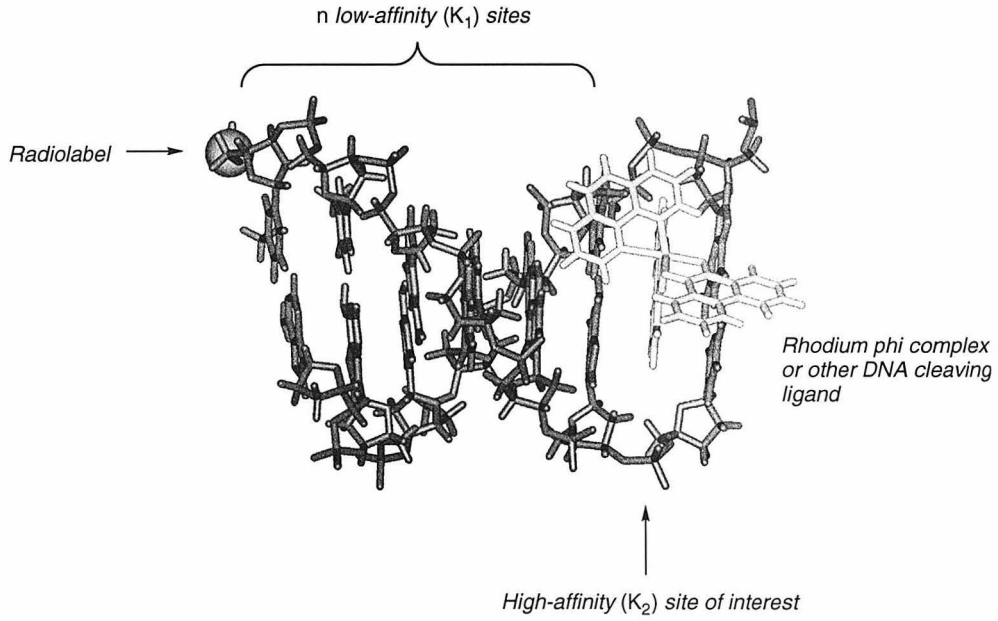

Figure 4.6. Modeled dissociation constant determination experiment.

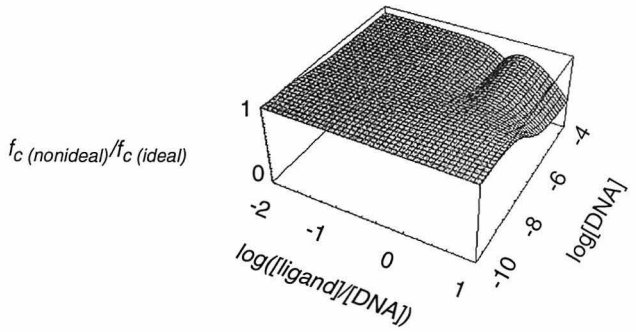

Figure 4.7. Effect of 10 binding sites (K_B = 10^6 M^{-1}, γ = 0.1) on observed fraction of site of interest (K_B = 10^8 M^{-1}, γ = 0.1) cleaved as a function of DNA concentration and ligand–DNA ratio.

and the fraction of bound complexes which lead to strand scission (γ), the effects of the lower-affinity sites on experimental dissociation constant measurements were investigated.

Inspection of a typical plot of the ratio of the fraction cleaved at the high affinity site in the presence of the lower-affinity sites to the fraction cleaved at the high affinity site in the absence of the lower-affinity sites (Figure 4.7) indicates that significant deviations occur at ligand–DNA ratios near unity and at extremely high ligand–DNA ratios. At DNA concentrations above the dissociation constant for the lower-affinity sites, there is a small deviation between the two values that is independent of the ligand–DNA ratio. The systemic error of dissociation constants derived from fitting photocleavage isotherms without accounting for the effects of the lower-affinity sites was assessed by simulating $F_{c,obs}$ data for a system with a K_B of 10^8 M^{-1} at the high-affinity site, a K_B of 10^6 M^{-1} at the lower-affinity sites, and a photocleavage efficiency (γ) of 1.0. Deviations between the input and output values of K_1 were acceptable (<21%) at ligand–DNA ratios below 1:2.[33] At a ligand–DNA ratio of 1:1 the systemic error was 42%, while at a ligand–DNA ratio of 1:10 the systemic error was 11%.

4.3.4. Determination of the dissociation constant of [Rh]-E10 for a 5'-CCA-3' sequence under conditions affording optimum selectivity. The thermodynamic dissociation constant of [Rh]-E10 for the sequence 5'-CCA-3' was determined by photocleavage titration. The concentration of the metallointercalator-peptide conjugate ranged from 7.2 x 10^{-6} M to 7.2 x 10^{-11} M, with a constant metallointercalator–unlabeled hairpin oligonucleotide ratio of 1:3. The hairpin oligonucleotide employed, 5'-AGAGCCACGAGATTTTTTCTCGTGGCTCT-3' (K_1-29), contains a T_5 loop and the three base pair target sequences 5'-CCA-3' flanked by four base pairs on the 5'-side and a C•G base pair followed by four base pairs on the 3'-side. The flanking sequence was optimized to eliminate sequences that are weakly recognized by [Rh]-E10. The use of a hairpin oligonucleotide ensured that melting would not occur under the nanomolar concentrations and elevated temperature of the experiment. Duplex hybridization under the experimental conditions was verified by determination of the melting temperatures of the 29-mer hairpin oligonucleotide (T_m 74.6 °C, $T_{m\,(rev)}$ 74.0 °C) by UV-visible spectroscopy at 0.1 μM in 10 mM Tris•HCl, pH 7.0.

An autoradiogram of the photocleavage titration of [Rh]-E10 with K_1-29 is shown in Figure 4.8. The derived cleavage isotherm (Figure 4.9) was fit to Equation 4.7, yielding a dissociation constant of 5.7 x 10^{-8} M. The intercalative dissociation constant of $[Rh(phi)_2(phen')]^{3+}$ at 55 °C in the presence of 5 mM $MnCl_2$ was determined by fitting the cleavage isotherm obtained by quantitation of the cleavage at all of the intercalation sites of the hairpin oligonucleotides K_1-29 and 5'-AATTCCACACAATTTTTTTGTGTGGAATT-3' (K_2-29) (Figure 4.6) to Equation 4.7, using a value of (hairpin oligonucleotide concentration)•(intercalation sites per oligonucleotide) as the concentration of binding sites. Comparison of the resulting value of 7.0 x 10^{-7} M with the dissociation constant of [Rh]-

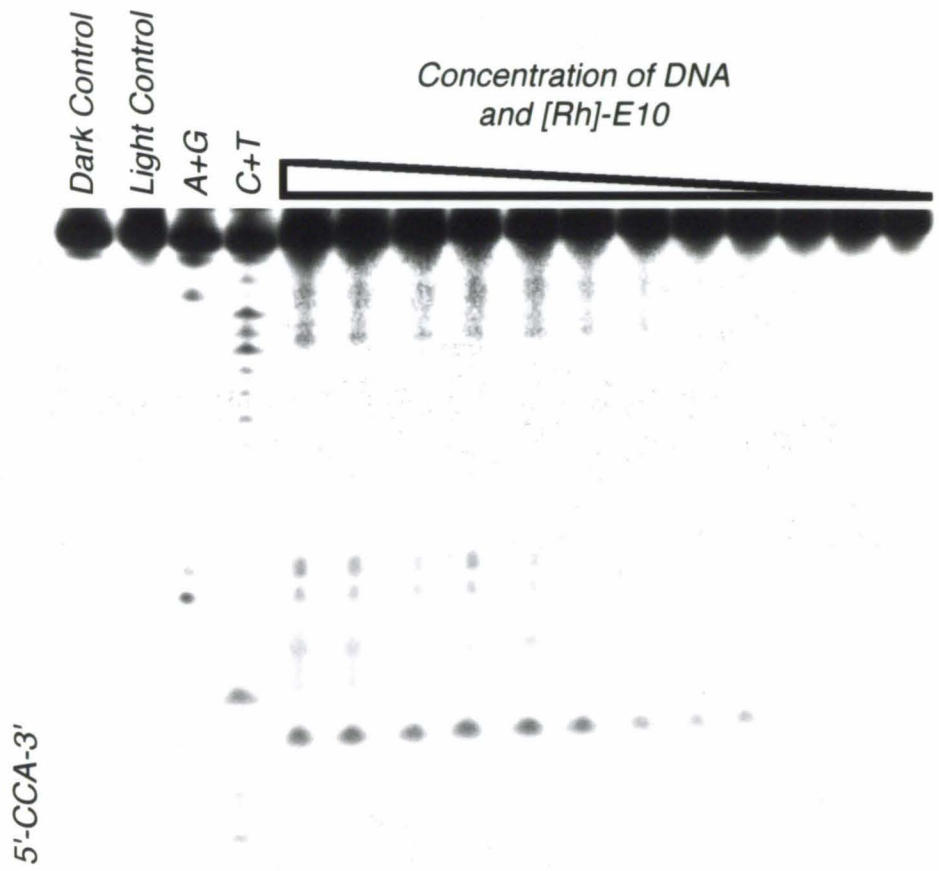

Figure 4.8. Autoradiogram of dissociation constant determination of [Rh]-E10 for 5'-CCA-3' by photocleavage titration. *Conditions*: 5 mM $MnCl_2$, 50 mM pH 7.0 sodium cacodylate, 3:1 K_2-29–[Rh]-E10, irradiated for 5 min at 313 nm, 55 °C.

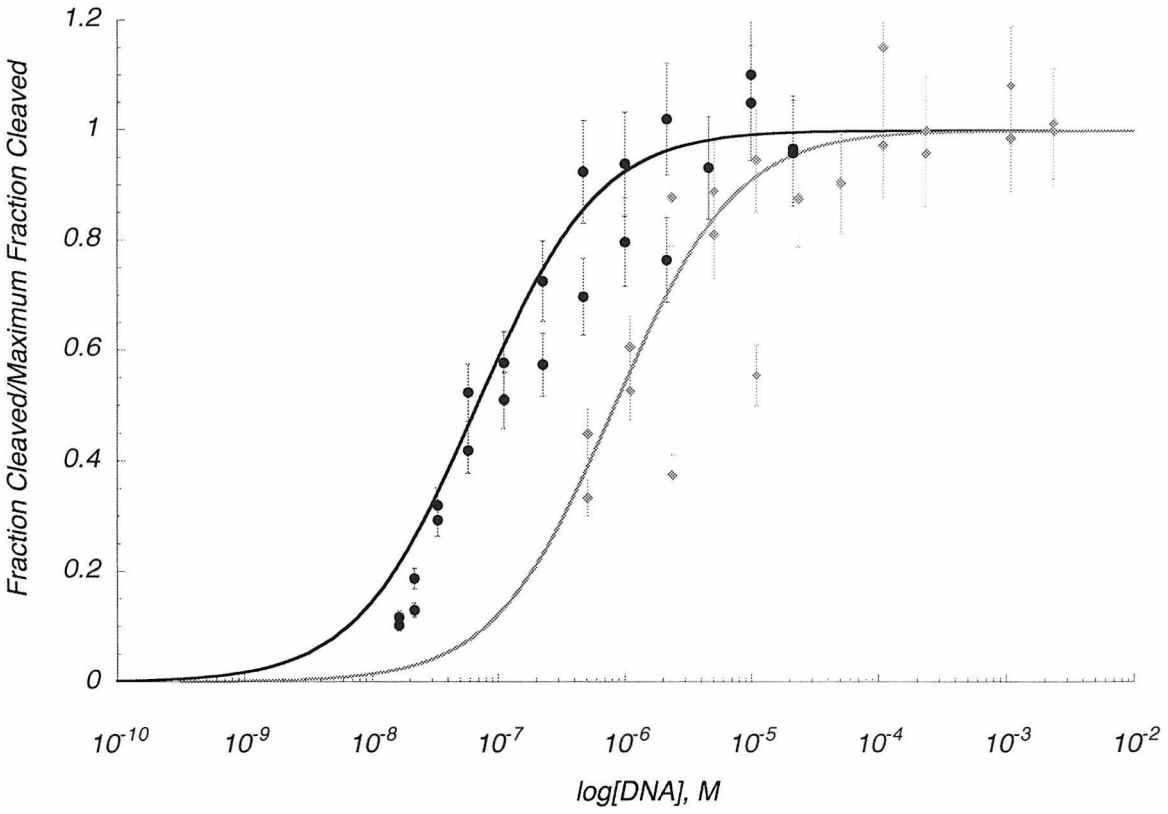

Figure 4.9. Photocleavage isotherms for [Rh]-E10 (black, K_d = 5.7 x 10^{-8} M)) and $[Rh(phi)_2(phen')]^{3+}$ (gray, K_d = 7.0 x 10^{-7} M). *Conditions*: 3:1 ratio of hairpin oligonucleotide–metallointercalator or metallointercalator-peptide conjugate, 5 mM $MnCl_2$, 50 mM sodium cacodylate buffer pH 7.0, 55 °C.

E10 for the target sequence 5'-CCA-3' indicated that at 55 °C, in the presence of 5 mM $MnCl_2$, the peptide appendage provides 13-fold tighter binding to the target sequence, corresponding to a free energy difference of 1.7 kcal•mol^{-1}.

4.3.5. Effect of temperature on metallointercalator-peptide conjugate selectivity and affinity. The origin of the enhanced DNA sequence selectivity of metallointercalator-peptide conjugates at elevated temperature was investigated by determining the dissociation constants at 23 °C and 55 °C of [Rh]-E10 with K_2-29, which also contains the target sequence 5'-CCA-3'. Cleavage isotherms generated from

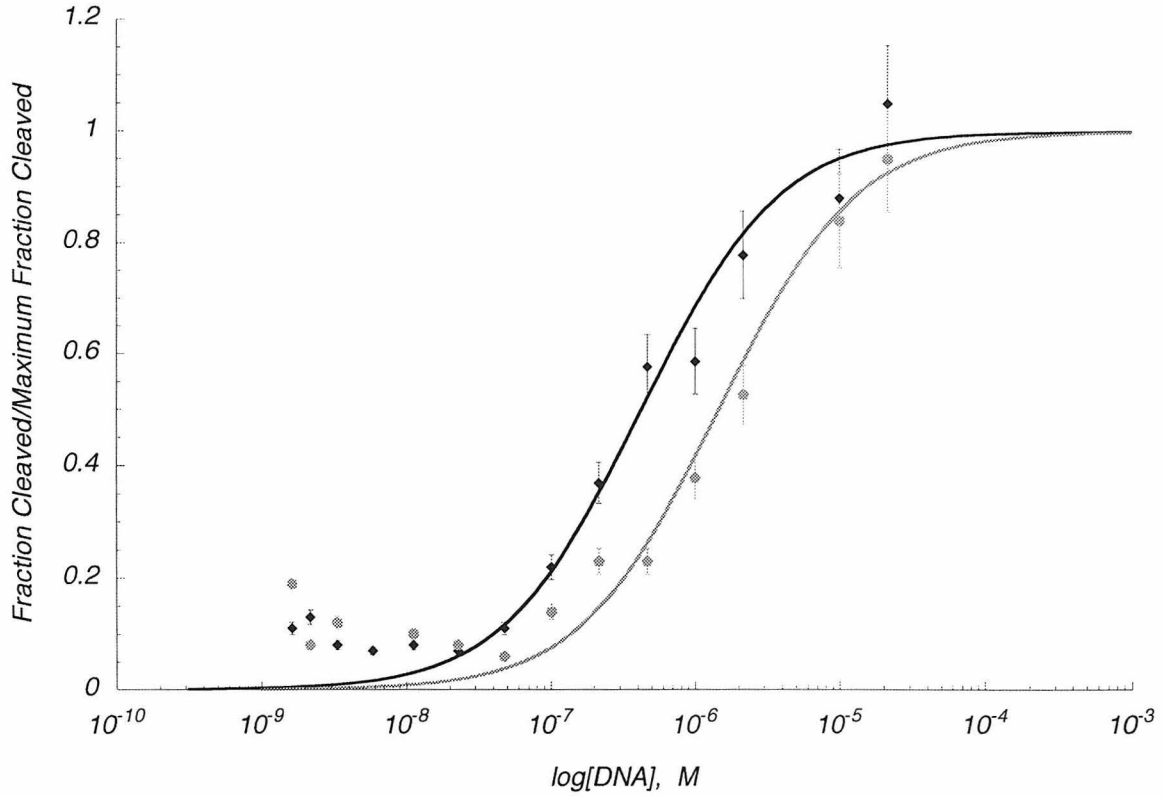

Figure 4.10. Temperature dependence of the dissociation constant of [Rh]-E10 for 5'-CCA-3'. *Conditions*: 3:1 ratio of K_2-29–[Rh]-E10, 5 mM $MnCl_2$, 50 mM sodium cacodylate buffer pH 7.0, 23 °C (gray, K_d = 1.2 x 10^{-6} M) or 55 °C (black, K_d = 2.3 x 10^{-7} M).

autoradiograms of photocleavage titration gel electrophoresis experiments revealed an increased affinity at elevated temperature (Figure 4.7). Determination of the dissociation constants derived from the cleavage isotherms indicated that [Rh]-E10 binds 5-fold more tightly at 55 °C (K_d = 2.3 x 10^{-7} M) than at 23 °C (K_d = 1.2 x 10^{-6} M) to the 5'-CCA-3' site of K_2-29, corresponding to a free energy difference of 2.0 kcal•mol^{-1}. Interestingly, a 2.5 μM sample of [Rh]-E10 in 5 mM $MnCl_2$ and 10 mM pH 7.0 Tris•HCl has no melting transition observable by CD between 5 °C and 95 °C.[40]

Table 4.3. Summary of measured dissociation constants.

Ligand	Conditions	Oligonucleotide	K_d
$[Rh(phi)_2(phen')]^{3+}$	pH 7.0, 5 mM $MnCl_2$, 55 °C	K_1-29 & K_2-29	$7.0 \pm 0.47 \times 10^{-7}$ M
[Rh]-E10	pH 7.0, 5 mM $MnCl_2$, 55 °C	K_1-29	$5.7 \pm 0.12 \times 10^{-8}$ M
[Rh]-E10	pH 7.0, 5 mM $MnCl_2$, 55 °C	K_2-29	$2.3 \pm 0.86 \times 10^{-7}$ M
[Rh]-E10	pH 7.0, 5 mM $MnCl_2$, 23 °C	K_2-29	$1.2 \pm 0.50 \times 10^{-6}$ M

4.3.6. Circular dichroism study of a metallointercalator-peptide conjugate bound sequence-selectively to DNA. Conformational changes associated with DNA binding by [Rh]-E10 were investigated by CD spectroscopy. In the absence of DNA, a 2.5 μM sample of [Rh]-E10 in 5 mM $MnCl_2$ and 10 mM pH 7.0 Tris•HCl at 55 °C shows a CD spectrum consistent with an α-helix with a helical content of 21%.[40] The CD spectrum of [Rh]-E10 in the presence of 5 μM DNA hairpin oligonucleotide K_2-29 under otherwise identical conditions was obtained by subtraction of the CD spectrum of the DNA from the CD spectrum of the DNA–metallointercalator-conjugate complex (Figure 4.11). Comparison of the CD spectrum of the metallointercalator-peptide conjugate in the absence of DNA with the derived CD spectrum of the metallointercalator-peptide conjugate in the presence of DNA indicated little change between 210 and 250 nm, suggesting that at 55 °C, DNA binding by [Rh]-E10 does not promote helix formation.

The origin of the induced negative CD between 275 and 300 nm was investigated by comparison of the CD spectrum of the DNA in 5 mM $MnCl_2$ and 10 mM pH 7.0 Tris•HCl at 55 °C in the absence and presence of 2.5 μM $[Rh(phi)_2(phen')]^{3+}$ (Figure 4.12). Little change occurs between 210 and 250 nm, indicating that the CD spectrum obtained by subtraction of the CD spectrum of the DNA from the CD spectrum of the [Rh]-E10•DNA complex is composed solely of the CD spectrum of [Rh]-E10 in the presence of DNA. In the presence of $[Rh(phi)_2(phen')]^{3+}$ the positive DNA CD between 275 and 285

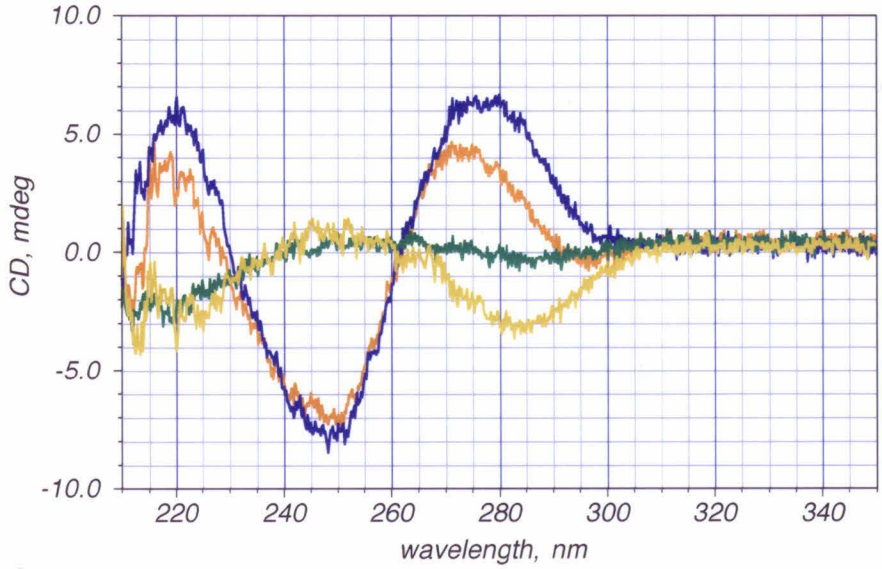

Figure 4.11. Comparison of CD spectra of [Rh]-E10 in the absence and presence of its DNA target sequence. *Shown*: K_2-29 (blue), [Rh]-E10 (green), [Rh]-E10•DNA complex (orange), derived CD spectrum of [Rh]-E10 in the presence of DNA (yellow). *Conditions*: 0 or 2.5 μM [Rh]-E10, 0 or 5.0 μM K_2-29, 5 mM $MnCl_2$, 10 mM pH 7.0 Tris•HCl, 55 °C.

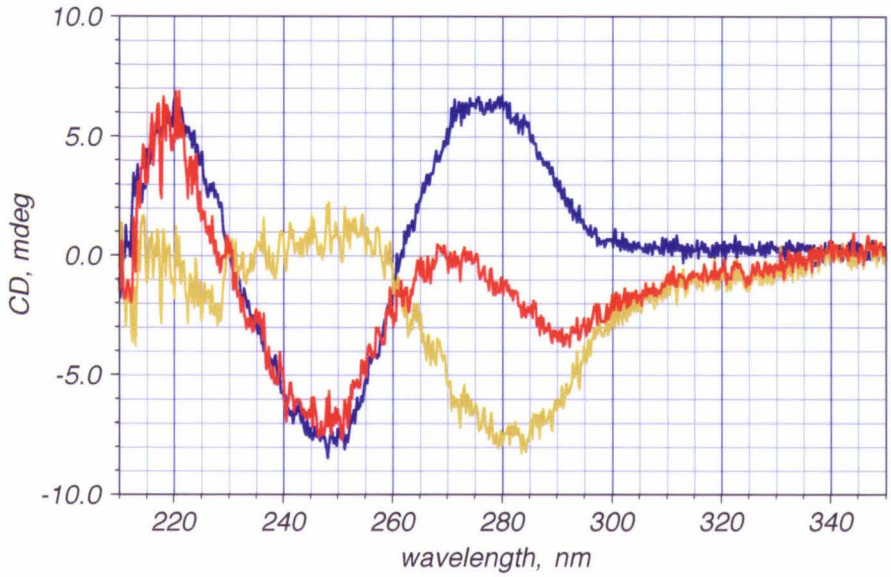

Figure 4.12. Effect of intercalative binding by $[Rh(phi)_2(phen')]^{3+}$ on CD spectrum of K_2-29. *Shown*: K_2-29 (blue), $[Rh(phi)_2(phen')]^{3+}$•DNA complex (orange), derived CD spectrum of $[Rh(phi)_2(phen')]^{3+}$ in the presence of DNA (red). *Conditions*: 0 or 2.5 μM $[Rh(phi)_2(phen')]^{3+}$, otherwise identical to Figure 4.11.

nm is more attenuated and the induced negative CD between 275 and 300 nm is more prominent than in the presence of [Rh]-E10, indicating that the induced negative CD between 275 and 300 nm is not associated with the E10 peptide.

4.4. Discussion

4.4.1. Energetics of DNA binding by [Rh]-E10. The design of an experimental protocol for determining sequence-selective and nonselective intercalative dissociation constants is complicated by the necessary presence of lower-affinity intercalation sites on the oligonucleotide containing the sequence of interest that compete for available ligand. Moreover, cleavage at the lower-affinity sites between the sequence of interest and the radiolabel attenuates the observed fraction cleaved at the sequence of interest. Although numerous spectroscopic methods have been developed for the measurement of dissociation constants between protein and small molecule ligands and bulk DNA,[41] these methods do not permit the determination of dissociation constants between DNA binding molecules and discrete nucleotide sequences in polymeric DNA. Because phi complexes of rhodium effect strand scission upon irradiation,[42] providing direct information about their binding positions, an assay based on DNA cleavage by the binding ligand was developed. In contrast to footprinting methods,[43] this internal cleavage assay eliminates any complicating signal from binding modes that do not promote strand scission.

The affinity of metallointercalator-peptide conjugates for specific sites is a function of the metal complex and the appended peptide. Previously, Sardesai *et al.* estimated the contribution of the peptide to specific binding as 1 kcal•mol^{-1} based on the cleavage intensities of [Rh]-E10 and [Rh(phi)$_2$(phen')]$^{3+}$ at a 5'-CCA-3' site and observed that a 100-fold excess of free peptide was incapable of competing with [Rh]-E10 for the DNA target.[18] Comparison of the dissociation constant of [Rh]-E10 for a 5'-CCA-3' sequence

and the bulk intercalative dissociation constant of $[Rh(phi)_2(phen')]^{3+}$ at 55 °C in the presence of 5 mM $MnCl_2$ affords a similar value of 1.7 kcal•mol^{-1} for the energetic advantage of specific complex formation.

Similar values have been reported for the energetic stabilization of specific complex formation by dimeric peptides derived from GCN4. Talanian *et al.* found that the disulfide-linked dimer of a 31-mer peptide derived bound to the GCN4 recognition element with a K_d of 5 x 10^{-8}.[44] Similarly, Cuenoud and Schepartz reported that an iron(II) *bis*-terpyridyl dimer of a 29-mer peptide bound to the GCN4 recognition element with a K_d of 1.3 x 10^{-7}.[45] These values correspond to free energies of complex formation of -10.2 kcal•mol^{-1} (0.17 kcal•mol^{-1} per amino acid residue) and -9.6 kcal•mol^{-1} (0.17 kcal•mol^{-1} per amino acid residue), respectively. In comparison, the energetic advantage of specific complex formation for [Rh]-E10 corresponds to a value of 0.13 kcal•mol^{-1} per amino acid residue, despite the small size and minimal secondary structure of the peptide.

DNA binding proteins derive most of their binding affinity from a combination of nonspecific electrostatic and hydrogen bonding interactions. Sequence discrimination is achieved through contacts made primarily by side chains of amino acid residues contained in a modular recognition domain. These results indicate that similarly, [Rh]-E10 derives the majority of its free energy of sequence-selective binding from intercalation, while base-specific interactions between the E10 peptide and the target DNA sequence provide sequence discrimination.

The sequence selectivity of metallointercalator-peptide conjugates is a function of the ratio between the dissociation constant for the target site and the dissociation constants for nontarget sites. Photocleavage results of metallointercalator conjugates of peptides derived from the P_{22} repressor have demonstrated that optimal selectivity in DNA binding is observed at elevated temperature.[18] In principle, either an increase in the affinity of the conjugate for the target sequence or a decrease in the affinity of the conjugate for nontarget

sequences could afford the observed increase in selectivity with increasing temperature. To discriminate between these possibilities, the effect of an increase in the temperature on the dissociation constant of [Rh]-E10 for its target site was determined. Remarkably, the metallointercalator-peptide conjugate binds 5-fold more tightly at 55 °C than at 23 °C.

A similar increase in affinity at elevated temperatures was reported by Lündback and coworkers in calorimetric studies of glucocorticoid receptor binding to target DNA sites, who postulated that release of ordered water at the transcription factor-response element interface was responsible for the observed thermodynamic data.[46] Macromolecular complex formation generally results in a large, negative change in the heat capacity (ΔC_p),[47] which has been attributed to a reduction in the solvent accessible surface upon complexation[47a,b] and to a reduction in the degrees of freedom at the complex interface.[47c,d] This heat capacity change results in opposite temperature dependencies of the enthalpic and entropic components of the free energy of binding. Accordingly, a value for $T\Delta S$ cannot be derived from the temperature dependence of the dissociation constant; however, it is possible to estimate $T\Delta S$ as a function of the effect of temperature changes on ΔH and $T\Delta S$. Increasing the temperature from 10 °C to 34 °C resulted in a 57% decrease in the value of ΔH and an 18% decrease in the absolute value of $T\Delta S$ for response element binding by the glucocorticoid receptor. If ΔH and $T\Delta S$ for sequence-selective DNA binding by [Rh]-E10 undergo identical percentage changes, a value of 16 kcal•mol^{-1} is obtained for $T\Delta S$ at 55 °C. If ΔH and $T\Delta S$ are temperature independent, $T\Delta S$ has a value of 20 kcal•mol^{-1} at 55 °C. The maximum entropic penalty for immobilization of a single water molecule in an ice or salt crystal has been estimated as 2 kcal•mol^{-1} at 27 °C.[48] Accordingly, the estimated values for $T\Delta S$ for sequence selective binding correspond to a minimum of 3 ordered waters released per recognized base pair. For comparison, the primary hydration shell of B-DNA consists of at least 11 to 12 water molecules per nucleotide, and at least 5 water molecules per base pair in the major groove.[49]

4.4.2. Conformational effects of DNA binding by [Rh]-E10. The E10 and R6A10 peptides confer specificities greater than 6:1 on $[Rh(phi)_2(phen')]^{3+}$ under optimal conditions, as measured by the ratio of cleavage by the sequence-selective metallointercalator-peptide conjugate to cleavage by $[Rh(phi)_2(phen')]^{3+}$ at the target DNA site.[18,50] These specificities are greater than the helical contents of [Rh]-E10 and [Rh]-R6A10 under the same conditions.[51] However, among the sequence-selective metallointercalator-peptide conjugates listed in Table 4.1, helical content in the absence of DNA correlates with selectivity for 5'-CCA-3'.[18] There are at least three possible explanations for this discrepancy: (1) some structural feature of the peptide correlates with the helical content yet is poorly detected by CD; this structural feature is essential for sequence-selective recognition; alternatively (2) the formation of specific DNA complexes promotes helix formation by metallointercalator-peptide conjugates; and/or (3) the transition between helix and random coil peptide conformations is rapid relative to the exchange rate of the intercalation complex between the DNA and the rhodium(III) anchor. In order to discriminate among these possibilities, changes in the helical content of [Rh]-E10 upon DNA binding were investigated.

Circular dichroism spectroscopy is exquisitely sensitive to changes in the conformation of biological macromolecules upon complex formation; in a recent example Uesugi identified an increase in the helical content of the basic region/helix-loop-helix/leucine zipper transcription factor Max upon binding a 21-mer oligonucleotide containing the target sequence 5'-CACGTG-3'.[52] Although intercalative binding by the rhodium complex perturbs the CD spectrum of the DNA, comparison of the CD spectrum of the DNA in the absence and presence of 0.5 equiv $[Rh(phi)_2(phen')]^{3+}$ indicates that the metallointercalator dependence of the CD spectrum of the DNA between 210 and 250 nm is very slight.[53] DNA binding by [Rh]-E10 does not appear to promote helix formation at 55 °C in the presence of 5 mM $MnCl_2$. This observation is consistent with a model for DNA

binding by [Rh]-E10 in which intercalative binding occurs first; subsequently, the peptide samples a helical conformation sufficiently frequently to slow the dissociation rate for intercalation complexes at the target site. Consequently, greater helical content in the absence of DNA results in greater stabilization of complexes at the target site, but high helicity is not a prerequisite for sequence selectivity.

4.5. Conclusions

Like DNA binding proteins, the metallointercalator-peptide conjugate studied in this chapter contains a recognition domain that confers sequence selectivity on a relatively sequence-neutral high affinity DNA binding domain. Determination of dissociation constants of [Rh]-E10 for discrete DNA sequences by photocleavage titration enabled the relative energetic contributions of these domains to sequence selective binding to be delineated; the peptide contributes a free energy of 1.7 kcal•mol^{-1} to complex formation between [Rh]-E10 and 5'-CCA-3'. Determination of the sequence-specific dissociation constants of [Rh]-E10 provided insight into the unusual increase in sequence selectivity observed at elevated temperature. The concomitant increases in specificity, determined from photocleavage data, and affinity, determined from dissociation constants, indicates that intercalation complexes of [Rh]-E10 at nontarget sequences enjoy less entropic stabilization than intercalation complexes at the target sequence, suggesting that like DNA binding proteins, metallointercalator-peptide conjugates achieve sequence selectivity through a variety of stabilizing interactions. Together, the dissociation constant and CD spectroscopic measurements of the [Rh]-E10•DNA complex have important implications for the design of future generations of metallointercalator-peptide conjugates having altered sequence selectivities. High specificity requires a combination of predisposition of the peptide to a conformation complementary to the target, energetically favorable base-specific

noncovalent interactions with the target sequence, and entropic benefits associated with complex formation.

4.6. References and Notes

1. (a) Brennan, R. G.; Matthews, B. W. *J. Biol. Chem.* **1989**, *264*, 1903. (b) Harrison, S. C.; Aggarwal, A. K. *Ann. Rev. Biochem.* **1990**, *59*, 933.
2. (a) Jones, N. *Cell* **1990**, *61*, 9. (b) Davis, R. L.; Cheng, P.-F.; Lassar, A. B.; Weintraub, H. *Cell* **1990**, *60*, 733. (c) Anthony-Cahill, S. J.; Benfield, P. A.; Fairman, R.; Wasserman, Z. R.; Brenner, S. L.; Stafford, W. F., III; Altenbach, C.; Hubbell, W. L.; DeGrado, W. F. *Science* **1992**, *255*, 979.
3. (a) Gehring, W. J.; Muller, M.; Affolter, M.; Percival-Smith, A.; Billeter, M.; Qian, Y. Q.; Otting, G.; Wüthrich, K. *Trends Genet.* **1990**, *6*, 323. (b) Gehring, W. J.; Qian, Y. Q.; Billeter, M.; Furukubo-Tokunaga, K.; Schier, A. F.; Resendez-Perez, D.; Affolter, M.; Otting, G.; Wüthrich, K. *Cell* **1994**, *78*, 211. (c) Pomerantz, J. L.; Pabo, C. O.; Sharp, P. A. *Proc. Natl. Acad. Sci. U.S.A.* **1995**, *92*, 9752.
4. Kerppola, T. K. *Curr. Opin. Struct. Biol.* **1991**, *1*, 71.
5. (a) Berg, J. M. *Science* **1986**, *232*, 485. (b) Berg, J. M. *Ann. Rev. Biophys. Biophys. Chem.* **1990**, *19*, 405. (c) Vallee, B.L.; Coleman, J.E.; Auld, D.S. *Proc. Natl. Acad. Sci. U.S.A.* **1991**, *88*, 999. (d) Schwabe, J. W. R.; Klug, A. *Nature Struct. Biol.* **1994**, *1*, 345.
6. Blackwell, T. K.; Bowerman, B.; Priess, J. R.; Weintraub, H. *Science* **1994**, *266*, 621.
7. (a) Cuenod, B.; Schepartz, A. *Science* **1993**, *259*, 510. (b) Talanian, R. V.; McKnight, C. J.; Kim, P. S. *Science* **1990**, *249*, 769. (c) Talanian, R. V.; McKnight, C. J.; Rutkowski, R.; Kim, P. S. *Biochemistry* **1992**, *31*, 6871. (d)

Morii, T.; Simomura, M.; Morimoto, S.; Saito, I. *J. Am. Chem. Soc.* **1993**, *115*, 1150. (e) Dervan, P. B. *Methods Enzymol.* **1991**, *208*, 497.

8. (a) O'Neil, K. T.; Hoess, R. H.; DeGrado, W. F. *Science* **1990**, *249*, 774. (b) Ueno, M.; Murakami, A.; Makino, K.; Morii, T. *J. Am. Chem. Soc.* **1993**, *115*, 12575.

9. (a) Chow, C. S.; Barton, J. K. *Methods Enzymol.* **1992**, *212*, 219. (b) Pyle, A. M.; Long, E. C.; Barton, J. K. *J. Am. Chem. Soc.* **1989**, *111*, 4520. (c) David, S. S.; Barton, J. K. *J. Am. Chem. Soc.* **1993**, *115*, 2984. (d) Krotz, A. H.; Luo, L. Y.; Shields, T. P.; Barton, J. K. *J. Am. Chem. Soc.* **1993**, *115*, 3877.

10. Sitlani, A.; Long, E. C.; Pyle, A. M.; Barton, J. K. *J. Am. Chem. Soc.* **1992**, *114*, 2303.

11. (a) Sitlani, A.; Dupureur, C. M.; Barton, J. K. *J. Am. Chem. Soc.* **1993**, *115*, 12589. (b) Krotz, A. H.; Hudson, B. P.; Barton, J. K. *J. Am. Chem. Soc.* **1993**, *115*, 12577. (c) Jackson, B. A.; Barton, J. K. *J. Am. Chem. Soc.* **1997**, *119*, 12986.

12. (a) Hudson, B. P.; Dupureur, C. M.; Barton, J. K. *J. Am. Chem. Soc.* **1995**, *117*, 9379. (b) Hudson, B. P.; Barton, J. K., submitted to *J. Am. Chem. Soc.*

13. The structural parameters for the base step (G_5pC_6 or G_5pC_{16}) at which intercalation occurs are: rise, 6.876 Å; slide, 1.460 Å; shift, -0.032 Å; twist, 51.928°; roll, -7.880 Å; tilt, 0.812°; shear, 0.088 Å; stretch, 0.030 Å, stagger, 1.053 Å; propeller twist, -20.072°; buckle, 29.443°.

14. (a) Sauer, R. T.; Pan, J.; Hopper, P.; Hehir, K.; Brown, J.; Poteete, A. R. *Biochemistry* **1981**, *20*, 3591. (b) Sauer, R. T.; Yocum, R. R.; Doolittle, R. F.; Lewis, M.; Pabo, C. O. *Nature* **1982**, *298*, 447. (c) Ptashne, M. *A Genetic Switch*, Cell Press and Blackwell Scientific Publications, Cambridge: 1986. (d)

Sevilla-Sierra, P.; Otting, G.; Wüthrich, K. *J. Mol. Biol.* **1994**, *235*, 1003. (e) Harrison, S. C.; Anderson, J. E.; Koudelka, G. B.; Mondragón, A.; Subbiah, S.; Wharton, R. P.; Wolberger, C.; Ptashne, M. *Biophys. Chem.* **1988**, *29*, 31.

15. Wharton, R. P.; Ptashne, M. *Nature* **1985**, *316*, 601.
16. Sardesai, N. Y., Barton, J. K. *J. Biol. Inorg. Chem.* **1997**, *2*, 762.
17. Lin, S. C. *Ph.D. Thesis*, California Institute of Technology, 1996.
18. Sardesai, N. Y.; Zimmerman, K.; Barton, J. K. *J. Am. Chem. Soc.* **1994**, *116*, 7502.
19. [Rh]-E10 was previously referred to as Sk-PD: see reference 18.
20. Still, W. C.; Kahn, M.; Mitra, A. *J. Org. Chem.* **1978**, *43*, 2923.
21. (a) Bodenhausen, G.; Kogler, H.; Ernst, R. R. *J. Magn. Reson.* **1984**, *58*, 370. (b) Marion, D.; Wüthrich, K. *Biochem. Biophys. Res. Commun.* **1983**, *113*, 967.
22. States, D. J.; Harberkorn, R. A.; Ruben, D. J. *J. Magn. Reson.* **1982**, *48*, 286.
23. *Felix User Guide*, version 95.0, Biosym/MSI, San Diego:1995.
24. Marion, D.; Ikura, M.; Bax, A. *J. Magn. Reson.* **1989**, *84*, 425.
25. Wolfram, S. *The Mathematica Book*, 3rd ed., Wolfram Media/Cambridge University Press, Cambridge, UK:1996.
26. Caruthers, M. H.; Barone, A. D.; Beaucage, S. L.; Dodds, D. R.; Fisher, E. F.; McBride, L. J.; Matteucci, M.; Stabinsky, Z.; Tang, J.-Y. *Methods Enzymol.* **1987**, *154*, 287.
27. (a) Stewart, J. M.; Young, J. D. *Solid Phase Peptide Synthesis*, Pierce Chemical Company, Rockford, Illinois: 1984. (b) Edmondson, J. M.; Klebe, R. J.; Zardeneta, G.; Weintraub, S. T.; Kanda, P. *BioTechniques* **1988**, *6*, 866.
28. Sardesai, N. Y.; Lin, S. C.; Zimmerman, K.; Barton, J. K. *Bioconj. Chem.* **1995**, *6*, 302.

29. (a) Cartwright, P. S.; Gillard, R. D.; Sillinpåå, E. R. J. *Polyhedron* **1987**, *6*, 105. (b) Dollimore, L. S.; Gillard, R. D. *J. Chem. Soc. Dalton. Trans.* **1973**, 933.

30. HF deprotection and cleavage from the resin of metallointercalator-peptide conjugates was performed by the Biopolymer Synthesis Facility, Department of Chemistry, California Institute of Technology.

31. Authentic sample courtesy of Dr. Sonya Franklin. The diastereomers of [Rh]-E10 (Δ and Λ at the metal center) are known to coelute under the HPLC column and gradient conditions described, see reference 18.

32. $[L]_f = - a / 3 + 2(- 3b + a^2)^{1/2} \cos(\arccos((- 27[L]_t / K_1K_2 - 9ab / (K_1K_2)^2 + 2a^3) / (2(3b - a^2)(- 3b + a^2)^{1/2})) / 3) / 3$, where a is $(K_1 + K_2 - K_1K_2[L]_t + K_1K_2[DNA]_t + K_1K_2n[DNA]_t) / K_1K_2$ and b is $(1 - K_1[L]_t - K_2[L]_t + K_1[DNA]_t + K_2n[DNA]_t) / K_1K_2$.

33. Simulations performed by Mr. Brian Jackson.

34. Maniatis, T.; Fritsch, E. F.; Sambrook, J. *Molecular Cloning*, Cold Spring Harbor Laboratory, Cold Spring Harbor: 1982.

35. Maxam, A. M.; Gilbert, W. *Proc. Natl. Acad. Sci. U.S.A.* **1977**, *74*, 560.

36. Sardesai, N. Y.; Lin, S.C.; Zimmermann, K.; Barton, J. K. *Bioconj. Chem.* **1995**, *6*, 302.

37. COSY and TOCSY spectra for [Δ-Rh]-E10 and a table of cross peak assignments are given in Appendix II.

38. Values for average chemical shift for amino acids are from Gross, K. H.; Kalbitzer, H. R. *J. Magn. Reson.* **1988**, *76*, 87.

39. Adapted from Jackson, B. A.; Hastings, C. A.; Johann, T. W.; Hudson, B. P.; Barton, J. K., manuscript in preparation.

40. The helical content is calculated by assuming that a fully helical peptide has a mean residue ellipticity ($[\theta_{222}]$) of -31,500 deg•cm^2•dmol^{-1}; see: Chen, Y. H.; Yang, J. T.; Martinez, H. M. *Biochemistry* **1972**, *11*, 4120. The mean residue ellipticity is defined as:

$$[\theta_{222}] = 100\theta_{222}/cnl$$

where θ_{222} is the ellipticity (mdeg) measured by CD spectroscopy, c is the peptide concentration (mM), n is the number of amino acids in the peptide, and l is the path length (cm) of the CD cell; see: Lehrman, S. R.; Tuls, J. L.; Lund, M. *Biochemistry* **1990**, *29*, 5590.

41. (a) Winzor, D. J.; Sayer, W. H. *Quantitative Characterization of Ligand Binding*; Wiley-Liss: New York, 1995. (b) Chaires, J. B.; Satyanarayana, S.; Suh, D.; Fokt, I.; Przewloka, T.; Priebe, W. *Biochemistry* **1996**, *35*, 2047-2053. (c) Takusagawa, F.; Wen, L.; Chu, W.; Li, Q.; Takusagawa, K. T.; Carlson, R. G.; Weaver, R. F. *1996* **1996**, *35*, 13240-13249. (d) Roche, C. J.; Berkowitz, D.; Sulikowski, G. A.; Danishefsky, S. J.; Crothers, D. M. *Biochemistry* **1994**, *33*, 936-942. (e) Wang, Y.; Killian, J.; Hamasaki, K.; Rando, R. R. *Biochemistry* **1996**, *35*, 12338-12346. (f) Pyle, A. M.; Rehmann, J. P.; Meshoyrer, R.; Kumar, C. V.; Turro, N. J.; Barton, J. K. *J. Am. Chem. Soc.* **1989**, *111*, 3051-3058. (g) Rentzeperis, D.; Marky, L. A.; Dwyer, T. J.; Geierstanger, B. H.; Pelton, J. G.; Wemmer, D. E. *Biochemistry* **1995**, *34*, 2937-2945. (h) Kalsbeck, W. A.; Thorp, H. H. *J. Am. Chem. Soc.* **1993**, *115*, 7146-7151. (i) Welch, T. W.; Thorp, H. H. *J. Phys. Chem.* **1996**, *100*, 13829-13836. (j) Carter, M. T.; Rodriguez, M.; Bard, A. J. *J. Am. Chem. Soc.* **1989**, *111*, 8901-8911. (l) Ding, L.; Bernadou, J.; Meunier, B. *Bioconj. Chem.* **1991**, *2*, 201-206.

42. Sitlani, A.; Long, E. C.; Pyle, A. M.; Barton, J. K. *J. Am. Chem. Soc.* **1992**, *114*, 2303.

43. (a) Goodisman, J.; Dabrowiak, J. C. in *Advances in DNA Sequence Specific Agents*; Hurley, L. H., Ed.; Jai Press: Greenwich, CT, 1992; Vol. 1, pp. 25-49. (b) Ward, B.; Rehfuss, R.; Goodisman, J.; Dabrowiak, J. C. *Biochemistry* **1988**, *27*, 1198-1205. (c) Guo, D. Q.; Gupta, R.; Lown, J. W. *Anti-Cancer Drug Design* **1993**, *8*, 369-397.

44. (a) Talanian, R. V.; McKnight, C. J.; Kim, P. S. *Science* **1990**, *249*, 769. (b) Talanian, R. V.; McKnight, C. J.; Rutkowski, R.; Kim, P. S. *Biochemistry* **1992**, *31*, 6871.

45. Cuenoud, B.; Schepartz, A. *Science* **1993**, *259*, 510.

46. (a) Lündback, T.; Zilliacus, J.; Gustaffson, J.-Å.; Carlstedt-Duke, J.; Härd, T. *Biochemistry* **1994**, *33*, 5955. (b) Lündback, T.; Härd, T. *Proc. Natl. Acad. Sci. U.S.A.* **1996**, *93*, 4754. For an additional example of entropy-driven binding to a biomacromolecule, see: Lopez, M. M.; Kosk-Kosicka, D. *Biochemistry* **1997**, *36*, 8864.

47. (a) Ha, J.-H.; Spolar, R. S.; Record, M. T., Jr. *J. Mol. Biol.* **189**, *209*, 801. (b) Spolar, R. S.; Record, M. T., Jr. *Science* **1994**, *263*, 777. (c) Ladbury, J. E.; Wright, J. G.; Sturtevant, J. M.; Sigler, P. B. *J. Mol. Biol.* **1994**, *238*, 669. (d) Hyre, D. E.; Spicer, L. D. *Biochemistry* **1995**, *34*, 3212.

48. Dunitz, J. D. *Science* **1994**, *264*, 670.

49. Falk, M.; Hartman, K. A., Jr.; Lord, R. C. *J. Am. Chem. Soc.* **1963**, *85*, 387.

50. See Chapter 5 of this thesis.

51. It is worth noting that the specificity (ratio of cleavage at the target site to the ratio of cleavage at nontarget sites) shows no marked difference between concentrations above and below the nonspecific dissociation constant. Accordingly, selective binding by only those metallointercalator-peptide conjugates in a helical conformation cannot account for the observed selectivity data.

52. Horiuchi, M.; Kurihara, Y.; Katahira, M.; Maeda, T.; Saito, T.; Uesugi, S. *J. Biochem.* **1997**, *122*, 711.

53. Similar results were observed in a CD study of DNA binding by the minor groove intercalator 2-methyl-9-hydroxyellipticinium acetate; see: Monnot, M.; Mauffret, O.; Lescot, E.; Fermandjian, S. *Eur. J. Biochem.* **1992**, *204*, 1035.

Chapter 5: Perturbing the DNA Sequence Selectivity of Metallointercalator-Peptide Conjugates by Single Amino Acid Modification

5.1. Introduction

5.1.1. Correlations between the amino acid sequences of DNA binding proteins and the nucleotide sequences of their targets. Selective binding interactions between biomolecules are crucial to a number of cellular processes. The selectivity of some binding interactions, such as base pairing of complementary DNA strands,[1] can be predicted by relatively simple rules. In contrast, no simple set of rules correlates the amino acid sequences of DNA binding proteins with the nucleotide sequences of their targets.[2] Crystallographic studies of transcription factor–operator complexes have revealed that multiple amino acids may be used to recognize a given base, and multiple bases may be recognized by the same amino acid (Table 5.1). Currently, combinatorial approaches are the most effective methods for obtaining oligopeptides that target specific nucleotide sequences.[3] A recognition code for protein–DNA interaction would find application in the development of repressors, transcription factors and nucleases with altered sequence selectivity.[4]

The classification of DNA binding proteins into superfamilies[5] has led to attempts to develop rules for given classes of DNA binding proteins that predict the target DNA sequence as a function of the amino acid sequence. Because of the modular fashion in which zinc finger transcription factors recognize DNA,[6] these proteins have been the subject of the most extensive attempts at developing a recognition code. Mutagenesis experiments have demonstrated that the construction of a family of zinc fingers that target different DNA sequences is possible. However, in many cases concerted amino acid changes are required to alter the specificity. Additionally, single amino acid changes can alter the DNA sequence selectivity at multiple positions of the DNA target.[7] These studies

Table 5.1. Base-specific contacts by amino acids in crystal structures of selected transcription factor-DNA complexes.[a,8]

	A	T	C	G
Arg		CAP		GR; Trp; Zif; CAP; Arc; Gli
Asn	en; GATA	Arc	Arc	λ
Asp			Gli	
Gln	λ; 434; Arc	434		434
Glu			CAP	
Gly		λ; Gr		
His				Zif
Ile		en		
Lys				GR; λ; MetJ; Gli
Ser	Gli			λ; Gli
Thr	MetJ			

[a]CAP, *E. Coli* CAP protein; en, *Drosophila* engrailed homeodomain; λ, λ-repressor; 434, *434* repressor; GR, glucocorticoid repressor; MetJ, *E. Coli* MetJ repressor; Trp, *E. Coli* Trp repressor; Zif, Zif268 zinc fingers; Arc, P_{22} Arc repressor; Gli, human *GLI* oncogene zinc fingers; GATA-1, erythroid-specific transcription factor GATA-1.

demonstrate the need for further research on the relationship between the amino acid sequences of DNA binding proteins and the nucleotide sequences of their targets.

5.1.2. Model for DNA recognition by metallointercalator-peptide conjugates derived from the P_{22} repressor. In previous work, Sardesai *et al.* tethered oligopeptides derived from the recognition domain of the P_{22} repressor to $[Rh(phi)_2(phen')]^{3+}$, conferring selectivity for the three base pair sequence 5'-CCA-3' on the relatively sequence-neutral metallointercalator. Unlike metallointercalator conjugates of peptides derived from the *434* repressor[9a] and the zinc fingers Sp1 and Adr1,[9c] the

sequence selectivity of the parent protein was not reproduced.[9] Instead, sequence selectivity for 5'-CCA-3' was observed with the metallointercalator-peptide conjugate $[Rh(phi)_2(phen')]^{3+}$-AANVAIAAWERAA-$CONH_2$ ([Rh]-E10).[10] Mutation of amino acid residues of [Rh]-E10 to alanine individually and pairwise indicated that Glu^{10} was critical in maintaining the secondary structure of the peptide and in making a base-specific contact to the DNA target. Modification of the amino acid sequence at sites other than Glu^{10} identified a number of metallointercalator-peptide conjugates with 5'-CCA-3' selectivity; the levels of selectivity correlated well with the helical content of the appended peptides. However, no new sequence selectivity was observed. From these and other results, Sardesai *et al.* proposed that [Rh]-E10 adopted a conformation similar to the one shown in Figure 5.1 when bound to its DNA target.

This chapter describes the results of modifications to the amino acid sequence of [Rh]-E10. These investigations were undertaken to develop [Rh]-E10 as a starting point for the predictable design of metallointercalator-peptide conjugates with altered sequence selectivity. This goal required that we identify positions in the sequence of the E10 peptide where amino acid changes resulted in altered DNA sequence selectivity. We also sought to explore the diversity of sequence selectivity that could be achieved by single amino acid modification of the parent metallointercalator-peptide conjugate, and to refine the model shown in Figure 5.1. Systematic variation in the position of the critical glutamate residue at position 10 led to the identification of new sequence-selective metallointercalator-peptide conjugate and the prediction of an additional residue of [Rh]-E10 that makes base-specific contacts. This prediction was tested by making further sequence changes at that position; these changes led to additional sequence selectivity. Thus, from [Rh]-E10 we can create a family of metallointercalator-peptide conjugates that exhibit a variety of sequence preferences.

5.2. Experimental

5.2.1. General procedures. All reagents were commercially obtained except where noted. When appropriate, reagents were purified prior to use. Except where noted, experimental procedures are as given in Chapter 4.

5.2.2. Instrumentation. MALDI-TOF mass spectroscopy was performed by the Protein and Peptide Microanalytical Facility, Beckman Institute, California Institute of Technology. Molecular mechanics simulations were performed with Discover[11] and rendered with InsightII[19] running on a Silicon Graphics Indigo^2 R10000 High Impact workstation.

1

5.2.3. Synthesis of [Rh(phi)$_2$(ethynylphen')]$^{3+}$. 1: TEA (1.9 mL, 13.6 mmol, 1.5 equiv), TBSCl (1.64 g, 10.9 mmol, 1.2 equiv), and 4-DMAP (110 mg, 0.9 mmol, 0.1 equiv) were added to a solution of 1 mL (9.06 mmol, 1 equiv) of 5-hexyn-1-ol in 25 mL CH_2Cl_2 at 0 °C. The resulting solution was stirred at 0 °C for 30 min. The reaction mixture was poured into 30 mL H_2O and extracted with 2 x 25 mL Et_2O. The organic layers were combined, dried over anhydrous Na_2SO_4, and concentrated *in vacuo*. The residue was purified by distillation (20 mTorr, 65 °C) to afford 1.75 g (90%) of **1** as a clear, colorless oil. ^{1}H NMR (300 MHz, $CDCl_3$) δ 3.66 (2H, t, J = 6.0 Hz, C1H_2), 2.22 (2H, m, C4H_2), 1.97 (1H, t, J = 1.8 Hz, C6H), 1.70-1.52 (4H, m, C2H_2 and C3H_2), 0.91 (9H, s, SiC(CH_3)$_3$), 0.08 (6H, s, Si(CH_3)$_2$) ppm.

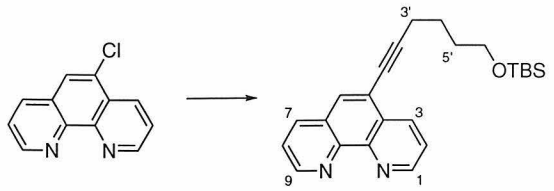

2

2: A solution of 1.00 g (4.65 mmol, 1.0 equiv) 5-chloro-1-phenanthroline, 100 mg (0.465 mmol, 0.1 equiv) CuI, 0.95 mL (7.0 mmol, 1.5 equiv) $^{i}Pr_2NH$, 750 mg (0.645 mmol, 0.15 equiv) $(PPh_3)_2PdCl_2$, and 2.5 g (11.6 mmol, 2.5 equiv) of **1** in 5 mL THF was sealed under Argon in a thick-walled glass bomb equipped with a Teflon valve, heated to 65 °C, and stirred for 48 h (*Caution:* use blast shield). The reaction mixture was cooled to 23 °C and 15 mL CH_2Cl_2 and 15 mL 1.0 M aqueous NaCN were added. The resulting slurry was vigorously stirred for 30 min. The aqueous layer was extracted with 2 x 10 mL CH_2Cl_2. The organic layers were combined, dried over anhydrous Na_2SO_4, and concentrated *in vacuo*. The residue was purified by chromatography on silica gel (25 x 120 mm, 1:2 EtOAc–CH_2Cl_2, R_f 0.30) followed by chromatography on reverse phase silica gel (25 x 80 mm, MeOH, R_f 0.40) to afford 1.65 g (90%) of **2** as a clear, colorless oil. ^{1}H NMR (500 MHz, $CDCl_3$) δ 9.25-9.23 (1H, m, C1*H* or C9*H*), 9.20-9.18 (1H, m, C1*H* or C9*H*), 8.77-8.75 (1H, m, C3*H* or C7*H*), 8.22-8.21 (1H, m, C3*H* or C7*H*), 7.96 (1H, d, *J* = 1.4 Hz, C6*H*), 7.74-7.71 (1H, m, C2*H* or C8*H*), 7.67-7.64 (1H, m, C2*H* or C8*H*), 3.72 (2H, t, *J* = 6.0 Hz, C3'H_2), 2.64 (2H, t, *J* = 6.6 Hz, C6'H_2), 1.82-1.76 (4H, m, C4'H_2 and C5'H_2), 0.91 (9H, s, SiC(CH_3)$_3$), 0.08 (6H, s, Si(CH_3)$_2$) ppm; ^{13}C NMR (126 MHz, $CDCl_3$) δ 150.5, 150.4, 145.7, 135.7, 135.0, 130.1, 128.7, 128.2, 123.4, 123.3, 120.8, 96.9, 62.6, 32.1, 26.0, 25.3, 19.6, 18.3, -5.3 ppm.

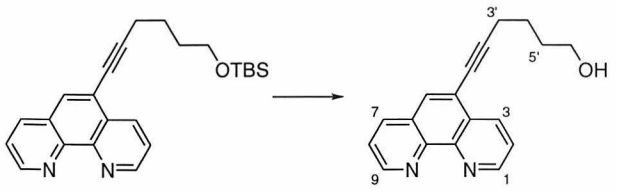

3

3: A solution of 1.62 g (4.15 mmol, 1.0 equiv) of **2** and 5.4 mL (5.4 mmol, 1.3 equiv) of a 1.0 M solution of TBAF in THF in 7.3 mL THF was stirred at 23 °C for 30 min. The reaction mixture was poured into 20 mL H_2O and extracted with 3 x 20 mL Et_2O. The organic layers were combined, dried over anhydrous Na_2SO_4, and concentrated *in vacuo*. The residue was purified by chromatography on reverse phase silica gel (25 x 80 mm, 4:1:0.5 EtOAc–CH_2Cl_2–MeOH, R_f 0.25) to afford 640 mg (55%) of **3** as a clear, colorless oil that solidified on standing. ^{1}H NMR (500 MHz, $CDCl_3$) δ 9.00 (1H, dd, *J* = 4.3, 1.6 Hz, C1*H* or C9*H*), 8.95 (1H, dd, *J* = 4.3, 1.7 Hz, C1*H* or C9*H*), 8.52 (1H, dd, *J* = 8.6, 1.7 Hz, C3*H* or C7*H*), 7.98 (1H, dd, *J* = 8.2, 1.6 Hz, C3*H* or C7*H*), 7.71 (1H, s, C6*H*), 7.52 (1H, dd, *J* = 8.2, 4.3 Hz, C2*H* or C8*H*), 7.42 (1H, dd, *J* = 8.6, 4.3 Hz, C2*H* or C8*H*), 3.59 (2H, t, *J* = 6.0 Hz, C3'H_2), 2.70 (1H, br s, O*H*), 2.47 (2H, t, *J* = 4.7 Hz, C6'H_2), 1.68-1.65 (4H, m, C4'H_2 and C5'H_2) ppm; ^{13}C NMR (126 MHz, $CDCl_3$) δ 150.3, 150.2, 145.6, 145.5, 135.6, 134.7, 130.0, 128.4, 128.0, 123.3, 120.5, 116.5, 96.7, 61.8, 31.8, 25.1, 19.4 ppm. HRMS (FAB) calculated for $C_{18}H_{16}N_2O$ 276.1262, calculated for $C_{18}H_{17}N_2O$ (M + H^+) 277.1341, found 277.1329.

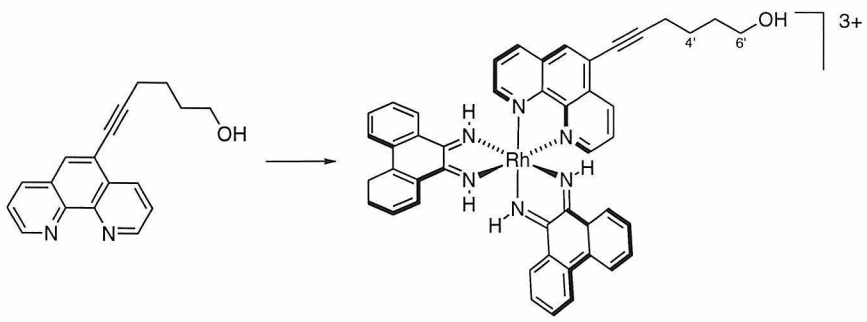

[Rh(phi)$_2$(ethynylphen')]Cl$_3$: AgOTf (124 mg, 0.482 mmol, 3.0 equiv) was added to a suspension of 100 mg (0.160 mmol, 1.0 equiv) [Rh(phi)$_2$Cl$_2$]Cl, prepared according to the literature procedure,[12] in 5 mL DMF. The resulting suspension was stirred at 65 °C for 16 h with protection from light. The precipitate was removed by filtration and 45 mg (0.160 mmol, 1.0 equiv) **3** was added. The resulting solution was stirred at 65 °C for 16 h with protection from light. The reaction mixture was cooled to 23 °C and diluted with 100 mL H_2O and 1 mL 1.0 M aqueous KCl. The precipitate was removed by filtration and the residue purified by cation-exchange chromatography (25 x 400 mm, stepped gradient 0.1 $\rightarrow$0.3 M aqueous KCl). The product eluted as a yellow-orange solution at 0.3 M KCl. Fractions containing the product were applied to a reverse phase silica gel column (25 x 80 mm). The column was washed with 500 mL Milli-Q H_2O and eluted with 3:1 0.1% aqueous TFA–MeCN. Lyophilization afforded 140 mg (97%) of the chloride salt of [Rh(phi)$_2$(ethynylphen')]$^{3+}$ as an orange powder. ^{1}H NMR (500 MHz, CD_3OD) δ 9.22 (1H, d, J = 8.5 Hz, ethynylphen' C2*H*, C4*H*, C7*H* or C9*H*), 9.08 (1H, d, J = 5.5 Hz, ethynylphen' C2*H*, C4*H*, C7*H* or C9*H*), 9.00 (1H, d, J = 5.5 Hz, ethynylphen' C2*H*, C4*H*, C7*H* or C9*H*), 8.94 (1H, d, J = 8.5 Hz, ethynylphen' C2*H*, C4*H*, C7*H* or C9*H*), 8.76 (2H, d, J = 7.9 Hz, two of phi C1*H*, C1'*H*, C10*H*, and C10'*H*), 8.49-8.47 (3H, m, ethynylphen' C3*H*, C6*H*, and C8*H*), 8.42-8.40 (4H, m, two of phi C4*H*, C4'*H*, C7*H*, or C7'*H* and two of phi C1*H*, C1'*H*, C10*H*, and C10'*H*), 8.20 (1H, dd, J = 8.5, 4.9 Hz, phi C4*H*, C4'*H*, C7*H*, or C7'*H*), 8.10 (1H, dd, J = 8.5, 4.9 Hz,

phi C4*H*, C4'*H*, C7*H*, or C7'*H*), 7.88 (2H, dd, *J* = 8.2, 8.0 Hz, two of phi C3*H*, C3'*H*, C8*H*, and C8'*H*), 7.80 (2H, dd, *J* = 8.2, 7.4 Hz, two of phi C3*H*, C3'*H*, C8*H*, and C8'*H*), 7.66 (2H, dd, *J* = 8.5, 8.2 Hz, two of phi C2*H*, C2'*H*, C9*H*, and C9'*H*), 7.54 (2H, t, *J* = 7.8 Hz, two of phi C2*H*, C2'*H*, C9*H*, and C9'*H*), 3.66 (2H, td, *J* = 6.2, 0.3 Hz, C6'H_2), 2.76 (1H, t, *J* = 6.6 Hz, one of C3'H_2), 2.72 (1H, t, *J* = 6.6 Hz, one of C3'H_2), 1.88-1.79 (4H, m, C4'H_2 and C5'H_2) ppm; ^{13}C NMR (126 MHz, CD_3OD) δ 175.9, 175.3, 155.8, 155.4, 147.8, 147.1, 141.6, 140.5, 138.1, 137.6, 136.0, 135.5, 132.8, 132.4, 132.1, 131.1, 131.0, 130.3, 129.9, 129.8, 128.8, 128.7, 126.7, 126.5, 126.3, 126.6, 124.1, 102.0, 76.6, 62.4, 33.0, 26.1, 20.3 ppm. MS (FAB) calculated for $C_{46}H_{36}Cl_3N_6ORh$ 896.1, calculated for $C_{46}H_{34}N_6ORh$ (M - 3Cl^- - 2H^+) 789.1, found 789.5.

5.2.4. Synthesis of metallointercalator-peptide conjugates. Peptide conjugates of $[Rh(phi)_2(phen')]^{3+}$ were synthesized using the procedure given in Chapter 4 for the synthesis of [Rh]-E10. Peptide conjugates of $[Rh(phi)_2(ethynylphen')]^{3+}$ were synthesized as follows: the resin-bound peptide (30 μmol, 1.0 equiv) was deprotected as described for the synthesis of peptide conjugates of $[Rh(phi)_2(phen')]^{3+}$, and dried *in vacuo*. The resin-bound peptide was suspended in 2 mL of a 50 mg/mL solution of CDI in 1,4-dioxane. The resulting slurry was stirred at 23 °C for 30 min. The resin-bound peptide was isolated by filtration, washed with 1,4-dioxane, and dried *in vacuo*. The resin-bound peptide was suspended in 1 mL DMF and 54 mg (60 μmol, 2.0 equiv) of $[Rh(phi)_2(ethynylphen')]Cl_3$, 1.0 μL (5.7 μmol, 0.2 equiv) DIEA and 0.2 mg (1.63 μmol, 0.05 equiv) 4-DMAP were added. The resulting slurry was stirred at 23 °C for 48 h with protection from light. The resin-bound peptide was isolated by filtration and successively washed with NMP, DMF, CH_2Cl_2, 1:1 CH_2Cl_2–MeOH, and EtOH. The resin-bound peptide was dried *in vacuo*. The metallointercalator-peptide conjugate was cleaved from the resin and the remaining protecting groups were removed by treatment with anhydrous HF

following standard protocols.[13,14] Peptide conjugates of $[Rh(phi)_2(ethynylphen')]^{3+}$ were purified by HPLC using a linear gradient of 15%→40% 0.1% TFA in MeCN in 0.1% aqueous TFA over 19 min followed by isocratic elution at 40% 0.1% TFA in MeCN in 0.1% aqueous TFA, at a flow rate of 4.5 mL/min.

5.2.5. Characterization of metallointercalator-peptide conjugates. Peptide conjugates of $[Rh(phi)_2(phen')]^{3+}$ were characterized by MALDI-TOF mass spectroscopy. Molecular ion peaks observed and calculated (in parentheses) for are as follows: [Rh]-E6, 2074.5 (2074.1); [Rh]-E7, 2117.4 (2117.2); [Rh]-E8, 2119.9 (2116.2); [Rh]-E12, 2189.3 (2187.3); [Rh]-E13, 2259.3 (2260.3); [Rh]-E6E10, 2132.9 (2132.1); [Rh]-R6A10, 2102.1 (2101.2); [Rh]-R6E10, 2160.7 (2159.2). Peptide conjugates of $[Rh(phi)_2(ethynylphen')]^{3+}$ fragmented upon both matrix assisted laser desorption and electrospray ionization. Therefore, these conjugates were characterized by UV-visible spectroscopy and comparison of HPLC retention times with the HPLC retention times of the free peptides to confirm the covalent linkage between the metal complex and the peptide.

5.2.6. Photocleavage of DNA restriction fragments. Plasmid pUC18 was digested with *EcoRI* restriction endonuclease, treated with calf intestinal alkaline phosphatase, and 5'-endlabeled with T4 polynucleotide kinase and [γ-^{32}P]-ATP. Alternatively, following digestion with *EcoRI* restriction endonuclease, the plasmid was 3'-endlabeled by treatment with the Klenow fragment of DNA polymerase I and [α-^{32}P]-ATP, dCTP, dGTP, and dTTP. Following 3'- or 5'-endlabeling, the DNA was digested with *PvuII* restriction endonuclease, yielding labeled fragments of 180 and 140 base pairs. The 180 base pair fragment was isolated by 6% nondenaturing polyacrylamide gel electrophoresis followed by electroelution.[15]

Photocleavage reactions were performed in 20 μL total volume contained in 1.7 mL presiliconized Eppendorf tubes. The reaction mixtures contained ~100,000 cpm labeled restriction fragment, 15 μM base pairs sonicated calf thymus DNA, 1 μM metallointercalator, 5 mM $MnCl_2$, and 50 mM pH 7.0 sodium cacodylate buffer. The reaction mixtures were incubated at 55 °C for 5 min and irradiated with 313 nm light at 55 °C for 10 min. Control reactions lacking metallointercalator were irradiated under identical conditions. Following irradiation 50 μL 7.5 M aqueous NH_4OAc and 200 μL EtOH were added. The DNA was isolated by precipitation and washed with cold 80% aqueous EtOH. The precipitated DNA was dried and resuspended in 5 μL 80% formamide sequencing loading buffer. Approximately 20,000 cpm of each sample, and Maxam-Gilbert A+T and C+G sequencing reactions[16] were loaded on a 6% denaturing polyacrylamide gel and electrophoresed at 1200 V for 2.5 h. The gel was transferred to paper and dried prior to autoradiography.

5.2.7. Photocleavage of oligonucleotides. Single stranded and hairpin oligonucleotides were 5'-endlabeled using T4 polynucleotide kinase and [γ-^{32}P]-ATP. Single stranded oligonucleotides were hybridized by annealing using a 10-fold excess of the complementary strand. The labeled duplex was purified by 20% nondenaturing polyacrylamide gel electrophoresis and isolated from the gel by the crush and soak method.[27]

Photocleavage reactions were performed in 20 μL total volume contained in 1.7 mL presiliconized Eppendorf tubes. Reaction samples contained ~100,000 cpm labeled oligonucleotide, unlabeled oligonucleotide and metallointercalator at the indicated concentrations, 5 mM $MnCl_2$, and 50 mM pH 7.0 sodium cacodylate buffer. The reaction mixtures were incubated at 55 °C for 5 min and irradiated with 313 nm light at 55 °C for 10 min. Control reactions lacking metallointercalator were irradiated under identical

conditions. Following irradiation 50 μL 7.5 M aqueous NH_4OAc and 200 μL EtOH were added. The DNA was isolated by precipitation and washed with cold 80% aqueous EtOH. The precipitated DNA was dried and resuspended in 5 μL 80% formamide sequencing loading buffer. Approximately 20,000 cpm of each sample, and Maxam-Gilbert A+T and C+G sequencing reactions,[28] were loaded on a 20% denaturing polyacrylamide gel and electrophoresed at 1200 V for 2.5 h. The gel was transferred to film prior to autoradiography.

5.3. Results

5.3.1. Synthesis and characterization of metallointercalators. The metallointercalators $[Rh(phi)_2(phen')]^{3+}$ and $[Rh(phi)_2(ethynylphen')]^{3+}$ were synthesized from the known complex $[Rh(phi)_2Cl_2]Cl$,[23] prepared from $RhCl_3 \cdot xH_2O$ and 9,10-

Scheme 5.1. Synthesis of alkynylphenanthroline-based metallointercalator.

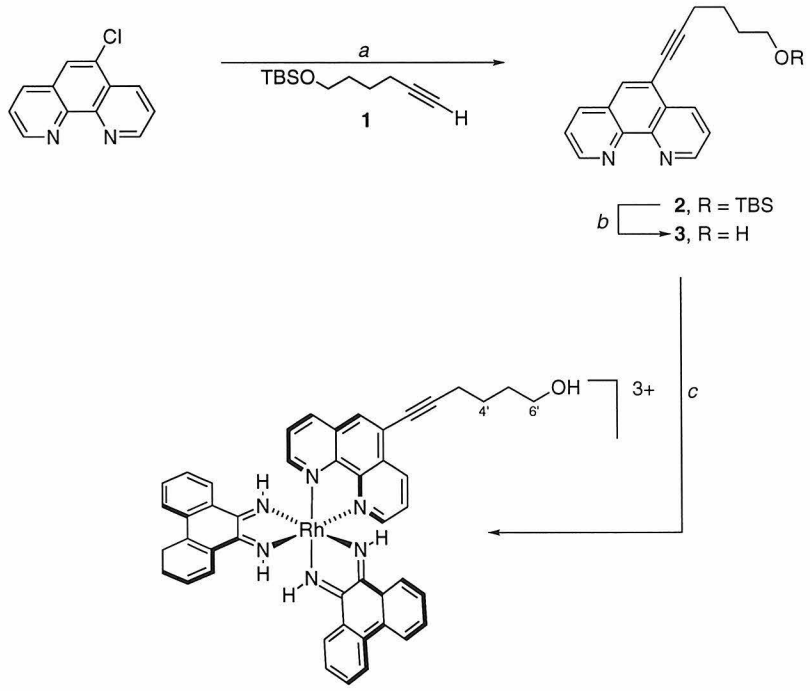

(a) CuI, $Pd(PPh_3)_2Cl_2$, DIEA, THF, 65 °C, 48 h (90%). (b) TBAF, THF, 23 °C, 30 min (55%). (c) $[Rh(phi)_2Cl_2]Cl$, AgOTf, DMF, 65 °C, 16 h, then **3**, 65 °C, 16 h (97%).

diaminophenanthrene in one step. Phen' and $[Rh(phi)_2(phen')]^{3+}$ were synthesized as described.[22] Ethynylphen' was prepared by palladium-catalyzed coupling of 5-chloro-1,10-phenanthroline with the copper acetylide of from **1**.[17] $[Rh(phi)_2(ethynylphen')]^{3+}$ was synthesized using the protocol for the preparation of $[Rh(phi)_2(phen')]^{3+}$. Treatment of $[Rh(phi)_2Cl_2]Cl$ with silver triflate in DMF, followed by reaction of the resulting solvent complex with alkynylphenanthroline **3**, afforded $[Rh(phi)_2(ethynylphen')]^{3+}$ (Scheme 5.1). Both $[Rh(phi)_2(phen')]^{3+}$ and $[Rh(phi)_2(ethynylphen')]^{3+}$ were purified by cation-exchange chromatography followed by reverse phase silica gel chromatography.

Although the UV-visible absorption spectra of $[Rh(phi)_2(phen')]^{3+}$ and $[Rh(phi)_2(ethynylphen')]^{3+}$ are similar, an additional transition between 320 and 330 nm causes the isosbestic points of $[Rh(phi)_2(phen')]^{3+}$ at 220, 280, 312 and 349 nm to be lost (Figure 5.1). Accordingly, solutions of $[Rh(phi)_2(ethynylphen')]^{3+}$ and peptide conjugates of $[Rh(phi)_2(ethynylphen')]^{3+}$ were quantitated by UV-visible spectroscopy using the isosbestic point at 422 nm. A value for ε_{422} of 11,300 $M^{-1}cm^{-1}$ was obtained from the UV-visible spectrum of $[Rh(phi)_2(phen')]^{3+}$ by comparison of the absorbance at 350 nm and 422 nm. As with other *bis*-phenanthrenequinone diimine complexes of rhodium(III), the optical spectrum of $[Rh(phi)_2(ethynylphen')]^{3+}$ shows a marked pH dependence. Titration of $[Rh(phi)_2(ethynylphen')]^{3+}$ from pH 3.0 to pH 9.0 results in a loss of intensity of 49% and a blue shift of 30 nm of the phi-centered transition between 352 and 382 nm. Plotting λ_{max} as a function of pH for the same transition yields a pK_a for $[Rh(phi)_2(ethynylphen')]^{3+}$

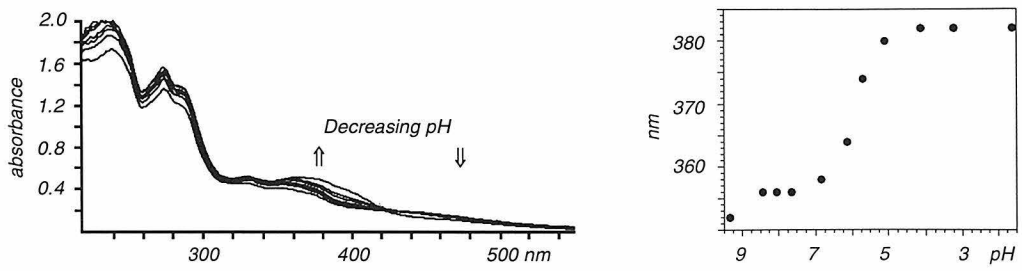

Figure 5.1. Absorbance spectrum of $[Rh(phi)_2(ethynylphen')]^{3+}$ as a function of pH.

of approximately 6.4 (Figure 5.1). In comparison, the pK_a of $[Rh(phi)_2(phen')]^{3+}$ is 6.4 and the phi-centered transition suffers a loss of intensity of 30% with a 29 nm blue shift,[26] while the pK_a of $[Rh(phi)_2(bpy')]^{3+}$ is 6.8-6.9 and the phi-centered transition suffers a loss of intensity of 34% with a 30 nm blue shift.[18]

5.3.2. Synthesis and characterization of metallointercalator-peptide conjugates. Peptide conjugates of $[Rh(phi)_2(phen')]^{3+}$ were synthesized as described by Sardesai *et al.* (Scheme 5.2).[22] Because of the instability of $[Rh(phi)_2(phen')]^{3+}$ and $[Rh(phi)_2(ethynylphen')]^{3+}$ to aqueous base, the formyl protecting group was removed from the tryptophan residue before coupling. Following coupling, the acid-labile

Scheme 5.2. Synthesis of peptide conjugates of $[Rh(phi)_2(phen')]^{3+}$.

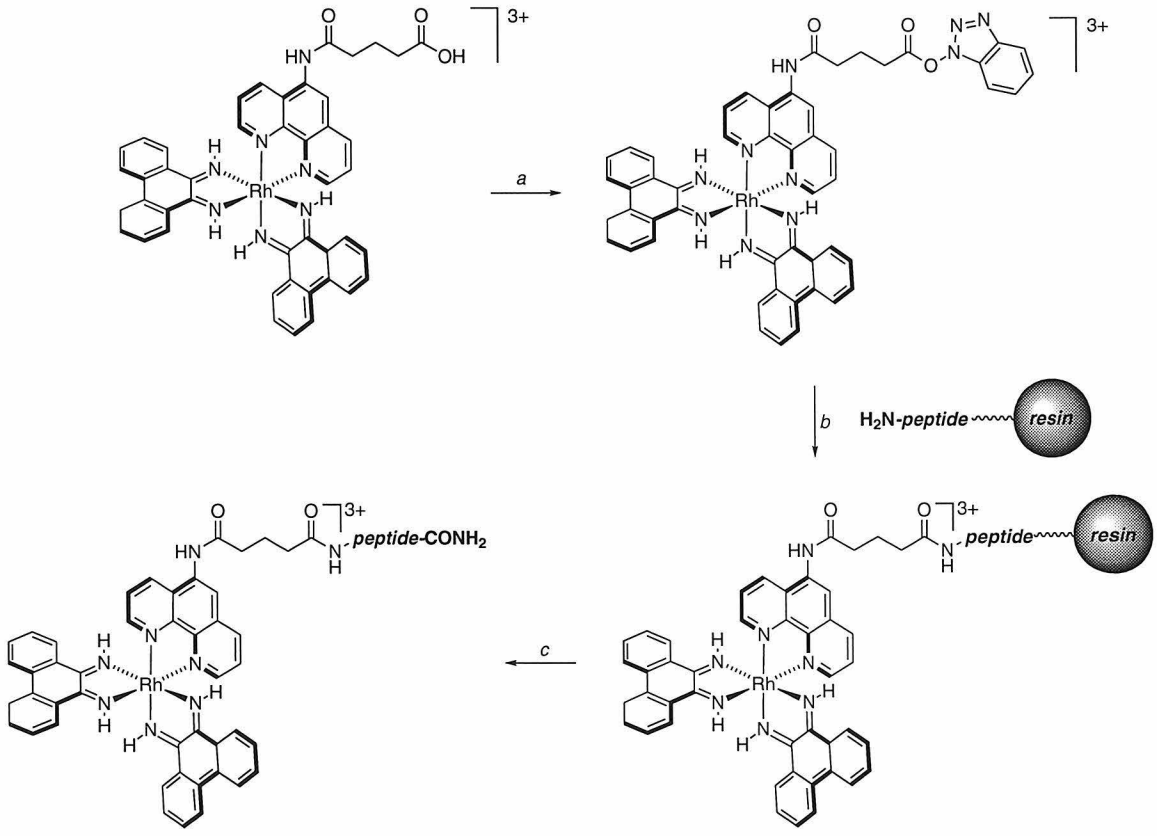

(a) DCC, HOBT, NMP, 23 °C, 15 min. (b) resin-bound peptide, 23 °C, 48 h. (c) anhydrous HF deprotection (2-5%).

Table 5.2. Peptide conjugates of $[Rh(phi)_2(phen')]^{3+}$ synthesized.

Conjugate	Peptide Sequence	Conjugate	Peptide Sequence
[Rh]-E6	AANVAEAAWARAA-$CONH_2$	[Rh]-E13	AANVAIAAWARAEAA-$CONH_2$
[Rh]-E7	AANVAIEAWARAA-$CONH_2$	[Rh]-E6E10	AANVAEAAWERAA-$CONH_2$
[Rh]-E8	AANVAIAEWARAA-$CONH_2$	[Rh]-R6A10	AANVARAAWARAA-$CONH_2$
[Rh]-E10	AANVAIAAWERAA-$CONH_2$	[Rh]-R6E10	AANVARAAWERAA-$CONH_2$
[Rh]-E12	AANVAIAAWAREAA-$CONH_2$	[Rh]-A6A10	AANVAIAAWARAA-$CONH_2$

protecting groups were removed and the peptide was cleaved from the resin with anhydrous HF.[16,17] Purification by HPLC afforded the conjugates in 2-5% yield as determined by UV-visible spectroscopy, based on 100% yield for the synthesis of the resin-bound peptide (Table 5.2). Chromatographic separation of the diastereomeric Δ- and Λ-metallointercalator-peptide conjugates was not observed.

Peptide conjugates of $[Rh(phi)_2(ethynylphen')]^{3+}$ were synthesized similarly (Scheme 5.3). Treatment of $[Rh(phi)_2(ethynylphen')]^{3+}$ with carbonyldiimidazole in anhydrous dioxane, as described by Hall *et al.* for the synthesis of metallointercalator-DNA conjugates,[19] afforded activated rhodium complex **4**. Prolonged stirring of resin-bound peptides with **4** in DMF, in the presence of catalytic 4-DMAP and diisopropylethylamine, removal of acid-labile protecting groups and cleavage of the peptide from the resin with anhydrous HF afforded peptide conjugates of $[Rh(phi)_2(ethynylphen')]^{3+}$. Following HPLC purification, the conjugates were obtained in 2-3% yield as determined by UV-visible spectroscopy, based on 100% yield for the synthesis of the resin-bound peptide (Table 5.3). Chromatographic separation of the diastereomeric Δ- and Λ-metallointercalator-peptide conjugates was not observed.

Table 5.3. Peptide conjugates of $[Rh(phi)_2(ethynylphen')]^{3+}$ synthesized.

Conjugate	Peptide Sequence
[Rhy]-E6	AANVAEAAWARAA-$CONH_2$
[Rhy]-E10	AANVAIAAWERAA-$CONH_2$

Scheme 5.3. Synthesis of peptide conjugates of $[Rh(phi)_2(ethynylphen')]^{3+}$.

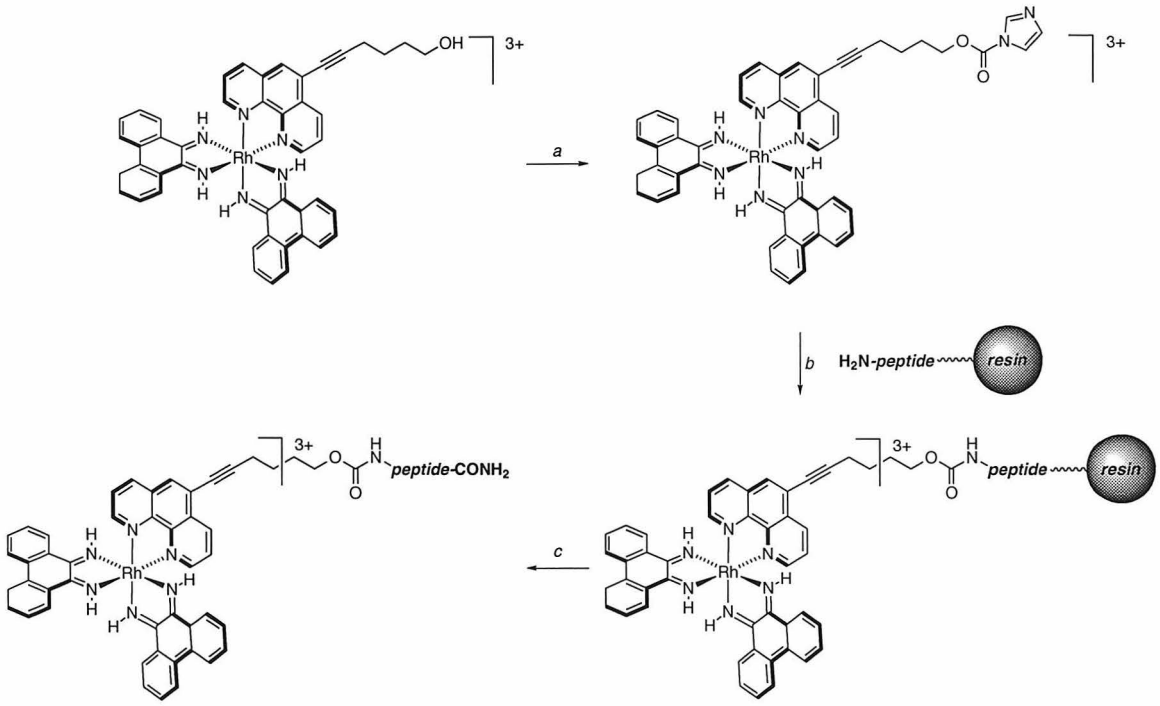

(a) carbonyldiimidazole, 1,4-dioxane, 23 °C, 30 min. (b) resin-bound peptide, DIEA, 4-DMAP, DMF, 23 °C, 48 h. (c) anhydrous HF deprotection (2-3%).

As Sardesai *et al.* have described, the UV-visible spectra of peptide conjugates of $[Rh(phi)_2(phen')]^{3+}$ and $[Rh(phi)_2(ethynylphen')]^{3+}$ are composites of the spectra of the parent rhodium complexes and the peptides alone (Figure 5.2).[20] Peptide conjugates of

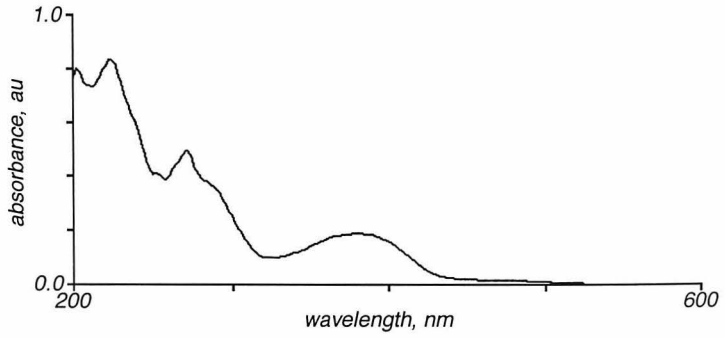

Figure 5.2. UV-visible spectrum of a representative peptide conjugate of $[Rh(phi)_2(phen')]^{3+}$ ([Rh]-R6E10, 10 μM in H_2O, not buffered, pH ~5.0).

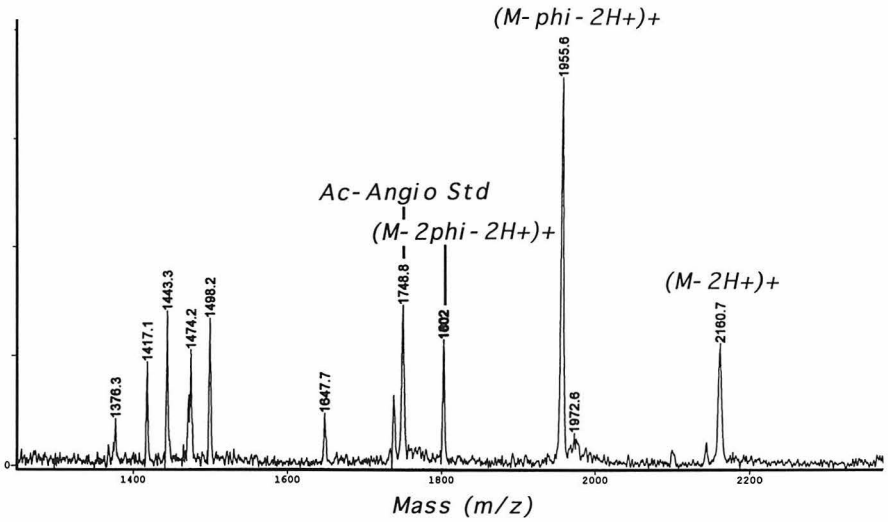

Figure 5.3. MALDI-TOF mass spectrum of a representative metallointercalator-peptide conjugate ([Rh]-R6E10).

$[Rh(phi)_2(phen')]^{3+}$ were also characterized by MALDI-TOF mass spectroscopy. The expected molecular ion peaks, as well as peaks derived from the loss of 1 and 2 phi ligands, were observed in all cases (Figure 5.3). In contrast, peptide conjugates of $[Rh(phi)_2(ethynylphen')]^{3+}$ fragmented upon both laser desorption ionization and electrospray ionization, affording ion peaks with *m/z* ratios consistent with the mass of the appended peptides. Therefore, peptide conjugates of $[Rh(phi)_2(ethynylphen')]^{3+}$ were characterized by UV-visible spectroscopy (Figure 5.4). Comparison of the HPLC retention times[21] of $[Rh(phi)_2(ethynylphen')]^{3+}$ (17.9 min) and the free E6 (13.7 min) and E10 (15.2 min) peptides with [Rhy]-E6 (20.5) and [Rhy]-E10 (21.6 min) supported the assignments for the coupled products. For comparison, the HPLC retention times of [Rh] and [Rh]-E10 are 15.1 min and 18.5 min under the same conditions, respectively.

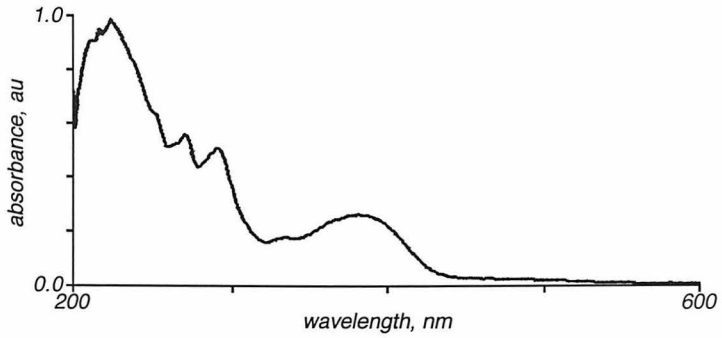

Figure 5.4. UV-visible spectrum of a representative peptide conjugate of $[Rh(phi)_2(ethynylphen')]^{3+}$ ([Rhy]-E10, 10 μM in H_2O, not buffered, pH ~5.0).

5.3.3. Site-selectivity of DNA photocleavage on restriction fragments by metallointercalator-peptide conjugates derived from [Rh]-E10 by varying the position of the critical glutamate. Previous work had indicated that the E10 peptide, and in particular Glu^{10}, is an essential determinant of the 5'-CCA-3' sequence selectivity of [Rh]-E10 and related metallointercalator-peptide conjugates.[9b] Systematic mutation of amino acid residues other than Glu^{10} did not alter the sequence selectivity of the parent metallointercalator-peptide conjugate. Instead, diminished specificity was observed with mutations that reduced the helical content of the peptide, while mutation of Glu^{10} to alanine or aspartate abolished specificity. We sought to develop a family of metallointercalator-peptide conjugates based on [Rh]-E10 that exhibited a variety of sequence preferences. Accordingly, our initial search focused on peptides in which the position of the essential glutamate was varied relative to the other amino acid residues. The family of metallointercalator-peptide conjugates constructed using this approach includes [Rh]-E6 (I6E, E10A), [Rh]-E7 (A7E, E10A), [Rh]-E8 (A8E, E10A), [Rh]-E12 (A12E, A14), and [Rh]-E13 (A13E, A14, A15).[22]

The new metallointercalator-peptide conjugates were screened for sequence-selective DNA photocleavage using the *EcoRI/PvuII* 180-mer restriction fragment of pUC18 (Figure 5.5). Photocleavage reactions were conducted at 55 °C in the presence of

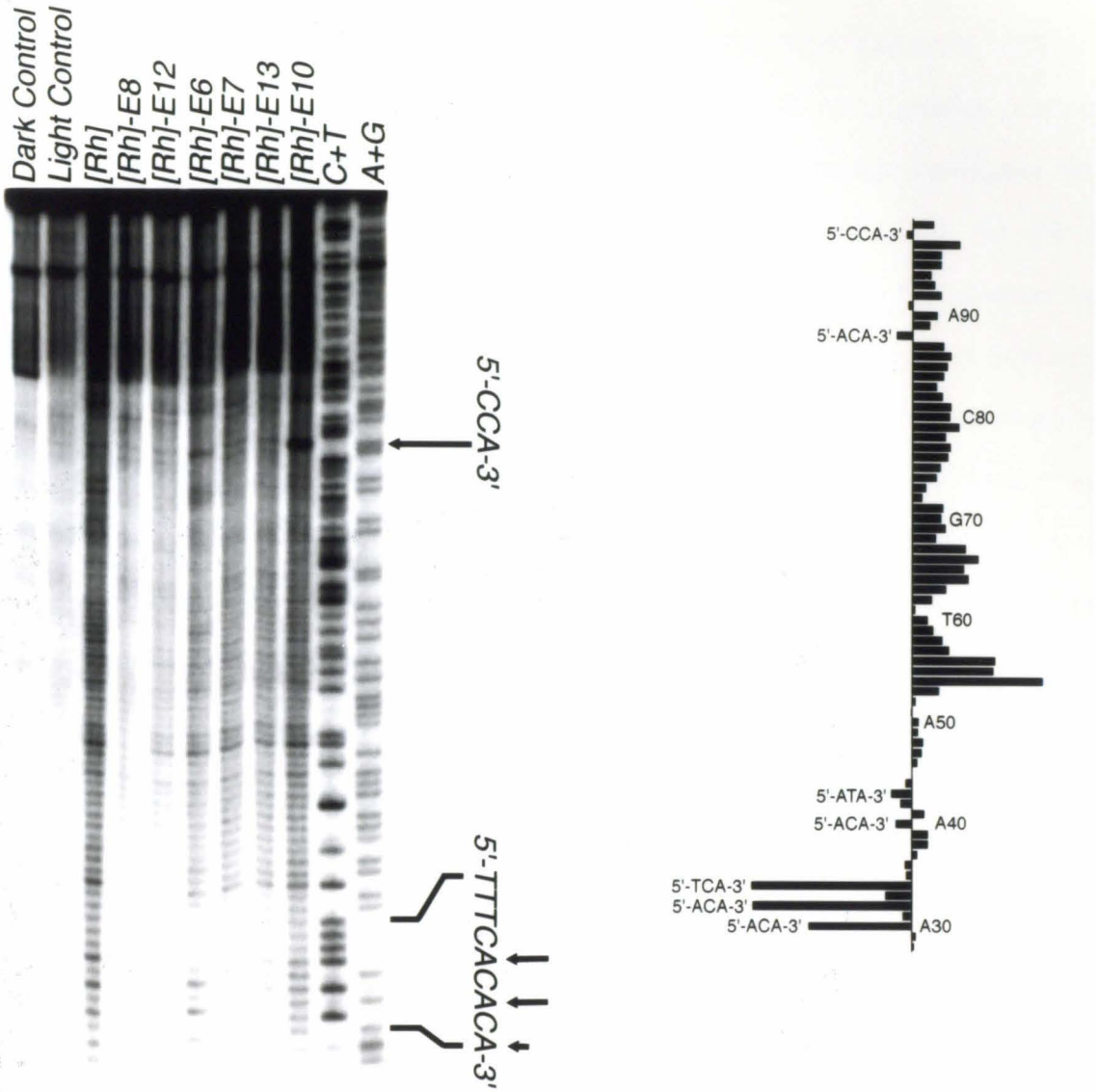

Figure 5.5. Photocleavage of pUC18 3'-endlabeled *Eco*RI/*Pvu*II 180-mer by first-generation metallointercalator-peptide conjugates at 55 °C in the presence of 5 mM $MnCl_2$. [Rh]-E10 cleaves at 5'-CCA-3' site. [Rh]-E6 cleaves at 5'-TTTC**ACACA**-3' site indicated. Small enhancements in cleavage by [Rh]-E6 are observed at other 5'-ACA-3' sites. Histogram indicates difference in cleavage between [Rh]-E6 and [Rh].

5 mM $MnCl_2$. These conditions result in optimal affinity and specificity of [Rh]-E10 for its target site.[23] New specificity was observed with [Rh]-E6. Conversely, [Rh]-E7, [Rh]-E8, [Rh]-E12, and [Rh]-E13 did not afford cleavage patterns that were discernibly different from that of $[Rh(phi)_2(phen')]^{3+}$. This result is consistent with the correlation between helical content and specificity observed with metallointercalator-peptide conjugates that target 5'-CCA-3'. Based on the model for DNA recognition by [Rh]-E10, the critical glutamate residue of [Rh]-E6 is located on the face of a putative α-helix that contacts the DNA. Conversely, in [Rh]-E7, [Rh]-E8, [Rh]-E12, and [Rh]-E13, the critical glutamate residue is not poised to make base-specific contacts with the DNA target. Cleavage by [Rh]-E6 on the 3'-endlabeled strand is more pronounced at the three adenosine bases of the sequence 5'-T^{38}TTC**ACACA**-3',[24] whereas cleavage by $[Rh(phi)_2(phen')]^{3+}$ is more pronounced at the cytosines. Similarly, on the 5'-endlabeled strand, enhanced cleavage by [Rh]-E6 is observed at A^{62}, A^{64}, and A^{67} of the sequence 5'-C^{58}CA**CACA**A**CA**TAC^{70}-3'. As with the parent conjugate, enhanced cleavage is not observed under the experimental conditions on the complementary strand. Significantly, enhanced cleavage by [Rh]-E6 is not observed at other 5'-pur-pyr-pur-3' sequences. Thus, the consensus sequence that emerges from analysis of the cleavage patterns observed with the *EcoRI/PvuII* 180-mer restriction fragment of pUC18 is 5'-ACA-3'.

5.3.4. Photocleavage of oligonucleotides by metallointercalator-peptide conjugates derived from [Rh]-E10 by varying the position of the critical glutamate. To demonstrate that the preferred binding site of [Rh]-E6 is 5'-ACA-3', photocleavage of a 31-mer oligonucleotide containing all four possible 5'-NCA-3' sequences separated by 5'-CGAG-3' spacers by [Rh]-E6 was investigated.[25] Concentrations of metallointercalator-peptide conjugate and unlabeled oligonucleotide ranged from 10^{-9} M to 10^{-5} M. At concentrations above the bulk intercalative dissociation

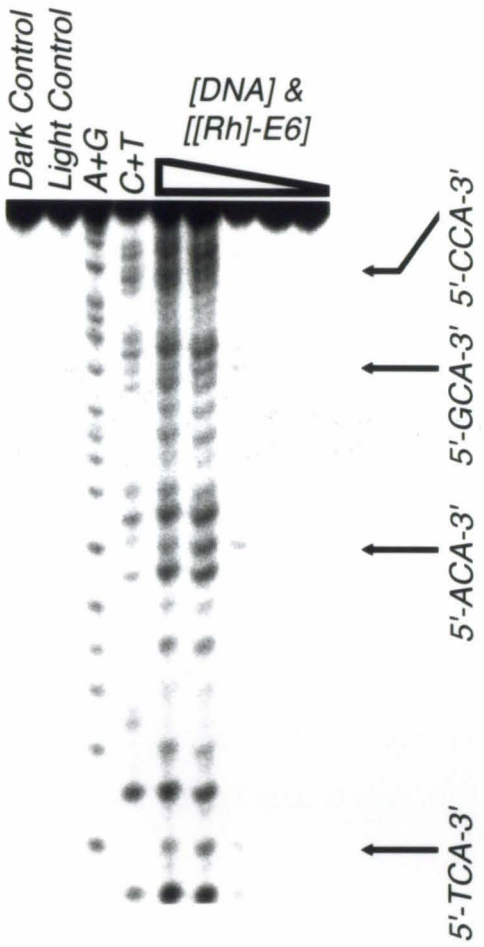

Figure 5.6. Photocleavage of a 31-mer oligonucleotide containing all four 5'-NCA-3' sites by [Rh]-E6 as a function of concentration. Concentration of [Rh]-E6 ranged from 10^{-5} M to 10^{-9} M, with a constant metallointercalator-unlabeled DNA oligonucleotide ratio of 1:1. Photocleavage reactions were conducted at 55 °C in the presence of 5 mM $MnCl_2$.

$$F_c = \frac{\gamma \bullet \left([DNA]_t + [L]_t + K_d - \left(\left([DNA]_t + [L]_t + K_d \right)^2 - 4 \bullet [DNA]_t \bullet [L]_t \right)^{1/2} \right)}{2 \bullet [DNA]_t} \quad (5.1)$$

constant of $[Rh(phi)_2(phen')]^{3+}$, there is little discernible difference in photocleavage intensity between the various recognition sites. However, at 10^{-7} M in metallointercalator-peptide conjugate and unlabeled oligonucleotide, photocleavage is most intense at the 5'-ACA-3' site, and weak photocleavage is observed at the 5'-TCA-3' site (Figure 5.6). Quantitation of the photocleavage intensities at the 3'-terminal adenine of the four 5'-NCA-3' sequences suggests that [Rh]-E6 binds approximately 1.5-fold more tightly to 5'-ACA-3' than to the other 5'-NCA-3' sites,[26] corresponding to an energy difference of approximately 0.3 kcal•mol^{-1}. For comparison, little difference in the photocleavage intensity at the four 5'-NCA-3' sequences is observed with $[Rh(phi)_2(phen')]^{3+}$. Under these conditions, [Rh]-E10 cleaves strongly at the 5'-CCA-3' site. Photocleavage by [Rh]-E10 is slightly stronger than photocleavage by $[Rh(phi)_2(phen')]^{3+}$ at the 5'-GCA-3' site. There is no discernible difference in photocleavage intensity by [Rh]-E10 and $[Rh(phi)_2(phen')]^{3+}$ at the 5'-ACA-3' and 5'-TCA-3' sites.

The thermodynamic dissociation constant of [Rh]-E6 for a 5'-ACA-3' site in a 29-mer hairpin oligonucleotide was measured by photocleavage titration.[27] The concentration of the metallointercalator-peptide conjugate ranged from 7.2 x 10^{-6} M to 7.2 x 10^{-11} M, with a constant metallointercalator–unlabeled hairpin oligonucleotide ratio of 1:3. The sequence of the hairpin oligonucleotide was 5'-AGAG**ACA**CGAGATTTTTTCTCGTGTCTCT-3' (K_3-29). An autoradiogram of a representative photocleavage titration is shown in Figure 5.7. A composite cleavage isotherm from several trials was fit to Equation 5.1,[28] yielding a dissociation constant of 9.9 x 10^{-8} M (Figure 5.8). Since the bulk intercalative dissociation constant of $[Rh(phi)_2(phen')]^{3+}$ is 7.0 x 10^{-7} M, at 55 °C, in the presence of 5 mM $MnCl_2$, the E6 peptide provides 7.1-fold tighter binding to the target sequence, corresponding to a

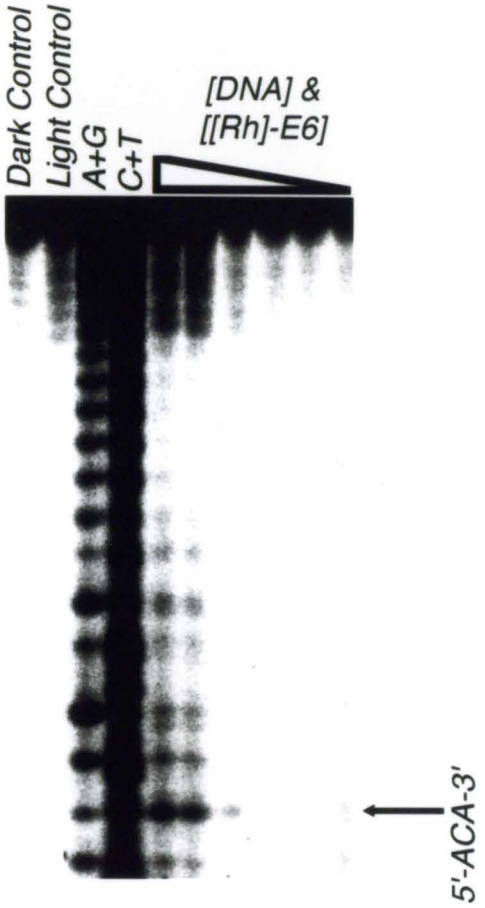

Figure 5.7. Dissociation constant determination for [Rh]-E6. Photocleavage reactions were conducted at 55 °C in the presence of 5 mM $MnCl_2$. The concentration of the metallointercalator-peptide conjugate in this experiment ranged from 1 x 10^{-6} M to 3.3 x 10^{-9} M, with a constant metallointercalator–unlabeled hairpin oligonucleotide ratio of 1:3.

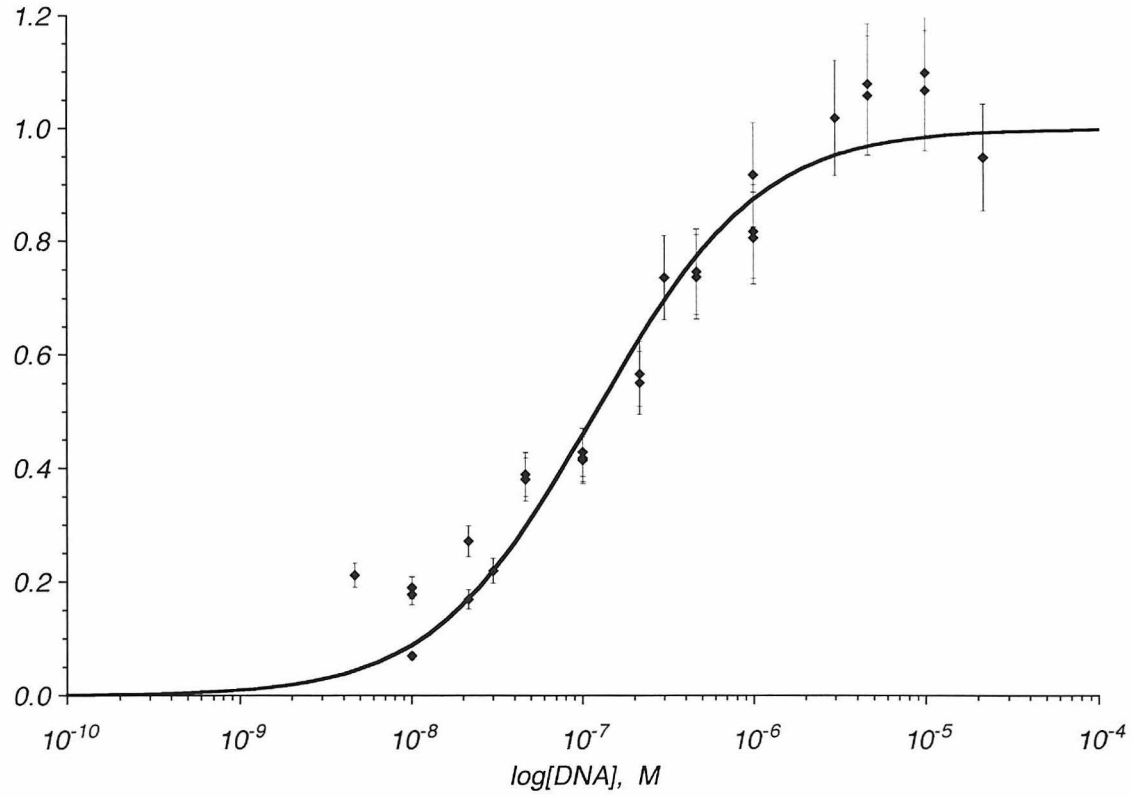

Figure 5.8. Photocleavage isotherm for [Rh]-E6 (K_d = 9.9 x 10^{-8} M). Conditions: 3:1 ratio of hairpin oligonucleotide–metallointercalator-peptide conjugate, 5 mM $MnCl_2$, 50 mM sodium cacodylate buffer pH 7.0, 55 °C.

free energy difference of 1.3 kcal•mol^{-1}. For comparison, the E10 peptide confers 13-fold tighter binding to its target sequence (5'-CCA-3') under these conditions, corresponding to an energy difference of 1.7 kcal•mol^{-1}.

5.3.5. DNA photocleavage by metallointercalator-peptide conjugates containing further amino acid sequence changes at positions 6 and 10. Photocleavage results with metallointercalator-peptide conjugates derived from [Rh]-E10 by varying the position of the critical glutamate suggest that the amino acids at positions 6 and 10 of these metallointercalator-peptide conjugates make contacts with the DNA that are

essential for sequence-selectivity. Therefore, further amino acid changes were restricted to these positions. Base-specific contacts between the arginine side chain and thymine and guanine nucleotides are common in crystal structures of transcription factor–operator complexes. Moreover, the positive charge associated with the guanidinium group of arginine was expected to increase the overall affinity of the metallointercalator-peptide conjugates for DNA. Accordingly, in addition to exploring the sequence-selectivity that could be achieved with various combinations of alanine, glutamate, and isoleucine at positions 6 and 10, the effects of arginine substitutions at position 6 were investigated. A second family of metallointercalator-peptide conjugates was synthesized; this family included [Rh]-E6E10 (I6E), [Rh]-I6A10 (E10A), [Rh]-R6E10 (I6R), and [Rh]-R6A10 (I6R, E10A), as well as conjugates of $[Rh(phi)_2(ethynylphen')]^{3+}$ with the E6 and E10 peptides, which were prepared to examine the consequences of increasing the conformational rigidity of the aliphatic linker.[21]

This family of metallointercalator-peptide conjugates was screened for sequence-selective DNA photocleavage using the *EcoRI/PvuII* 180-mer restriction fragment of pUC18 (Figure 5.9). As before, screening was conducted at 55 °C in the presence of 5 mM $MnCl_2$. Enhanced cleavage by [Rh]-R6A10 was observed at a number of sites on both the 5'-endlabeled and 3'-endlabeled restriction fragments. However, none of the other metallointercalator-peptide conjugates afforded cleavage patterns that were discernibly different from that of $[Rh(phi)_2(phen')]^{3+}$. Interestingly, the E6 and E10 peptides, which conferred sequence selectivity on $[Rh(phi)_2(phen')]^{3+}$, did not afford sequence-selective cleavage when appended to $[Rh(phi)_2(ethynylphen')]^{3+}$. There is no discernible difference in the photocleavage patterns of $[Rh(phi)_2(phen')]^{3+}$ and $[Rh(phi)_2(ethynylphen')]^{3+}$; consequently, it is unlikely that a change in the interaction of the metallointercalator with DNA is responsible for the observed lack of sequence selectivity.

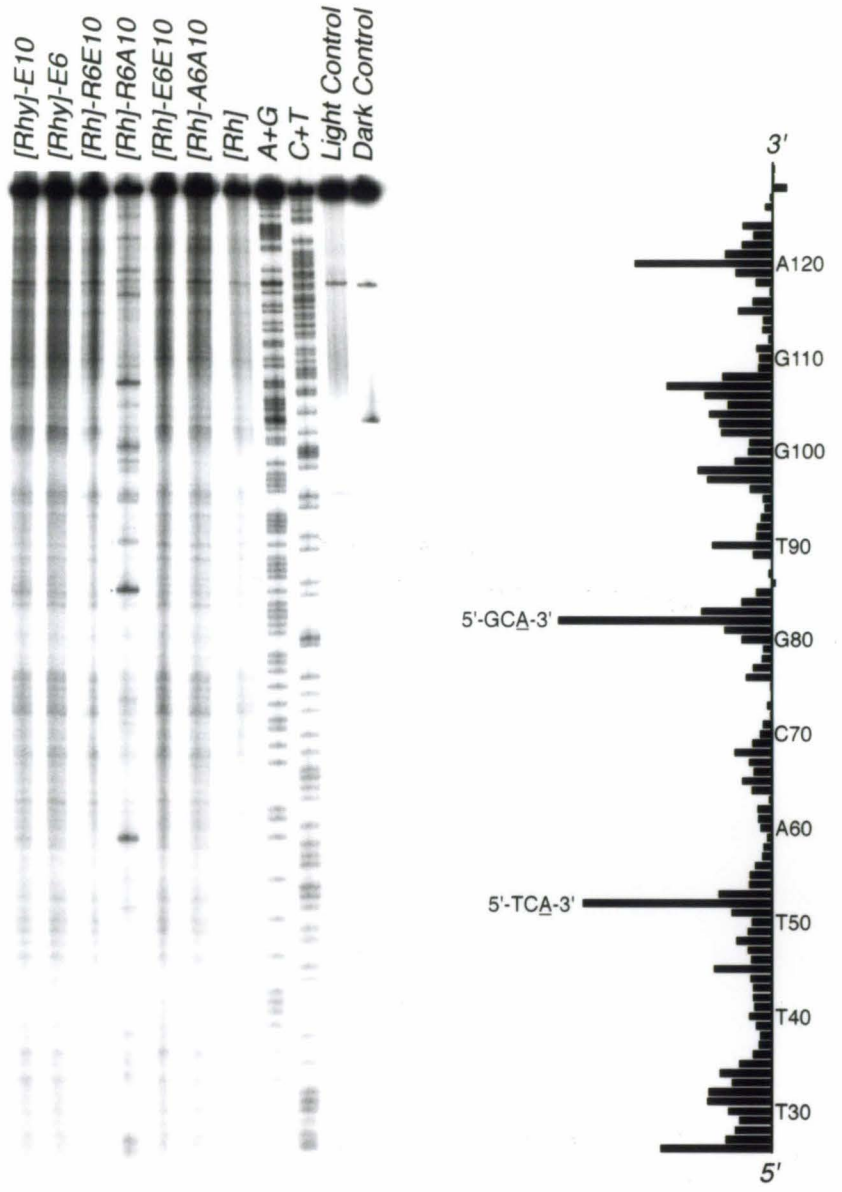

Figure 5.9. Photocleavage of pUC18 5'-endlabeled *Eco*RI/*Pvu*II 180-mer by second-generation metallointercalator-peptide conjugates at 55 °C in the presence of 5 mM $MnCl_2$. Histogram represents difference in cleavage by [Rh]-R6A10 and cleavage by [Rh] at each base. Cleavage site is underlined.

Photocleavage by [Rh]-R6A10 was more pronounced than photocleavage by $[Rh(phi)_2(phen')]^{3+}$ at several positions along both strands of the pUC18 180-mer. A three-base-pair consensus sequence does not emerge, yet new specificity, distinct from that observed with [Rh]-E6 and [Rh]-E10, is apparent. Comparison of the nucleotide sequences that flank positions where enhanced photocleavage is observed with [Rh]-R6A10 suggests a sequence preference for [Rh]-R6A10 (Table 5.4). Two three-base-pair recognition sequences, 5'-GCA-3' and 5'-TCA-3', afford the most intense photocleavage and match at least two of three sequential nucleotides flanking the cleavage site for all of the sequences where enhanced photocleavage is observed.[29] Unlike [Rh]-E6 and [Rh]-E10, photocleavage does not always occur with 5'-asymmetry.

5.3.6. Photocleavage of oligonucleotides by [Rh]-E6E10.

Photocleavage of the *EcoRI/PvuII* 180-mer restriction fragment of pUC18 by [Rh]-E6E10 is not discernably different from photocleavage by $[Rh(phi)_2(phen')]^{3+}$. However, the sequence selectivity observed with [Rh]-E6 and [Rh]-E10 suggests that each of the glutamate residues of [Rh]-E6 is capable of making specific contacts with the cytosine bases in a 5'-CCA-3' recognition site. Accordingly, photocleavage of a 31-mer oligonucleotide containing all four possible 5'-NCA-3' sequences separated by 5'-CGAG-3' spacers by [Rh]-E6E10 was investigated. In the absence of Mn^{2+}, [Rh]-E6E10 cleaved at the 5'-CC**A**-3' site with a similar intensity as [Rh]-E10, while sequence-selective cleavage by [Rh]-E6 and [Rh]-R6A10 was not observed (Figure 5.10). Interestingly, in the absence of Mn^{2+}, cleavage by both [Rh]-E10 and [Rh]-E6E10 was seen at the adenine of the 5'-GC**A**-3' site.

Table 5.4. Nucleotide sequences from the *EcoRI/PvuII* 180-mer restriction fragment of pUC18 that show enhanced photocleavage by [Rh]-R6A10.

Sequence	Strand and Position	Relative Intensity[a]	Sequence	Strand and Position	Relative Intensity[a]
5'-TGT**T**TCC-3'	5', T26	52	5'-GCC**T**AAT-3'	5', T106	31
3'-ACAAAGG-5'			3'-CGGATTA-5'		
5'-CTG**T**GTG-3'	5', T32	29	5'-GAG**T**GAG-3'	5', T113	5
3'-GACACAC-5'			3'-CTCACTC-5'		
5'-GTG**T**GAA-3'	5', T34	24	5'-CTA**A**CTC-3'	5', A120	64
3'-CACACTT-5'			3'-GATTGAG-5'		
5'-TTA**T**CCG-3'	5', T45	27	5'-CTC**A**CTG-3'	5', A144	27
3'-AATAGGC-3'			3'-GAGTGAC-5'		
5'-CTC**A**CAA-3'	5', A52	**88**	5'-CGC**T**TTC-3'	5', T153	nq
3'-GAGTGTT-5'			3'-GCGAAAG-5'		
5'-ACA**T**ACG-3'	5', T68	17	5'-GTC**G**GGA-3'	5', G162	nq
3'-TGTATGC-5'			3'-CAGCCCT-5'		
5'-AGC**A**TAA-3'	5', A82	**100**	5'-CTG**T**CGT-3'	5', T172	nq
3'-TCGTATT-5'			3'-GACAGAC-5'		
5'-GTG**T**AAA-3'	5', T90	28	5'-GTC**G**TGC-3'	5', G174	nq
3'-CACATTT-5'			3'-CAGCACG-5'		
5'-GCC**T**GGG-3'	5', T97	30	5'-CGC**T**CGT-3'	3', T72	29
3'-CGGACCC-5'			3'-GCGAGCA-5'		
5'-GGG**T**GCC-3'	5', T102	23	5'-GGC**A**CCC-3'	3', A102	33
3'-CCCACGG-5'			3'-CCGTGGG-5'		
5'-GTG**C**CTA-3'	5', C104	29			
3'-CACGGAT-5'					

[a]Relative intensity = (fraction cleaved by [Rh]-R6A10) - (fraction cleaved by $[Rh(phi)_2(phen')]^{3+}$), with the intensity at A82 defined as 100. nq = not quantitated.

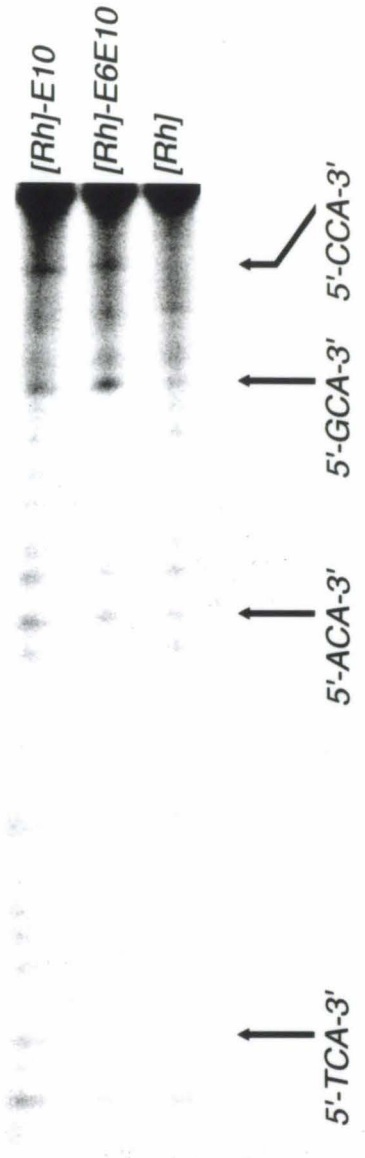

Figure 5.10. Cleavage of a 31-mer oligonucleotide containing all 4 5'-NCA-3' sequences by [Rh]-E6 and [Rh]-E10 in the absence of Mn^{2+}. Photocleavage reactions were conducted at 55 °C and contained 2.5 x 10^{-7} M metallointercalator or metallointercalator-peptide conjugate and 1 x 10^{-6} M unlabeled oligonucleotide.

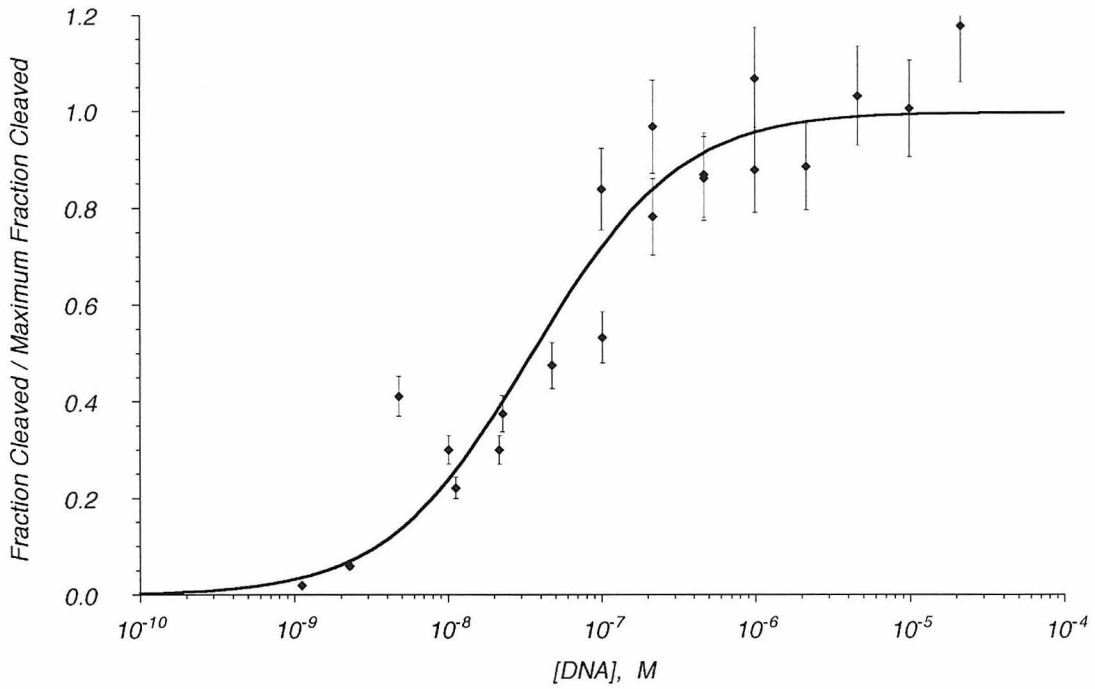

Figure 5.11. Photocleavage isotherm for [Rh]-E6E10 (K_d = 3.0 x 10^{-8} M). Conditions: 3:1 ratio of hairpin oligonucleotide–metallointercalator-peptide conjugate, 50 mM sodium cacodylate buffer pH 7.0, 55 °C.

The dissociation constant of [Rh]-E6E10 for a 5'-CCA-3' site in a 29-mer oligonucleotide with the sequence 5'-AGAG**CCA**CGAGATTTTTTCTCGTGTCTCT-3' (K_3-29) was measured by photocleavage titration at 55 °C. The concentration of the metallointercalator-peptide conjugate ranged from 7.2 x 10^{-6} M to 7.2 x 10^{-11} M, with a constant metallointercalator–unlabeled hairpin oligonucleotide ratio of 1:3. The isotherm obtained by quantitating the fraction cleaved at the adenine of the recognition site was fit to Equation 5.1, yielding a dissociation constant of 3.0 x 10^{-8} (Figure 5.11). Since the bulk intercalative dissociation constant of $[Rh(phi)_2(phen')]^{3+}$ is 7.0 x 10^{-7} M, at 55 °C, in the presence of 5 mM $MnCl_2$, the E6E10 peptide provides 23-fold tighter binding to the target sequence, corresponding to a free energy difference of 2.1 kcal•mol^{-1}. A summary of DNA

Table 5.5. Summary of DNA recognition by peptide conjugates of $[Rh(phi)_2(phen')]^{3+}$ and $[Rh(phi)_2(ethynylphen')]^{3+}$.

Conjugate	Peptide Sequence	DNA Recognition Site(s)[a]	K_d[b], x 10^{-8} M
[Rh]-E6	$[Rh(phi)_2(phen')]^{3+}$-AANVA**E**AAWARAA-$CONH_2$	5'-AC**A**-3', weak 5'-TC**A**-3'	9.9 ± 1.2
[Rh]-E7	$[Rh(phi)_2(phen')]^{3+}$-AANVAI**E**AWARAA-$CONH_2$	–	
[Rh]-E8	$[Rh(phi)_2(phen')]^{3+}$-AANVAIA**E**WARAA-$CONH_2$	–	
[Rh]-E10	$[Rh(phi)_2(phen')]^{3+}$-AANVAIAAW**E**RAA-$CONH_2$	5'-CC**A**-3'	5.7 ± 0.12
[Rh]-E12	$[Rh(phi)_2(phen')]^{3+}$-AANVAIAAWAR**E**AA-$CONH_2$	–	
[Rh]-E13	$[Rh(phi)_2(phen')]^{3+}$-AANVAIAAWARA**E**AA-$CONH_2$	–	
[Rh]-R6E10	$[Rh(phi)_2(phen')]^{3+}$-AANVA**R**AAW**E**RAA-$CONH_2$	–	
[Rh]-I6A10	$[Rh(phi)_2(phen')]^{3+}$-AANVAIAAWARAA-$CONH_2$	–	
[Rh]-E6E10	$[Rh(phi)_2(phen')]^{3+}$-AANVA**E**AAW**E**RAA-$CONH_2$	weak 5'-CC**A**-3'	3.0 ± 0.5
[Rh]-R6A10	$[Rh(phi)_2(phen')]^{3+}$-AANVA**R**AAWARAA-$CONH_2$	consistent with 5'-(G/T)C**A**-3'	
[Rhy]-E6	$[Rh(phi)_2(phen')]^{3+}$-AANVA**E**AAWARAA-$CONH_2$	–	
[Rhy]-E10	$[Rh(phi)_2(phen')]^{3+}$-AANVAIAAW**E**RAA-$CONH_2$	–	

[a]The primary photocleavage site is indicated in bold.

[b]K_d's measured at 55 °C in the presence of 5 mM $MnCl_2$, except for [Rh]-E6E10, which was measured in the absence of $MnCl_2$. The bulk intercalative dissociation constant of $[Rh(phi)_2(phen')]^{3+}$ is 7.0 ± 0.47 x 10^{-7} M.

recognition sequences and measured dissociation constants for the metallointercalator-peptide conjugates studied in this chapter is shown in Table 5.5.

5.3.7. Photocleavage efficiency of metallointercalator-peptide conjugates. Comparison of the specificity of [Rh]-E10, as determined by the ratio of the dissociation constant to the bulk intercalative dissociation constant of $[Rh(phi)_2(phen')]^{3+}$, with the ratio of the fraction cleaved at the 5'-CCA-3' site to the fraction cleaved at the same sites by $[Rh(phi)_2(phen')]^{3+}$ provides some insight into the photocleavage efficiencies of [Rh]-E10. Similar analyses are possible for [Rh]-E6 and [Rh]-E6E10. [Rh]-E10 provides 6.5-fold stronger cleavage at a 5'-CCA-3' site than $[Rh(phi)_2(phen')]^{3+}$.[9b] Comparison of the dissociation constant of [Rh]-E10 for the sequence 5'-CCA-3' to the bulk intercalative dissociation constant of $[Rh(phi)_2(phen')]^{3+}$ indicates that this metallointercalator-peptide conjugate binds 13-fold more tightly to its target than $[Rh(phi)_2(phen')]^{3+}$. Therefore, the photocleavage efficiency of [Rh]-E10 is approximately half that of $[Rh(phi)_2(phen')]^{3+}$. Similarly, [Rh]-E6 binds 7.1-fold more tightly to the sequence 5'-ACA-3', as determined by comparison of dissociation constants. Photocleavage by [Rh]-E6 is approximately 3.2-fold stronger than photocleavage by $[Rh(phi)_2(phen')]^{3+}$ at the sequence 5'-ACA^{32}-3' (Figure 5.5). Conversely, [Rh]-E6E10 binds 23-fold more tightly to 5'-CCA-3' than $[Rh(phi)_2(phen')]^{3+}$. However, cleavage by [Rh]-E6E10 is only 4.1-fold more intense than cleavage by $[Rh(phi)_2(phen')]^{3+}$ at this site (Figure 5.10). Thus, the photocleavage efficiency of the metallointercalator is dependent on the attached peptide and its interaction with the DNA target. These results are consistent with the variation in photocleavage efficiency of [Rh]-R6A10 at various sites on the 5'-endlabeled *EcoRI/PvuII* 180-mer restriction fragment of pUC18. Despite the similarity between the two sequences, cleavage at the highlighted adenine of the sequence 5'-

CTCA^{52}CAA-3' is 3.3-fold stronger than cleavage at the highlighted adenine of the sequence 5'-CTCA^{144}CTG-3'.

5.3.8. Circular dichroism of metallointercalator-peptide conjugates.

Circular dichroism spectra of the metallointercalator-peptide conjugates studied in this chapter were recorded at 23 °C at pH 7.0 in the absence and presence of 5 mM $MnCl_2$ and trifluoroethanol (TFE) to explore correlations between sequence selectivity and secondary structure content (Table 5.6). Under these conditions, CD spectra consistent with an α-helical conformation are observed for all of the metallointercalator-peptide conjugates, with helical contents ranging from 1% to 33% (Figure 5.12). Addition of Mn^{2+} or TFE results in increases in the helical content of all of the metallointercalator-peptide conjugates. These additives also increase the specificity of DNA recognition by [Rh]-E6 and [Rh]-E10. In contradistinction, the specificity of [Rh]-E6E10 does not increase upon addition of Mn^{2+}. Interestingly, [Rh]-E6E10 has a relatively low helical content, and little change is observed

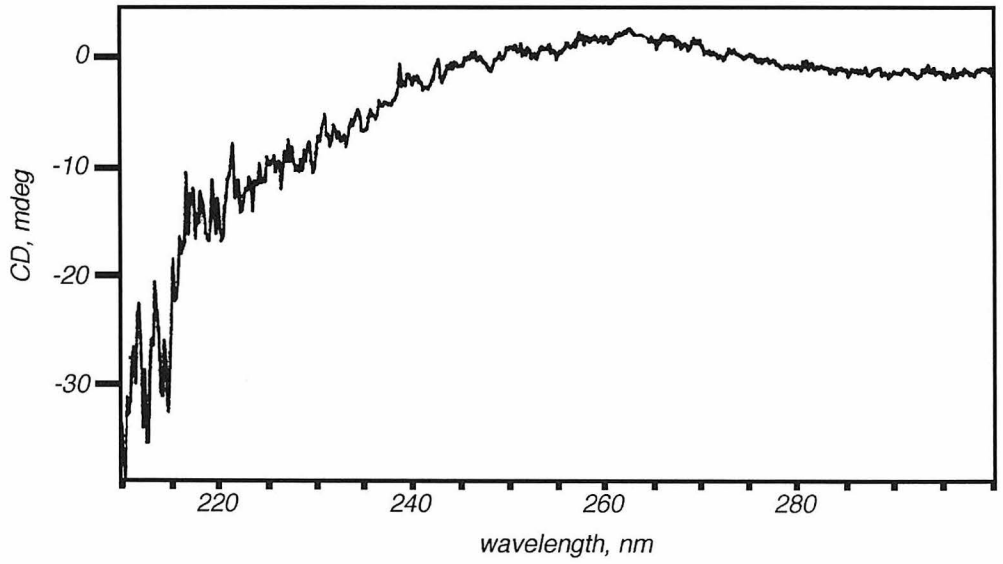

Figure 5.12. CD spectrum of [Rh]-E6 (50 μM) in 5 mM $MnCl_2$, 10 mM Tris•HCl, pH 7.0.

Table 5.6. Helical content of peptide conjugates of $[Rh(phi)_2(phen')]^{3+}$.[30]

Conjugate	Helical Content (pH 7.0, 23 °C, 10 mM Tris•HCl)	Helical Content (pH 7.0, 23 °C, 5 mM $MnCl_2$, 10 mM Tris•HCl)	Helical Content (pH 7.0, 23 °C, 25% TFE, 7.5 mM Tris•HCl)
[Rh]-E6	<1%	5%	8%
[Rh]-E7	4%	8%	7%
[Rh]-E8	3%	6%	8%
[Rh]-E10	17%	21%	24%
[Rh]-E12	<1%	1%	2%
[Rh]-E13	5%	6%	8%
[Rh]-E6E10	3%	5%	5%
[Rh]-R6A10	2%	8%	10%
[Rh]-R6E10	4%	6%	10%
[Rh]-A6A10	18%	25%	33%

upon addition of Mn^{2+} or TFE. Together, these results suggest that helix formation is an important component of DNA recognition by these metallointercalator-peptide conjugates.

5.4. Discussion

5.4.1. DNA recognition by metallointercalator-peptide conjugates derived from [Rh]-E10 by varying the position of the critical glutamate. Hydrogen bonding contacts between the glutamate side chain carboxylate and N4 of cytosine are a common recognition motif in crystal structures of transcription factor-operator complexes.[31] Previous work has demonstrated that Glu^{10} is critical to recognition of 5'-CCA-3' by [Rh]-E10.[9b] We chose to vary the position of Glu^{10} relative to the other amino acids of the E10 peptide to identify additional positions in the sequence that might make base-specific contacts with DNA targets. This approach indicated that a glutamate residue at position 6, but not positions 7, 8, 12, or 13, conferred sequence selectivity on $[Rh(phi)_2(phen')]^{3+}$ in conjunction with an alanine residue at position 10.

Although DNA binding does not appear to increase the helicity of [Rh]-E10,[32] helical content correlates with selectivity in a family of metallointercalator-peptide conjugates that target 5'-CCA-3'.[9b] The lack of sequence selectivity of these metallointercalator peptide conjugates agrees with the observation that helical content is important for specificity. When these peptides adopt helical conformations, the side chains of the amino acid residues at positions 6 and 10 are located on the same face of the helix and are capable of making specific contacts with the DNA target. When the structure of the peptide is poorly defined, the ability of the amino acid side chains at positions 6 and 10 to make specific contacts with the DNA is diminished. When the critical glutamate residue is not located at position 6 or 10, specificity is not observed.

Despite the sequence selectivity exhibited by [Rh]-E6 and [Rh]-E10, sequence selectivity is not observed when these peptides are conjugates to $[Rh(phi)_2(ethynylphen')]^{3+}$. These results point out the importance of the metallointercalator in correctly orienting these peptides in the major groove. Both $[Rh(phi)_2(phen')]^{3+}$ and $[Rh(phi)_2(ethynylphen')]^{3+}$ can bind by intercalation of either diastereomeric phi ligand, and the linkers of both metallointercalators possess some degrees of freedom. Accordingly, multiple orientations are available to peptides appended to either metallointercalator. However, qualitative comparisons of the differences between these orientations are possible. Superimposition of the phenanthroline ligands of $[Rh(phi)_2(phen')]^{3+}$ and $[Rh(phi)_2(ethynylphen')]^{3+}$ suggests that differences in the preferred position of C_α of the N-terminal amino acid residue are about 2-3 Å.

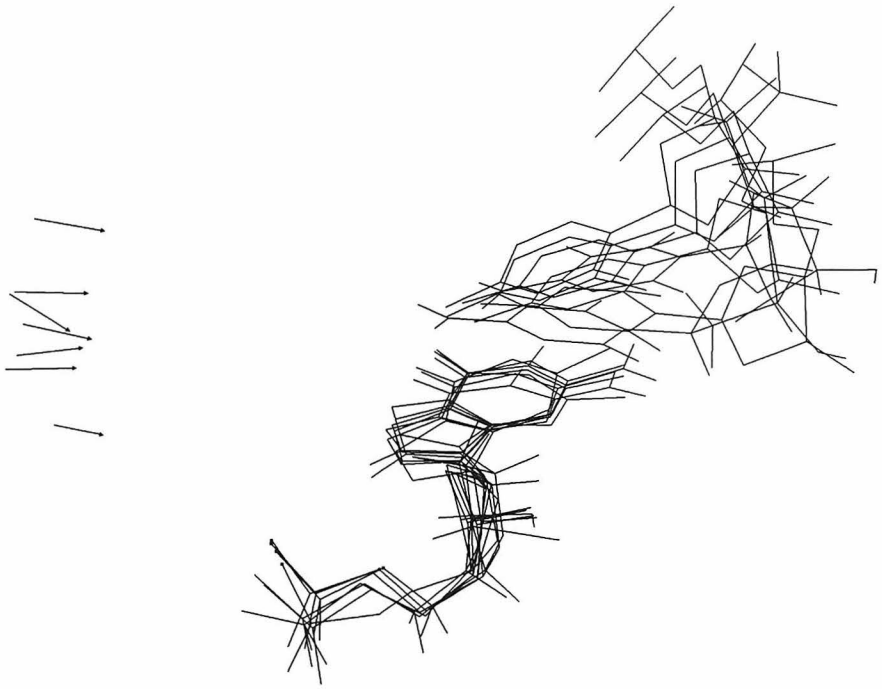

Figure 5.13. $C_\alpha \rightarrow C_\beta$ vectors for arginine residues from the *E. Coli* CAP protein, the glucocorticoid receptor, and Zif268 that target guanine, after superimposition of the contacted residues.

5.4.2. Model for DNA recognition by [Rh]-E6 and [Rh]-E10. Many amino acids with functional side chains are capable of making base-specific contacts with more than one type of base (Table 5.1). However, DNA binding proteins can specify their operator sites with single-base accuracy. Although the factors that determine which of several possible bases will be specified by a given amino acid in a given recognition domain are not clear, it has been suggested that the position and orientation of the peptide backbone with respect to the DNA determines the types of contacts that individual amino acids are capable of making. Conversely, for recognition of a given nucleotide by a given amino acid, certain positions and orientations of the peptide backbone with respect to the DNA are preferred.[33] To illustrate this point, $C_\alpha \rightarrow C_\beta$ vectors for arginine residues from

the *E. Coli* CAP protein, the glucocorticoid receptor, and Zif268 that make base-specific contacts with guanosine and thymine bases are shown in Figure 5.13.

Based on the sequence preferences of the metallointercalator-peptide conjugates studied in this chapter, it is possible to refine our previous model for sequence-selective DNA binding by [Rh]-E10.[9b] Together, photocleavage results with [Rh]-E6, [Rh]-E10, and [Rh]-E6E10 indicate that glutamate residues at positions 6 and 10 of these metallointercalator-peptide conjugates are capable of making specific contacts with cytosine bases. The effect of substituting arginine for glutamate at position 6 of [Rh]-E6 confirm the importance of this residue in sequence-selective DNA recognition. These results form the basis for our refined model.

The refined model (Figure 5.14) was constructed by energy minimization[34] using the following restraints: (1) the DNA was constrained to adopt canonical B-form torsion angles, except at the intercalation site; (2) the DNA structural parameters (helical twist and helix rise) at the intercalation site, and the position of the intercalated phi ligand, were derived from the solution structure of Δ-α-[Rh[(*R,R*)-Me_2trien]phi]$^{3+}$ bound to 5'-TGCA-3';[35] (3) the relative position of the glutamate side chain carboxylate and the 5'-cytosine of the 5'-CCA-3' recognition site was constrained to match the relative position of Glu^{180} and its target cytosine in the *E. Coli* CAP protein-operator complex;[36] and (4) the initial conformation of the peptide was a canonical α-helix. A similar analysis was performed for [Rh]-E6, with the relative position of the glutamate side chain carboxylate and the cytosine of the 5'-ACA-3' recognition site constrained to match the relative position of Glu^{180} and its target cytosine in the *E. Coli* CAP protein-operator complex.

5.4.3. Implications of the model. Although mutation studies have identified a contact between the critical glutamate residue and one of the cytosine bases of the recognition site of both [Rh]-E6 and [Rh]-E10, these studies have shed little light on

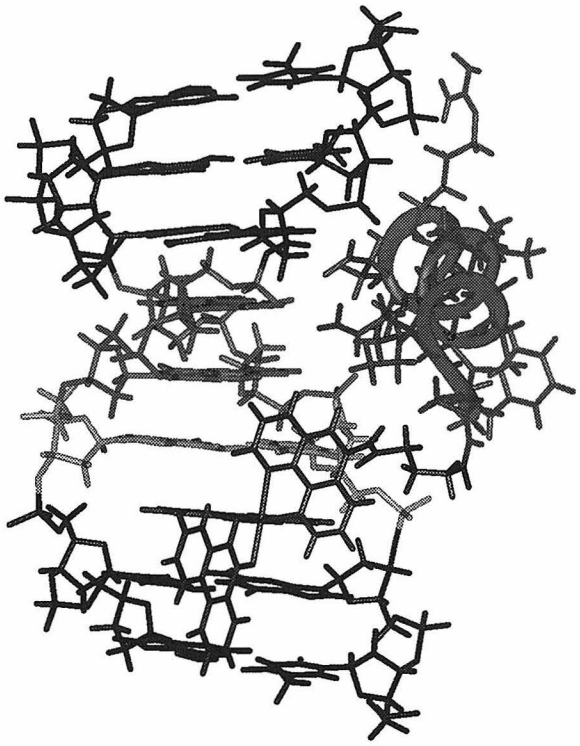

Figure 5.14. Model for DNA recognition by [Rh]-E10.

additional, base-specific contacts that specify the remainder of the recognition site. In order be able to rationally modify the sequence selectivity of these metallointercalator-peptide conjugates, it is necessary to identify additional contacts that determine the observed sequence preferences. Some inferences about the nature of these contacts may be drawn by examination of the models.

[Rh]-E10 is capable of high levels of discrimination between 5'-CCA-3' and 5'-CAA-3', 5'-CGA-3', or 5'-CTA-3'. Amino acid modification studies have indicated that the residue at position 6 plays an important role in determining the sequence selectivity of the metallointercalator-peptide conjugates derived from [Rh]-E10. Therefore, a possible role for Ile^6 in determining the sequence preferences of [Rh]-E10 was considered. Figure 5.15 shows the Connolly surfaces of the central C•G base pair and the isoleucine residue at position 6. No other amino acid side chains of the E10 peptide are in proximity to this base

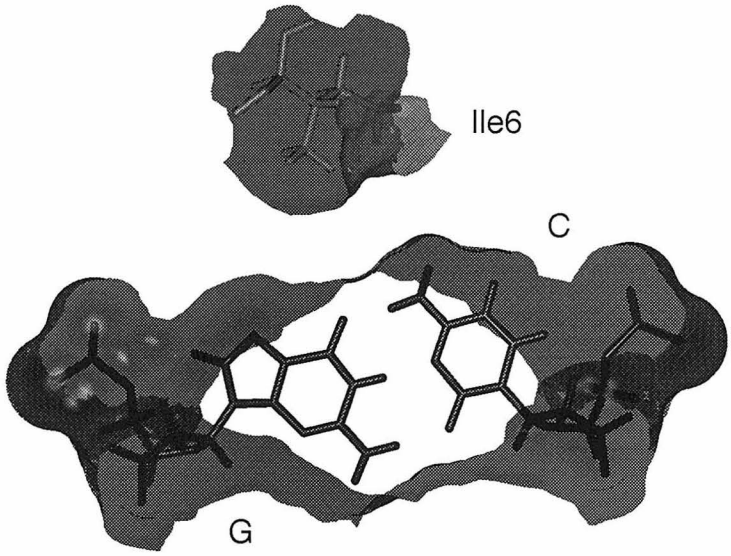

Figure 5.15. Recognition of C•G by shape-selectivity.

pair, suggesting that shape complementarity between the preferred C•G base pair and the isoleucine side chain and a lack of shape complementarity between the alternative G•C, A•T, and T•A base pairs and the isoleucine side chain is an important determinant of the observed sequence selectivity.

[Rh]-E6 is capable of discriminating between 5'-ACA-3' and 5'-CCA-3' or 5'-GCA-3', and to a lesser extent, between 5'-ACA-3' and 5'-TCA-3'. In the model for DNA recognition by [Rh]-E6, the side chain methyl group of Ala^{10} is in contact with the thymine C5-methyl group. Together, photocleavage results with [Rh]-E10 and [Rh]-E6E10, which implicate amino acid residues at position 10 in mediating sequence-selective recognition of DNA, and the three-dimensional model described above suggest that a methyl-methyl interaction is primarily responsible for the observed sequence selectivity. The lessened ability of [Rh]-E6 to discriminate between 5'-ACA-3' and 5'-TCA-3' may arise from methyl-methyl interactions between other alanine residues and a putative T•A base pair at the 5'-position of the recognition sequence.

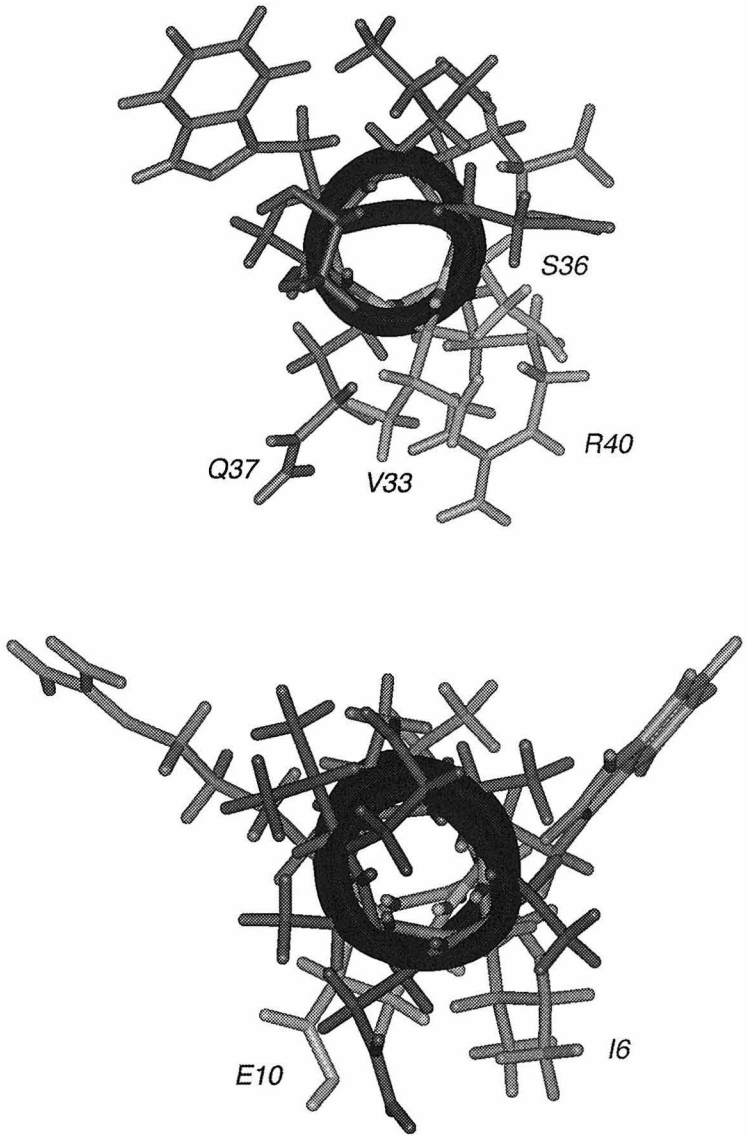

Figure 5.16. Structure of the P_{22} α_3 helix and structure the E10 peptide drawn using canonical α-helix torsion angles.

Why do the metallointercalator-peptide conjugates studied in this chapter not reproduce the sequence selectivity of the parent protein? The structure of the E10 peptide drawn using canonical α-helix torsion angles suggests an origin for this discrepancy (Figure 5.16). In the NMR structure of the P_{22} repressor, Trp^{38} is buried in the hydrophobic core of the protein and Ser^{36} and Arg^{40} poised to contact the DNA target. In the canonical α-helix representation of the E10 peptide, Trp^{9} and Arg^{11} define two faces of

the helix, only one of which is capable of lying in the major groove without steric clashes between the sugar-phosphate backbone and the Trp and Arg side chains. Consistent with this view, specificity is observed with the E6 and E10 peptides, both of which have the critical glutamate located on this face. Specificity is not observed with peptides where the glutamate residue is moved away from this face (E7, E8, E12, E13).

5.4.4. Effect of the E6R mutation on the DNA sequence selectivity of [Rh]-E6. Photocleavage of the 5'-endlabeled *EcoRI/PvuII* 180-mer restriction fragment of pUC18 by [Rh]-R6A10 reveals that a single amino acid change can cause complex changes in the DNA recognition characteristics of these metallointercalator-peptide conjugates. This change confirms the predictions made on the basis of the sequence selectivities observed with metallointercalator-peptide conjugates derived from [Rh]-E10 by changing the position of the critical glutamate residue.

How can a single amino acid change cause such a complex change in the photocleavage characteristics of a metallointercalator-peptide conjugate? A comparison of $C_\alpha \rightarrow C_\beta$ vectors for arginine residues that make hydrogen bonding contacts with guanine-O6 in the crystal structures of operator complexes of CAP, the glucocorticoid receptor, and Zif268, generated by superimposition of the guanosine bases, is shown in Figure 5.13. Although there is some variation in the C_α position, all of the C_α atoms located slightly to the 3' side of the guanosine base and along the base pair axis all of the C_α atoms lie to the guanine side of the guanine-cytosine interface. In the lone example of a hydrogen bonding interaction between glutamate and cytosine-N4 in the crystal structures of operator complexes of CAP, the glucocorticoid receptor, and Zif268, Glu C_α is found to the cytosine side of the guanine-cytosine interface along the base pair axis and to the 5'-side of the contacted base. The distance between C_α of Arg^{466} in the glucocorticoid receptor-operator complex and C_α of Glu^{180} in the CAP-operator complex after superimposition of

the cytosine bases of the C•G base pairs they contact is 6.41 Å. Assuming that the preferred recognition sequence of [Rh]-R6A10 includes C•G adjacent to the position cleaved, the difference between the preferred position of the C_α of Glu^6 of [Rh]-E6 and the preferred position of Arg^6 of [Rh]-R6A10 would produce a significant shift in the position of the α-helix relative to the DNA. Such a shift would affect both the amino acid side chain(s) that are presented to the base pair at the 5'-position of the recognition sequence and the position of the metal complex in the intercalation site. Consequently, both the sequence preferences at the 5'-position of the recognition sequence and the photocleavage characteristics of the metallointercalator-peptide conjugate could be perturbed. This result is consistent with the degeneracy in Table 5.1; judicious selection of the amino acid used to recognize a given base affords the opportunity to control the orientation of the DNA-binding protein relative to the DNA target, thereby modulating the sequence preferences of amino acids at nearby positions in a transcription factor-operator complex.

5.5. Conclusions

This investigation demonstrates the usefulness of metallointercalator-peptide conjugates as small-molecule systems within which to explore the correlation between the amino acid sequence of DNA-binding proteins and the DNA sequences they target. The rhodium(III) complexes used as anchors provide high levels of nonspecific affinity for DNA and a well-defined coordination geometry with which to orient appended peptides in the major groove. Screening of peptide conjugates of $[Rh(phi)_2(phen')]^{3+}$ using a photocleavage assay identified new sequence selectivity and resulted in the prediction of base-specific contacts by residues at position 6 in metallointercalator-peptide conjugates derived from the P_{22} repressor recognition α-helix. Using data from crystal structures of transcription factor–operator complexes, and the solution structure of a rhodium(III) phi complex bound to DNA by intercalation from the major groove, a model was constructed

that accounts for the observed sequence selectivity the metallointercalator-peptide conjugates studied. Correlations between the amino acid sequence and the DNA sequence selectivity of these metallointercalator-peptide conjugates suggest that Ile^6 is responsible for the observed C•G selectivity of [Rh]-E10 at the central base pair of the 5'-CCA-3' target sequence. Predictably, an amino acid substitution at this position caused complex changes in the DNA sequence preferences of the modified metallointercalator-peptide conjugate.

5.6. References and Notes

1. Watson, J. D.; Crick, F. H. C. *Nature* **1953**, *171*, 737.
2. For recent reviews, see: (a) Pabo, C. O.; Sauer, R. T. *Ann. Rev. Biochem.* **1992**, *61*, 1053. (b) Rhodes, D.; Schwabe, J. W. R.; Chapman, L.; Fairall, L *Phil. Trans. R. Soc. Lond.* B **1996**, *351*, 501.
3. For a recent examples, see: Choo, Y.; Sánchez-García, I.; Klug, A. *Nature* **1994**, *372*, 642.
4. For an example of *in vivo* repression of an oncogene by a designed, site-specific DNA binding protein, see reference 3.
5. For examples, see: helix-turn-helix: Brennan, R. G.; Matthews, B. W. *J. Biol. Chem.* **1989**, *264*, 1903. (b) Harrison, S. C.; Aggarwal, A. K. *Ann. Rev. Biochem.* **1990**, *59*, 933; helix-loop-helix: (c) Jones, N. *Cell* **1990**, *61*, 9. (d) Davis, R. L.; Cheng, P.-F.; Lassar, A. B.; Weintraub, H. *Cell* **1990**, *60*, 733. (e) Anthony-Cahill, S. J.; Benfield, P. A.; Fairman, R.; Wasserman, Z. R.; Brenner, S. L.; Stafford, W. F., III; Altenbach, C.; Hubbell, W. L.; DeGrado, W. F. *Science* **1992**, *255*, 979; homeodomain: (f) Gehring, W. J.; Muller, M.; Affolter, M.; Percival-Smith, A.; Billeter, M.; Qian, Y. Q.; Otting, G.; Wüthrich, K. *Trends Genet.* **1990**, *6*, 323. (g) Gehring, W. J.; Qian, Y. Q.; Billeter, M.; Furukubo-Tokunaga, K.; Schier, A. F.; Resendez-Perez, D.; Affolter, M.; Otting, G.;

Wüthrich, K. *Cell* **1994**, *78*, 211. (h) Pomerantz, J. L.; Pabo, C. O.; Sharp, P. A. *Proc. Natl. Acad. Sci. U.S.A.* **1995**, *92*, 9752; basic region-leucine zipper: (i) Kerppola, T. K. *Curr. Opin. Struct. Biol.* **1991**, *1*, 71; zinc finger: (j) Berg, J. M. *Science* **1986**, *232*, 485. (k) Berg, J. M. *Ann. Rev. Biophys. Biophys. Chem.* **1990**, *19*, 405. (l) Vallee, B.L.; Coleman, J.E.; Auld, D.S. *Proc. Natl. Acad. Sci. U.S.A.* **1991**, *88*, 999. (m) Schwabe, J. W. R.; Klug, A. *Nature Struct. Biol.* **1994**, *1*, 345.

6. For the first cocrystal structure of a zinc finger protein with DNA, see: (a) Pavletich, N. P.; Pabo, C. O. *Science* **1991**, *252*, 809. (b) Pavletich, N. P.; Pabo, C. O. *Science* **1993**, *261*, 1701.
7. (a) Desjarlais, J. R.; Berg, J. M. *Proc. Natl. Acad. Sci. U.S.A.* **1992**, *89*, 7345. (b) Choo, Y.; Klug, A. *Proc. Natl. Acad. Sci. U.S.A.* **1994**, *91*, 11168. (c) Nardelli, J.; Gibson, T.; Charnay, P. *Nucl. Acids Res.* **1992**, *20*, 4137. (d) Desjarlais, J. R.; Berg, J. M. *Proteins* **1992**, *12*, 101. (e) Thukral, S. K.; Morrison, M. L.; Young, E. T. *Mol. Cell Biol.* **1992**, *12*, 2784.
8. Adapted from reference 2a and from Sardesai, N. Y. *Ph.D. Thesis*, California Institute of Technology, 1995.
9. The consensus operator site of the P_{22} repressor is 5'-ANTNAAG-3'; see: reference 2a.
10. [Rh]-E10 was formerly referred to as Sk-PD; see reference 8b.
11. *InsightII User Guide*, version 2.3.0, Biosym Technologies: San Diego, 1993.
12. Pyle, A. M.; Chiang, M. Y.; Barton, J. K. *Inorg. Chem.* **1990**, *29*, 4487.
13. (a) Stewart, J. M.; Young, J. D. *Solid Phase Peptide Synthesis*, Pierce Chemical Company, Rockford, Illinois: 1984. (b) Edmondson, J. M.; Klebe, R. J.; Zardeneta, G.; Weintraub, S. T.; Kanda, P. *BioTechniques* **1988**, *6*, 866.

14. HF deprotection and cleavage from the resin of metallointercalator-peptide conjugates was performed by the Biopolymer Synthesis Facility, Department of Chemistry, California Institute of Technology.

15. Maniatis, T.; Fritsch, E. F.; Sambrook, J. *Molecular Cloning*, Cold Spring Harbor Laboratory, Cold Spring Harbor: 1982.

16. Maxam, A. M.; Gilbert, W. *Proc. Natl. Acad. Sci. U.S.A.* **1977**, *74*, 560.

17. Suffert, J.; Ziessel, R. *Tetrahedron Lett.* **1991**, *32*, 757-760

18. Pyle, A. M. *Ph. D. Thesis*, Columbia University, 1989.

19. Hall, D. B.; Holmlin, R. E.; Barton, J. K. *Nature*, **1996**, *382*, 731.

20. Sardesai, N. Y.; Lin, S. C.; Zimmermann, K.; Barton, J. K. *Bioconj. Chem.* **1995**, *6*, 302.

21. Determined on a Vydac 218TP510 semipreparative reverse-phase C_{18} column using a linear gradient of 15%→40% 0.1% TFA in MeCN in 0.1% aqueous TFA over 19 min followed by isocratic elution at 40% 0.1% TFA in MeCN in 0.1% aqueous TFA, at a flow rate of 4.5 mL/min.

22. Throughout this chapter, all amino acid substitutions are indicated relative to the sequence of [Rh]-E10 (H_2N-AANVAIAAWERAA-$CONH_2$).

23. See reference 8b and Chapter 4 of this thesis.

24. Numbering refers to positions of the complementary base on the 5'-strand. The sequence of the pUC18 3'-endlabeled *EcoRI/PvuII* 180-mer is 5'-CTGGC ACGAC^{171} AGGTT TCCCG^{161} ACTGG AAACG^{151} GGGCA GTGAG^{141} CGCAA CGCAA^{131} TTAAT GTGAG^{121} TTAGC TCACT^{111} CATTA GGCAC^{101} CCCAG GCTTT^{91} ACACT TTATG^{81} CTTCC GGCTC^{71} GTATG TTGTG^{61} TGGAA TTGTG^{51} AGCGG ATAAC^{41} AATTT CACAC^{31} AGGAA ACAGC^{21} TATGA CCATG^{11} ATTAC GAATT^{1}-3'.

25. The sequence of the labeled strand of the oligonucleotide was 5'-GAG**TCA**CGAG**ACA**CGAG**GCA**CGAG**CCA**CGAG-3'.
26. This analysis assumes that the photocleavage efficiency is comparable at all four 5'-NCA-3' sites. A similar derivation of the stabilization energy for specific complex formation by [Rh]-E10 was confirmed by independent measurement of dissociation constants; see Chapter 4 of this thesis.
27. For a protocol for dissociation constant determination by photocleavage titration, see Chapter 4 of this thesis.
28. For Equation 5.1, $[DNA]_t$ is the total DNA concentration in duplexes, $[L]_t$ is the total ligand concentration, and γ is the fraction of bound complexes at a given site that produce strand scission under the conditions of the experiment.
29. This may be demonstrated by consideration of the identity of the cleaved base. Where the cleaved base is A, sequences with no common nucleotides at adjacent positions may be identified, *e.g.*, A82 and A120. Where the cleaved base is C, G, or T, such sequences may not be identified. A similar analysis may be performed for the other positions of the putative recognition sequence. The above analysis excludes cleavage at C104, which has no apparent similarity with any of the other recognition sequences, and may be associated with recognition of the 5'-GCA-3' sequence on the complementary strand (cleavage associated with recognition of this sequence is visible at T102).
30. The helical content is calculated by assuming that a fully helical peptide has a mean residue ellipticity ($[\theta_{222}]$) of -31,500 deg•cm^2•dmol^{-1}; see: Chen, Y. H.; Yang, J. T.; Martinez, H. M. *Biochemistry* **1972**, *11*, 4120. The mean residue ellipticity is defined as:

$$[\theta_{222}] = 100\theta_{222}/cnl$$

where θ_{222} is the ellipticity (mdeg) measured by CD spectroscopy, c is the peptide concentration (mM), n is the number of amino acids in the peptide, and l is the path length (cm) of the CD cell; see: Lehrman, S. R.; Tuls, J. L.; Lund, M. *Biochemistry* **1990**, *29*, 5590.

31. (a) Schultz, S. C.; Shields, G. C.; Steitz, T. A. *Science* **1991**, *253*, 1001. (b) Raskin, C. A.; Diaz, G.; Joho, K.; McAllister, W. T. *J. Mol. Biol.* **1992**, *228*, 506.
32. See Chapter 4 of this thesis.
33. Pabo, C. O., personal communication. See also: Pomerantz, J. L.; Pabo, C. O.; Sharp, P. A. *Proc. Natl. Acad. Sci. U.S.A.* **1995**, *92*, 9752.
34. Molecular mechanics calculations were performed using the CVFF forcefield (Dauber-Osguthorpe, P; Roberts, V. A.; Osguthorpe, D. J.; Wolff, J.; Genest, M.; Hagler, A. T. *Proteins: Structure, Function and Genetics* **1988**, *4*, 31). Minimization involved 1000 iterations of steepest descents minimization followed by 1000 iterations (1 picosecond) dynamics with temperature of 300 K and 5000 iterations of steepest descents minimization. The DNA and the intercalator were fixed throughout the calculation. An ensemble of structures was generated in this fashion. For the respective metallointercalator-peptide conjugates, all of the structures were essentially identical. A representative structure of [Rh]-E10 is shown in the text.
35. (a) Hudson, B. P.; Dupureur, C. M.; Barton, J. K. *J. Am. Chem. Soc.* **1995**, *117*, 9379. (b) Hudson, B. P.; Barton, J. K., submitted to *J. Am. Chem. Soc.*
36. Parkinson, G.; Wilson, C.; Gunasekera, A.; Ebright, Y. W.; Ebright, R. E.; Berman, H. M. *J. Mol. Biol.* **1996**, *260*, 395.

Chapter 6: Conclusions and Perspectives

6.1. Conclusions

In an effort to understand the molecular basis of sequence-specific DNA recognition by proteins, we have investigated DNA binding by peptide conjugates of the metallointercalators $[Rh(phi)_2(phen')]^{3+}$ and $[Rh(phi)_2(ethynylphen')]^{3+}$. These small, well-defined systems possess the high nonspecific affinity for DNA, and permit DNA binding sites to be determined with single-base resolution. Consequently, these systems are excellent models for the recognition of individual operator half-sites by monomeric recognition domains.

We have optimized the solid-phase coupling strategy of Sardesai *et al.*[1] This strategy permits rapid access to families of metallointercalator-peptide conjugates. Thus, we have been able to explore the effects of incremental variations in the amino acid sequences of the appended peptides. The optimized synthetic strategy has enabled us to prepare micromolar quantities of a metallointercalator-peptide conjugate using enantiomerically pure Δ-$[Rh(phi)_2(phen')]^{3+}$. Consequently, we are able to examine metallointercalator-peptide conjugates, and their interactions with DNA, by multidimensional NMR.

We have examined the effects of modifying the amino acid sequence of a sequence-selective metallointercalator-peptide conjugate in a systematic fashion. $[Rh(phi)_2(phen')]^{3+}$-AANVAIAAWERAA-$CONH_2$ ([Rh]-E10) targets the three-base-pair sequence 5'-CCA-3'. Previous studies have demonstrated that the presence of a glutamate residue at position 10 is critical to sequence-selective DNA recognition by [Rh]-E10. We have explored the DNA recognition characteristics of a family of metallointercalator-peptide conjugates derived from [Rh]-E10 by changing the position of the glutamate residue in the amino acid sequence. These studies resulted in the identification of a new sequence-selective

metallointercalator-peptide conjugate, $[Rh(phi)_2(phen')]^{3+}$-AANVAEAAWARAA-$CONH_2$ ([Rh]-E6), which targets the three-base-pair sequence 5'-ACA-3'. Notably, the glutamate residue of [Rh]-E6 is located on the same face of a putative α-helix as the glutamate residue of [Rh]-E10. Sequence selectivity was not observed when the critical glutamate residue was located at positions 7, 8, 12, and 13, which are not on the same face of the helix. These results support our hypothesis that base-specific interactions between these metallointercalator-peptide conjugates and their DNA targets require the peptide to adopt a helical conformation.

Based on the sequence-selectivities of [Rh]-E6 and [Rh]-E10, we have constructed a model for DNA binding by these metallointercalator-peptide conjugates. With this model, we predicted additional interactions between [Rh]-E6 and [Rh]-E10 and their respective DNA targets. To test our predictions, we made further amino acid changes at positions 6 and 10. Substitution of arginine for glutamate at position 6 caused a complex change in the DNA recognition characteristics of [Rh]-E6. Thus, we confirmed that the amino acid residue at position 6 plays an important role in determining the DNA sequence selectivity of these metallointercalator-peptide conjugates.

6.2. Perspectives

The metallointercalator-peptide conjugates studied in this thesis afford the possibility of targeting phenanthrenequinone diimine complexes of rhodium(III) to predictable sites in duplex DNA. Such tunable sequence specificity would have widespread practical application. Conversely, the metallointercalator-peptide conjugates studied in this thesis also permit the DNA recognition characteristics of individual amino acids to be studied in the context of a small, readily synthesized, well-defined system.

Being able to target metallointercalator-peptide conjugates to any sequence will require a deeper understanding of the factors that are responsible for sequence specificity.

The investigations described in this thesis cover only a small subset of the available combinations of the naturally occurring amino acids. Within this subset, we have observed complex recognition characteristics. Further studies of the recognition characteristics of [Rh]-R6A10 will facilitate design. Screening of additional sequence variants at the critical positions 6 and 10 should lead to the identification of additional sequence selectivity.

Rational design of metallointercalator-peptide conjugates with predictable sequence specificities will also require the structural details of DNA binding by these constructs to be elucidated. In this thesis, we have demonstrated that sufficient quantities of a peptide conjugate of enantiopure Δ-$[Rh(phi)_2(phen')]^{3+}$ for multidimensional NMR study can be synthesized. The structure determination of the complex between [Δ-Rh]-E10 and an oligonucleotide containing a 5'-CCA-3' sequence is currently in progress in the Barton laboratory.[2]

The metallointercalator-peptide conjugates studied in this thesis afford many possibilities for practical applications. The overall affinity and sequence specificity of the metallointercalator for DNA may be controlled. Among other applications, Barton and coworkers have demonstrated that phenanthrenequinone diimine complexes of rhodium(III) may be used to repair thymine dimers[3] and to block transcriptional activation.[4] Appending oligopeptides to these complexes may permit these processes to be carried out in a sequence-specific fashion. Finally, peptide conjugates of $[Rh(phi)_2(bpy')]^{3+}$ that hydrolyze the phosphodiester backbone of DNA have been developed in this laboratory.[5] Consequently, it may be possible to construct a small-molecule equivalent of a restriction endonuclease by appending two peptides, one of which confers sequence-specific binding and one of which carries out the chemical transformation, to a metallointercalator.

6.3. References and Notes

1. Sardesai, N. Y.; Lin, S. C.; Zimmermann, K.; Barton, J. K. *Bioconj. Chem.* **1995**, *6*, 302.
2. Franklin, S. J.; Hastings, C. A.; Barton, J. K. *unpublished results.*
3. Dandliker, P. J.; Holmlin, R. E.; Barton, J. K. *Science* **1997**, *275*, 1465.
4. Johann, T. W. *Ph.D. Thesis*, California Institute of Technology, 1997.
5. Fitzsimons, M. P.; Barton, J. K. *J. Am. Chem. Soc.* **1997**, *119*, 3379.

Appendix I: X-ray Crystallographic Data for (±)-15 (Chapter 2).

Table I.1. Crystallographic data for (±)-15.

Formula	$C_{18}H_{20}O_3$	Scan Rate, deg/min	5.49
Formula Weight	284.36	Scan Width, deg	0.9 + 0.350tanΘ
Crystal dimensions, mm	0.13 x 0.25 x 0.48	hkl ranges, h	-13 to 13
Radiation Wavelength, Å	Mo, 0.71073	hkl ranges, k	0 to 12
Temperature, °C	25 ± 1	hkl ranges, l	-15 to 16
Crystal System	monoclinic	2Θ range, deg	2.0 - 50.0
Space Group	$P2_1/c$	Structure solution	Direct methods
a, Å	11.338 (3)	No. of unique data	3014
b, Å	10.536 (2)	No. of data used in refinement	1620
c, Å	13.154	Weighting scheme, w	$4F_o^2/[\sigma(F_o)^2]^2$
β, deg	105.99 (2)	No. of parameters refined	190
V, Å^3	1511 (1)	R[a]	0.0746
Z	4	R_w[b]	0.0748
Density, g/cm^3	1.25	GOF	0.53
Absorption coeff., μ, cm^{-1}	0.8	Largest shift/esd	0.00
Rel. transmission coeff.	0.000 - 0.000	High peak in diff map, e/Å^3	0.31 (6)
Scan type	Ω-2Θ		

[a] $R = \Sigma(|F_o| - |F_c|)/\Sigma|F_o|$ [b] $R_w = [\Sigma w(|F_o| - |F_c|)^2/\Sigma w|F_o|^2]^{1/2}$

Table I.2. Positional parameters for (±)-15.

Atom[a]	x	y	z	B (A^2)
O1	0.9197 (3)	0.2000 (3)	0.8090 (3)	3.34 (7)
O2	0.9412 (3)	0.0445 (3)	1.0958 (3)	3.25 (7)
O3	0.7900 (4)	0.0569 (4)	0.7260 (3)	4.39 (9)
C1	0.9862 (4)	0.2590 (5)	0.9019 (4)	2.7 (1)
C2	1.0660 (5)	0.3526 (5)	0.8857 (4)	3.5 (1)
C3	1.1398 (5)	0.4141 (5)	0.9719 (4)	3.6 (1)
C4	1.1337 (5)	0.3852 (5)	1.0714 (4)	4.0 (1)
C5	1.0531 (5)	0.2931 (5)	1.0870 (4)	3.4 (1)
C6	0.9785 (4)	0.2287 (4)	1.0013 (4)	2.49 (9)
C7	0.8856 (4)	0.1336 (5)	1.0152 (4)	2.6 (1)
C8	0.8070 (4)	0.0775 (5)	0.9097 (4)	2.8 (1)
C9	0.8336 (4)	0.1051 (5)	0.8093 (4)	3.0 (1)
C10	0.8434 (5)	-0.0085 (6)	1.1312 (4)	4.1 (1)

C11	0.7485 (5)	0.0958 (5)	1.1244 (4)	3.5 (1)
C12	0.7669 (4)	0.1840 (5)	1.0372 (4)	2.7 (1)
C13	0.6991 (4)	0.1533 (5)	0.9243 (4)	2.9 (1)
C14	0.5990 (5)	0.1899 (5)	0.8550 (4)	3.5 (1)
C15	0.4983 (5)	0.2776 (5)	0.8691 (5)	4.0 (1)
C16	0.5333 (7)	0.4124 (6)	0.8501 (8)	9.2 (3)
C17	0.3793 (6)	0.2441 (7)	0.7891 (6)	6.9 (2)
C18	0.4787 (6)	0.2657 (8)	0.9782 (6)	7.6 (2)
H2	1.068	0.375	0.816	6.0*
H3	1.196	0.477	0.962	6.0*
H4	1.185	0.429	1.131	6.0*
H5	1.050	0.273	1.157	6.0*
H8	0.807	-0.077	1.087	6.0*
H10B	0.807	-0.012	0.900	6.0*
H10A	0.874	-0.038	1.202	6.0*
H11B	0.667	0.063	1.106	6.0*
H11A	0.764	0.139	1.190	6.0*
H12	0.753	0.266	1.061	6.0*
H14	0.588	0.157	0.786	6.0*
H16A	0.472	0.470	0.858	10.0*
H16B	0.610	0.433	0.899	10.0*
H16C	0.541	0.418	0.780	10.0*
H17A	0.315	0.297	0.797	10.0*
H17B	0.390	0.254	0.720	10.0*
H17C	0.360	0.158	0.799	10.0*
H18A	0.415	0.321	0.985	10.0*
H18B	0.458	0.181	0.990	10.0*
H18C	0.553	0.288	1.029	10.0*

[a]Starred atoms were refined isotropically. Anisotropically refined atoms are given in the form of the isotropic equivalent displacement parameter defined as $(4/3)*[a^2*B(1,1) + b^2*B(2,2) + c^2*B(3,3) + ab(\cos\gamma)*B(1,2) + ac(\cos\beta)*B(1,3) + bc(\cos\alpha)*B(2,3)]$.

Table I.3. General displacement parameters - U for (±)-15.[a]

Atom	U(1,1)	U(2,2)	U(3,3)	U(1,2)	U(1,3)	U(2,3)
O1	0.054 (2)	0.039 (2)	0.033 (1)	-0.008 (2)	0.011 (1)	0.001 (2)
O2	0.042 (2)	0.038 (2)	0.044 (2)	0.006 (2)	0.013 (1)	0.014 (2)
O3	0.066 (2)	0.054 (2)	0.045 (2)	-0.007 (2)	0.012 (2)	-0.017 (2)
C1	0.036 (2)	0.029 (2)	0.038 (2)	0.005 (2)	0.009 (2)	-0.001 (2)
C2	0.051 (3)	0.037 (3)	0.046 (3)	0.001 (2)	0.017 (2)	0.007 (2)
C3	0.047 (3)	0.034 (3)	0.062 (3)	-0.006 (2)	0.024 (2)	0.003 (3)

C4	0.045 (3)	0.050 (3)	0.052 (3)	-0.014 (3)	0.008 (2)	-0.007 (3)
C5	0.044 (3)	0.043 (3)	0.040 (2)	-0.001 (2)	0.010 (2)	0.002 (2)
C6	0.034 (2)	0.025 (2)	0.034 (2)	0.004 (2)	0.008 (2)	0.004 (2)
C7	0.032 (2)	0.029 (2)	0.037 (2)	0.002 (2)	0.008 (2)	0.004 (2)
C8	0.039 (2)	0.023 (2)	0.044 (2)	0.003 (2)	0.012 (2)	-0.004 (2)
C9	0.037 (2)	0.032 (3)	0.042 (2)	0.009 (2)	0.009 (2)	-0.003 (2)
C10	0.059 (3)	0.048 (3)	0.058 (3)	0.005 (3)	0.032 (2)	0.011 (3)
C11	0.050 (3)	0.043 (3)	0.042 (2)	-0.001 (3)	0.018 (2)	0.003 (2)
C12	0.036 (2)	0.027 (2)	0.041 (2)	0.000 (2)	0.015 (2)	-0.000 (2)
C13	0.034 (2)	0.026 (2)	0.048 (3)	-0.001 (2)	0.008 (2)	-0.007 (3)
C14	0.042 (3)	0.036 (3)	0.051 (3)	-0.001 (2)	0.008 (2)	-0.007 (3)
C15	0.035 (3)	0.043 (3)	0.066 (3)	0.006 (3)	0.000 (2)	-0.005 (3)
C16	0.085 (5)	0.037 (4)	0.231 (9)	0.015 (4)	0.052 (5)	-0.008 (5)
C17	0.049 (3)	0.080 (5)	0.122 (6)	0.015 (4)	0.002 (4)	-0.009 (5)
C18	0.083 (4)	0.104 (5)	0.109 (5)	0.046 (4)	0.042 (3)	-0.001 (5)

[a]The form of the anisotropic displacement parameter is: $\exp[-2\pi^2\{h^2a^2U(1,1) + k^2b^2U(2,2) + l^2c^2U(3,3) + 2hkabU(1,2) + 2hlacU(1,3) + 2klbcU(2,3)\}]$, where a, b, and c are reciprocal lattice constants.

Appendix II: NMR Spectra and Cross Peak Assignments for [Δ-Rh]-E10 (Chapter 4).

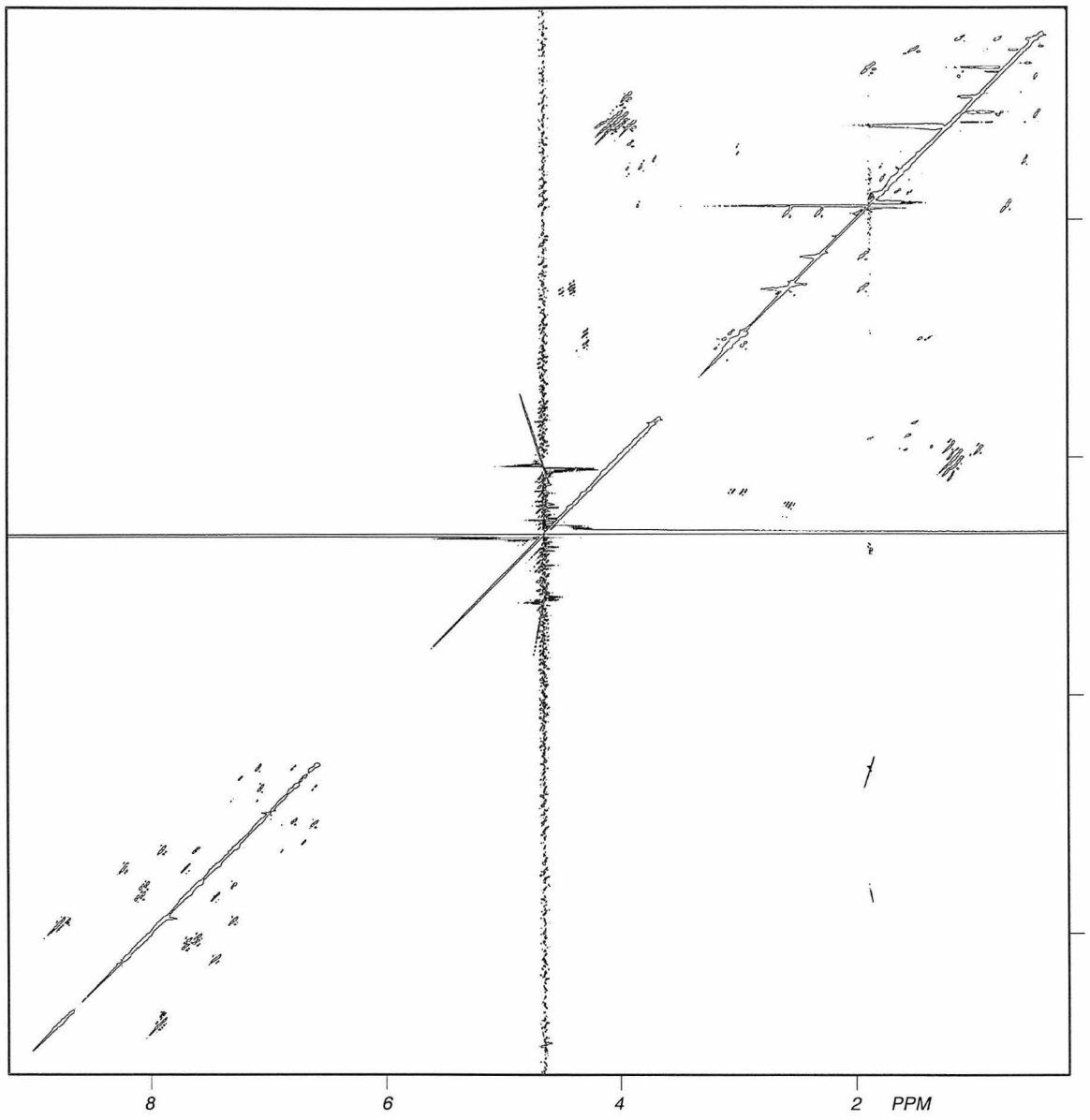

Figure II.1. COSY spectrum of [Δ-Rh]-E10 (500 MHz, D_2O).

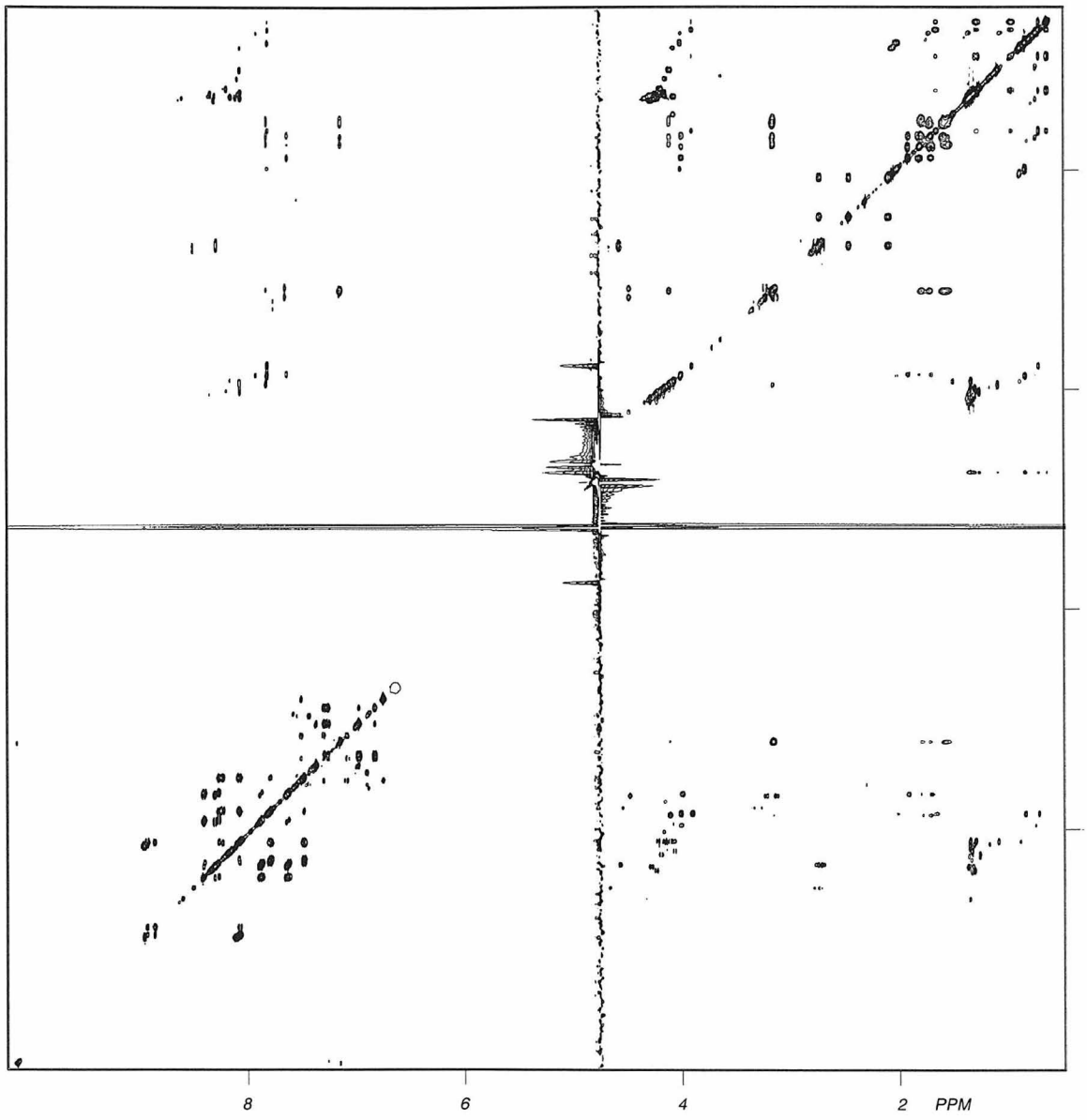

Figure II.2. TOCSY spectrum of [Δ-Rh]-E10 (600 MHz, 90:10 H_2O–D_2O).

Table II.1. Observed COSY (500 MHz, D_2O) cross peaks for [Δ-Rh]-E10.

Signal	Signal	δ_1	δ_2	Signal	Signal	δ_1	δ_2
Ala[7] H_α	Ala[7] H_β	4.06	1.07	phen H_2	phen $H_{1\text{ or }3}$	8.02	8.88
Ala[7] H_β	Ala[7] H_α	1.07	4.05	phen $H_{2'}$	phen $H_{1,3}$	8.07	8.91
Ala H_α	Ala H_β	4.15	1.29	phi $H_{1'}$	phi $H_{2'}$	8.03	7.42
Ala H_β	Ala H_α	1.28	4.17	phi $H_{2'}$	phi $H_{3'}$	7.42	7.72
Arg H_α	Arg H_β	4.04	1.69	phi $H_{2'}$	phi $H_{1'}$	7.42	8.03
Arg H_β	Arg H_α	1.68	4.05	phi $H_{3'}$	phi $H_{2'}$	7.74	7.43
Arg H_δ	Arg H_γ	3.11	1.56	phi $H_{3'}$	phi $H_{4'}$	7.73	8.19
Arg H_γ	Arg H_δ	1.55	3.12	phi $H_{4'}$	phi $H_{3'}$	8.18	7.73
Asn H_α	Asn H_β	4.54	2.70	phi $H_{1''}$	phi $H_{2''}$	8.35	7.58
Asn H_β	Asn H_α	2.68	4.53	phi $H_{2''}$	phi $H_{3''}$	7.58	7.83
Glu H_α	Glu H_β	3.94	1.68	phi $H_{2''}$	phi $H_{1''}$	7.57	8.35
Glu H_β	Glu H_α	1.67	3.94	phi $H_{3''}$	phi $H_{2''}$	7.82	7.57
Ile H_α	Ile H_β	3.81	1.61	phi $H_{3''}$	phi $H_{4''}$	7.82	8.22
Ile H_β	Ile Me_2	1.61	0.67	phi $H_{4''}$	phi $H_{3''}$	8.22	7.82
Ile H_β	Ile H_α	1.60	3.83	Trp H_4	Trp H_5	7.21	6.73
Ile Me_2	Ile H_β	0.67	1.61	Trp H_5	Trp H_6	6.74	6.90
Ile Me_1	Ile $H_\gamma 1$	0.59	0.90	Trp H_5	Trp H_4	6.73	7.20
Ile Me_1	Ile $H_\gamma 2$	0.59	1.23	Trp H_6	Trp H_5	6.90	6.73
Ile $H_{\gamma 1}$	Ile Me_1	0.91	0.59	Trp H_6	Trp H_7	6.91	7.19
Ile $H_{\gamma 2}$	Ile Me_1	1.24	0.59	Trp H_7	Trp H_6	7.18	6.91
linker $H_{1'}$	linker $H_{2'}$	2.69	2.04	Trp H_α	Trp $H_{\beta 1}$	4.41	3.17
linker $H_{2'}$	linker $H_{3'}$	2.05	2.42	Trp H_α	Trp $H_{\beta 2}$	4.41	3.08
linker $H_{2'}$	linker $H_{1'}$	2.04	2.69	Trp $H_{\beta 1}$	Trp H_α	3.16	4.41
linker $H_{3'}$	linker $H_{2'}$	2.41	2.05	Trp $H_{\beta 2}$	Trp H_α	3.07	4.41
phen $H_{1',3'}$	phen $H_{2'}$	8.91	8.06	Val H_α	Val H_β	3.96	2.00
phen $H_{1\text{ or }3}$	phen H_2	8.82	8.03	Val H_β	Val H_γ	2.00	0.83
phen $H_{1\text{ or }3}$	phen H_2	8.87	8.03	Val H_β	Val H_α	1.99	3.96
phen H_2	phen $H_{1\text{ or }3}$	8.02	8.82	Val H_γ	Val H_β	0.84	2.00

[c]Phen H_2-H_4 and H_7-H_9 spin systems were not distinguished and are labeled phen H_1-H_3 and $H_{1'}$-$H_{3'}$.

[d]There are two pairs of accidentally isochronous phi spin systems. The individual spin systems were not distinguished and are labeled phi $H_{1'}$-$H_{4'}$ and $H_{1''}$-$H_{4''}$.

Table II.2. Observed TOCSY (600 MHz, 90:10 H_2O–D_2O) cross peaks for Δ-[Rh]-E10.

Signal	Signal	δ_{D1}	δ_{D2}	Signal	Signal	δ_{D1}	δ_{D2}
Ala^7 H_α	Ala^7 Me	4.11	1.08	Glu H_N	Glu H_β	7.64	1.68
Ala^7 H_α	Ala^7 H_N	4.11	8.12	Ile H_α	Ile Me_2	3.91	0.72
Ala^7 H_N	Ala^7 Me	8.07	1.08	Ile H_α	Ile Me_1	3.91	0.64
Ala^7 H_N	Ala^7 H_α	8.07	3.93	Ile H_α	Ile $H_{\gamma 2}$	3.91	1.28
Ala^7 Me	Ala^7 H_α	1.10	3.95	Ile H_α	Ile $H_{\gamma 1}$	3.92	0.96
Ala^7 Me	Ala^7 H_N	1.10	8.11	Ile H_α	Ile H_β	3.91	1.64
Ala^8 H_α	Ala^8 Me	4.07	1.32	Ile H_α	Ile H_N	3.91	7.86
Ala^8 H_α	Ala^8 H_N	4.07	8.20	Ile H_β	Ile Me_1	1.67	0.64
Ala^8 H_N	Ala^8 Me	8.16	1.33	Ile H_β	Ile Me_2	1.67	0.72
Ala^8 H_N	Ala^8 H_α	8.16	3.91	Ile H_β	Ile $H_{\gamma 1}$	1.66	0.96
Ala^8 Me	Ala^8 H_α	1.35	3.92	Ile H_β	Ile $H_{\gamma 2}$	1.67	1.27
Ala^8 Me	Ala^8 H_N	1.35	8.20	Ile H_β	Ile H_α	1.66	3.79
Ala^{12} H_α	Ala^{12} Me	4.16	1.29	Ile H_β	Ile H_N	1.67	7.86
Ala^{12} H_α	Ala^{12} H_N	4.16	8.12	Ile $H_{\gamma 1}$	Ile H_β	0.97	1.64
Ala^{12} H_N	Ala^{12} Me	8.06	1.28	Ile $H_{\gamma 1}$	Ile $H_{\gamma 2}$	0.98	1.27
Ala^{12} H_N	Ala^{12} H_α	8.07	3.98	Ile $H_{\gamma 1}$	Ile Me_2	0.98	0.71
Ala^{12} Me	Ala^{12} H_α	1.31	3.99	Ile $H_{\gamma 1}$	Ile Me_1	0.98	0.64
Ala^{12} Me	Ala^{12} H_N	1.31	8.11	Ile $H_{\gamma 2}$	Ile Me_1	1.30	0.64
Ala^5 H_α	Ala^5 Me	4.19	1.25	Ile $H_{\gamma 2}$	Ile Me_2	1.30	0.71
Ala^5 H_α	Ala^5 H_N	4.19	8.24	Ile $H_{\gamma 2}$	Ile $H_{\gamma 1}$	1.30	0.96
Ala^5 H_N	Ala^5 Me	8.19	1.25	Ile $H_{\gamma 2}$	Ile H_β	1.29	1.64
Ala^5 H_N	Ala^5 H_α	8.19	4.02	Ile H_N	Ile $H_{\gamma 1}$	7.83	0.96
Ala^5 Me	Ala^5 H_α	1.27	4.01	Ile H_N	Ile Me_2	7.81	0.71
Ala^5 Me	Ala^5 H_N	1.27	8.23	Ile H_N	Ile Me_1	7.83	0.64
Ala^2 H_α	Ala^2 Me	4.24	1.30	Ile H_N	Ile H_β	7.83	1.64
Ala^2 H_α	Ala^2 H_N	4.24	8.39	Ile H_N	Ile H_α	7.83	3.79
Ala^2 H_N	Ala^2 Me	8.34	1.30	Ile Me_1	Ile Me_2	0.66	0.71
Ala^2 H_N	Ala^2 H_α	8.34	4.05	Ile Me_1	Ile $H_{\gamma 1}$	0.66	0.95
Ala^2 Me	Ala^2 H_α	1.32	4.04	Ile Me_1	Ile $H_{\gamma 2}$	0.66	1.27
Ala^2 Me	Ala^2 H_N	1.33	8.38	Ile Me_1	Ile H_β	0.66	1.64
Ala^{13} H_α	Ala^{13} Me	4.22	1.34	Ile Me_1	Ile H_α	0.66	3.78
Ala^{13} H_α	Ala^{13} H_N	4.22	8.12	Ile Me_1	Ile H_N	0.66	7.87
Ala^{13} H_N	Ala^{13} Me	8.07	1.34	Ile Me_2	Ile Me_1	0.73	0.63
Ala^{13} H_N	Ala^{13} H_α	8.07	4.04	Ile Me_2	Ile $H_{\gamma 1}$	0.74	0.96
Ala^{13} Me	Ala^{13} H_α	1.36	4.03	Ile Me_2	Ile $H_{\gamma 2}$	0.73	1.27
Ala^{13} Me	Ala^{13} H_N	1.36	8.11	Ile Me_2	Ile H_β	0.74	1.63
Ala^1 H_α	Ala^1 Me	4.28	1.36	Ile Me_2	Ile H_α	0.74	3.78
Ala^1 H_α	Ala^1 H_N	4.29	8.35	Ile Me_2	Ile H_N	0.73	7.87

Ala^1 H_N	Ala^1 Me	8.31	1.36	$linker_{1'}$	$linker_{2'}$	2.73	2.07
Ala^1 H_N	Ala^1 H_α	8.30	4.09	$linker_{1'}$	$linker_{3'}$	2.74	2.42
Ala^1 Me	Ala^1 H_α	1.37	4.06	$linker_{2'}$	$linker_{3'}$	2.10	2.42
Ala^1 Me	Ala^1 H_N	1.38	8.35	$linker_{2'}$	$linker_{1'}$	2.10	2.68
Arg H_α	Arg H_δ	4.12	3.10	$linker_{3'}$	$linker_{1'}$	2.47	2.69
Arg H_α	Arg $H_{\beta2}$	4.11	1.75	$linker_{3'}$	$linker_{2'}$	2.46	2.07
Arg H_α	Arg $H_{\beta1}$	4.12	1.69	phen $H_{1,3}$	phen H_2	8.96	8.16
Arg H_α	Arg H_γ	4.12	1.55	phen H_2	phen $H_{1,3}$	8.11	8.99
Arg H_α	Arg H_{guan}	4.11	7.21	phen $H_{1'}$	phen $H_{3'}$	8.93	8.90
Arg H_α	Arg H_N	4.11	7.88	phen $H_{1'}$	phen $H_{2'}$	8.93	8.12
Arg $H_{\beta1}$	Arg H_δ	1.73	3.10	phen $H_{2'}$	phen $H_{3'}$	8.08	8.90
Arg $H_{\beta1}$	Arg H_α	1.73	3.95	phen $H_{3'}$	phen $H_{1'}$	8.86	8.97
Arg $H_{\beta1}$	Arg H_γ	1.72	1.57	phen $H_{2'}$	phen $H_{1'}$	8.08	8.96
Arg $H_{\beta1}$	Arg $H_{\beta2}$	1.74	1.76	phen $H_{3'}$	phen $H_{2'}$	8.86	8.12
Arg $H_{\beta1}$	Arg H_{guan}	1.73	7.22	phi $H_{1'}$	phi $H_{3'}$	8.40	7.94
Arg $H_{\beta1}$	Arg H_N	1.72	7.88	phi $H_{1'}$	phi $H_{2'}$	8.39	7.69
Arg $H_{\beta2}$	Arg H_δ	1.80	3.10	phi $H_{1'}$	phi $H_{4'}$	8.41	8.33
Arg $H_{\beta2}$	Arg H_α	1.80	3.96	phi $H_{2'}$	phi $H_{4'}$	7.64	8.34
Arg $H_{\beta2}$	Arg H_γ	1.79	1.55	phi $H_{2'}$	phi $H_{1'}$	7.64	8.44
Arg $H_{\beta2}$	Arg $H_{\beta1}$	1.78	1.71	phi $H_{2'}$	phi $H_{3'}$	7.64	7.94
Arg $H_{\beta2}$	Arg H_{guan}	1.80	7.21	phi $H_{3'}$	phi $H_{1'}$	7.89	8.44
Arg $H_{\beta2}$	Arg H_N	1.79	7.88	phi $H_{3'}$	phi $H_{4'}$	7.89	8.34
Arg H_δ	Arg H_α	3.16	3.97	phi $H_{3'}$	phi $H_{2'}$	7.89	7.68
Arg H_δ	Arg H_γ	3.16	1.55	phi $H_{4'}$	phi $H_{3'}$	8.30	7.94
Arg H_δ	Arg $H_{\beta1}$	3.18	1.70	phi $H_{4'}$	phi $H_{2'}$	8.29	7.70
Arg H_δ	Arg $H_{\beta2}$	3.17	1.77	phi $H_{4'}$	phi $H_{1'}$	8.29	8.45
Arg H_δ	Arg H_{guan}	3.16	7.21	phi $H_{1''}$	phi $H_{2''}$	8.26	7.84
Arg H_δ	Arg H_N	3.15	7.88	phi $H_{1''}$	phi $H_{3''}$	8.26	7.54
Arg H_γ	Arg H_δ	1.58	3.10	phi $H_{1''}$	phi $H_{4''}$	8.26	8.13
Arg H_γ	Arg H_α	1.58	3.96	phi $H_{2''}$	phi $H_{4''}$	7.80	8.12
Arg H_γ	Arg $H_{\beta1}$	1.59	1.69	phi $H_{2''}$	phi $H_{1''}$	7.80	8.29
Arg H_γ	Arg $H_{\beta2}$	1.58	1.77	phi $H_{2''}$	phi $H_{3''}$	7.80	7.54
Arg H_γ	Arg H_{guan}	1.57	7.20	phi $H_{3''}$	phi $H_{4''}$	7.49	8.12
Arg H_γ	Arg H_N	1.57	7.88	phi $H_{3''}$	phi $H_{1''}$	7.50	8.29
Arg H_{guan}	Arg H_α	7.16	3.97	phi $H_{3''}$	phi $H_{2''}$	7.49	7.84
Arg H_{guan}	Arg H_δ	7.15	3.11	phi $H_{4''}$	phi $H_{3''}$	8.08	7.54
Arg H_{guan}	Arg $H_{\beta2}$	7.16	1.76	phi $H_{4''}$	phi $H_{2''}$	8.09	7.85
Arg H_{guan}	Arg $H_{\beta1}$	7.16	1.70	phi $H_{4''}$	phi $H_{1''}$	8.09	8.30
Arg H_{guan}	Arg H_γ	7.15	1.55	Trp H_2	Trp $H_{N\ arom}$	7.16	10.14
Arg H_N	Arg H_α	7.83	3.96	Trp H_4	Trp H_7	7.30	7.32
Arg H_N	Arg H_δ	7.83	3.11	Trp H_4	Trp H_6	7.31	7.04
Arg H_N	Arg $H_{\beta2}$	7.83	1.77	Trp H_4	Trp H_5	7.30	6.90

Arg H_N	Arg $H_{\beta 1}$	7.83	1.70	Trp H_5	Trp H_6	6.84	7.04
Arg H_N	Arg H_γ	7.84	1.55	Trp H_5	Trp H_4	6.83	7.37
Asn H_α	Asn $H_{\beta 12}$	4.58	2.69	Trp H_5	Trp H_7	6.83	7.32
Asn H_β	Asn H_N	2.74	8.33	Trp H_6	Trp H_5	6.98	6.90
Asn H_N	Asn $H_{\beta 12}$	8.29	2.69	Trp H_6	Trp H_7	6.98	7.32
$CONH_{2\,(1)}$	$CONH_{2\,(1)}$	7.38	7.05	Trp H_6	Trp H_4	6.98	7.36
$CONH_{2\,(1)}$	$CONH_{2\,(1)}$	6.99	7.43	Trp H_7	Trp H_4	7.26	7.36
$CONH_{2\,(2)}$	$CONH_{2\,(2)}$	6.76	7.57	Trp H_7	Trp H_6	7.26	7.05
$CONH_{2\,(2)}$	$CONH_{2\,(2)}$	7.51	6.82	Trp H_7	Trp H_5	7.26	6.90
Glu H_α	Glu $H_{\gamma 2}$	4.00	1.88	Trp $H_{N\,arom}$	Trp H_2	10.11	7.22
Glu H_α	Glu $H_{\gamma 1}$	4.00	1.80	Trp H_α	Trp $H_{\beta 1}$	4.49	3.07
Glu H_α	Glu H_β	4.01	1.69	Trp H_α	Trp $H_{\beta 2}$	4.49	3.16
Glu H_α	Glu H_N	4.00	7.70	Trp $H_{\beta 1}$	Trp H_N	3.14	7.71
Glu H_β	Glu $H_{\gamma 2}$	1.71	1.88	Trp $H_{\beta 2}$	Trp H_N	3.23	7.72
Glu H_β	Glu $H_{\gamma 1}$	1.72	1.78	Trp H_N	Trp $H_{\beta 1}$	7.65	3.08
Glu H_β	Glu H_α	1.70	3.87	Trp H_N	Trp $H_{\beta 2}$	7.65	3.17
Glu H_β	Glu H_N	1.71	7.68	Val H_α	Val $Me_{1,2}$	4.05	0.86
Glu $H_{\gamma 1}$	Glu H_β	1.81	1.67	Val H_α	Val H_β	4.02	2.01
Glu $H_{\gamma 1}$	Glu $H_{\gamma 2}$	1.82	1.88	Val H_α	Val H_N	4.02	7.87
Glu $H_{\gamma 1}$	Glu H_α	1.81	3.87	Val H_β	Val $Me_{1,2}$	2.05	0.86
Glu $H_{\gamma 1}$	Glu H_N	1.82	7.70	Val H_β	Val H_α	2.02	3.88
Glu $H_{\gamma 2}$	Glu $H_{\gamma 1}$	1.92	1.78	Val H_β	Val H_N	2.01	7.87
Glu $H_{\gamma 2}$	Glu H_β	1.92	1.68	Val H_N	Val H_β	7.82	2.00
Glu $H_{\gamma 2}$	Glu H_α	1.92	3.86	Val H_N	Val $Me_{1,2}$	7.82	0.85
Glu $H_{\gamma 2}$	Glu H_N	1.93	7.69	Val H_N	Val H_α	7.83	3.86
Glu H_N	Glu H_α	7.63	3.86	Val $Me_{1,2}$	Val H_β	0.88	2.01
Glu H_N	Glu $H_{\gamma 2}$	7.64	1.89	Val $Me_{1,2}$	Val H_α	0.88	3.90
Glu H_N	Glu $H_{\gamma 1}$	7.64	1.78	Val $Me_{1,2}$	Val H_N	0.86	7.86

[a]C-terminal and Asn side chain $CONH_2$ groups were not distinguished and are labeled $CONH_{2\,(1)}$ and $CONH_{2\,(2)}$.

[c]Phen H_2-H_4 and H_7-H_9 spin systems were not distinguished and are labeled phen H_1-H_3 and $H_{1'}$-$H_{3'}$.

[d]There are two pairs of accidentally isochronous phi spin systems. The individual spin systems were not distinguished and are labeled phi $H_{1'}$-$H_{4'}$ and $H_{1''}$-$H_{4''}$.

Table II.3. Observed NOESY (600 MHz, 90:10 H_2O–D_2O) cross peaks for Δ-[Rh]-E10.

Signal	Signal	δ_{D1}	δ_{D2}	Signal	Signal	δ_{D1}	δ_{D2}
Ala^{12} H_α	Ala^{12} Me	4.18	1.34	Ile H_α	Ala^{7} H_N	3.92	8.10
Ala^{12} H_α	Ala^{13} H_N	4.18	8.10	Ile H_β	Ile $H_{\gamma 1}$	1.68	1.00
Ala^{12} Me	Ala^{12} H_α	1.33	4.19	Ile H_β	Ile Me_2	1.70	0.75
Ala^{13} H_α	Ala^{13} Me	4.22	1.39	Ile $H_{\gamma 1}$	Ile Me_1	1.02	0.68
Ala^{13} H_α	Ala^{13} H_N	4.26	8.09	Ile $H_{\gamma 1}$	Ile H_β	1.00	1.69
Ala^{13} H_N	Ala^{12} H_α	8.08	4.18	Ile $H_{\gamma 2}$	Ile $H_{\gamma 1}$	1.31	1.01
Ala^{13} H_N	Ala^{13} H_α	8.08	4.26	Ile $H_{\gamma 2}$	Ile Me_1	1.30	0.69
Ala^{13} H_N	Ala^{13} Me	8.08	1.39	Ile H_N	Ile H_α	7.83	3.93
Ala^{13} Me	Ala^{13} H_α	1.38	4.25	Ile H_N	Ala^{5} H_α	7.83	4.22
Ala^{1} H_α	Ala^{1} Me	4.31	1.41	Ile Me_1	Ile $H_{\gamma 1}$	0.66	1.00
Ala^{1} H_α	Ala^{2} H_N	4.31	8.37	Ile Me_1	Ile $H_{\gamma 2}$	0.67	1.32
Ala^{1} H_N	Ala^{2} Me	8.36	1.35	Ile Me_2	Ile H_β	0.74	1.69
Ala^{1} H_N	Ala^{1} H_α	8.33	4.32	Linker 3'	Ala^{1} H_N	2.48	8.34
Ala^{1} Me	Ala^{1} H_α	1.40	4.31	Linker 1'	Linker 2'	2.74	2.12
Ala^{2} H_α	Asn H_N	4.26	8.31	Linker 2'	Linker 1'	2.13	2.75
Ala^{2} H_α	Ala^{2} Me	4.25	1.35	Linker 3'	Linker 2'	2.50	2.12
Ala^{2} H_α	Ala^{2} H_N	4.26	8.37	Phen $H_{1,3}$	Phen H_2	8.96	8.15
Ala^{2} H_N	Ala^{1} Me	8.33	1.41	Phen H_2	Phen $H_{1,3}$	8.13	8.96
Ala^{1} H_N	Linker 3'	8.33	2.49	Phen H_6	Phen H_7	8.44	8.97
Ala^{2} H_N	Ala^{2} H_α	8.37	4.26	Phen H_7	Phen H_6	8.95	8.44
Ala^{2} H_N	Ala^{1} H_α	8.37	4.32	Phen H_7	Phen H_8	8.94	8.10
Ala^{2} Me	Ala^{1} H_N	1.34	8.36	Phen H_8	Phen H_9	8.10	8.90
Ala^{2} Me	Ala^{2} H_α	1.34	4.27	Phen H_8	Phen H_7	8.09	8.96
Ala^{5} H_α	Ala^{5} Me	4.21	1.29	Phen H_9	Phen H_8	8.88	8.10
Ala^{5} H_α	Ile H_N	4.21	7.84	Phi H_N	Phi H_1	10.60	8.43
Ala^{5} H_N	Val H_α	8.21	4.04	Phi H_N	Phen H_1	10.61	8.98
Ala^{5} H_N	Ala^{5} Me	8.20	1.30	Trp H_2	Trp $H_{N\ arom}$	7.18	10.13
Ala^{5} H_N	Ala^{5} H_α	8.21	4.22	Trp H_2	Trp $H_{\beta 2}$	7.18	3.25
Ala^{5} Me	Ala^{5} H_N	1.29	8.21	Trp H_2	Trp $H_{\beta 1}$	7.18	3.16
Ala^{5} Me	Val H_N	1.29	7.84	Trp H_2	Ala^{7} Me	7.17	1.12
Ala^{5} Me	Ala^{5} H_α	1.28	4.23	Trp H_6	Trp H_7	6.98	7.29
Ala^{7} H_α	Ala^{7} Me	4.11	1.13	Trp H_7	Trp $H_{N\ arom}$	7.28	10.13
Ala^{7} H_α	Ala^{7} H_N	4.13	8.10	Trp H_7	Trp H_6	7.28	6.97
Ala^{7} H_N	Ile H_α	8.09	3.93	Trp H_7	Trp $H_{\beta 1}$	7.32	3.16
Ala^{7} H_N	Ala^{7} H_α	8.09	4.13	Trp H_7	Trp $H_{\beta 2}$	7.32	3.24
Ala^{7} H_N	Ala^{7} Me	8.09	1.12	Trp H_α	Trp H_N	4.50	7.66
Ala^{7} H_N	Ala^{7} Me	1.12	8.10	Trp H_α	Trp $H_{\beta 1}$	4.49	3.15
Ala^{7} Me	Ala^{7} H_α	1.13	4.13	Trp $H_{\beta 1}$	Trp H_α	3.15	4.51

Ala^8 H_α	Ala^8 Me	4.09	1.37	Trp $H_{\beta1}$	Trp H_2	3.16	7.19
Ala^8 H_α	Ala^8 H_N	4.11	8.19	Trp $H_{\beta1}$	Trp $H_{\beta2}$	3.11	3.25
Ala^8 H_α	Trp H_N	4.09	7.67	Trp $H_{\beta1}$	Trp H_N	3.27	7.67
Ala^8 H_N	Ala^7 Me	8.17	1.12	Trp $H_{\beta1}$	Trp H_N	3.13	7.67
Ala^8 H_N	Ala^8 H_α	8.17	4.12	Trp $H_{\beta2}$	Trp H_α	3.27	4.51
Ala^8 H_N	Ala^8 Me	8.17	1.37	Trp $H_{\beta2}$	Trp H_2	3.25	7.19
Ala^8 Me	Ala^8 H_N	1.37	8.18	Trp $H_{\beta2}$	Trp $H_{\beta1}$	3.29	3.16
Ala^8 Me	Ala^8 H_α	1.36	4.11	Trp H_N	Trp H_α	7.66	4.52
Ala^7 Me	Trp H_2	1.12	7.19	Trp H_N	Ala^8 H_α	7.67	4.10
Arg H_α	Arg H_β	4.12	1.76	Trp H_N	Trp $H_{\beta2}$	7.66	3.24
Arg H_α	Arg H_N	4.14	7.85	Trp H_N	Trp $H_{\beta1}$	7.66	3.16
Arg H_β	Arg H_α	1.81	4.14	Trp $H_{N\ arom}$	Trp H_7	10.12	7.30
Arg H_δ	Arg H_γ	3.18	1.60	Trp $H_{N\ arom}$	Trp H_2	10.13	7.19
Arg H_N	Glu H_α	7.85	4.03	Val H_α	Val H_β	4.03	2.05
Arg H_N	Arg H_α	7.85	4.13	Val H_α	Val $Me_{1,2}$	4.03	0.88
Asn H_β	Val H_N	2.77	8.31	Val H_α	Val H_N	4.01	7.85
Asn $H_{\beta1}$	Asn H_α	2.77	4.60	Val H_α	Ala^5 H_N	4.03	8.22
Asn $H_{\beta2}$	Asn H_α	2.71	4.60	Val H_β	Val $Me_{1,2}$	2.06	0.88
Asn H_N	Asn H_α	8.31	4.61	Val H_β	Val H_N	2.05	7.84
Asn H_N	Ala^2 H_α	8.31	4.26	Val H_β	Val H_α	2.05	4.03
Asn H_N	Ala^2 Me	8.30	1.35	Val H_N	Val H_α	7.84	4.02
Glu H_α	Glu H_N	4.02	7.65	Val H_N	Asn H_α	7.83	4.60
Glu H_α	Arg H_N	4.03	7.85	Val H_N	Val H_β	7.84	2.04
Glu H_N	Glu H_α	7.65	4.02	Val H_N	Val $Me_{1,2}$	7.83	0.88
Glu H_N	Trp H_α	7.65	4.52	Val H_N	Ala^5 Me	7.83	1.30
Ile H_α	Ile H_N	3.92	7.83	Val $Me_{1,2}$	Val H_β	0.85	2.05
Ile H_α	Ile Me_2	3.92	0.77	Val $Me_{1,2}$	Val H_N	0.87	7.84
Ile H_α	Ile H_β	3.92	1.68				